THE UNIVERSITY OF MICHIGAN

INDUSTRY PROGRAM OF THE COLLEGE OF ENGINEERING

ELECTROTRANSPORT IN SOME LIQUID METAL ALLOYS

John D. Verhoeven

A dissertation submitted in partial fulfillment
of the requirements for the degree of
Doctor of Philosophy in the
University of Michigan
Chemical and Metallurgical Department
1963

January, 1963

IP-603

Doctoral Committee:

Professor Edward E. Hucke, Chairman
Professor Ernst Katz
Professor Donald R. Mason
Professor Giuseppe Parravano
Professor David V. Ragone
Professor Maurice J. Sinnott

ACKNOWLEDGMENTS

The present investigation was carried out at the Department of Chemical and Metallurgical Engineering, University of Michigan, Ann Arbor, Michigan under the direction of Professor E. E. Hucke. The author would like to express his sincere thanks to Professor Hucke for stimulating his interest in this problem and encouraging his work.

The author would also like to thank, in particular, Professor D. V. Ragone, whose strong influence encouraged the author to continue his studies and to Dr. J. C. Angus, whose friendship and technical advice as a fellow graduate student were deeply appreciated.

The United States Atomic Energy Commission provided the funds which made this work possible, under contract No. AT (11-1)-771. The Jones and Laughlin Steel Company provided the author with a fellowship for one year of his graduate study.

The author is also grateful to the analytical group and to Fanny, Bill, and John of the Chem. Met. Shops.

TABLE OF CONTENTS

TABLE OF CONTENTS (CONT'D)

LIST OF TABLES

LIST OF TABLE (CONT'D)

LIST OF FIGURES

LIST OF FIGURES (CONT'D)

LIST OF APPENDICES

NOMENCLATURE

A_m	Mean cross sectional area of capillary cells
A_i	Atomic scattering cross section for electrons and component i
A_i^*	Atomic scattering cross section for electrons and activated component i
$\overline{A_i}$	Average atomic scattering cross section for electrons and component i
$\overline{A}$	Average atomic scattering cross section for electrons and the atoms or ions of a material
A_e	Cross sectional area at entrance of capillary cells, or the atomic cross section for electrons and a component
A_p	Atomic cross section for positive carriers and a component
a	A constant in Equation (93) and Equation (101) and the capillary cell length in the solution of the partial differential Equation (144)
a_i	Activity of component i
B_i	Absolute mobility of component i
B	Statistical constant defined in Equation (182)
b'	Constant in Equation (H-2)
b	Constant in Equation (101), (156), and (H-1), and the interatomic distance in Equation (32)
C'	Constant in Equation (44)
C	Dimensionless concentration defined by Equation (143)
C_m	Mean dimensionless concentration within the capillary

D_i	Intrinsic diffusion coefficient of component i with container as reference velocity
D^*	Self diffusion coefficient
D	Diffusion coefficient
e^*_i	Negative charge of transport for component i defined by Equation (63)
e	Charge on an electron
E	Electric field intensity
E_F	Energy at the Fermi level
f	Correlation constant in Equation (7) or the slope of the mole fraction versus resistivity curve
F	Faraday constant or the total external force on a system
F_i	Net force on component i
F_{ei}	Frictional force of electrons on an ion of component i
F_{ed}	Frictional force of electrons on a defect
F_d	Net force on a defect
F_A	Average net force on solute atom "A"
F_n	Average net force on nearest neighbor atom "n"
F_{fi}	The force exerted upon component i by an electric field
I	Electric current
j	Electric current per unit area
J_i^a	Flux of component i in moles per area and time referred to reference velocity "a"
J_i	Flux of component i in moles per area and time referred to the observer or container velocity

$J_o(b)$	Bessel function
$J_2(b)$	Bessel function
h	Plank's constant
k	Boltzmon constant
K	Constant defined in Equation (59)
K_i	Electrotransport constant defined by Drakin
K_n	Constant defined in Equation (90)
ℓ, ℓ_e	Mean free path length of the electrons
ℓ_p	Mean free path length of the positive charge carriers
L	Length of capillary cell
L_{ik}	Phenomenological constant
m_e, m	Mass of an electron
m*	Effective mass of an electron
M	Molecular weight
n_i'	Number of ions or atoms of component i
n_i	Number of ions or atoms of component i per unit volume
n_e	Number of electrons per unit volume
n_p	Number of positive charge carriers per unit volume
n_d	Number of defects per unit volume
n_o	Number of atoms of solvent material per unit volume
n_A	Number of atoms of component A per unit volume
N_n	Average number of nearest neighbors
$(N_i)_m$	Mean number of moles of component i per unit volume within the capillary
N_i	Number of moles of component i per unit volume

N, N_o	Number of moles of solvent per unit volume, i.e. molar density
N_i	Number of moles of component i
P_i, p_i	Momentum of component i
P	Momentum
r_{ik}	Friction coefficient between components i and k
r_{ie}	Friction coefficient between components i and electrons
r_{Au}	Friction coefficient between activated and unactivated ions
r_{ue}	Friction coefficient between unactivated ions and electrons
r_{Ae}	Friction coefficient between activated ions and electrons
r_{iAu}	Friction coefficient between activated i ions and unactivated ions
r_{lA2A}	Friction coefficient between activated 1 ions and activated 2 ions
r_i^*	Friction coefficient between activated i ions and electrons
$\bar{r}$	Average friction coefficient between solvent ions and electrons
S	Dimensionless ratio defined by Equation (143)
t	Dimensionless time defined by Equation (143)
t_i	Transference number of component i
T	Temperature
u	Electric mobility
u_i^v	Electric mobility of component i with reference to the volume velocity
u_i^A	Electric mobility of component i with reference to the mean atom velocity
u_i^M	Electric mobility of component i with reference to the mean mass velocity

u_i Electric mobility of component i with reference to the container velocity

u_A Electric mobility of component A

u_{AN} Electric mobility of component A with reference to the nearest neighbor velocity

u_N Electric mobility of the nearest neighbors

U_{12} Differential electric mobility

v_i^a Velocity of component i with respect to reference velocity "a"

v_o Velocity of the bulk material with reference to the container velocity

v_ν Volume velocity with reference to the container

v_i Velocity of component i with reference to the container

$\bar{v}_i$ Average of v_i

v_e Velocity of the electrons with reference to the container

$\overline{v_e}$ Average of v_e

$\overline{v_{ie}}$ Average velocity of ions with respect to the electrons

$\overline{v_{12}}$ Average velocity of component 1 with respect to component 2

$\overline{v_{Au}}$ Average velocity of the activated ions with respect to the unactivated ions in a pure material

v_A Velocity of the activated ions with respect to the container or the mean atom velocity with respect to the container

v_M Mean mass velocity with respect to the container

V' Total volume

$\bar{V}_o$ Volume per atom of total material

$\bar{V}$ Volume per mole of total material, specific molar volume

$\bar{V}_i$, $\bar{V}_k$	Volume per mole of component i or k, partial molar volume
$\bar{V}_e$	Specific molar volume of the metal at the entrance of the capillary cell
$\bar{V}_m$	Mean specific molar volume of the metal within the capillary cell
V, V_c	Voltage drop across the cell
V_s	Voltage drop across the shunt
$(V_s)_o$	Initial voltage drop across the shunt
V_{tc}	Voltage output of the thermocouple
X'_i	Mass fraction of component i
X_k, X_i	Mole fraction of component i or k
X_{iA}	Mole fraction of activated component i
X_A	Mole fraction of component A or of the activated ions of a pure material
X_e	Mole fraction of the electrons
X_{iu}	Mole fraction of unactivated component i
X_u	Mole fraction of unactivated ions in a pure material
$(X_i)_m$	Mean value of component i within the capillary cell
Z	Length of the capillary cell
Z_i	Valence of component i
$\bar{Z}$	Average value of the valence of the ions or atoms of a material
Z^*, Z_A	Valence of the activated ions of a pure material
Z_u	Valence of the unactivated ions of a pure material
Z_i^*	Valence of the activated ions of component i
Z_i^o	Effective valence of component i

Greek Symbols

α	A constant defined in connection with Equation (30)
δ_i, δ_{ei}	Momentum transfer coefficient between electrons and component i
$\overline{\delta}$	Mean value of δ_i over the solvent atoms or ions
$\zeta_i, \zeta_A, \zeta_u$	A parameter specifying the degree of ionization of component i and of the activated and unactivated ions of a pure material
θ	Time or the Debye temperature
μ	Gibbs chemical potential
$\rho_i, \Delta\rho_i$	Resistivity decrement due to presence of component i
ρ_o	Resistivity of pure solvent or matrix material
ρ_d	Resistivity decrement due to presence of a defect
ρ_m	Mean resistivity of the metal within the capillary cell
ρ_e	Resistivity associated with conduction by negative carriers
ρ_p	Resistivity associated with conduction by positive carriers
σ	Conductivity of a pure material
τ_e, τ	Mean free collision time for electrons with a material
τ_i	Mean free time for collisions of electrons with component i
τ_A	An averaged mean free collision time defined in Equation (47)
τ_{ni}	The reciprocal of the viscosity of a metal for component i
τ_n	The reciprocal of the viscosity of a metal
τ_d	Mean free time for collisions of electrons with defects.

ABSTRACT

Recent theories on the electrolysis of metals, referred to as electrotransport, are reviewed. A literature survey presents recent experimental data on self transport in pure solid metals, electrotransport in solid metals containing interstitial solutes and solid solution solutes, electrotransport in solid semiconductors and liquid metals, and the Haeffner effect. Two experimental techniques are developed for measuring the electric mobility in liquid metal alloys at elevated temperatures. With the first technique the mobility is measured in dilute solutions of two binary systems and four ternary systems using bismuth as the solvent. The mobility is measured as a function of composition and temperature in the Bi-Sn system with the second technique. The precision of the second technique is quite good, giving a deviation of 1% at the 95% confidence level on a Student t distribution, for the average mobility of 8 measurements. A simple phenomenological description is presented and the data on Bi-Sn are thereby converted to the effective valence, or charge, employing literature data for the mutual diffusion coefficient. Analysis of the data indicates the true charge of Sn in Bi to be +1.8 at 500°C. The data agree fairly well with the recent work of Belashchenko.

INTRODUCTION

When an electric field is applied to a metal, a relatively large current is produced due to the ease with which electrons move among the ions within the metal. The electric field also produces a force on the ions which might cause them to migrate and thus carry a certain fraction of the total current. Such a migration of metallic ions does occur under certain conditions, but is only a very small fraction of the total current. The process of the migration of metal ions under an electric field will be referred to hereafter as electrotransport.

The oldest known observation of electrotransport in metals is attributed to Gerardin.[1] In 1861 Gerardin noticed that after electrolysis in the molten state a lead-tin alloy became soft at one end and brittle at the other, and that a sodium mercury alloy would only decompose water at one end. As one might expect, electrotransport in solid metals occurs at a much slower rate than in liquid metals. Consequently, for a number of years it was thought that the effect did not occur in solid metals. However, in the early 1930's a number of investigators experimentally demonstrated electrotransport in solid metals by using sufficiently high current densities and temperatures. General reviews of electrotransport in liquid and solid metals have been published by Schwarz,[2] Jost[3] and Seith.[4] The first chapters of this report present a review of the more recent experimental and theoretical work on electrotransport in solid metals, semiconductors, and liquid metals.

The original motivation for the work of this thesis was prompted by a very practical problem. At the time, there was considerable interest in a liquid metal fuel reactor using liquid bismuth as a carrier for uranium fuel. Some of the fission products were found to be quite difficult to remove by the usual techniques. It was felt that electrotransport might prove to be a practical method of separation. If the fission products and the uranium migrated in opposite directions, or with sufficiently different velocities, it would be possible to perform the separation within the reactor, and the heat generation could conceivably be utilized. Examination of electrotransport data on 39 liquid metal alloy systems revealed that in all but two of the systems the heavy component migrated to the anode. Since uranium is heavier than its fission product, it was therefore expected that it would migrate to the cathode relative to its fission products, thus providing the necessary requirement for a successful separation.

The process of electrotransport may be described by the mobility of the individual ions measured with respect to a specified reference velocity, or alternately by the transference number. Such parameters have only been reported quantitatively for liquid metals in dilute mercury amalgams around room temperature. It was the object of this investigation, to devise a technique for experimentally determining the differential mobility in liquid metal systems as a function of temperature and composition; and to compare the results with the current theories.

The terms anode and cathode are frequently encountered in this report. To avoid any possibility of confusion here, the following definition of these terms is presented. The anode is the electrode toward which

normal negative electrons migrate within the cell under the influence of an electric field; the cathode, of course, is the opposite electrode.

CHAPTER I

ELECTROTRANSPORT IN METALS

The theoretical treatment of electrotransport in metals is complicated by the presence of the conducting electrons. In a current carrying metal the conducting electrons possess a considerable momentum which they continually transfer to the metal ions. Consequently, in addition to the electric field force exerted upon the metal ions, there is a drag force resulting from the ion-electron collisions. If all of the atoms of a metal are considered to be positively charged due to the loss of electrons to the "electron gas," the resultant force produced by an electric field on a metal alloy may be expressed as

$$F = \sum_i n_i e Z_i E - n_e e E \ , \tag{1}$$

where the electron valence is taken as -1. Since there is no net charge within the metal this force must necessarily be zero.

If we designate the frictional force of the electrons upon component i as F_{ei}, and assume that it is proportional to the electric field, we may write,

$$F_{ei} = \delta_{ei} E \ , \tag{2}$$

where δ_{ei} is a friction coefficient. Since the conducting electrons move through the lattice with a steady state velocity, we may write,

$$n_e e E = \sum_i n_i \delta_{ei} E \ . \tag{3}$$

By combining Equation (3) with Equation (1) where F is zero we have

$$\sum_i n_i eE \left[Z_i - \frac{\delta_{ei}}{e}\right] = 0. \tag{4}$$

The net force on component i of charge Z_i must be

$$F_i = eE \left[Z_i - \frac{\delta_{ei}}{e}\right] . \tag{5}$$

When an external force is applied to an ion within an alloy of uniform composition the ion will move with a terminal velocity. The magnitude of this velocity for a given force is determined by the frictional drag force of the lattice. The absolute mobility is defined as the terminal velocity per unit of force and it is supposedly independent of the nature of the external force. In his theory of the Brownian motion Einstein[5] has shown that the absolute mobility is related to the diffusion coefficient of the moving ion by the relation

$$B_i = \frac{D_i}{kT} . \tag{6}$$

It was first pointed out by Herring[6] that this equation must be modified when it is applied to crystalline solids because the diffusion jumps are not completely random. The modified Einstein equation is usually written as

$$B_i = \frac{D_i}{fkT} , \tag{7}$$

where f is a correlation coefficient. Calculation of f for various lattice structures has been discussed by a number of authors.[7,8,9] Based on a model that requires an activation energy to produce a diffusion jump, Frenkel[10] has shown that Einstein's relation holds for the

movement of an ion as long as the external force is $\ll \frac{2kT}{\delta}$ where δ is the jump distance. If the electric field, E, were the only force acting upon an ion then Equation (7) would hold for $E \ll 10^6$ volt/cm. Although Frenkel's model probably holds for solids it is debatable whether it applies for liquids.(11)

Using Equation (5) and the absolute mobility, the velocity of an ion undergoing electrotransport may be expressed as follows,

$$v_i = B_i F_i = B_i e E \left[Z_i - \frac{\delta_{ei}}{e}\right] . \qquad (8)$$

A mobility, u_i is now defined as the velocity per unit electric field, v_i/E, where u_i may be related to B_i as follows,

$$u_i = B_i e \left[Z_i - \frac{\delta_{ei}}{e}\right] . \qquad (9)$$

In order to avoid confusion between these two mobilities, the mobility u_i will be called the electric mobility since it is connected with a force specifically electric. Applying Equation (7) then, we have for the electric mobility

$$u_i = \frac{D_i}{fkT} e \left[Z_i - \frac{\delta_{ei}}{e}\right] . \qquad (10)$$

Equation (1) illustrates why the presence of the conducting electrons complicates the interpretation of electric mobility data. Since u_i and D_i are the only quantities that may be obtained from transport type experiments, it is not possible to directly determine the individual terms within the brackets. Consequently, the true charge on a component, Z_i, can only be obtained if the frictional coefficient δ_{ei} can be determined independently, or vice versa. The bracketed term

in Equation (10) is generally referred to as the effective valence, Z_i^o, so that we may write

$$u_i = \frac{D_i}{fkT} e Z_i^o , \tag{11}$$

where Z_i^o has the form

$$Z_i^o = [Z_i - \frac{\delta_{ei}}{e}] . \tag{12}$$

Consequently Equation (5) can be written in the following simple form,

$$F_i = e E Z_i^o . \tag{13}$$

The direction of transport of component i in an electrotransfer experiment will be predicted by the sign of Z_i^o in solid metals and dilute metallic alloys. A negative sign indicates that electron friction forces predominate and transport occurs toward the anode. A positive effective charge means that the field force is greater than the friction force and transport is toward the cathode. The theoretical treatments which will be discussed are concerned with developing an expression for δ_{ei} which would then allow the determination of Z_i from experimental measurements.

Many investigators have presented data on electrotransfer experiments in terms of a transport number rather than a mobility. The transport number, t_i, is usually defined as the g-ions of component i transported per Faraday of charge. The flux of component i in terms of t_i can then be expressed as $t_i \cdot j_i/F$, where j_i is the current density in amps/cm^2. Equating this expression to $N_i U_i E$, the relationship between transference number and electric mobility is obtained,

$$t_i = \frac{u_i N_i F}{\sigma_i} . \tag{14}$$

CHAPTER II

DISCUSSION OF RECENT THEORIES

Theoretical treatments of electrotransport in metals have met with very little success in explaining experimental data. Two early investigators, Skaupy[12] and Lewis,[13] have proposed qualitative theories which are complete in that they consider both the field force and the electron friction force. Subsequent theories were developed in an attempt to quantitatively explain the data on electrotransport. However, these theories neglected to account for the frictional electron force, apparently because of its complexity. Wagner[14] presented a theory which he claimed to be only an approximation because of the neglect of the frictional force. He also worked on a more complete theory which was never published, (see Mangelsdorf[15] footnote 9, and Huntington[16] footnote 4). Schwarz[17] also developed a theory in which the effect of the electron friction was not treated directly. Although Schwarz claimed good experimental agreement, the theoretical justification of his treatment appears somewhat dubious. A more detailed discussion of these treatments is presented by Angus,[18] Mangelsdorf,[15] and Schwarz.[2]

In the last decade a number of new theoretical attempts have been made in an effort to quantitatively describe electrotransport in metals. These theories may be classified under two categories. In the first category the problem is treated from a phenomenological approach employing the methods of irreversible thermodynamics. In the second category the problem is approached on the atomic scale where the momentum exchange of the electron-atom interaction is examined in detail.

V. B. Fiks[19]

Fiks has presented a theoretical treatment of electrotransfer in metals which is used by all of the recent Soviet investigators. In this treatment an expression is derived for the force exerted by the electrons upon a metal ion as a function of the ion scattering cross section for electrons. A brief account can be given as follows. In each collision the electrons are assumed to lose only that portion of their momentum which they have acquired since their last collision, $\Delta P = eE\tau$, where τ is the electron mean free time and may be related to the mean free path and average electron velocity as, $\tau = \ell/v_e$. The number of collisions per second is equal to the electron flux, $n_e v_e$, times the atomic scattering cross section, A_i. Consequently, the force of the electrons on an ion may be expressed as follows,

$$F_{ei} = -eE\ell n_e A_i \ . \qquad (15)$$

A rather detailed mathematical development is presented which derives this expression more rigorously from a quantum mechanical approach.

It was pointed out by Mott,[20] that the resistance due to a small portion of foreign atoms in solid solution could be expressed under cetain restrictions as follows, $\Delta P_i = (mv_e X_i A_i / n_e e^2 \bar{v}_o)$. Using this expression and assuming that the free electron to atom ratio is exactly one, Fiks relates the electron drag force to the residual resistance by the following equation,

$$F_{ei} = -eE \frac{1}{X_i} \frac{\Delta\rho_i}{\rho_o} \ . \qquad (16)$$

The force calculated by this equation is said to be too large. This is attributed to the fact that the $\Delta \rho_i$ results not only from the foreign ion but also from all other distorted ions produced by its presence.

Following the ideas of Frenkel presented earlier, it is assumed that migration occurs through the movement of activated atoms and that these activated atoms have a different scattering cross section, A_i^*, and a different charge, Z_i^*. The total force on an activated ion is expressed as,

$$F_i = eE \left[Z_i^* - n_e \ell A_i^* \right] . \tag{17}$$

Fiks then assumes that the net force on the average unactivated ion is zero so that

$$\bar{Z} = n_e \ell \bar{A} . \tag{18}$$

Equation (17) then reduces to the following form,

$$F_i = eE \left[Z_i^* - \bar{Z} \frac{A_i^*}{\bar{A}} \right] . \tag{19}$$

The sign of the electric mobility is determined by the relation

$$Z_i^* \bar{A} \gtrless \bar{Z} A_i^* \tag{20}$$

In Klemm's treatment of this problem from the approach of irreversible thermodynamics, the concept of activated and non-activated atoms was also employed. Fiks shows that the criterion for the sign of the electric mobility expressed in Equation 20 is exactly analogous to the criterion that Klemm obtained.

Hall measurements in some metals have shown that a portion of the charge carriers have a positive sign. Glinchuk[21] has pointed out that momentum transfer from positive charge carriers would be opposite to the electron momentum transfer and consequently he has modified Fiks theory accordingly. Including this modification Equation (15) becomes

$$F_{ei} = eE\,(\ell_p n_p A_p - \ell_e n_e A_e). \tag{21}$$

The pertinence of the work of Barnett[22] to this problem was first pointed out by Klemm.[23] Barnett's experiments indicate that electrons in a metal which has a positive Hall coefficient show a negative e/m ratio when accelerated with respect to the lattice. Glinchuk's formulation would then appear incorrect. There appears to be considerable experimental work, however, in support of cathode-directed momentum transfer between defect electrons and the ions which move in the metal. This will be discussed in Chapter III.

S. E. Bresler and G. E. Pikus[24]

In this treatment the electron friction force in a pure metal is determined in a relatively simple manner. The total electron momentum per unit volume is expressed as, $m_e n_e \bar{v}_e = -m_e j/e$. The electron-ion interaction force is then determined from the rate of change of this momentum expression as follows,

$$F_{ei} = -\frac{m_e}{n_{ie}}\frac{d_j}{d\theta} = -\frac{m_e j}{n_{ie}\tau} = -\frac{m_e \sigma E}{n_{ie}\tau}. \tag{22}$$

A "modified classical" formula, $n_e e^2 \tau / m_e^*$, is then substituted for the electrical conductivity and the electron to atom ration, n_e/n_i, is replaced by an average charge $\bar{Z}$ giving,

$$F_{ei} = - \bar{Z} e E \left(\frac{m}{m^*}\right)_e . \tag{23}$$

The effective mass, m_e^*, of the electrons is used to account for the polarization of the electron cloud by the lattice potential.

It is assumed that the total force acting on an ion of pure metal is zero, so that the field force is given by Equation (23) with a plus sign.

$$F_{fi} = -F_{ei} = \bar{Z} e E \left(\frac{m}{m^*}\right)_e . \tag{24}$$

The electron drag force on component i in an alloy is assumed to be directly proportional to the contribution of component i to the total resistivity. This electron drag force is then expressed by writing Equation (23) in terms of resistivity

$$F_{ei} = -Ze \left(\frac{m}{m^*}\right)_e \rho_i j = -Ze \left(\frac{m}{m^*}\right)_e \frac{\rho_i}{\rho_o} E . \tag{25}$$

The field force on component i in an alloy is assumed equal to the field force on pure component i as expressed by Equation (24). The net force per atom on an ion of component i in an alloy then becomes,

$$\begin{aligned} F_i &= \bar{Z} e \left(\frac{m}{m^*}\right)_e \left[E - \frac{\rho_i}{\rho_o} E\right] \\ &= \bar{Z} e E \left(\frac{m}{m^*}\right)_e \left[\frac{\Delta \rho_i}{\rho_o}\right] . \end{aligned} \tag{26}$$

The assumptions in this derivation seem quite broad. Recent experiments done on self transport in solid metals show that the net

force on the average atom in a pure metal cannot be zero. Consequently, the assumption of zero net force only seems valid if it is applied to unactivated atoms, as was done by Fiks, since these atoms are defined as being stationary. The field force assumed in Equation (24) is only an approximation. Also, the derivation of Equation (23) forces the drag force to always equal the field force in the case of free electrons.

H. B. Huntington and A. R. Grone[16]

In this treatment it is assumed that the electrons are only scattered by the defects. It is also assumed that the defects are decoupled from the lattice. These assumptions are said to be rather arbitrary restrictions which result in scattering without the annihilation or creation of phonons. The rate of momentum transfer between the electrons and defects is then calculated from a quantum mechanical approach in which the electron momentum is expressed as m_e times the group velocity of the Block wave. The common assumption of a mean free time independent of the wave number is made and F_{ed} is found to be,

$$F_{ed} = - \frac{m_e j}{n_d e \tau_d} \quad . \tag{27}$$

This is analogous to the expression found by Bresler and Pikus [Equation (22)] in a less rigorous manner.

Rough calculations are presented which indicate that the collision rate is high enough to assume that the average force from the scattering process can be approximated as continuous. The mean free time for electron-defect collisions is then related to the resistivity contribution of the defects as $\Delta \rho_d = |m_e^*| / n_e e^2 \tau_d$, and n_e is replaced

by $\bar{Z}n_o$, where o designates the matrix atoms, to give for F_{ed},

$$F_{ed} = - \frac{m_e j}{n_d} \cdot \frac{\Delta\rho_d(\bar{Z} \cdot n_o)e}{|m_e^*|} = - e\bar{E}\bar{Z} \left(\frac{\Delta\rho_d \cdot n_o}{\rho_o \cdot n_d}\right) \frac{m_e}{|m_e^*|} . \qquad (28)$$

This result indicates that the friction force is proportional to the ratio of the resistivity of a defect site to the resistivity of a lattice site. It is also proportional to the ratio of the electron mass to the absolute value of the effective mass.

The above result indicates that even when the electrons act as holes (negative mass) they still transfer momentum to the anode. This agrees with the work of Barnett mentioned earlier. Barnett's work has been extended to a number of other positive Hall coefficient metals by Ginzburg.[25] Electrotransfer experiments in metals containing both n and p type conduction mechanisms as measured by a Hall coefficient will be discussed in Chapter III.

An analysis is presented which modifies the Einstein equation [Equation (6)] for a particle whose charge varies with position. It is assumed that the activated ion has a different charge than the unactivated ion. The force on the moving ion is arbitrarily expressed as a periodic function with a wave length corresponding to the jump length. For the function chosen, it is shown that the Einstein equation is modified by a constant factor of 1/2 when it is applied to the net flow of atoms due to electron friction. The final form for the mobility of self transport in pure metals then becomes,

$$u_i = \frac{\alpha D_i}{fkT} e\bar{E}\bar{Z} \left[1 - 1/2 \left(\frac{\Delta\rho_d \cdot n_o}{\rho_o \cdot n_d}\right) \frac{m_e}{|m_e^*|}\right] . \qquad (29)$$

Comparison with Equations (11) and (13) gives the following expression for the net force on an ion,

$$F_i = eE\bar{Z}\alpha \left[1 - \frac{1}{2} \cdot \frac{\Delta\rho d}{\rho_o} \cdot \frac{n_o}{n_d} \frac{m_e}{|m_e^*|}\right] . \qquad (30)$$

Huntington and Grone[16,26] have presented experimental data to support their theoretical work. This data will be discussed in more detail in Chapter III. In their work the velocity of self transport is related to the velocity of marker indentations in the metal specimens. It is pointed out that this procedure is subject to two assumptions, (1) no void formation, and (2) no changein lateral dimensions. If either assumption is not met, the value of u_i will be reduced below the true value. The factor α is introduced to express this mathematically, and consequently must meet the restriction, $\alpha \leq 1$.

In an article which is to appear shortly, Huntington[27] has revised the above treatment slightly. The revised treatment uses the pseudo momentum rather than m_e times the Block wave group velocity as the electron mementum. The result is that the electron mass, m_e in the numerator of Equations (27) to (30) should be replaced by the effective electron mass, m_e^*. Hence, the revised theory predicts that the electron friction force does depend on the sign of the effective electron mass.

C. Bosvieux and J. Friedel[28]

In this treatment, which appeared very recently in the literature, the net force produced by an electric field on three different types of defects in a metal is determined. The defects considered are, intersititials, holes and substitutional defects. The calculations are

quantum mechanical in nature. A number of assumptions are made and the results are only claimed to be approximately quantitative.

For the case of interstitials the following expression is obtained for the net force exerted on the defect interstitial,

$$F_d = -eE\bar{Z}\frac{\Delta\rho_d \cdot n_o}{\rho_o \cdot n_d} \quad , \tag{31}$$

where the subscript o refers to the matrix or solvent atoms. It is seen that the result is essentially the same expression obtained by Huntington for the electron-defect friction force. The derivation indicates that when the carriers are electrons the net force is toward the anode, when they are positive holes it is toward the cathode. According to this derivation the interstitial defect does not feel any direct force from the electric field because of a screening effect from the charge carriers. A qualitative explanation of this effect is presented. When the carriers are electrons, the effect of the displaced Fermi surface is to slow the electron velocity on the anode side of the interstitial and increase their velocity on the cathode side. The electron density on the anode side is therefore increased, causing more screening and an increase of charge on the anode side which results in movement to the anode.

Equation (31) indicates that for a given charge carrier the direction of motion of an interstitial defect is not a function of the charge of the defect. This result would appear to be contradicted by the migration of carbon to the cathode in nickel,[78,81] since Hall measurements indicate the predominate charge carrier is negative. However, this analysis is not directly applicable to metals of the transition group because of mixed conductivity between 4-S electrons and 3-d holes.

The authors have pointed out that experiments on interstitial electrotransport in Cu, Ag, or Au would provide a good test of their theory.

The mechanism of self transport in metals is probably the movement of atoms into neighboring lattice holes, occurring in such a pattern as to produce a net transfer. The authors have calculated an expression for the effective force exerted upon an ion moving from a lattice point into a neighboring lattice hole. In this analysis an expression is determined for the force on the ion which is valid at the initial lattice point. The ion at the saddle point is assumed to act as an interstitial so that Equation (31) expresses the force exerted upon it at that position. The force as a function of ion position is then estimated by connecting the above two values by a sine function. The final result for the force on an ion moving into a lattice hole is,

$$F_i = -\frac{1}{2} eE\bar{Z} \left[\frac{\Delta\rho_d \cdot n_o}{\rho_o \cdot n_d} - \frac{4\pi\bar{Z}}{3\pi} (J_o(b) - 2J_2(b) - 1\right] , \qquad (32)$$

where $\Delta\rho_d n_o/\rho_o n_d$ is to be evaluated for a lattice atom at the saddle point, J_o and J_2 are Bessel functions, and b is the interatomic distance.

Another expression similar to this, which is based on the same model is presented for the substitutional case in dilute solutions. It is not clear to this author how the value of the resistivity of a lattice ion at the saddle point could be determined.

P. C. Mangelsdorf[15,29]

Mangelsdorf has developed a theory for electrotransport in dilute molten alloys from two slightly different analyses. The first

analysis[29] is more phenomenological and will be discussed here. In the second analysis[15] a sort of quasi-phenomenological development is made on two rather complex problems accompanying electrotransfer theory: the origin of possible electrical forces on an ion, and the volume of disturbed solvent produced by an isolated solute atom. The results of both analyses are essentially the same.

The frictional force between the electrons and metal ions is assumed to be proportional to the electron flux,

$$F_{ei} = -\delta_i n_e v_e, \tag{33}$$

where δ_i is an arbitrarily defined friction coefficient. The steady state force balance on the electrons is written as,

$$-en_eE + \sum_i n_i \delta_i n_e v_e = 0 . \tag{34}$$

The average velocity of the electrons, $\bar{v}_e$, is related to the conductivity through Ohm's law and the average charge per ion, $\bar{Z}$, is taken as the electron-atom ratio. Combining Equation (34) with Ohm's law, the electrical conductivity is expressed as,

$$\sigma = \frac{e^2\bar{Z}}{\bar{\delta}} . \tag{35}$$

The net force on an ion is written as,

$$F_i = Z_i eE - \delta_i n_e \bar{v}_e, \tag{36}$$

which, when combined with Equation (35) through Ohm's law, gives an expression analogous to Fiks' Equation (19),

$$F_i = eE \left[Z_i - \bar{Z} \frac{\delta_i}{\bar{\delta}}\right] . \tag{37}$$

Now by differentiating Equation (35) with respect to the mole fraction of solute, X_A, an expression is obtained for the conductivity decrement produced by the solute A. This expression is combined with Equation (37) to give for a dilute solution,

$$eE\bar{Z}\,\frac{1}{\sigma}\left(\frac{\partial\sigma}{\partial x_A}\right)_{dil} = \sum_i F_i \left(\frac{\partial n_i}{\partial n_A}\right)_{dil} . \qquad (38)$$

Physically, the quantity $(\partial n_i/\partial n_A)$ is taken to be the number of i type ions generated by addition of a solute atom A. Consequently, the right hand side of Equation (38) must be interpreted as the total force exerted on solute A due to the electric field, F_A. According to previous notation then, the net force exerted on an ion i in dilute solution is,

$$F_i = eE\bar{Z}\left(\frac{1}{\sigma}\frac{\partial\sigma}{\partial x_i}\right)_{dil} = -eE\bar{Z}\left(\frac{1}{\rho}\frac{\partial\rho}{\partial x_i}\right)_{dil} = -eE\bar{Z}\left[\frac{n_o}{\rho_o}\frac{\Delta\rho_i}{n_i}\right]_{dil} . \qquad (39)$$

This result indicates, as did a previous one, that the direction of motion is not a function of the charge of the solute atom. The author indicates that this result is independent of the nature of the charge carriers as long as the current mechanism is electronic.

In describing the electromigration of solute atoms in the liquid state, the author assumes that as the solute atoms migrate they have a tendency to drag along some of the solvent atoms in the near vicinity. Consequently, he envisions electromigration occurring through the movement of atom clusters. As an approximation he assumes the cluster to consist of the solute atom plus its nearest neighbors. Equation (38) may then be written as

$$F_A + N_n F_n = eE\bar{Z}\left[\frac{1}{\sigma}\frac{\partial\sigma}{\partial x_A}\right]_{dil} , \qquad (40)$$

where F_n is the average force on the nearest neighbors and N_n is the average number of nearest neighbors. Under this model the mobility is written as,

$$u_A = u_{AN} + u_N \ , \tag{41}$$

where u_{AN} is the mobility of the solute atom with respect to its nearest neighbors and u_N is the mobility of the neighbors with respect to the reference system. Obviously, such a distinction complicates the description of the solute velocity. However, for a strongly solvated solute atom u_{AN} will approach zero, so that the velocity of the solute can be described with a single mobility.

By expressing the total force on an ion as a function of the effective charge in accord with Equation (13), it is possible to write,

$$F_A + N_n F_n = eEZ_i^o = eE\bar{Z} \left(\frac{1}{\sigma} \frac{\partial \sigma}{\partial x_i}\right)_{dil} \ . \tag{42}$$

Hence, a plot of Z_i^o against $\left(\frac{1}{\sigma} \frac{\partial \sigma}{\partial x_i}\right)_{dil}$ for different solutes in the same solvent should produce a straight line with the slope being equal to the mean charge of the solvent ions, provided the solute is strongly solvated. The author has examined the electrotransfer of different solutes in mercury. Since the diffusion coefficients of the alkali metals are lower than those of other solutes, and since the alkali's have large positive heats of solution, he assumes strong solvation for alkali metals dissolved in mercury. The above plot for K, Na, and Li does give a straight line as predicted and the slope indicates an electron to atom ratio of 0.3. The data of Schulz[30] on optical absorbtivity and of

Cusack[31] and Tieche[32] on Hall coefficients seem to indicate fairly conclusively that the electron to atom ratio in pure mercury is around 2.0. Manglesdorf points out that this discrepancy may result from the assumption that the electrical force is only effective in producing relative motion between the bulk Hg ions and the solvated mercury ions.

Another discrepancy of the theory pointed out by the author is its failure to qualitatively predict the motion of Pb, Tl, and Bi in mercury. All of these elements increase the conductivity of Hg and therefore should migrate to the cathode. However, Pb and Tl do not migrate at all and Bi migrates to the anode. This difficulty is accounted for by assuming that the force on the solvated mercury atoms predominate in total so that the solute is actually pushed backwards to the anode.

This treatment points up some of the additional difficulties encountered when interpreting electrotransport experiments in liquid metals.

Manglesdorf[33] has published an article in which he considers the isotope separation in the Haeffner effect. Applying the formality of irreversible thermodynamics, he shows that there is a heat flux produced by the electric field at constant temperature. If the fluxes are thought to be linear functions of the forces, it is seen that this "isothermal flux" would give rise to a force which in turn would contribute to the isotope separation. From available data Mangelsdorf shows that this effect could be responsible in large part for the Haeffner effect.

P. G. de Gennes[34]

This theoretical treatment was developed in an effort to quantitatively describe the separation of isotopes in liquid metals through electrotransport. The author treats the normal lattice scattering through a viscosity coefficient rather than an absolute mobility or a self diffusion coefficient. The force on an ion due to lattice scattering is given as the product of a mean impulse, p_i, times the viscosity of the metal for isotope i, $1/\tau_{ni}$, which can be expressed in terms of mean velocity as,

$$F_i = \frac{p_i}{\tau_{ni}} = \frac{m_i \bar{v}_i}{\tau_{ni}} \quad . \tag{43}$$

A mean value for this viscosity is related to a mean value for the diffusion coefficient by the expression

$$\tau_n = C' \frac{MD}{kT} \quad , \tag{44}$$

where the constant $C' \approx 1$, and M is a mean value of the atomic masses.

A force balance is made for steady state electrotransport (zero concentration gradient) assuming $M_i \approx M$,

$$\bar{v}_i \left(\frac{kT}{D}\right) \frac{1}{C'} = ZeE - F_{ei} \quad , \tag{45}$$

where it was assumed that each isotope contributes the same number of electrons to the "electron gas."

In each collision the electron is assumed to lose only that portion of its momentum acquired since its last collision, $eE\tau_e$. The mean time between electron collisions upon species i is designated τ_i.

If the collisions of the electrons per unit time are equated to the electron collisions upon all the isotopes per unit time the following relation is obtained

$$\frac{Z}{\tau_e} = \frac{X_1}{\tau_1} + \frac{X_2}{\tau_2} , \tag{46}$$

where the metal has only two components, X is the mole fraction, and Z the free electron to atom ratio. The quantity $1/\tau_A$ is defined as an average of the collision rates weighted according to atomic fraction, so that

$$\frac{1}{\tau_A} = X_1 \left(\frac{1}{\tau_1}\right) + X_2 \left(\frac{1}{\tau_2}\right) = \frac{Z}{\tau_e} . \tag{47}$$

The electron-ion interaction force can now be expressed as,

$$F_{ei} = \frac{eE\tau_e}{\tau_i} = eEZ \frac{\tau_A}{\tau_i} . \tag{48}$$

Hence, the mean velocity of component i becomes,

$$\bar{v}_i = C' \left(\frac{D}{kT}\right) eEZ \left[\frac{\tau_i - \tau_A}{\tau_i}\right] . \tag{49}$$

It is recognized that only a difference in velocities is measured so that a differential velocity Δv is defined,

$$\Delta v = \bar{v}_1 - \bar{v}_2 = C' \left(\frac{D}{kT}\right) eEZ \left(\frac{\tau_1 - \tau_2}{\tau_A}\right) , \tag{50}$$

where it has been assumed that $\tau_A^2 = \tau_1\tau_2$.

The electron-ion interactions are analyzed in terms of the probability of transitions. The results of this fairly complicated mathematical analysis is expressed as follows,

$$\frac{\Delta\tau}{\tau} = \frac{1}{12} \frac{\Delta M}{M} \left(\frac{\Theta}{T}\right)^2 , \tag{51}$$

where Θ is the Debye temperature.

The final formula can be written in terms of the differential mobility as

$$U_{12} = \frac{\Delta v}{E} = \frac{C'}{12} \left(\frac{D}{kT}\right) eZ \left(\frac{\Theta}{T}\right)^2 \frac{\Delta M}{M} . \qquad (52)$$

The results predict that the lighter isotope will move to the anode in accord with experiments. This is explained physically as meaning that the lighter isotope has a larger vibration amplitude and hence feels more of the electron friction force. In comparing the quantitative predictions of his theory with the data available at the time, the author found numerical disagreement. This disagreement was attributed to the assumptions required in the development.

A. Klemm[35,38]

In a paper appearing in 1953[35] Klemm has presented a theoretical treatment of transport processes based on the thermodynamics of irreversible processes. Instead of writing the fluxes as a linear function of the forces as is more common, he has written the forces as linear functions of the fluxes. This treatment led to the following general expression,

$$F_i = \sum_k^N r_{ik} X_k (v_i - v_k), \quad r_{ik} = r_{ki} , \qquad (53)$$

for a system of N components, where r_{ik} is defined as a friction coefficient. Rencently, Laity[36] has pointed out that Klemm's result was implicitly contained in Onsager's[37] paper, and that the coefficients r_{ik} are a most suitable choice for describing transport phenomena. Contrary to Fick's diffusion coefficient and other such phenomenologically defined coefficients, the friction coefficients, r_{ik}, have a microscopic

interpretation. They are the proportionality constant between the velocity i relative to k and the force applied to i, with allowance for the fraction of i's environment that consists of k.

In a later paper Klemm[38] presented a theoretical development on the electrotransport of isotopes in liquid metals based on his earlier work.[35] In this treatment the electrotransport is considered to produce three fluxes, two isotope fluxes and the electron flux. From Equation (53) then, three equations result, one for each flux. In these equations the force is expressed as a product of the charge times the field gradient. The charge per atom is expressed as $\zeta_i Z_i$, where Z_i is the electrochemical valence, and ζ_i, a parameter specifying the degree of ionization. The valence of both isotopes is the same, Z, and the electron valence is taken as one. The three equations are combined to obtain the following expression,

$$\frac{v_{12}}{\bar{v}_{ie}} = \left[\left(\frac{\zeta_1 - \zeta_2}{\bar{\zeta}_i}\right) - \left(\frac{r_{1e} - r_{2e}}{\bar{r}_{ie}}\right)\right]/\left(1 - \frac{r_{12}}{Z\bar{r}_{ie}}\right) . \qquad (54)$$

In this expression $\bar{v}_{ie}$, $\bar{r}_{ie}$, $\bar{\zeta}_i$, are some kind of averages over the respective values of v_{ie}, r_{ie}, ζ_i, where i refers to the two isotopes. Hence the velocity $\bar{v}_{ie}$ is the same as that previously specified $\bar{v}_e$. Klemm does not state how these averages were taken. This author was unable to derive the above expression. However, if one assumes $\bar{v}_{ie} \approx v_{1e} \approx v_{2e}$ and averages r and ζ through the mole fractions, an expression similar to the one above is obtained except for the absence of the 1 in the denominator.

Klemm proceeds to make an estimate of each of the terms in the above expression. This analysis, which requires a number of assumptions

about the relative degree of ionization and relative friction forces, indicates that the above equation disagrees with experimental data by at least four orders of magnitude. On the basis of this disagreement Klemm postulates a different model for electrodiffusion. Each of the two isotopes is assumed to exist in two states, an activated and an unactivated state. The unactivated isotopes are assumed to be indistinguishable so that the metal is treated as a mixture of four components. The following expression results,

$$\frac{v_{12}}{\bar{v}_{ie}} = \left[\frac{(X_{1A} + X_{2A})\,\bar{v}_{Au}}{(X_1 + X_2)\,\bar{v}_{ie}}\right] \left(\frac{r_{2Au} - r_{1Au}}{\bar{r}_{Au}}\right) \Big/ \left(1 + \left(\frac{X_{1A} + X_{2A}}{X_{1u} + X_{2u}}\right) \frac{r_{1A2A}}{\bar{r}_{Au}}\right). \quad (55)$$

It can be seen that the bracketed term is related to the self transport number. Subscript A refers to activated ions and u to unactivated ions. Unfortunately, the expression is quite complex and contains terms difficult to determine experimentally. The justification of treating the liquid as a mixture of mobile and immobile ions is not conclusive. It rests upon the assumptions employed in showing Equation (54) to be inadequate.

By comparison with isotopic electrotransport experiments on solid and liquid molten iodides, Klemm has estimated the terms in parenthesis in Equation (55) to have a value of approximately 10^{-3}. From the experimental data of Haeffner[39] the self transport number of liquid mercury was then determined to be approximately 10^{-4}, directed toward the anode. This result predicts that the mobile atoms move toward the anode relative to the immobile atoms. This is in agreement with the majority of the data on self transport in solid which is discussed in Chapter III.

If a pure metal is thought to consist of mobile and immobile atoms or activated and unactivated atoms, then the analysis which led to Equation (54) may be applied and the result will be an expression for the self transport. By further assuming that r_{Ae} and r_{ue} are negligible relative to r_{Au}, Klemm has determined the following expression which is related to self transport,

$$\frac{v_{Au}}{\bar{v}_{ie}} = \frac{(\zeta_A r_{ue} - \zeta_u r_{Ae})X_e}{(X_A\zeta_A + X_u\zeta_u)r_{Au}} . \tag{56}$$

It can be shown that this same equation may be obtained directly from Equation (53) with only the following assumption, $\bar{v}_{ie} \approx v_{Ae} \approx v_{ue}$.

Equation (56) may be rearranged for a more direct comparison with the previous authors. The average velocity of the electrons may be related to the conductivity, $\bar{v}_{ie} = \sigma E/n_e e$. The friction coefficient may be related to the self diffusion coefficient as described by Laity,[36] $r_{Au} = RT/D$. The degree of ionization, ζ_i, may be converted to the effective valence, Z_i, because it appears in a ratio. If the immobile ions are assumed to be stationary, then the velocity of self transport becomes,

$$v_{Au} = v_A = \frac{\sigma E}{n_e e}\left(\frac{D}{RT}\right)\frac{(Z_A r_{ue} - Z_u r_{Ae})X_e}{(X_A Z_A + X_u Z_u)} . \tag{57}$$

If the effective valence of the electrons is taken as 1, it can be seen from a charge balance that $X_e = X_A Z_A + X_u Z_u$. Hence the equation becomes,

$$v_A = \frac{\sigma E}{F \cdot n_e}\left(\frac{D}{kT}\right) r_{ue}\left[Z_A - Z_u \frac{r_{Ae}}{r_{ue}}\right] . \tag{58}$$

Comparison with the uncorrelated Einstein equation then yields the following expression for the net force per ion,

$$F_i = eEK\left[Z_A - Z_u \frac{r_{Ae}}{r_{ue}}\right] = eEK\left[Z_i^* - \bar{Z}\ \frac{r_i^*}{\bar{r}}\right], \qquad (59)$$

where K is a constant equal to r_{ue}/Fn_e, and the notation has been changed to be consistent with previous results. This equation is also applicable to the electrotransport of interstitials where the interstitial is considered as the activated ion. A similarity of this result to Fiks' and Mangelsdorf's is apparent.

B. Baranowski[39-44]

Baranowski has applied the thermodynamics of irreversible processes to the problem of electrotransport in metals. In his treatment the fluxes are written as linear functions of the forces. The flow of electrons is treated as a separate flux so that for a binary system the flux equations are written as,

$$J_i = \sum_k^3 L_{ik}X_k, \quad (i = 1,2,3)(L_{ik} = L_{ki}), \qquad (60)$$

where L_{ik} are phenomenological coefficients and X_k are thermodynamic forces expressed as follows,

$$X_k = -\text{grad}\ \mu_i - Z_i F\ \text{grad}\ \phi\ . \qquad (61)$$

In this treatment on liquid metals Baranowski[40,42] applies the restriction of constant volume, $J_1\bar{V}_1 + J_2\bar{V}_2 = 0$. This produces the following relations,

$$\sum_{k=1}^{2} L_{ik}\bar{V}_k = 0. \qquad i = 1,2,3 \qquad (62)$$

A transport parameter is defined in the following manner for both components,

$$(J_3/J_1)_{X_3 = X_2 = 0} \equiv e_1^*, \quad (J_3/J_2)_{X_3 = X_1 = 0} \equiv e_2^* . \tag{63}$$

These parameters are a measure of the conduction electrons transferred per ion in the absence of an electric field. Analogous to the heat of transport, they might be termed the negative charge of transport. It is easily seen that they are related to the phenomenological coefficients as follows,

$$e_1^* = \frac{L_{31}}{L_{11}}, \quad e_2^* = \frac{L_{32}}{L_{22}} . \tag{64}$$

By combining Equations (60), (62) and (64), the following expression is obtained for J_1,

$$J_1 = L_{11} \left(X_1 - \frac{\bar{V}_1}{\bar{V}_2} X_2 + e_1^* X_3\right) . \tag{65}$$

Baranowski now assumes that the gradient of the chemical potential of the electrons is zero. He also limits himself to dilute solutions where $\text{grad}\ \mu_2 = 0$. For the steady state where $J_1 = 0$, he obtains,

$$\frac{d\ell n N_1}{dZ} = \frac{\left[\frac{\bar{V}_1}{\bar{V}_2} Z_2 - Z_1 + \frac{e_1^*}{e}\right] eE}{kT} , \tag{66}$$

where the activity coefficient has been assumed to be 1.

An expression for the electrotransport flux may be written as $N_1 u_1 E$. At steady state this electrotransport flux is exactly counterbalanced by the diffusion flux given by Fick's equation so that,

$$\frac{d\ell n N_1}{dZ} = \frac{u_1}{D_1} E . \tag{67}$$

If u_1 is now substituted from Equation (11), the following relation is obtained for the steady state distribution,

$$\frac{d\ell nN_1}{dZ} = \frac{eEZ_1^o}{fkT} . \tag{68}$$

By comparison to Equations (66) and (13), it can be seen that Baranowski's treatment gives the following expression for the force on an ion,

$$F_1 = eE \left[\frac{\bar{V}_1}{\bar{V}_2} Z_2 - Z_1 + \frac{e_1^*}{e}\right] , \tag{69}$$

where the term in brackets is the effective valence.

It can be demonstrated that Baranowski did not need to specify a dilute solution. If the same analysis is carried through employing the Gibbs-Duhem equation, the result is the same as Equation (66), with the following term as a coefficient of kT in the denominator,

$[1 + X_1\bar{V}_1/X_2\bar{V}_2]$.

Baranowski[43] has presented a slightly different treatment of this problem for solid state electrotransport where the constant volume restriction does not apply. The following assumptions are needed. (1) The cross effect between components 1 and 2 is zero so that, $L_{12} = L_{21} = 0$. (2) The gradient of the chemical potential of the electrons is zero. (3) The contribution to the electron flux from the transport of metal ions is negligible, so that L_{33} may be directly related to the electrical conductivity by Ohm's law. The transport number is then expressed as follows,

$$t_1 = \frac{L_{11}Fe}{\sigma} \left[Z_1 - \frac{e_1^*}{e} F\right] . \tag{70}$$

If Fick's diffusion equation is expressed as $J_i = -D_i \text{ grad } C_i$, the phenomenological coefficient L_{11} may be related to the diffusion coefficient. Using this relation and Equation (14) the following expression is obtained for the mobility from Equation (70).

$$u_1 = \frac{d\ell nX_1}{d\ell na_1} \frac{D_1}{kT} e \left[Z_1 - \frac{e_1^*}{e}\right] , \tag{71}$$

where a_1 is the activity coefficient. From Equations (11) and (13) then, the net force per ion is,

$$F_i = eE \left[\frac{d\ell nX_i}{d\ell na_i} \left(Z_i - \frac{e_i^*}{e}\right)\right] . \tag{72}$$

These results indicate that the transference parameter e_i^* characterizes the electron-ion interaction force. This seems logical, since the electron-ion interaction is characterized by L_{13}, which is directly related to e_i^*. The interpretation of e_i^* from Equation (63) would seem to indicate that there is a direct connection between the number of conduction electrons transported per ion in the absence of a field and the electron friction produced by a field.

D. K. Belashchenko[45,46]

The Russian investigator Belashchenko has treated the problem of electrotransport using irreversible thermodynamics. His treatment parallels quite closely the general approach discussed by Denbigh.[47] It is difficult to understand the significance of the interpretation Belashchenko gives to his results.

A long thermodynamic argument is presented which justified writing the general flux equation as the difference of the electric

diffusion flux and the ordinary diffusion flux,

$$J_1 = N_1 u_1 E - D_1 \frac{dN_1}{dZ} . \tag{73}$$

The effective valence of a metal ion is defined by the following relation,

$$u_i = \frac{d\ell nN_i}{d\ell na_i} \frac{D_i}{kT} eZ_i^o . \tag{74}$$

The flux J_1 is set to zero for steady state conditions and the following relation is obtained,

$$\frac{d\ell na_i}{dZ} = \frac{eEZ_i^o}{kT} . \tag{75}$$

This equation is also derived using Thomson's method.

Belashchenko compares his result to Baranowski's, Equation (66), and claims that Baranowski's results are wrong in the general sense. It is interesting to note, that it is possible to reduce Equation (75) to Equation (66) without using any equations other than those appearing in Belashchenko's[45] article except those necessary to take into account the difference between activity and concentration. In a recent article[44] Baranowski has commented that Belashchenko's interpretation of his equation is incorrect. These authors have formally exchanged views on their articles in a recent publication[48,49] which this author has not yet been able to obtain.

S. I. Drakin[50]

Applying classical thermodynamics to electrotransport, Drakin has derived the following expression for dilute solutions,

$$\frac{d\ell nN_1}{dZ} = \frac{[Z_2 - Z_1]\, eE}{kT} \tag{76}$$

It was pointed out by Baranowski,[51] that the application of classical thermodynamics did not have any theoretical justification since the electrotransfer process is highly irreversible. By comparison with Equation (66) Baranowski[40] has shown that Drakin's assumptions are only justified in the case of zero electron friction force and equal partial molal volumes. A good discussion of Drakin's theory has been presented by Angus.[18]

Other Work

Gurov[52] has recently published an article in which he attempts to extend Fiks' treatment to quantities more directly measurable by experiment. He presents a rather detailed analysis of the ion movement based on a quasi-static hole distribution in the metal. Using Mott's formula [see Equation (87)] he has developed an expression for the excess charge of a migrating ion in a dilute solution which is a function of the Fermi energy.

Summary of Theories

The results of the different theoretical developments have been summarized in Table I. The expression giving the net force per ion resulting from the electric field is listed. The effective charge is simply the coefficient of eE in each expression.

The electron-ion friction coefficients defined by Mangelsdorf, δ_i, and Klemm, r_i, and the scattering cross section of Fiks, A_i are all interrelated. The relationship between them is presented in Appendix A, Equations (A-12), (A-18), and (A-19). It can be seen, that the ratio

of an individual coefficient to its average value will be the same for all three coefficients. Hence Mangelsdorf's expression,

$$F_i = eE \left[Z_i - \bar{Z} \frac{\delta_i}{\bar{\delta}}\right] , \tag{37}$$

reduces exactly to Fiks' Equation (19) in the case where transport occurs by the movement of activated ions. It also reduces to Klemm's Equation (59) divided by the constant K, in the case of activated transport. The three treatments appear to be quite consistent, with Mangelsdorf's being slightly more general.

By combining Equation (36) with Ohm's Law, Mangelsdorf's treatment gives,

$$F_i = eE \left[Z_i - \frac{\delta_i}{e^2 \rho}\right] . \tag{77}$$

This equation is interesting because it predicts that, if the electron-ion friction coefficient is independent of temperature, the electron-ion friction forces will vary with temperature in a known manner, as $1/\rho$. Since such an assumption is quite likely, it can be seen that an analysis of mobility versus temperature data based on this model would allow a determination of the true charge, Z_i.

In Huntington's development an expression is obtained for the electron-ion interaction force, Equation (28), which Bosvieux also obtained by a more sophisticated treatment for the case of electron-interstitial interaction force. If the defect in Huntington's treatment is treated as an interstitial rather than a marker indentation, the following equation is obtained for net force per interstitial,

$$F_i = eE \alpha \left[Z_i - \frac{1}{2} \bar{Z} \left(\frac{\Delta\rho_d \cdot n_o}{\rho_o \quad n_d}\right) \frac{m_e}{|m_e^*|}\right] . \tag{78}$$

In his treatment Huntington has assumed that the resistivity due to a defect of some sort in the lattice could be written as $\Delta\rho_d = m_e^*/n_e e^2 \tau_i$, where τ_i is the mean free time between electron-defect collisions. In Appendix A it is shown that under the same assumption for the resistivity decrement due to a foreign ion, the development of Fiks gives the following equation,

$$F_i = eE \left[Z_i - \bar{Z} \left(\frac{\Delta\rho_i \cdot n_o}{\rho_o \cdot n_i}\right)\right] . \qquad (79)$$

In Appendix A it is shown that the same assumption applied to Mangelsdorf's Equation (37) gives the very same expression. From the relationship of Klemm's treatment to Mangelsdorf's, previously discussed, it is easily shown that Klemm's Equation (59) reduces to the above equation times the constant K. The result of these three theories then, represented by Equation (79), is essentially the same as Huntington's Equation (78) for the case of interstitial transport. All four treatments appear quite consistent.

It is interesting that both Bosvieux's theory for interstitial transport and Mangelsdorf's results for infinitely dilute solutions lead to the following expression for the net force per interstitial,

$$F_d = -eE\bar{Z} \left(\frac{\Delta\rho_d \cdot n_o}{\rho_o \cdot n_d}\right) . \qquad (31)$$

Hence both treatments, along with that of Pikus, indicate that the transport of an interstitial should be unaffected by its charge. This conflict with the above theories could be resolved experimentally.

It may be concluded, that a rigorous treatment of electrotransport in metals is extremely difficult due to the complexity of the electron-ion interaction and the difficulty of describing a specific charge to a metal atom in a lattice.

TABLE I

SUMMARY OF THEORETICAL TREATMENTS

Author	Net Force per Ion	Eq. No.	Comments
Fiks	$eE\left[Z_i^* - \bar{Z}\frac{A_i^*}{\bar{A}}\right]$	19	Activated ion model
Pikus	$eE\left[\bar{Z}\left(\frac{m}{m^*}\right)_e \frac{\Delta\rho_i}{\rho_o}\right]$	26	Field force on i assumed equal to field force on pure ion
Huntington	$eE\bar{Z}\alpha\left[1 - \frac{1}{2}\left(\frac{\Delta\rho_d \cdot n_o}{\rho_o \cdot n_d}\right)\frac{m_e^*}{\lvert m_e^*\rvert}\right]$	30	Self transport Lattice model
Bosvieux	$-eE\left[\bar{Z}\left(\frac{\Delta\rho_d \cdot n_o}{\rho_o \cdot n_d}\right)\right]$	31	Interstitial defect Lattice model
	$eE\bar{Z}\left[\frac{2\tau\bar{Z}}{3\pi}\left(J_o(b) - 2J_2(b) + 1 - \frac{1}{2}\left(\frac{\Delta\rho_d \cdot n_o}{\rho_o \cdot n_d}\right)\right)\right]$	32	Self transport Lattice model
Mangelsdorf	$eE\left[Z_i - \bar{Z}\frac{\delta_i}{\bar{\delta}}\right]$	37	General
	$-eE\left[\bar{Z}\left(\frac{\Delta\rho_i \cdot n_o}{\rho_o \cdot n_i}\right)\right]$	39	Infinitely dilute solution
deGennes	$eEZC\left[\frac{\tau_i - \tau_A}{\tau_i}\right]$	49	Isotope transference
Klemm	$eEK\left[Z_i - \bar{Z}\frac{r_i^*}{\bar{r}}\right]$	59	Self transference or interstitial defect
Baranowski	$eE\left[\frac{\bar{V}_1}{\bar{V}_2}Z_2 - Z_1 + \frac{e_1^*}{e}\right]$	69	Dilute solution, constant volume
	$eE\frac{d\ell nX_1}{d\ell na_1}\left[Z_1 - \frac{e_1^*}{e}\right]$	72	Negligible interaction between component fluxes, $L_{12} = L_{21}$

CHAPTER III

REVIEW OF RECENT EXPERIMENTAL WORK

An increased interest in electrotransport has developed in recent years. In liquid metals, this interest was initiated by the work of Haeffner in 1953, illustrating the effectiveness of electrotransport as a means of separating isotopes and in solid metals by the work of Seith and Wever in 1953, presenting a method of determining absolute migration rates. Wever's work in 1956 on self transport in solid copper appears to have initiated the recent interest in this area. The number of studies of electrotransport in semiconductors has also been increasing. A good review of much of this work was given by Heumann[53] in 1958. Since that time a large volume of work by Soviet workers has appeared in the literature. The following is a review emphasizing the more recent work since Heumann's article. The method used by the authors in presenting their data is reviewed with a fair degree of detail to allow comparison to the theoretical developments discussed in Chapter II.

Self Transport in Solid Metals

The first quantitative measurements of self electrotransport in solid metals were made by Wever[54] in 1956 on solid copper. The mass transport of the copper caused a separation of uniformly spaced microhardness impressions on the cold end of the specimen where the moving ions came to rest and a shortening between impressions on the cold end from which they came. In the past few years this work has been followed up by a number of investigations on self electrotransport in solid metals.

Work of Wever--Wever has investigated self transport in the pure metals Ni, Fe,[55] and Cu.[54] In reporting his data he has used

the following expression for the transference number,

$$t = \frac{D^*}{fkT} FN\rho\, e(Z + z). \tag{80}$$

According to Equation (14), the transference number is simply equal to the electric mobility times the product $F \cdot N \cdot \rho$, for a pure metal. From Equation (11) then, the transference number for a pure metal would be,

$$t = \frac{D^*}{fkT} FN\rho\, eZ^o \ . \tag{81}$$

Hence it can be seen that the quantity which Wever reports as $(Z + z)$ is equal to the effective valence Z^o, defined by Equation (13). Rearrangement of Equation (13) gives,

$$Z_i^o = \frac{F_i}{eE} \ . \tag{82}$$

Consequently, it is apparent that the effective valence is the ratio of the actual force exerted on the ion to the field force exerted on an ion having a true valence of +1. A negative effective valence means movement toward the anode. In such cases the friction force of the ion-electron interaction is directed toward the anode and is larger than the field force, which must always be directed to the anode for positive metal ions. A positive effective valence means movement toward the cathode.

If one postulates that in some metals the momentum transfer between the current carriers and the activated ions may be directed toward the cathode, then a positive effective valence can mean one of two things. Either the electron-ion friction force is directed toward the anode and the field force exceeds the friction force, or both forces are directed toward the cathode.

TABLE II

RESULTS OF WEVER ON SELF TRANSPORT

Metal	Temp T (°C)	Tr. No. t g-ion/F x 10^9	Eff. Valence Z^*(1)	Ref
Cu	900	-3	-14	54
	1000	+3	+12	
Ni	1190	-6	-5	55
	1255	-6	-2.1	
	1300	-10	-1.8	
	1385	-23	-1.5	
Fe	1190	+35	+43	55
	1300	+53	+12	
	1325	+65	+9	

(1) Negative sign means anode-directed migration

The results of Wever's work are presented in Table II. A very interesting result was found for copper. Between 900°C and 1000°C the direction of migration reverses from anode to cathode. This is attributed to a relative decrease in the electron-ion friction force with increasing temperature. It is pointed out that Huntington's theory predicts a temperature variation in accord with $1/\rho$ for the friction force. Hence, the reversal is qualitatively explained.

In his analysis of this data, Wever assumes that the defect electrons of a p-conducting metal transfer momentum in the cathode direction. Consequently, for Ni, which is predominantly n-conducting, the friction force appears to be slightly larger than the field force. For iron, which is predominantly p-conducting, both forces act toward the cathode, and hence the effective valence is considerably larger. The data

on iron at 1190°C indicate that the net force per ion is 40 times larger than the field force on an ion having a true valence of +1. Wever has pointed out that due to the screening effects of the electrons the valence of the metal ions would probably not be greater than +1. Even if the ion had a true valence of +4, the net force would still be 10 times larger than the field force. Hence, if the data is correct, it appears that the iron atoms are receiving a considerable, cathode directed force other than the field force.

In another paper, Wever and Seith[56] have discussed the problem of cathode-directed momentum transfer from defect electrons. As mentioned earlier, it is known from the work of Barnett[22] that the overall electron momentum transfer must be anode-directed even in p-conductors. Consequently, they have postulated that the defect electrons of the p-conducting metal interact preferentially with the activated ions. Such preferential interaction could allow a net movement toward the cathode while still maintaining the overall electron momentum transfer in the anode direction.

Work of Huntington and Grone--These authors have studied self-electrotransport in Au[16] and Cu[57] by measuring the movement of marker indentations. The data is reported as a plot of v/j as a function of the reciprocal of the absolute temperature. If Equation (11) is rearranged it may be written for pure metals as,

$$\frac{v}{j} = \alpha \frac{D^*}{fk} \frac{\rho}{T} eZ^\circ , \qquad (83)$$

where α is a factor introduced by these authors to account for void formation or lateral dimension change. For gold, α is taken as 1/3, for copper, $\alpha = 1$. The results for Au are presented as a plot of the

effective valence, Z° versus temperature, and for Cu, a plot of $Z^\circ - 1$ versus temperature. Estimates from these plots are presented in Table III. It can be seen that both metals migrate to the anode with Cu reversing direction at temperatures above 1000°C. The reversal confirms Wever's results but appears to occur about 50°C higher. The inverse temperature dependence of Z° appears to be of the same magnitude as that found by Wever for Ni and Fe.

TABLE III

RESULTS OF HUNTINGTON AND GRONE ON SELF TRANSPORT

Metal	Temp. °C	Eff. Valence Z°(1)	Pseudo-Activation Energy kcal/g-at	Self Diff. Act. Energy kcal/g-at	Ref
	800	-8.3			
Au	900	-6.5	35	41.7	16
	1000	-5.0			
	800	-5			
Cu	900	-2	49.5	47	57
	1000	0			

(1) Negative sign means anode-directed migration

As previously discussed, the authors have derived the following expression for the effective valence

$$Z^\circ = \bar{Z}\left[1 - \tfrac{1}{2}\frac{\Delta\rho_d}{\rho_o}\frac{n_o}{n_d}\frac{m_e^*}{|m_e^*|}\right]. \qquad (84)$$

For both Au and Cu the values of $\bar{Z}$ and $m_e^*/|m_e^*|$ are taken as +1, and Equation (84) is solved for $\Delta\rho_d n_o/n_d$. This quantity is found to be quite insensitive to temperature. The authors interpret this result in support of their theory, since one would not expect the scattering from defects to

be influenced by the thermal vibration of neighboring ions. This is evidence that the friction coefficient of Mangelsdorf, Equation (77), and the activated scattering cross section of Fiks, Equation (19), are temperature independent.

From the temperature dependence of v/j, a pseudo-activation energy has been determined. Since the resistivity is generally a linear function of temperature, the factor ρ/T in Equation (83) should be temperature independent; and since Z° decreases slowly with temperature, one would expect the temperature variation of v/j to be slightly less than the temperature variation of the self diffusion coefficient. Hence, one would expect the pseudo-activation energy to be sligtly lower than the self diffusion activation energy. From Table III it is seen that the pseudo-activation energy is slightly lower for Au, and slightly higher for Cu, than the self diffusion activation energy. The discrepancy for Cu may be attributed to the much higher scatter in the data on copper.

Equations (83) and (84) show that Huntington's approximate theory predicts that the velocity of transport should be a linear function of the current density. This prediction was confirmed in the work on gold for a factor of two change in current density.

In Huntington's article now in press[27] quantitative results are presented on self transport in platinum and qualitative results are presented from a study on aluminum. The experimental technique has been refined to give more precise results and the data has been corrected for thermal diffusion effects and creep due to surface forces. The presentation of the data on platinum is similar to that on gold. The effective valence drops linearly from +0.32 at 1675°C to +0.23 at 1475°C. The pseudo-

activation energy is 12 percent higher than literature data on the activation energy for self diffusion. The quantity $(\Delta\rho_d n_o/n_d)$ is again found to be fairly insensitive to temperature. The interesting result here is the sign of the effective valence; the transport is cathode-directed. Platinum has a negative Hall coefficient so that the electric field force predominates in the self electrotransport of platinum. This result is unique for all of the measurements on self transport with the exception of Cu at high temperature. Such a statement assumes, however, that the measured Hall coefficients used to determine the sign of the charge carriers apply at the temperature of the electrotransport experiments. The electrotransport of aluminum was found to be anode directed and relatively large. The effective valence was fairly temperature independent and the mobility was not a function of current density. The results will be published in more detail by Dr. R. V. Penney.

Work of Kuz'menko and Khar'kov--A considerable amount of work has been done recently in the Russian Ukraine by Kuz'menko and co-workers. They have studied self-electrotransport in Ag and Zn,[58,59,60] using a radioactive tracer and a weighing technique, and in Cd,[59] Al,[61] Cu, Pb, Sn,[60] and Au,[62] using a weighing technique. Kuz'menko[63] has recently published a review article on this data. The authors have presented their data directly as the velocity of migration and have used the correlated Einstein equation to determine the effective valence. Some of the data is presented in Table IV. It can be seen from the sign of the effective valence that all of the metals migrate toward the anode. Contrary to the work of both Wever and Grone, no reversal was found in the direction of migration of Cu at 1000°C. Also, the values of the

effective valence for Au appear to be about a factor of four higher than those obtained by Huntington. These discrepancies might be attributable to differences in method. Wever and Huntington both used the movement of surface scratches as a measure of the mass transport while Kuz'menko used the weighing method for Au and Cu. It is interesting to note that the metals Zn, Cd, and Sn have been reported to have a positive Hall coefficient. Contrary to the theory of Wever, these metals were transported to the anode.

TABLE IV

RESULTS OF KUZ'MENKO ON SELF TRANSPORT

Metal	Temp. °C	Eff. Valence Z° (2)	True Valence Z	Ref. (1)
Ag	745	-26	0.86	58, 60
	800	-27	0.88	
	875	-22	0.85	
Cu	900	-38	1.3	60
	950	-18	0.92	
	1000	-22	1.2	
Au	750	-38	1.2	62
	800	-34	1.2	
	900	-33	1.2	
Al	500	-28	1.6	61
	550	-19	1.3	
	570	-16		
Zn	350	-4.0	.60	59
	370	-4.3	.63	
Cd	250	-5	.64	59
Pb	250	-47	3.6	60
	310	-45	3.6	
Sn	190	-80	4.1	60

(1) All data is presented in reference (63)
(2) Negative sign means anode-directed migration

It can be seen that the temperature dependence of the effective valence is qualitatively the same as that found by Wever and Huntington. Kuz'menko has done a very thorough study of the effect of current density on the velocity of migration. For Cd and Zn the current density was varied by a factor of 10-15 and for Ag, Sn, and Pb by a factor of 5-8. In all cases the ion velocity varied linearly with current density within the limits of experimental error. Hence, it appears that the effective valence is not a function of the field strength. For Ag an activiation energy was determined from the velocity versus temperature data. At constant field strength, a value of 40.5 kcal/mole was obtained compared to 44.8 kcal/mole for self diffusion. The difference is attributed to the presence of the factor T in the denominator of the correlated Einstein equation. Huntington's pseudo-activation energy appears to be a better parameter since this factor is cancelled out.

Based on the theory of Fiks, Kuz'menko[63,64] has developed a method of determining the effective charge on an activated ion. The electrical resistivity is taken as $\rho = m/n_e e^2 \tau$. The mean free time is equated to ℓ/v_e, the electron velocity is related to the Fermi energy $E_F = \frac{1}{2} m v_e^2$, and the equation is solved for the product $n_e \cdot \ell$,

$$n_e \ell = \frac{(2mE_F)^{\frac{1}{2}}}{\rho e^2} = \frac{\bar{Z}}{\bar{A}} , \qquad (85)$$

and from Fiks' Equation (18) the product equals $\bar{Z}/\bar{A}$. On the basis of his experimental work Kuz'menko assumes that the field force is negligible compared to electron friction force so that Fiks' expression for the effective valence may be rearranged to give

$$A^* = Z^\circ \frac{\bar{A}}{\bar{Z}} = Z^\circ \frac{e^2 \rho}{(2mE_F)^{\frac{1}{2}}} . \qquad (86)$$

The value of A* was determined for Ag from 675°C to 900°C assuming E_F = 5.5 ev. An average value of 3.6×10^{-16} cm^2 was found with no temperature dependence within the limits of experimental error. This temperature insensitivity is in qualitative agreement with Huntington's results.

An analytical expression for the activated cross section has been derived[64] by a method similar to that used by Mott[20],

$$A^* = \frac{\pi}{2} \frac{Z^{*2} e^6}{E_F^2} \left[\ln \left(1 + \frac{1}{y}\right) - \frac{1}{1+y} \right] , \qquad (87)$$

where $y = 5.14 \times 10^{-8} n_e^{1/3}$. From Equations (86) and (87) the true value of the valence of an activated ion is estimated. These values are listed in Table IV. A discussion of the validity of Equation (87) as a measure of the true valence of an activated ion undergoing electrotransport has been presented by Kuz'menko[63]. The results of this analysis are similar to those of Gurov[52].

Related Work--It seems appropriate in this section to discuss the recent work of some Soviet investigators who have studied the electrotransfer of iron in alloys of iron containing small amounts of solute. I. N. Frantsevich and co-workers have studied the electrotransfer of Fe^{59} in iron-carbon alloys containing 1 w/o carbon. This work has been reported in four different articles.[65-68] These authors analyse their data based on the model of Frenkel previously mentioned. In their analysis however, they neglect the electron friction force with no apparent justification. The experimental results are quite interesting and are presented in Table V. The iron migrated to the anode below 1150°C and probably to

the cathode above that temperature as in pure iron, although the actual reversal was not reported. Apparently, the addition of 1% carbon to iron causes the iron to migrate to the anode rather than to the cathode as Wever found in pure iron.

S. D. Gertsriken[69] and co-workers have measured the electromigration of iron in iron-carbon alloys by following the motion of molybdenum markers within the samples. Their work was done on alloys containing 0.35 and 0.70 w/o carbon. The results are shown in Table V and confirm the direction of transport found by Frantsevich. It is apparent though, that Gertsriken's results indicate higher migration velocities and an increasing rather than decreasing temperature dependence.

Using the same method, Gertsriken[70,71] has also measured the electrotransport of iron in alloys of Al-Fe containing 2.5 and 8 w/o Al. In this work the iron migrated to the cathode as in the case of self transport found by Wever.

TABLE V

ELECTROTRANSPORT OF IRON IN ALLOYS OF IRON PLUS SOLUTE

Alloy	Element Transported	Temp °C	Tr.No. x 10^6 (1)	Reference
Fe-1.0C	Fe^{59}	950	-1.86	68
		1000	-1.08	
		1050	-0.49	
		1100	-0.13	
		1150	0.0	
Fe-.35C	Fe	945	-6.4	69
		1020	-15.0	
Fe-.70C	Fe	945	-5.3	69
		1020	-6.9	
Fe-2.5Al	Fe	1300	+4.6	70
Fe-8Al	Fe	1300	+3.4	70

(1) Negative sign means anode directed migration

Electrotransport of Interstitial Solutes

Study of electrotransfer of interstitials has the advantage that the mobility is determined directly rather than a differential or relative mobility, since the velocity of the interstitial is on the order of 100 times greater than the velocity of transport of the lattice ions. A summary of the quantitative results of the work done on electrotransport of interstitials through 1956 has been presented by Seith[4] and Heumann.[53] A qualitative review will be presented here within the framework of the previous discussion. Electrotransport of oxygen has been investigated in β-titanium[72] and zirconium,[73] and in both cases the oxygen migrated to the anode. Nitrogen was also found to migrate to the anode in γ-iron.[74] It is difficult to say whether the field force or the electron friction force predominates here. If one could assume that the electron friction force were cathode-directed because of the defect electron conduction in these metals, then the interstitial ions would have to be present as negative ions in these metals. Two papers[75,76] on the diffusion of hydrogen in palladium have shown that hydrogen migrates to the cathode. If hydrogen is assumed to be present in metals as a positive ion, then the field force would be cathode-directed. Since palladium is predominately n-conducting the electron friction force would be anode directed. Consequently, the field force would predominate. More recently data has been published on the electrotransport of oxygen in yttrium metal,[77] which is predominantly n-conducting at room temperature. At 1230 and 1370°C oxygen migrated to the anode.

Yavoiskii[78] has investigated the electrotransport of hydrogen in steels in the austenitic temperature region. A series of steels was investigated and a small separation was observed in only three samples:

high carbon, medium carbon, and Mn steels. The fact that a separation was not observed in the other steels is undoubtedly due to the low current densities used, 10-30 amps/cm^2.

The electrotransport of interstitial carbon has been studied quite extensively, especially in an iron matrix. Good reviews of the older works in the literature are given by Kalinovich.[79,80] In recent years Russian workers have made a number of studies using radioactive techniques employing C^{14}. Babikova[81-83] has studied carbon transport in α-Fe, Fe-Cr, Fe-Ni, Fe-Mn, Fe-Si, Ni and Ni-Cr between 500 and 900°C. Frantsevich and Kalinovich[65,68,84] have studied carbon transport in γ-Fe between 900 and 1100°C. In all of these studies, as in the previous studies, carbon migrates to the cathode. Unfortunately, all of these authors analyse their data implicitly assuming a negligible electron-friction force. Their discussion concerning the charge of the carbon atom and the corresponding donor-acceptor reactions are, therefore, subject to question. This implicit assumption has recently been pointed out by Kalinovich,[80] who has recalculated his data in γ-iron and some of Balikova's data in α iron in terms of the effective valence. The recalculated data are presented in Table VI. The temperature dependence of the effective charge in γ-iron appears to be roughly the same as that found in the self transport experiments. The magnitude of the effective charge indicates that there is a cathode-directed force in addition to the field force, since it is unlikely that the carbon atom is ionized more than +4. This could be attributed to the momentum transfer of the defect electrons in the p-conducting iron, or also to inaccurate data. It would be interesting to recalculate Babikova's data on pure nickel because here one would expect a lower effective charge since nickel is n-conducting.

TABLE VI

ELECTROTRANSPORT OF CARBON IN STEEL

Alloy	Temp °C	Eff. Valence Z^{o}(1)	Recalculated from Reference
α-Fe	600	+49	83
	950	+13.4	
	1000	+11.0	
γ-Fe	1050	+ 7.7	65
	1100	+10.6	
	1150	+ 8.1	

(1) Plus sign means cathode-directed migration

Two interesting studies have recently appeared by Frantsevich on the transport of carbon in Fe, Ni, Co[85] and Ti, Ta, W.[86] The data have been analysed by a method based on the theory of Fiks. The authors have presented the details of their analysis in reference (87). Following Glinchuck, the authors assume that the electron friction force is produced by both positive and negative carriers in a metal. From Equation (21) it can be seen that the effective charge has the following form,

$$Z_i^o = Z_i - \ell_e n_e A_e + \ell_p n_p A_p \quad . \tag{88}$$

An expression for the conductivity as a function of the carrier concentration and mean free path is used, which may be derived as follows. The electrical conductivity is taken as $\sigma = n_e e^2 \tau_F / m$. The mean free time at the Fermi level is equated to ℓ_e / v_F, and the electron velocity is related to the Fermi energy $E_F = \frac{1}{2} m v_e^2$, giving,

$$\sigma = \frac{n_e e^2 \ell_e}{(2mE_F)^{\frac{1}{2}}} \quad . \tag{89}$$

The free electron approximation for the Fermi energy, $E_F = h^2/2m \cdot (3n_e/8\pi)^{2/3}$, is now substituted into Equation (89) to give

$$\sigma = \left(\frac{8\pi}{3}\right)^{1/3} \frac{e^2}{h} \ell_e n_e^{2/3} = K_n \ell_e n_e^{2/3}, \qquad (90)$$

where K_n is a constant. It is assumed that Equation (90) applied for both postive and negative electrons, and it is substituted into Equation (88) to give for the effective valence,

$$Z_i^o = Z_i - \frac{\sigma_e A_e n_e^{1/3}}{K_n} + \frac{\sigma_p A_p n_p^{1/3}}{K_n} . \qquad (91)$$

The conductivity is expressed as $\sigma = \sigma_e + \sigma_p$; and it is assumed that the total resistivity ρ as well as ρ_e are linear functions of temperature. The resistivity is expressed as $\rho = \rho_o + \alpha T$ and $\rho_e = \rho_{oe} + \alpha_e T$ and substitution into Equation (91) gives a fairly complex algebraic expression for Z_i. It is further assumed that the scattering cross section A_e, A_p and the carrier concentrations n_e, n_p are temperature independent. The algebraic expression then reduces to the following form,

$$AX^2 + B Z_i^o X - CX - Z_i^o + Z_i = 0 , \qquad (92)$$

where $X = \left(T + \frac{\rho_o}{\alpha}\right)^{-1}$ and A, B, C, are constants. Hence, by determining Z^o at various temperatures, the true valence, Z_i, may be calculated. If the resistivity is assumed to be a linear function of concentration, the same type of analysis gives an expression similar to Equation (92) so that the true valence, Z_i may also be determined from data of Z_i^o as a function of composition under assumptions similar to those above. It is pointed out that if ρ_e/ρ_p = constant in the temperature range of investigation,

Equation (92) is reduced from its hyperbolic form to a linear form,

$$Z_i^o = Z_i - \frac{a}{\rho} \quad . \tag{93}$$

In their experimental work the authors have used a radioactive technique employing C^{14}. They obtain the diffusion coefficient in addition to the electrical mobility from their experiments. Equation (11) is used to calculate the effective charge which is then fitted into Equation (92) by the method of least squares. The results are shown in Table VII.

TABLE VII

ESTIMATES OF TRUE CARBON VALENCE

Alloy	Temp. Range °C	True Carbon Valence(1)	Reference
Fe-C	800-1400	+3.7	
Co-C	600-1400	+2.8	85
Ni-C	600-1400	+1.8	
Ti-0.1C	950-1650	+4.0	
Ta-0.1C	600-2600	+2.8	86
W-0.1C	1800-2800	+0.6	

(1) Postive valence means cathode-directed migration

Unfortunately, these authors do not present their data for Z_i^o versus T, so that it is not possible to check their results. They claim that all of the curves were hyperbolic except Ta-C which was linear. They do not give any statistical measure of the fit.

This analysis is much more sound theoretically than those of the previous investigators who simply neglected the electron friction force. It does make a number of assumptions though, which appear questionable.

It is interesting to note that if it is assumed that defect electrons do not produce a cathode directed friction force, as seems quite reasonable from Barnett's work and the results of Kuz'menko of self transport in Sn, Cd, and Zn, then the effective valence may be written as Equation (93) directly from the theories of Mangelsdorf, Fiks, Huntington and Klemm. All theories predict "a" in Equation (93) to be directly proportional to the electron-ion scattering cross section which Huntington and Kuz'menko have shown to be insensitive to temperature. Hence, if it were demonstrated that the data for Z^{o} versus $1/\rho$ (T) fit a hyperbolic curve much better than a linear curve, this would be evidence in favor of Glinchuk's and Wever's theory of cathode-directed momentum transfer from defect electrons. If it fit a linear curve better, it could be concluded that either ρ_e/ρ_p = constant, or that the cathode-directed momentum transfer from defect electrons was negligible.

Electrotransport of Solid Solution Components in Solid Metals

In electrotransfer experiments on solid solution metallic phases a relative transport of both components occurs. Consequently, transport numbers or electric mobilities determined with respect to fixed reference system are frequently a measure of relative movement. Such parameters are related to a differential mobility or transport number. Seith and Wever[167] were the first investigators to determine both the relative transference number and the true transference number in solid solution metallic phases. They have conducted a number of experiments which have been summarized by Heumann.[53] Contrary to some of the results on interstitial and self transport, these authors found the mobility in β Cu-Al and in Ag-Zn to be a function of current density. Concerning

the direction of the electron-ion momentum transfer, an interesting correlation was found with conduction mechanism. In the Cu-Al system, going from the β to γ phase, the conduction mechanism changes from n to p-conducting, and the direction of migration of Al was found to change from anode to cathode. In the Cu-Sn and Ag-Zn systems, the same correlation was found across a phase change. This is additional evidence that led to Wever's hypothesis of cathode-directed momentum transfer between defect electrons and activated ions.

In the past few years a considerable amount of work has been published by two groups of investigators in the Russian Ukraine. These investigators have employed techniques involving the use of radioactive tracers. It is generally possible to determine the diffusion coefficient from the electrotransport experiment by these methods. A summary of the methods employed is given by Kuz'menko.(63)

Work of Frantsevich, Kalinovich and Co-Workers--These authors generally use a technique in which they follow the movement of a radioactive zone deposited onto a wire of the alloy under study. In their initial work they have implicitly assumed that the electron-ion interaction force is negligible. In their more recent work however, they have presented data in terms of effective valence, Table VIII. The temperature dependence of the effective valence appears to be quite consistant with that found for interstitial and self transport experiments. In the work on Ni-Cr(94) the authors have investigated surface electrotransfer. By successively analysing and removing the outside layers of wire specimens, they claim to have shown that surface transport is larger by a factor of four. In the work on Ni-W, Fe-W, and W-Fe, the authors found that the transport

decreased with temperature and became experimentally unmeasurable at around 1100°C.

TABLE VIII

DATA OF FRANTSEVICH AND CO-WORKERS

Alloy	Conc. Migrating Element Wt%	Temp °C	Eff. Z*	Direction of Migration	Reference
Ni-Cr	4.36 w/o Cr	950	57.6	Cathode	94
		1000	42.5		
		1050	34.7		
		1100	27.6		
Mo-Ni	90.76 w/o Ni	1150	25.7	Anode	95
		1200	20.9		
		1250	18.0		
		1300	15.0		
Mo-Cr	9.92 w/o Cr	1200-1350	--	Cathode	88
Ni-W	W	850-1100	--	Cathode	89
Fe-W	0.49 W	900-1150	--	Cathode	65,68,85,90,91
Fe-Cr	7.4 Cr	900-1200	--	Cathode	65,68,85,92
Fe-Mo	2,4.5 Mo	950-1100	--	Anode	65,68,85,93
W-Fe	Fe	900-1150	--	Anode	85,91
Cr-Fe	Fe	900-1200	--	Anode	85,92
Mo-Fe	Fe	950-1100	--	Cathode	85
Co-W	0.82 W	1100-1350	10	Cathode	98

These authors have developed a technique for determining the true charge which was discussed in the section on interstitial transport. They have used this technique on Mo-W and Ni-Cr, Table IX. In the Mo-W system the true valence was determined by measuring Z_i^o as a function of temperature, and in the Ni-Cr system, by measuring Z_i^o as a function of concentration. In neither case was the data on effective charge presented;

only the results were given. It is interesting that the results in three cases indicate a large negative valence for the migrating metallic ion. The presence of the "electron gas" requires that the average metal ion be positively charged, so that this negative charge would be necessarily limited to the ion in its activated position. The results indicate that the true valence of activated molybdenum changes from -4.7 to +2.4 in going from 75 to 25 atom % Mo in W.

TABLE IX

DATA OF FRANTSEVICH AND CO-WORKERS

Alloy	Conc. Migrating Element At%	Temp °C	True Valence	Direction of Migration	Ref
Mo-W	25W	1500-2200	-2.7	Cathode	
Mo-W	75W	1900-2500	+3.0	Cathode	87,96
W-Mo	75Mo	1900-2500	-4.7	Anode	
W-Mo	25Mo	1500-2200	+2.4	Anode	
Ni-Cr	4.8-19.7 Cr	1250	-4.2	Cathode	87,97
Cr-Ni	80.3-95.2 Ni	1250	+1.1	Anode	

Work of Kuz'menko and Co-Workers--The experimental technique generally used by Kuz'menko was to coat a radioactive layer on the polished surface of two specimens, place them in contact and run a high current through them at the temperature of interest, separate the specimens at the original interface, and analyse the activity distribution in each half. The experimental results presently in the literature are given in Table X. The authors have calculated the effective valence by a rearranged form of Equation (11). The true valence is determined by the method described previously in the section on self transference. The authors interpret this true charge as being the charge which a conduction

electron experiences in the vicintiy of an activated ion. From data on residual resistance they have calculated the true charge of non-activated ions.[104] The true valence of the activated ions was smaller than the non-activated ions. This could be attributable to screening effects upon the activated ions.

TABLE X

DATA OF KUZ'MENKO AND CO-WORKERS

Alloy Conc: At%	Migrating Element	Temp °C	Effective Valence	True Valence	Direction of Migration	Ref
Al	Ag^{110}	599	17	1.3(1)	Anode	
Al-.84 Zn	Zn^{65}	560	11	1.1(1)	Anode	101
Al-5.0 Zn	Zn^{65}	577	12	1.1(1)	Anode	
Zn-50 Ag	Ag^{110}	670	1.6	---	Anode	
Zn-50 Ag	Ag^{110}	519	1.9	---	Anode	100
Zn-30 Ag	Ag^{110}	577	33	---	Anode	
Zn-50 Ag	Zn^{65}	434	0.6	---	Anode	
Cu	Sb^{124}	1100	42	1.35	Anode	
Cu	Co^{60}	1202	32	1.2	Anode	102
Cu	Fe^{59}	1317	40	1.4	Anode	
Fe-23,35,40 Al	Al	1000-1340	---	---	Cathode	99
Fe-23,35,40 Al	Fe^{59}	1000-1340	---	---	Anode	
Cu	Sn	1075-1153	57-20	1.4	Anode	
Cu-0.1 Sn	Sn	1101-1159	51-28	1.3	Anode	103
Ag-1.0 Sn	Sn	997-1205	48-23	1.2	Anode	

(1) Valence of Al assumed to be 3.

Electrotransport in Semiconductors

One might expect the electrotransport properties in semiconductors to be similar in nature to those in metals, since the possibility of an

electron-ion friction force is present. The electron scattering cross section in semiconductors is large, so that even though the electron concentration is low relative to metals, an appreciable friction force might be expected.

Apparently, Kubaschewski[105] was the first investigator to measure electrotransfer in a semiconducting type material. In Mg_3Bi_2 he found Bi accumulated at the anode and Mg at the cathode. In the past few years a number of investigations have been reported in the literature and they are quite interesting. Fuller[106] has investigated the electrotransport of Li in Ge and Si, and of Cu in Ge. He made a direct measure of the electric mobility by measuring the displacement of spot-zone, doped with the impurity element under investigation. Diffusion coefficients calculated from the Einstein relation appeared to agree quite satisfactorily with previous measurements. This would indicate that the electron-ion scattering force was negligible in this work. The author points out that Cu acts as a negative ion in Ge at room temperature, and that his electrotransport data indicate that at the higher temperatures it switches to a positive ion.

The remaining investigators discussed here all use essentially the same technique. A radioactive layer of the element to be investigated is coated onto the polished surface of two blocks of the semiconducting material which are then butted against each other. After passing a high current, an activity profile is made on the sample. Gallagher[107] has presented the solution to the differential equation for this problem and has shown that the ratio of u/D may neatly be determined from the activity profile. From the Einstein equation then, he has determined

the effective charge from his data on electrotransport of Cu in Si, Table XI. Apparently copper moves with a positive valence of 1 in silicon with no appreciable electron drag. The author qualitatively confirmed Fuller's work on Cu in Ge and was unable to detect movement of Fe or Au in silicon at 1100°C.

TABLE XI

ELECTROTRANSPORT DATA ON SEMICONDUCTORS

Semiconductor	Migrating Element	Temp °C	Eff. Valence Z°	Direction of Transport	Ref
Si	Cu	1000	+0.83	Cathode	107
		1125	+1.23		
		1200	+1.03		
Se	Tl	100	+2.85	Cathode	108
		175	+3.59		
		215	+3.34		

Ibragimov[108] has investigated electrotransport of thallium in selinium. He uses the same technique as Gallagher, and uses a similar method to analyse his data, which are presented in Table XI. It is concluded that thallium moves with a charge of +3. On the basis of an evaluation of Fiks' expression for the electron-ion friction force he concludes that this force is negligible.

Contrary to the results of Gallagher, Boltaks[109] found an electrotransport of Au in Si. An analysis similar to Gallagher's was used. It was also checked by a slightly different analysis which does not require the diffusion coefficient to determine the electric mobility. The results shown in Table XII indicate that the electrotransport increases up to 1230°C and then drops sharply and changes direction at around 1280°C.

This change in direction has been considered by Fiks,[110] who attributes it to the temperature dependence of the electron scattering cross section. From an analytical expression for the electron scattering cross section on semiconductors he estimated an inversion temperature from the function which he has developed for the effective valence. In Si it is approximately 1325°C and in Ge, 725°C. Such an explanation is similar to that used by Wever to explain the inversion of self transport found in copper.

TABLE XII

ELECTROTRANSPORT DATA ON SEMICONDUCTORS

Semiconductors	Migrating Element	Temp °C	Mobility $(cm^2/V\text{-}s)x10^6$	Direction of Migration	Ref
Si	Au	1160	+1	Cathode	109
		1230	+10	Cathode	
		1350	-100	Anode	
Ge	In	300-500	-.15 to -3.6	Anode	111
		800-900	+9.8 to +50	Cathode	
Ge	Sb	500-600	+1.6 to +4.2	Cathode	111
		800-900	-12 to -37	Anode	

Konstantinov[111] has recently presented data on electrotransport of In and Sb in Ge. In analyzing his data he was able to determine the mobility directly from the displacement of the radioactive peak at the interface. The mobilities obtained were much larger than would be expected from calculations using the Einstein relation and measured diffusion coefficients. This might be attributable to the electron drag force. It can be seen that with both impurities a reversal of migration direction occurred between 500 and 800°C. These temperatures agree well with Fiks' calculations. It is significant that Konstantinov obtained the same results using either p or n-conducting germanium.

From the data on electrotransport in semiconductors it appears that only in some cases might the electron-ion friction force be appreciable relative to the field force.

Electrotransport in Liquid Alloys

The Austrian investigator, R. Kremann, has done a very large amount of work on electrotransport in liquid alloys. This and other pertinent work done before 1940 have been summarized by K. Schwarz.[2] In recent times the interest in electrotransport in liquid alloys has diminished considerably. The work available in the literature since 1940 is discussed below.

Work of Drakin--In a paper published in 1950, Drakin[112] has shown that a eutectic alloy may be separated into its solid solution components by electrotransport. If a eutectic alloy is electrolysed just above its melting point, one would imagine that the components would migrate in opposite directions and that concentration changes would begin to occur first at the electrode boundaries. A small concentration change would cause solidification of the component solid solution phase at each electrode; and if plain front solidification were maintained, these solid phases would grow down the separation tube until all of the eutectic alloy was solidfied into its component solid solution phases. Drakin has studied the eutectic systems Bi-Sn and Bi-Cd. In experiments conducted on 1 mm I.D. capillaries he was able to approach a complete separation.

Drakin and Maltsev[113] have made a systematic study of electrotransport in the Na-K system at 100°C. They used a looped capillary and measured the composition changes by following the resistivity changes

with electrodes sealed into the capillary. The experiments were run to steady state and from plots of the log of the end concentration differences versus voltage drop an "electrodiffusion constant", K_i, was determined in accord with a relation which is written for dilute solutions as,

$$\ln \frac{N_1}{N_2} = \frac{K_1 E L}{T} , \tag{94}$$

where L is the tube length and N_1 and N_2 are end concentrations. Comparison of this equation in differential form with Equation (68) gives the relation between K_i and the effective valence,

$$K_i = \frac{e}{k} Z_i^o . \tag{95}$$

The authors observed the interesting result that the direction of transport reverses itself with composition change; below 48 w/o Na, electrotransport of sodium is anode-directed, above this percentage it is cathode-directed. This effect occurs in other systems and has been discussed by Schwarz.[2]

In two recent papers Drakin[114,115] has determined the electrodiffusion constant, K_i, for a number of dilute solutions of elements in sodium and potassium. The same technique as above was used. The results along with some on Na-K are given in Table XIII. Drakin offers a qualitative explanation of this data as follows. The alkali-heavy metal interaction is stronger than the alkali-alkali interaction, and hence, the heavy metals are more completely solvated and are therefore driven more strongly to the anode by the friction force. It is concluded that in metals where the electron friction dominates the electrotransfer process, a solute will always migrate to the anode. Such a conclusion qualitatively explains the reversal found in the Na-K system.

TABLE XIII

ELECTROTRANSPORT DATA OF S. I. DRAKIN

Alloy	At% of Migrat. Ele.	Temp °C	$K_i \times 10^{-4}$ deg/V	Eff. Valence Z_i^o	Direction of Migration	Ref
K-Na	5.5 Na	100	0.54	0.46	Anode	113
K-Hg	0.4 Hg	100	12	10	Anode	114
K-Pb	0.6 Pb	100	26	22	Anode	114
K-Tl	0.19 Tl	110	23	20	Anode	115
Na-K	1.6 K	100	0.97	0.84	Anode	113
Na-Hg	0.6 Hg	110	21	18	Anode	115
Na-Hg	1.1 Hg	110	9.0	7.7	Anode	115
Na-Pb	0.45 Pb	110	25	21	Anode	115
Na-Cd	.21 Cd	110	15	13	Anode	115

An interesting correlation is presented without a theoretical explanation. Drakin[113] has determined the electrodiffusion constant, K_i, as a function of composition in Na-K at 100°C. If the slope of the conductivity versus molar concentration curve is plotted as a function of composition, it has exactly the same shape as the plot of K_i versus composition. If such a correlation were general, it would mean that in any system having a maximum or minimum in the conductivity versus molar composition curve, a corresponding reversal of migration would be predicted. It might be pointed out, that in cases where the electron friction predominates, most of the theoretical developments indicate the direction of transfer to be a function of the sign of the slope of the resistivity versus mole fraction curve.

Work of Belashchenko--In an article published in 1960, Belashchenko[116] has reported an investigation of electrotransport in molten Bi-Sn alloys

at 300°C using a radioactive tracer technique for analysis. In this work a reversal of transport direction was found at approximately 65 At% Sn. In a more recent article, Belashchenko[117] has stated that this investigation was in error due to inaccuracies in the radiochemical analysis involving Sn^{113}.

Belashchenko[117] has presented an interesting phenomenological derivation of an expression for the effective valence in a binary alloy. He assumes a zero net force on the bulk of the alloy and writes a force balance on the elements, considering both field force and electron friction force. If Equations 2 and 4 are combined, the force balance may be written as,

$$\sum_i n_i (eEZ_i - F_{ei}) = 0. \tag{96}$$

If this equation is expanded for a two component system and solved for the electron-ion interaction force on component 1, it becomes,

$$F_{e1} = \frac{eE(n_1Z_1 + n_2Z_2)}{n_1 + n_2 (F_{e2}/F_{e1})} \tag{97}$$

It is assumed that the electron-ion friction force is a linear function of the electric field, so that the ratio of the two forces in a binary system may be written as,

$$\frac{F_{e2}}{F_{e1}} = \frac{A_2}{A_1} = \frac{\delta_2}{\delta_1} = \frac{r_{2n}}{r_{1n}} , \tag{98}$$

depending on whether one employs an electron scattering cross section after Fiks, (see Equation 15) or a friction coefficient after Klemm or Mangelsdorf, (see Equations 33 and A-18). Hence, the net force on an ion is given as,

$$F_1 = eEZ_1 - F_{ei} = eE\left(\frac{n_2(A_2Z_1 - A_1Z_2)}{n_1A_1 + n_2A_2}\right) \qquad (99)$$

The effective valence is the term in parenthesis,

$$Z_1^o = \frac{n_2\,(A_2Z_1 - A_1Z_2)}{n_1A_1 + n_2A_2} \,. \qquad (100)$$

In dilute solutions it is noted that this equation becomes

$$Z_1^o = (Z_1 - Z_2\,\frac{A_1}{A_2}) \,, \qquad n_2 \approx o \,. \qquad (101)$$

This relationship has the same form as the equation of Fiks, Mangelsdorf and Klemm, which were previously discussed.

Belashchenko has conducted some interesting experiments in connection with these equations. In all of his work he has determined the effective valence by measuring the steady-state concentration distribution in a capillary by means of chemical or radio-chemical analysis. Work on electrotransport in a number of dilute alloys has been reported in two references (118, 119). It was assumed that the electron scattering cross section is proportional to the square of the true valence, so that Equation (101) is written as,

$$Z_1^o = \left(Z_1 - \frac{Z_1^{\,2}}{Z_2}\right). \qquad (102)$$

Such an assumption would follow from Mott's work as presented by Kuz'menko, see Equation (87). The experimental values of the effective valence were compared with those computed from Equation (102), when the electrochemical valence was substituted for Z_i. The results are given in Table XIV. There appears to be a fairly good correlation. The direction of migration is correctly predicted in every case. The data also appears to agree

TABLE XIV

DATA OF BELASHCHENKO COMPARED TO KREMANN

	Belashchenko[118,119]					R. Kremann[2]		
Alloy	Conc. Solute Wt.%	Temp °C	Experimental Effective Valence, Z_1^o	$Z_1 - \frac{Z_1^2}{Z_2}$	Direction of Migration	Conc. Wt%	Temp °C	Direction of Migration
Bi-Cd	2.5 Cd	300	+1.36	+1.20	Cathode	25-75Cd	---	Cathode
Bi-Se	.08 Se	300	-0.90	-1.20	Anode			
Cd-Bi	4.7 Bi	350	-16.4	-7.50	Anode	25-75Bi	---	Anode
Cd-Sn	.41 Sn	360	-5.40	-4.00	Anode	25-75Sn	300	Anode
Pb-Zn	.04 Zn	360	+0.7	+1.00	Cathode			
Pb-Se	.05 Se	360	-3.00	-3.00	Anode			
Sn-Bi	4.8 Bi	350	-0.80	-1.25	Anode	12-75Bi	200,300	Anode
Sn-Ca	0.1 Ca	300	+0.60	+0.75	Cathode			
Bi-Ag	.001 Ag	300	+0.15	+0.80	Cathode	30Ag	---	Cathode
Pb-Ag	.001 Ag	360	+0.33	+0.75	Cathode	50-80Ag	1000	Cathode

qualitatively with that of Kremann taken at higher concentrations.

In a more recent report, Belashchenko[120] has measured the electrotransport of small quantities of silver and gold in a number of solvents using Ag^{110} and Au^{198}. In this work the correlation just described did not hold up, as might be guessed from the poor agreement found on Bi-Ag and Pb-Ag. In this work the true valence of the migrating solute was calculated from Equation (102) using the electrochemical valence of the solvent for Z_2 and the measured effective valence. The results are given in Table XV.

TABLE XV

ELECTROTRANSPORT OF DILUTE SOLUTIONS OF Ag AND Au

	Solute = Ag^{110}			Solute = Au^{198}		
Solvent	Effective Valence Z°_{Ag}	True Valence Z_{Ag}	Direction of Migration	Effective Valence Z°_{Au}	True Valence Z_{Au}	Direction of Migration
Cd	-1.25	-0.6	Anode	-2.2	-1.3	Anode
In	-0.74	-0.6	Anode	---	---	
Sn	-1.07	-0.9	Anode	-2.2	-1.5	Anode
Hg(1)	+1.43	---	Cathode	+1.47	---	Cathode
Tl	+0.64	+0.9	Cathode	-0.28	-0.26	Anode
Pb	+0.48	+0.56	Cathode	-0.1	-0.1	Anode
Bi	+0.2	+0.2	Cathode	-0.18	-0.18	Anode

(1) Data taken from Schwarz[2]

Five of these systems have been measured by Kremann[2] at higher solute concentrations. The direction of transport agrees in the systems Ag-Pb and Ag-Bi. There is disagreement in the systems Ag-Sn, Au-Pb, and Au-Bi indicating either a reversal in direction or experimental errors. The metals Cd, In, Sn are 5th period and Hg, Tl, Pb, Bi are 6th period.

Belashchenko notes that the true valence is little affected by a change in group number of the solvent but consistently affected by a change in the period numbers. This is related to the solvent-solute interaction by the phase diagrams which indicate a more positive energy of mixing for Ag and Au with the 6th period metals. One might equally conjecture however, that it could be connected with the mass difference between the elements of the 5th and 6th period. It is interesting to note that this analysis, like that of Frantsevich's for solids, indicates a negative value for the solute ion in some cases.

Belashchenko[117] has also studied electrotransport as a function of composition in the systems Cd-Sn, Bi-Cd, and Bi-Sn. It is noted that Equation (100) may be rearranged into the following form,

$$Z_1^o = \frac{X_2(\frac{A_2}{A_1} Z_1 - Z_2)}{1 - (1 - A_2/A_1)X_2} = \frac{aX_2}{1 - bX_2}, \qquad (103)$$

where a and b are constants. The value of Z_i is determined as a function of composition and the data are fitted to Equation (103). This treatment assumes Z_1, Z_2 and A_1/A_2 to be independent of composition. The data appear to fit this equation fairly well. Values of $A_{Sn}/A_{Bi} = 0.644$, $A_{Cd}/A_{Sn} = 0.187$, and $A_{Bi}/A_{Cd} = 8.77$ were obtained. The author notes that the product of these three quantities should be unity, and it is found to be 0.95. Belashchenko interprets this result as an indication that Z_1, Z_2, and A_1/A_2 are concentration independent in these eutectic systems. The author is also able to check the previous assumptions that A_i is proportional to the square of the electrochemical valence. A plot of log A_i/A_{Bi} as a function of the log of the electrochemical valence of component i for Cd, Bi, and Sn gave a fairly straight line, but indicated the scattering cross

section to be proportional to the 2.36 power of the electrochemical valence.

In a very recent article not yet available to this author, Belashchenko[168] has reported on the electrotransport of Th and Co in metals of the 5th and 6th periods. The results are apparently quite similar to those found for Ag and Au, with the transport being anode-directed.

Other Work--Mangelsdorf[29,121] has measured the mobility of a number of solutes in Hg at room temperature with a very neat experimental apparatus employing resistivity techniques to measure composition change. His data are in good agreement with the data of Schwarz[2] on these same systems taken by means of diffusion potential measurements and direct velocity measurements.

Rabkin[122] has studied the electrotransport of carbon and sulfur in liquid iron at 1280-1300°C. The results are only qualitative in nature but definitely show that carbon is transported to the cathode as in the solid state. The results on sulfur are not as definite but indicate migration is probably also cathode-directed.

Yavoiskii[123] has studied the electrotransport of hydrogen in melts of aluminum, copper and steel. The results indicate an appreciable mobility of hydrogen toward the cathode. Angus[124] has studied the temperature dependence of the electrotransport in the Na-Hg system around the composition 0.5 At% Na, where the reversal occurs. At high temperatures he found that the reversal no longer occurred. This result is interpreted as being consistent with a theory which postulates that the reversal is caused by associations in the liquid, since at higher temperatures one would

imagine that the associations would disappear. Pikus[24] has found a maximum in the Na-Hg resistivity curve at room temperature near the point of reversal which supports his theoretical predictions. It would be interesting to see if this maximum disappears at higher temperatures. Epstein and Weeks[162] have studied the electromigration of Cr and Fe in liquid Bi. The solubility of these elements is extremely low, with Cr, 40 ppm and Fe, 13 ppm at 495°C. They found that Cr migrates to the anode and Fe to the cathode.

The Haeffner Effect

Since the experiments of Haeffner in 1953, the process of separating isotopes in a liquid metal by means of electrotransport has generally been referred to as the Haeffner effect. In recent years many reports have been published on this subject. Lodding and co-workers[125-130] have studied a number of different metals, K, In, Li, Cd, Zn, Sn. Two additional metals have been studied by others workers, Hg[131-134] and Ga.[135-136] In all of the metals studied to date the heavy isotope concentrates at the cathode. Two different techniques have been used to measure the effect. Lodding reports his data in terms of a parameter called the mass effect, μ, which is defined as

$$\mu = \frac{\Delta v/-v_e}{\Delta M/M} \quad , \tag{104}$$

where Δv is the difference in migration velocities of the two isotopes and ΔM is the isotopic mass difference. This parameter may be written in terms of the differential mobility, U_{12}, as follows,

$$\mu = \frac{U_{12}(e\, n_e \rho_o)}{\Delta M/M} \quad . \tag{105}$$

It can be seen that the mass effect, μ, is a measure of the differential mobility per fraction of isotopic mass difference. It is determined experimentally by a simple mass balance on the separation tube before and after the experiment, under the restriction that the time of the experiment is less than the critical time required for the concentration gradient to extend to the middle of the tube. The electron-ion ratio is also assumed to be one, so that $N_e = N_o$. Such a technique has the disadvantage that run-times greater than the critical time give low results. Lodding[130] has indicated that much of his original work suffered from this error. This technique has the advantage, however, that it is not a function of the diffusion coefficient, and consequently is not affected by large effective diffusion coefficients due to convective mixing, which may be an inherent result of the high current densities involved.

Bogoyavlenskii[134] has presented data on Hg and recalculated data on Hg, Ga, K, and In in terms of the parameter β, which is defined as,

$$\beta = \frac{U_{12}/u}{\Delta M/M} = \frac{U_{12}(kT/D^*e)}{\Delta M/M} , \qquad (106)$$

where D^* is the self diffusion coefficient of the liquid metal, and the effective valence is taken as 1. When an experiment is run to steady state conditions the electrotransport flux is counterbalanced by a back diffusion flux so that an expression such as Equation (67) may be used to describe the steady state condition. It is shown in Chapter IV that the steady state concentration distribution may also be written as a function of U_{12}/D. One may write a general flux equation, similar to Equation (141), which includes transport due to the electric field and also concentration gradient diffusion.

It is then possible to obtain the concentration distribution as a function of $U_{12}/\bar{D}$ and time by solving the partial differential equation obtained by applying the continuity equation to this general flux expression. This has been done by Bagoyavlenskii[136] and Pikus[169] for different boundary conditions. Consequently, the parameter β may be determined from analysis of the concentration distribution in the separation tube at any time t, or at the steady state. A disadvantage of this method is that β is a function of the diffusion coefficient and will therefore be affected by any errors resulting from convection. The values of β are on the order of 10^{-1}. The values of μ are on the order of 10^{-5}.

The temperature dependence of β has been determined in Hg by Bogoyavlenskii[134] and in Ga by Roth.[136] Both investigators found β to be a linear increasing function of T, which means that the differential mobility, U_{12}, should be exponential in temperature following the diffusion coefficient. This does not agree with de Gennes theory, (see Equation 52) which predicts U_{12} to vary as D/T^3. Lodding[130] has recently remeasured the temperature dependence of μ in Rb, K, and In. He found μ to be proportional to T^3, which means that the differential mobility U_{12} should be proportional to T^2. This result is not in agreement with Bogoyavlenskii's but does seem closer to de Gennes' theory.

Lodding's thesis[137] on the Haeffner effect has recently been published. An excellent review is provided and the details of the results published in reference (130) are given. Some interesting work on self diffusion coefficients is also presented. Both parameters β and μ were determined and D* was calculated from them. In the case of indium it is possible to compare the results with data on D* obtained by the

capillary technique. The electrotransport value is 42×10^{-5} cm^2/sec compared to an average literature value of 31×10^{-5}. The electrotransport value of the activation energy is 1.64 kcal/mole compared to 2.52 by the capillary technique. The discrepancy is in the direction predicted by errors resulting from convection.

It might also be noted that Haeffner[132] has found a small isotope separation on passing a high D.C. current through a solid uranium wire. Lodding[137] has done some unpublished work on solid indium metal.

CHAPTER IV

ELECTROTRANSPORT IN LIQUID METAL ALLOY SYSTEMS

In this chapter a rather simplified phenomenological theory of electrotransport in liquid metal alloys is presented. It is based largely on the theoretical developments discussed in Chapter II. In addition, a discussion is presented of the influence of the electrokinetic effect upon the experimental determination of electrotransport in liquid metal alloys.

Discussion of Theoretical Aspects

Transport processes, by their nature, involve the flow of a component within a system. This flow is generally described as the flux of the moving component, where the flux is defined as the quantity of material passing across a plane perpendicular to the flow per unit area and unit time. The magnitude of such a flux depends upon the coordinate system chosen as a reference. Consequently, in order to fully specify a flux, it is necessary to explicitly state the reference system. In general, the flux of component i can be expressed as the velocity of component i times its concentration. The flux then, can be specified by the following equation,

$$J_i^a = N_i v_i^a \,, \tag{107}$$

where the superscript ,a, refers to the velocity of the coordinate system chosen as a reference. A number of different reference systems can be chosen to describe any experiment. These reference systems are frequently different from that of an observer who remains stationary with respect to

the apparatus containing the material under investigation. To avoid confusion concerning reference systems, the following nomenclature will be used. A superscript will be used to specify the reference coordinate system velocity, as in Equation (107). However, no superscript will be used when the reference velocity is an observer who is stationary with respect to the apparatus holding the material under investigation. Equation (107) may also be written as follows,

$$J_i^a = N_i(v_i - v_a) \quad . \tag{108}$$

The total flux of component i with respect to the observer may be expressed as,

$$J_i = N_i v_i \quad . \tag{109}$$

If one now combines Equations (108) and (109) the total fluxes of the two components of a binary system may be written as,

$$J_1 = N_1(v_1 - v_a) + N_1 v_a \quad , \tag{110}$$

$$J_2 = N_2(v_2 - v_a) + N_2 v_a \quad . \tag{111}$$

Equations (110) and (111) combine to give,

$$J_1 X_2 - J_2 X_1 = X_1 X_2 N_o (v_1 - v_2) \quad , \tag{112}$$

where the molar concentration has been written as $X_i N_o$. This equation is completely general. It is the relation between the observed fluxes and the relative velocity of the migrating components in a binary system.

In Chapter I the electric mobility of a component was defined as the velocity per unit electric field. This may be stated more generally as,

$$u_i = \left[\frac{v_i}{E}\right]_{\Delta N_i,\ \Delta T = 0} . \tag{113}$$

Hence for an electrotransport experiment performed under conditions of constant composition and temperature, Equation (112) may be written as,

$$J_1 X_2 - J_2 X_1 = X_1 X_2 N_o (u_1 - u_2) E . \tag{114}$$

A differential mobility is now defined as,

$$U_{12} = u_1 - u_2, \quad U_{21} = u_2 - u_1 . \tag{115}$$

This differential mobility is independent of the reference system velocity.

In order to determine U_{12} from experiment it is necessary to measure J_1 and J_2 independently. If the experimental technique imposes a relation between the two fluxes it is only necessary to measure one flux. In this work electrotransport is measured in liquid metals across the mouth of a closed end capillary tube. It is shown in Chapter V that the conditions of constant volume are maintained in this technique under certain restrictions. The relation between the observed fluxes may therefore be written as,

$$J_1 \bar{V}_1 + J_2 \bar{V}_2 = 0 . \tag{116}$$

By combining Equations (114), (115) and (116), the expression for the fluxes of component 1 and 2 may be written as,

$$J_1 = U_{12} N_1 N_2 \bar{V}_2 E, \quad J_2 = U_{21} N_1 N_2 \bar{V}_1 E. \tag{117}$$

Alternate expressions for the fluxes are easily obtained from Equation (114) for other experimental conditions, such as those of zero mean mole or mass velocity.

It is possible to relate the differential mobility to the mutual diffusion coefficient. From Equations (9) and (12) the electric mobility may be related to the absolute mobility as,

$$u_i = eB_i Z_i^o \ . \tag{118}$$

Therefore Equation (115) may be written as,

$$U_{12} = e\ [B_1 Z_1^o - B_2 Z_2^o] \ . \tag{119}$$

By combining Equations (12) and (4) the force balance may be written, for a binary system as,

$$N_1 Z_1^o + N_2 Z_2^o = 0 \ . \tag{120}$$

Substitution of Equation (120) in Equation (119) gives,

$$U_{12} = eZ_1^o\ [B_1 + B_2 \frac{N_1}{N_2}] \ . \tag{121}$$

Darken[138] has shown that if one takes the driving force for diffusion to be the gradient of the Gibbs chemical potential, the "intrinsic" diffusion coefficient may be related to the absolute mobility as,

$$D_1 = kTB_1 \frac{d\ell na_1}{d\ell nN_1} \ , \tag{122}$$

where D_1 is the diffusion coefficient measured using the gradient of the concentration in Fick's first law. The differential mobility may

then be written as,

$$U_{12} = \frac{eZ_1^o}{kT} \left[D_1 \frac{d\ell nN_1}{d\ell na_1} - \frac{X_1}{X_2} D_2 \frac{d\ell nN_2}{d\ell na_2} \right] . \tag{123}$$

If one assumes that the molar density, or alternately the molar specific volume, is constant during the experiment, it is possible to show by manipulation of the Gibbs-Duhem equation that

$$\frac{d\ell nN_1}{d\ell na_1} = \frac{d\ell nN_2}{d\ell na_2} . \tag{124}$$

It might be pointed out that it would not be necessary to assume constant molar volume if the diffusion coefficient were measured using the gradient of the mole fraction rather than molar concentration. However, since most of the literature data uses the concentration gradient, the above assumption is employed. Darken[138] had defined the mutual diffusion coefficient, $\bar{D}$, as $X_1D_2 + X_2D_1$. Substitution of this definition and Equation (124) into Equation (123) gives the following relation for the differential mobility,

$$U_{12} = \frac{eZ_1^o\bar{D}}{X_2kT} \frac{d\ell nN_1}{d\ell na_1} . \tag{125}$$

As pointed out in Chapter II, Mangelsdorf has given a fairly general development of an expression for the effective charge. If the electron-ion friction force is taken to be equal to the electron momentum flux times a friction coefficient, δ_i, the net force per ion becomes,

$$F_i = eZ_iE - \delta_i n_e v_e . \tag{126}$$

Such a formulation neglects momentum transfer from positive charge carriers. In Chapter II it was pointed out, that in view of Barnett's work, the theoretical justification for cathode-directed momentum transfer from defect electron is subject to question. Also, in Chapter III it was noted that Kuz'menko's results on self transport in Zn, Cd, and Sn indicate the absence of cathode-directed momentum transfer from defect electrons. In addition, Tieche[139] has recently published data on the Hall effect of ten liquid metals which indicate that all of the metals have negative coefficients including Zn and Cd, which have positive Hall coefficients in the solid state. This result would indicate that in liquid metals only a small percentage of the charge is transported by defect electrons. Neglect of cathode-directed momentum transfer from positive charge carriers in Equation (126) is justified on the basis of these arguments.

If Equation (126) is combined with Ohm's law and Equation (13), the expression for the effective valence becomes,

$$Z_i^o = \left[Z_i - \frac{\delta_i}{e^2\rho}\right] . \qquad (127)$$

The differential mobility may then be expressed as,

$$U_{12} = \frac{e\bar{D}}{X_2 kT} \frac{d\ell nN_1}{d\ell na_1} \left[Z_1 - \frac{\delta_1}{e^2\rho}\right] . \qquad (128)$$

Tieche[139] found that in eight out of nine liquid metals the Hall coefficient was independent of temperature; Cusack[31] and Tieche[32] obtained the same results for liquid mercury. It would appear then, that the true valence, Z_i, is probably temperature independent. It was

noted in Chapter III, that both Huntington and Kuz'menko have shown by experiment that the friction coefficient, δ_i, is independent of temperature in solid pure metals. Consequently, it should be possible to predict the temperature dependence of the differential mobility from a knowledge of the temperature dependence of the mutual diffusion coefficient, the resistivity, and the activity.

In dilute solutions Equation (128) reduces to,

$$U_{12} = \frac{eD_1}{kT} \frac{d\ell nN_1}{d\ell na_1} \left[Z_1 - \frac{\delta_1}{e^2\rho}\right] \tag{129}$$

$$U_{21} = \frac{eD_2}{kT} \frac{d\ell nN_2}{d\ell na_2} \left[Z_2 - \frac{\delta_2}{e^2\rho}\right] . \tag{130}$$

In a dilute solution the measured transport velocity of the solvent approaches zero and its electric mobility therefore appraoches zero, so that $U_{12} = u_1$ in Equation (129) and $U_{21} = u_2$ in Equation (130). The fact that the measured electric mobility of the solvent approaches zero in dilute solutions indicates that the self transport of the solvent is negligibly small in these experiments.

There is an alternate way of presenting data which might have been used. Equation (110) is written for an arbitrary reference velocity. A volume velocity, v_v, may be defined as the reference velocity from a volume balance across a plane perpendicular to the flow direction at the capillary mouth,

$$N_o v_v \bar{V} = v_v = \sum_{i=1}^{n} N_i v_i \bar{V}_i . \tag{131}$$

Equation (110) may be rewritten as,

$$J_1 = J_1^v + N_1 v_v . \tag{132}$$

Because Equation (116) applies in the work on the Bi-Sn system at any point along the capillary, it is apparent from Equation (131) that the volume velocity v_v is zero. Consequently, the fluxes may have been written as,

$$J_1 = N_1 u_1^v E \ , \quad J_2 = N_2 u_2^v E \ . \tag{133}$$

By comparison to the flux equations used in this work, Equations (117), the relation between the mobility using the volume velocity reference and the differential mobility may be obtained,

$$u_1^v = U_{12} N_2 \bar{V}_2 \ . \tag{134}$$

Other reference velocities, such as the mean mass velocity or mean atom velocity, might also have been used to present the data. The resulting mobility for each reference velocity is slightly different. If the reference velocity is taken as the mean atom velocity, v_A, or the mean mass velocity, v_M, it may be shown by similar arguments that,

$$u_1^A = X_2 U_{12} \ , \quad u_1^M = X_2' U_{12} \ . \tag{135}$$

The mean velocities used here are simply the total net atom or mass flux divided by the overall atom or mass density. The data can be presented in terms of any one of the above mobilities. The differential mobility has the advantage that it may be related to the mutual diffusion coefficient rather than the intrinsic coefficient. In the case of dilute solutions, all of the above mobilities become equal.

It may be noted from Chapter III, that much of the experimental work on electrotransport has been done by analysis of steady state

experiments, i.e., experiments which have been run to the point where the electrotransport flux is exactly balanced by a back diffusion flux so that there is no net mass transfer. It is therefore useful to relate the differential mobility to the results of steady state experiments. When the mass transport is produced by both an electric field and a concentration gradient, the flux equation for the components of a binary system may be written as,

$$J_1 = N_1 u_1 E - D_1 \frac{dN_1}{dZ} , \tag{136}$$

$$J_2 = N_2 u_2 E - D_2 \frac{dN_2}{dZ} . \tag{137}$$

At the conditions of steady state there is no net mass transport within the system, so that both fluxes would be zero. Therefore, Equations (136) and (137) may be combined to give the following relation for steady state conditions,

$$\frac{U_{12}}{\bar{D}} = \frac{N_o}{N_2 E} \frac{d\ell n N_1}{dZ} , \tag{138}$$

where constant molar density has been assumed. Hence, the steady state results may be interpreted in terms of the differential mobility and the mutual diffusion coefficient. If the mutual diffusion coefficient is measured using the concentration gradient, this relation is limited by the assumption of constant molar density. If mole fraction gradient is used when measuring $\bar{D}$, the relation is general, however, N_1 must be replaced by X_1.

The above steady state relationship may be reduced to the following form by combination with Equation (125),

$$\frac{d\ln a_1}{dZ} \frac{eEZ_1^o}{kT} . \tag{139}$$

This is the same equation derived by Belashchenko. Since the mutual diffusion coefficient does not appear, the relation is not limited by the assumption of constant molar density.

Discussion of Experimental Aspects

Two independent studies on electro-kinetic effects in liquid metals have recently appeared in the literature. The problem is treated theoretically by Fiks and Pikus,[140,141] and both theoretically and experimentally by Klemm.[142,143] The theoretical treatments are similar. Due to diffusive reflection of conduction electrons at the container walls, the electron-ion drag force is diminished slightly as the wall is approached. Consequently, the field force outweighs the electron-drag force in the boundary layer, and the ions are pulled toward the cathode. In experiments on liquid mercury, Klemm[142] has observed transport to the cathode as predicted. He characterizes the flow with the electrokinetic mobility, α, defined as the velocity per unit electric field in a medium where the pore diameter is much larger than the mean free path of the electrons. The values of α at 80°C were found to be around 2.5×10^{-3} cm^2/volt-sec in containers of iron, platinum, glass, and p or n-germanium. The effect appears to be approximately a factor of 10 larger than the electric mobilities of solutes in mercury.

In electrotransport experiments on liquid metals in a closed capillary, this electrokinetic effect would cause a longitudinal flow of the metal at the capillary walls relative to the metal in the central

portion of the capillary. This counter-flow would produce convection currents in the capillary, and the diffusion would be characterized by an effective diffusion coefficient which would be the sum of the convective and the ordinary diffusion coefficients. It can be seen from Equation (138), that the concentration profile in steady state electrotransport experiments is a function of the mutual diffusion coefficient. Consequently, large effective diffusion coefficients would cause an error in the results of such experiments. This difficulty will not arise in experiments which determine the differential mobility independent of concentration gradients, such as the experiments of Mangelsdorf[121] and Lodding.[129]

Belashchenko[120] has conducted some experiments to estimate the effective diffusion coefficient in steady-state electrotransport experiments. He has determined the effective valence as a function of field strength in the Co-Sn system at 350°C. At high current densities the effective valence decreases. This decrease is attributed to convective mixing arising from the electrokinetic effect. Unfortunately, the units of the field strength are not given so that it is not possible to determine the range of current densities over which the effective charge is a function of field strength.

CHAPTER V

EXPERIMENTAL INVESTIGATIONS

As mentioned in Chapter III, a considerable amount of work has been done in the past on electrotransport in liquid alloy systems. In most of this work however, the data is subject to errors due to convective mixing within the capillary and segregation upon freezing. The aim of the experimental program of this work was to develop a technique, free from the above mentioned errors, for quantitatively determining the electric mobility at high temperatures.

General Considerations

After a number of preliminary experiments it appeared that a one ended reservoir method provided the best experimental technique. This method is similar to the capillary technique used for determining diffusion coefficients in liquid metals. A metal electrode is sealed into one end of a capillary and the capillary tube is held vertically beneath the surface of a relatively large reservoir of the alloy under investigation. A D.C. electric current is passed through the metal within the capillary causing the solute to diffuse in-to or out-of the open end of the tube depending on the polarity. Under the constant volume restriction of Equation (116), the total mass transport of solute across the tube mouth may be expressed as,

$$J_1 = U_{12} N_1 N_2 \bar{V}_2 E \ . \qquad (140)$$

Since the reservoir is very large compared to the capillary, the composition of the reservoir will be essentially constant. This means that all the terms of Equation (140) will be constant for a given isothermal experiment,

since the metal at the capillary mouth is in direct contact with the reservoir. Such a conclusion assumes the absence of a concentration buildup in the region of the reservoir surrounding the capillary mouth. The total mass transfer between the capillary and reservoir can be determined from the difference in the composition of the reservoir metal and the average composition of the capillary metal. The differential mobility, U_{12}, may then be determined by a simple mass balance using Equation (140).

This technique does not require a concentration profile in order to determine the mobility. Since the capillary may be separated from the reservoir before solidification, the method is not subject to errors due to segregation. Three basic requirements must be fulfilled however: (1) the composition must be constant at the capillary mouth, (2) there must not be any transport across the tube mouth by a diffusion process, and (3) the constant volume restriction of Equation (116) must hold.

The following considerations indicate that the first requirement will generally be fulfilled. By manipulation of Equation (140) it can be shown that the divergence of the net mass flow across the tube mouth and out into the reservoir is zero; i.e., the net mass flow is independent of the area of the conducting column. Consequently, the solute is not simply deposited into the reservoir at the capillary mouth, but is moved right out into the reservoir, thereby avoiding a concentration buildup. The same argument holds for the case where the solute is run into the capillary.

The second requirement may be analysed as follows. Since the initial composition in the capillary is uniform, the electric field produces a constant flux of solute at all points inside the capillary except at the upper closed end where the flux is necessarily zero. Consequently, after the current is turned on, the capillary composition will remain constant

throughout, except at the closed end, where it will either increase or decrease depending on the polarity. As time proceeds, this changing composition will broaden out toward the mouth of the tube and eventually establish a concentration gradient at the capillary mouth as shown in Figure 1. The rate of broadening will depend upon the magnitude of the diffusion coefficient. Convective mixing will simply increase the rate of broadening; it will not produce a net flux across the tube mouth since the concentration is constant across the amouth. And so, contrary to the steady state method used by many investigators, this technique is not subject to errors due to the convection such as might be produced by the electrokinetic effect discussed in the last chapter. In order to fulfill the second requirement then, it is simply necessary to terminate the experiment before an appreciable gradient is established at the tube mouth.

A detailed discussion of the third requirement is given in Equations (160) to (165). It is concluded that the constant volume restriction holds in ideal solutions and also in dilute solutions. The nature of this third requirement is different than that of the first two, since it is the result of the form of the flux equation, Equation (140). Other experiments could be devised which would require alternate restrictions such as constant mass or constant moles. The constant volume restriction was used here because it is valid for the systems studied with the present experimental technique.

This experimental technique requires some method of determining the mean concentration of the capillary metal. Two methods have been developed, one employing chemical analysis and the other a resistivity analysis. The resistivity technique has proven to be much more precise.

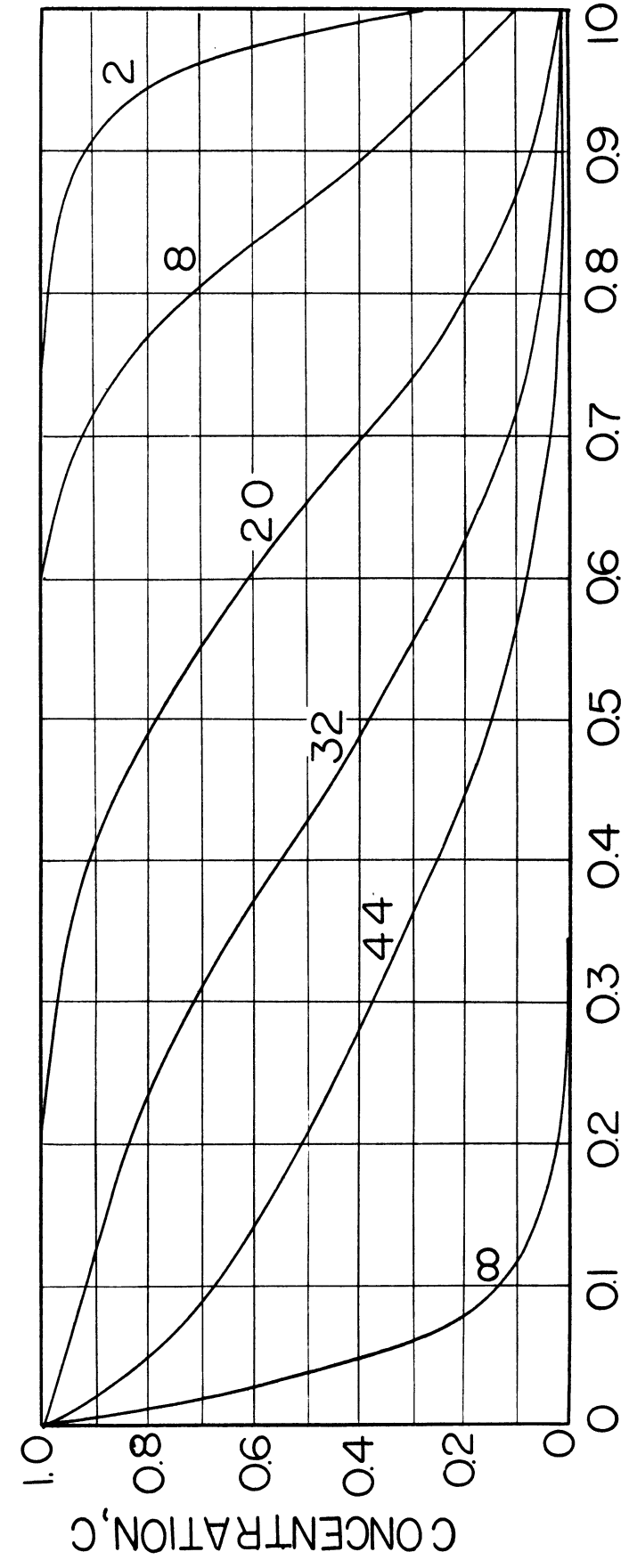

Figure 1. Concentration Distribution, Parameters of Time in Hours, S = -20, $D/a^2 = 9 \times 10^{-4}$ per sec.

Mathematical Description

In order to facilitate the design of experiments a mathematical description of the process has been worked out. The general flux expression including mass transport from both an electric field and a concentration gradient may be written as follows,

$$J_1 = N_1 u_1 E - D_1 \, dN_1/dZ \, . \qquad (141)$$

The mobility and the diffusion coefficient in this expression have the observer as a reference velocity. The general partial differential equation for the process may be obtained from a differential mass balance, which is equivalent to applying the continuity equation, $\partial N_1/\partial\theta = -\partial J/\partial Z$. It is assumed that u_1, D_1, and E are constant with E approximated by the total voltage drop, V, divided by the capillary length, a, to give,

$$\frac{\partial N_1}{\partial \theta} = D_1 \frac{\partial^2 N_1}{\partial Z^2} - \left(\frac{u_1 V}{a}\right) \frac{\partial N_1}{\partial Z} \, . \qquad (142)$$

This partial differential equation is simplified by substitution of the following dimensionless groups,

$$X = \frac{Z}{a} \, , \quad S = \frac{u_1 V}{D_1} \, , \quad C_1 = \frac{N_1}{N_o} \, , \quad t = \frac{D\theta}{a^2} \qquad (143)$$

so that Equation (142) becomes,

$$\frac{\partial C_1}{\partial t} = \frac{\partial^2 C_1}{\partial X^2} - S \frac{\partial C_1}{\partial X} \, , \qquad (144)$$

under the additional assumption that the total molar density, N_o, is constant. This is the same partial differential equation encountered in sedimentation and thermal diffusion experiments. It has been solved by Mason and Wever,(144)

Furth,[145] DeGroot,[146] and Drakin[147] for various boundary conditions. None of these authors present the solutions for the boundary conditions of the present experiments, although two of them[144,147] have solved the equation for the case of a semi-infinite tube where the concentration remains constant at one end.

In collaboration with Mr. John Angus and Mr. Ward Bowsma, the author has solved this equation for the boundary conditions of the present experiments. The details of the mathematics involved have been presented in a separate report.[148] The solutions are presented in Appendix B. They are of a different form depending on whether the value of S is equal to, greater than, or less than 2. A literature search did not reveal a complete set of the roots of the eigenfunctions. Therefore, a listing of the roots of the two eigenfunctions, as calculated on a digital computer using the half interval method, are also included in Appendix B.

Figure 1 is the predicted concentration profile as a function of time and distance in an experiment where the solute is moved out of the capillary. The figure predicts that the experiment would have to be terminated sometime between 20 and 32 hours in order to avoid errors due to back-diffusion across the capillary mouth. By integrating the mathematical solutions over the length of the capillary, an expression is obtained for the mean tube concentration, C_m, as a function of time. Figure 2 shows the variation of the mean tube concentration versus a dimensionless time, τ. Positive values of S correspond to solute migration into the tube, negative values to migration out of the tube. Initially, C_m, varies linearly with time; then the effect of the back-diffusion flux at the tube mouth shows up as a departure from linearity and a gradual approach to a steady state value.

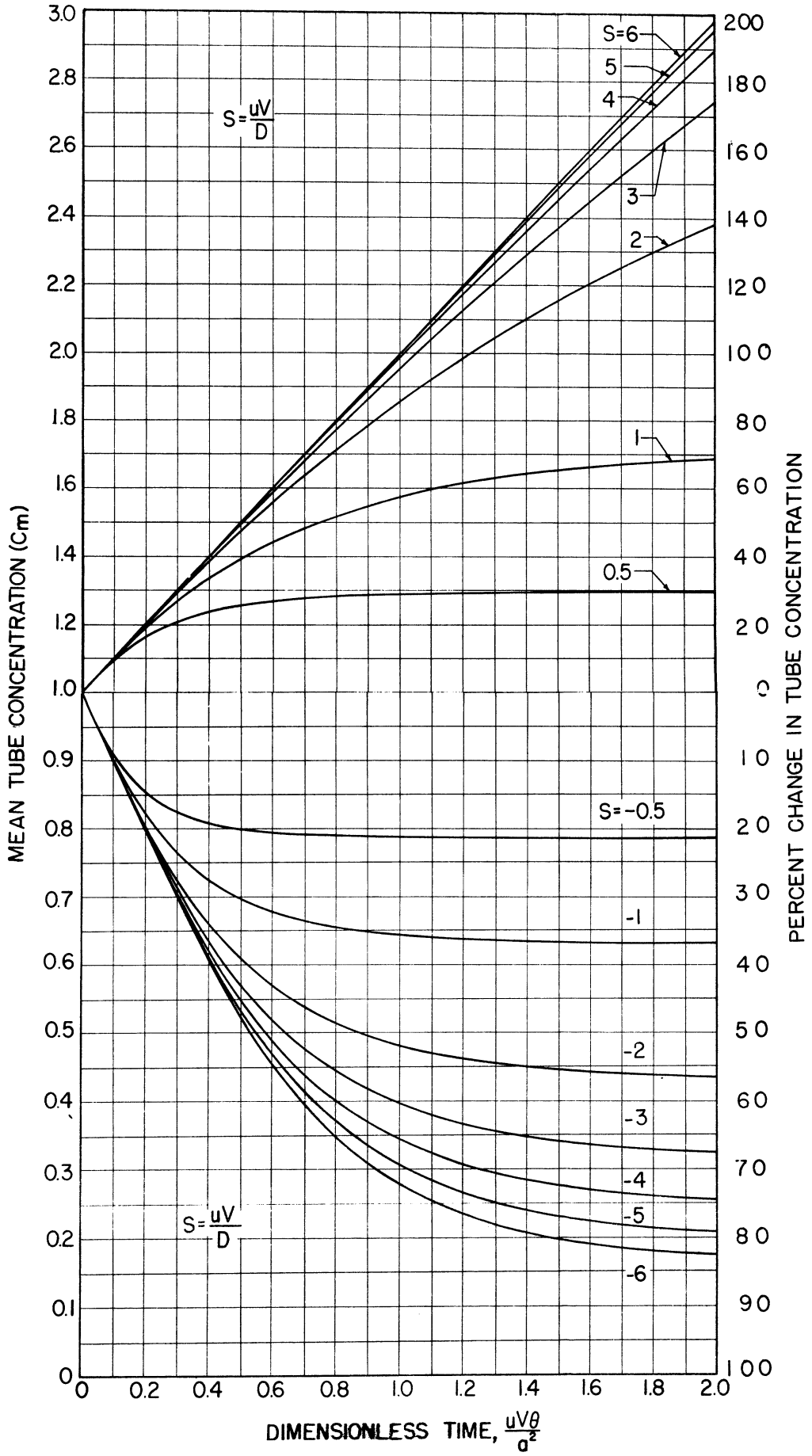

Figure 2. Cm vs. τ.

Equation (141) may be written in terms of the velocity of component 1 as follows,

$$v_1 = u_1 E - \frac{D_1}{N_1} \frac{dN_1}{dZ} \quad . \tag{145}$$

If this equation along with the corresponding expression for component 2 is substituted into Equation (112) and the constant volume restriction of Equation (116) is applied the following expression is obtained,

$$J_1 = U_{12} N_1 N_2 \bar{V}_2 E - N_o \bar{V}_2 \bar{D} \frac{dN_1}{dZ} \quad , \tag{146}$$

where it is necessary to assume constant molar density. Again, it may be noted that this assumption would not be required if the driving force for diffusion were written as the gradient of the mole fraction. The mobility and the diffusion coefficient in the solution of the partial differential equation may be related to the differential mobility and the mutual diffusion coefficient by comparing Equations (141) and (146). Hence, in the present experiments, the mobility of Equation (141) is related to the differential mobility by Equation (134); the diffusion coefficient of Equation (141) is equal to the mutual diffusion coefficient times $N_o \bar{V}_2$.

The mathematical description of this process may also be obtained by first applying the restriction of constant volume to the flux expression and then forming the partial differential equation from the resulting flux equation. Using this method, Pikus[165] has shown that if one assumes constant molar density, constant electric field, and $[(D_1 - D_2)/D_1] << 1$, the partial differential equation may be reduced to a solvable non-linear equation in the dependent variable $N_1 \cdot \bar{V}_1$. If one further assumes the

partial molar volume, $\bar{V}_1$, to be constant, a solution may be obtained for the differential mobility, U_{12}, as a function of composition and time. Bogoyavlenskii[133] has presented the solution of this non-linear equation for the boundary conditions of the present experiments. This approach has the disadvantage that it is necessary to solve a non-linear partial differential equation.

Chemical Analysis Technique

Acknowledgement--This technique was developed in collaboration with fellow graduate student, John C. Angus. The work is therefore included in this thesis with the qualification that it is only partially the original work of this author.

Experimental Design--The changing capillary composition is followed in this technique by means of chemical analysis. The experimental apparatus is shown in Figure 3. After heating to temperature under vacuum, the capillaries are lowered beneath the surface of the molten alloy and then filled by introducing helium pressure. Current is passed down one tube and up the other for a given time; the tubes are then raised out of the melt, solidified, and the composition of the entire capillary is determined by chemical analysis. The difference of the mean capillary composition and the reservoir composition is related to the atoms transported, $\Delta N_2'$ in-to or out-of the reservoir. By making a simple mass balance across the capillary mouth using Equation (140) the following expression is obtained for the electric mobility,

$$U_{12} = \frac{1}{N_1 N_2 \bar{V}_2 \rho I} \frac{\Delta N_1'}{\Delta \theta} \quad . \tag{147}$$

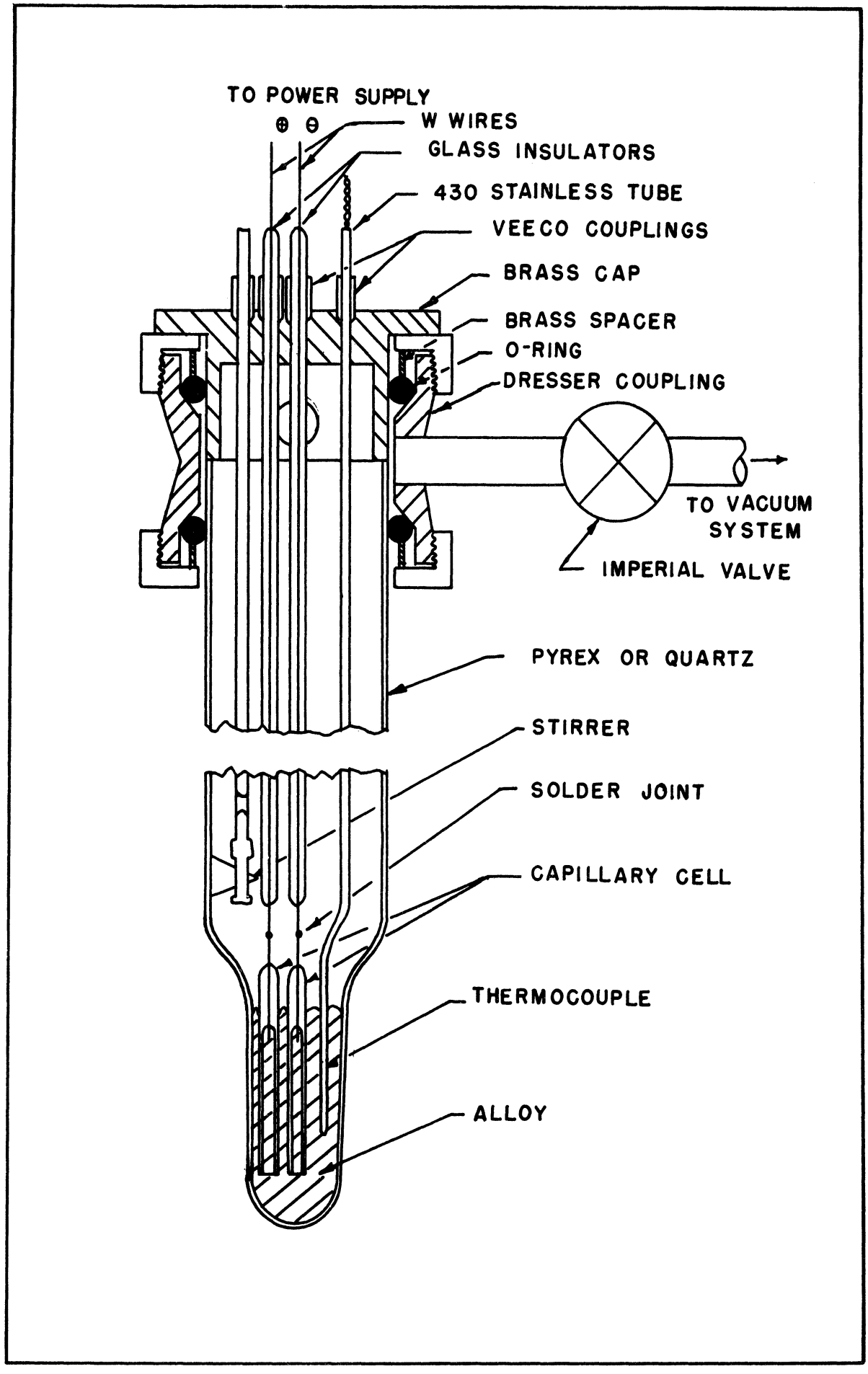

Figure 3. Electrotransport Cell.

For a dilute solution of 1 in 2, $N_2\bar{V}_2 \cong 1$, and U_{12} approaches u_1 so that this equation simplifies to the following form,

$$u_1 = \frac{1}{N_1 \rho I} \cdot \frac{\Delta N_1'}{\Delta \theta} \quad . \tag{148}$$

The resulting mobility is determined for the conditions of composition and temperature prevailing at the mouth of the capillary.

The solutions to the partial differential equation described above have been used to estimate experimental design which would minimize errors due to back diffusion. From the solutions it is possible to calculate the ordinary diffusion flux across the tube mouth as a function of time. The error in the mobility due to this diffusion flux may then be calculated as a function of the percent change in tube concentration as in Figure 4. From these plots it is seen that at constant S, the error is much smaller when the solute is run into the tubes. Also, larger values of S give smaller errors. The electric mobility and the diffusion coefficient are fixed by the system so that S can only be increased by increasing the voltage drop, V, across the capillary. This may be done by increasing the field strength or the tube length. The field strengths are limited by the I^2R heat generation to values of around 0.2 V per cm. It can be seen from Figure 2, that the effect of increasing the tube length, a, will be to increase the time required for a given concentration change.

There is always a certain error associated with chemical analysis. Unfortunately, the mobility is calculated from the difference of the capillary analysis and the reservoir analysis. For small concentration changes, these numbers will be of the same magnitude, and hence the analytical error will show up as a much larger error in the mobility. The factor by which the

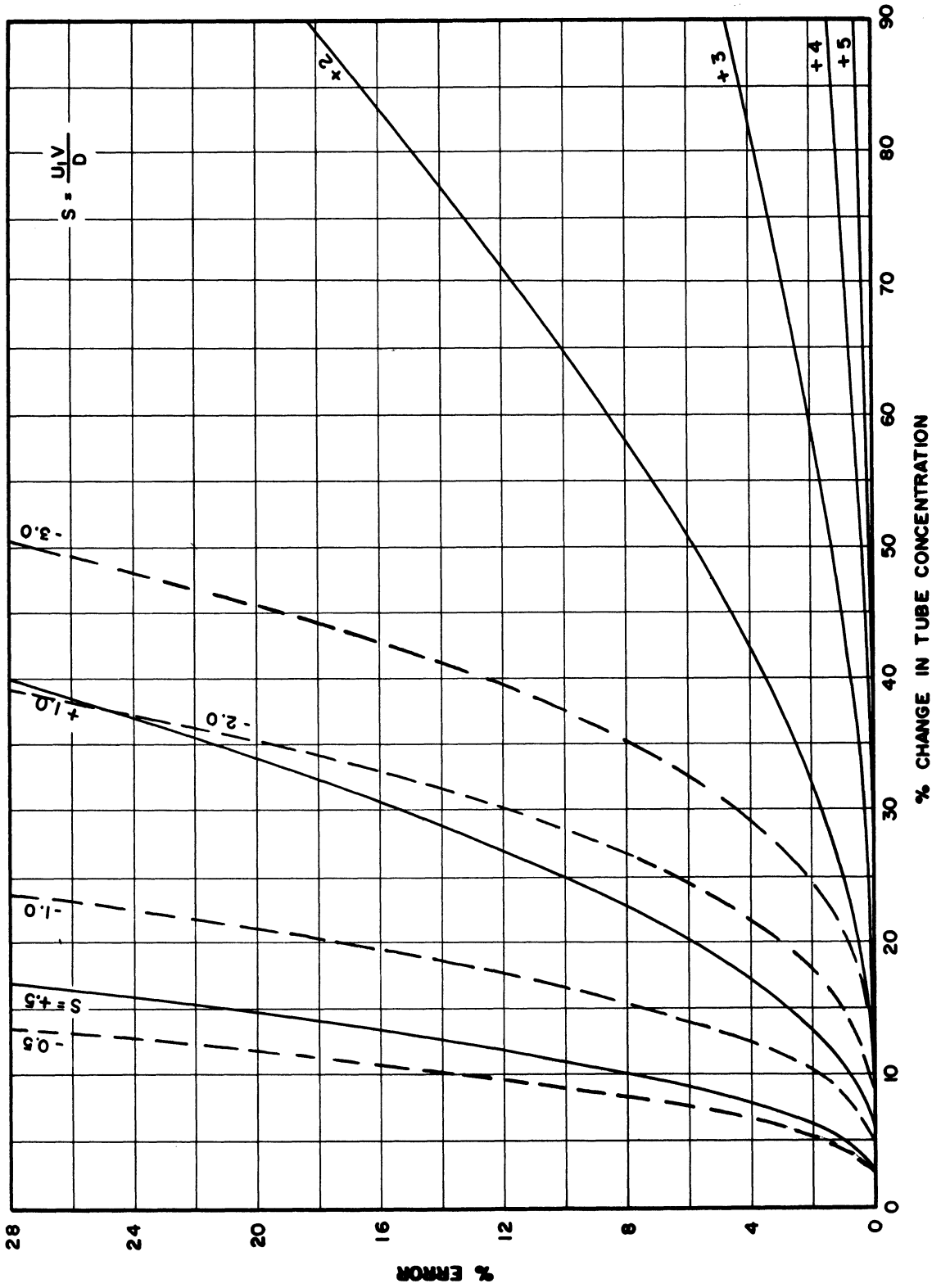

Figure 4. Percent Error in Mobility vs. Percent Change in Tube Concentration.

analytical error is magnified is shown as a function of the percent change of capillary concentration in Figure 5. This error may be reduced slightly by analysing more than one sample from the reservoir (n in Figure 5).

The errors due to ordinary diffusion across the mouth increase with concentration change according to Figure 4, while the analytical errors decrease with concentration change according to Figure 5. Hence, it is possible to design experiments from these plots in Figure 2, which produce concentration changes corresponding to minimum errors. The design may be checked experimentally by determining the reproducibility of the mobility for different concentration changes.

Experimental Procedure--The apparatus is shown in Figure 3. The capillaries were made of pyrex or quartz with a 0.008-in. tungsten electrode sealed into one end. The wall thickness was varied between 0.13 and 0.26 mm and the inside diameter between 0.5 and 1.0 mm. The capillary length was varied between 3 and 10 cm and in some runs the capillary was bent into a U-shape to reduce convection effects. The stirrer consisted of a sheet of molybdenum cut into the shape of a disk slightly smaller than the reservoir diameter. The disk was supported horizontally on the end of a Pyrex rod; an up-and-down vertical motion through the melt gave a thorough mixing action. AISI No. 430 ferritic stainless was used as a thermocouple shield material. It contains Fe, Cr, and C, none of which are appreciably soluble in the bismuth alloys investigated. The apparatus was heated to temperature in a resistance wound hinged furnace made by Hevi-Duty. Temperature control was provided by either an on-off Leeds and Northrup Micromax or a proportionating Wheelco controller. The maximum temperature variation throughout a run was generally ± 5°C. In order to avoid convection the top of the

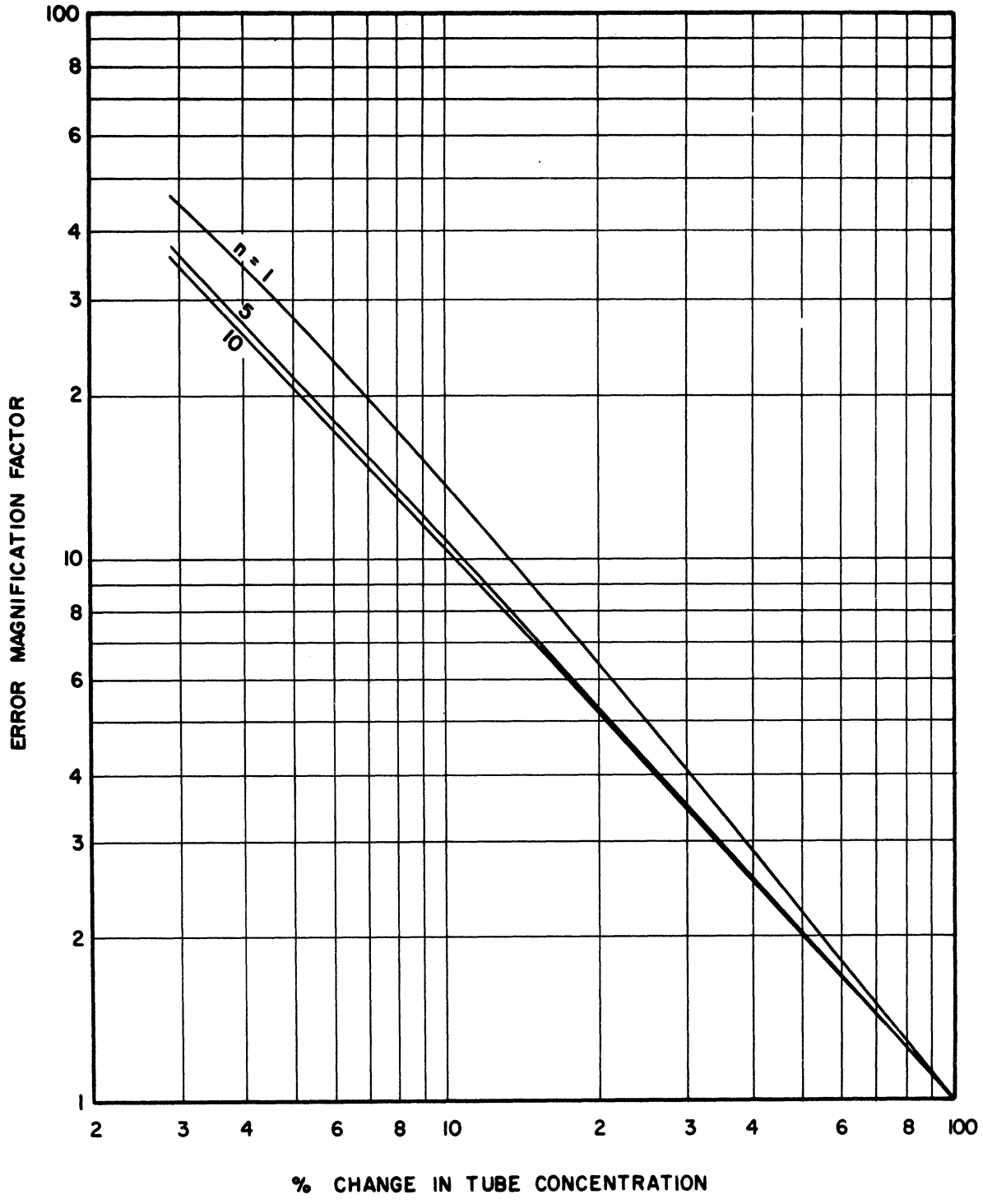

Figure 5. Error Magnification in Mobility Calculation.

reservoir was maintained slightly hotter than the bottom. The gradient was around 0.7°C per cm. The current was determined by measuring the voltage drop across a maganin shunt which was previously calibrated against Leeds and Northrup 0.1 ohm No. 301185 standard resistor. Voltages were measured with Leeds and Northrup model 8662 potentiometer. The current was supplied by either a Udylite model 2006-DU2 or Nobatron model E-28-10 rectifier. The ripple was less than 2% as measured on an oscilloscope and the current remained constant to ±1% in all of the runs. Matched 28 ga. Chromel-Alumel thermocouple wire was used to measure the temperature. During the course of the experiments, a number of thermocouples were used, all from the same spools. Two couples were calibrated against Leeds and Northrup No. 1035408 standard Pt-10% Rh thermocouple wire and against the melting point of bismuth; the results are shown in Appendix C. The couples were consistently 1 to 2°C off. All of the temperature measurements were made with an ice bath cold junction and a Leeds and Northrup No. 8662 potentiometer. The vacuum system consisted of a liquid nitrogen cold trap and a Cenco Hyvac-2 fore pump connected with copper tubing and teflon diaphragm Imperial Brass Valves. The pressure was measured with an RCA 1946 thermocouple gauge at a point adjacent to the valve shown in Figure 3, on the pump side. The gauge was calibrated against a McLeod gauge and the system was capable of maintaining indicated pressures of around 10^{-3} to 10^{-4} mm Hg. The suppliers and their quoted purity on the metals used were as follows: Bi, Belmont Smelting, 99.998%; Cu, Baker and Adamson, 99.98%; Pd, Chemical Commerce, 99.98%; Ni, Allied Chemical, 99.5%; U, Mallinckrodt, 99.97%; Mg, Down Chemical Company, 99.98%.

The general operating procedure was as follows. With the capillaries, stirrer, and thermocouple raised above the weighed alloy in the bottom of

the pyrex or quartz outer tube, the apparatus was heated to about 100°C above the operating temperature under vacuum. After outgassing at this temperature overnight with occasional stirring, the capillaries were lowered into the melt and filled by introducing one atmosphere of helium pressure. The temperature was reduced to its operating value and the current was turned on for the desired time. The capillaries were then raised out of the melt and the apparatus was air cooled. In order to obtain samples of the reservoir, a number of short capillaries were sealed at one end and attached, mouth downward, parallel to the capillary cells. These were automatically filled during the run and provided reservoir samples of the same geometry as the capillary samples. The reservoir and run-tube samples were then analysed. Details of the analytical procedures are given in Appendix D.

Experimental Results--In all of the work bismuth metal was used as the solvent. The binaries Ni-Bi, Pd-Bi and the ternaries Cu-Ni-Bi, Cu-Mg-Bi, Cu-U-Bi, and Mg-Ni-Bi were studied. The raw data are listed in Appendix E.

The unrejected results for the binary systems are shown in Table XVI and the ternaries in Table XVII. The electric mobility, u_1, was calculated from Equation (148). The calculations are based on the resistivity and density of pure liquid bismuth. It is possible to make an estimate of the error in the mobility due to back diffusion for each individual run from the solution of the partial differential equation. This determination is simplified by constructing the cross plot of Figures 1 and 4 shown in Figure 6. Knowing the average value of the mobility, the dimensionless time is calculated and the corresponding error is obtained from Figure 6. The back diffusion error, calculated in this manner is

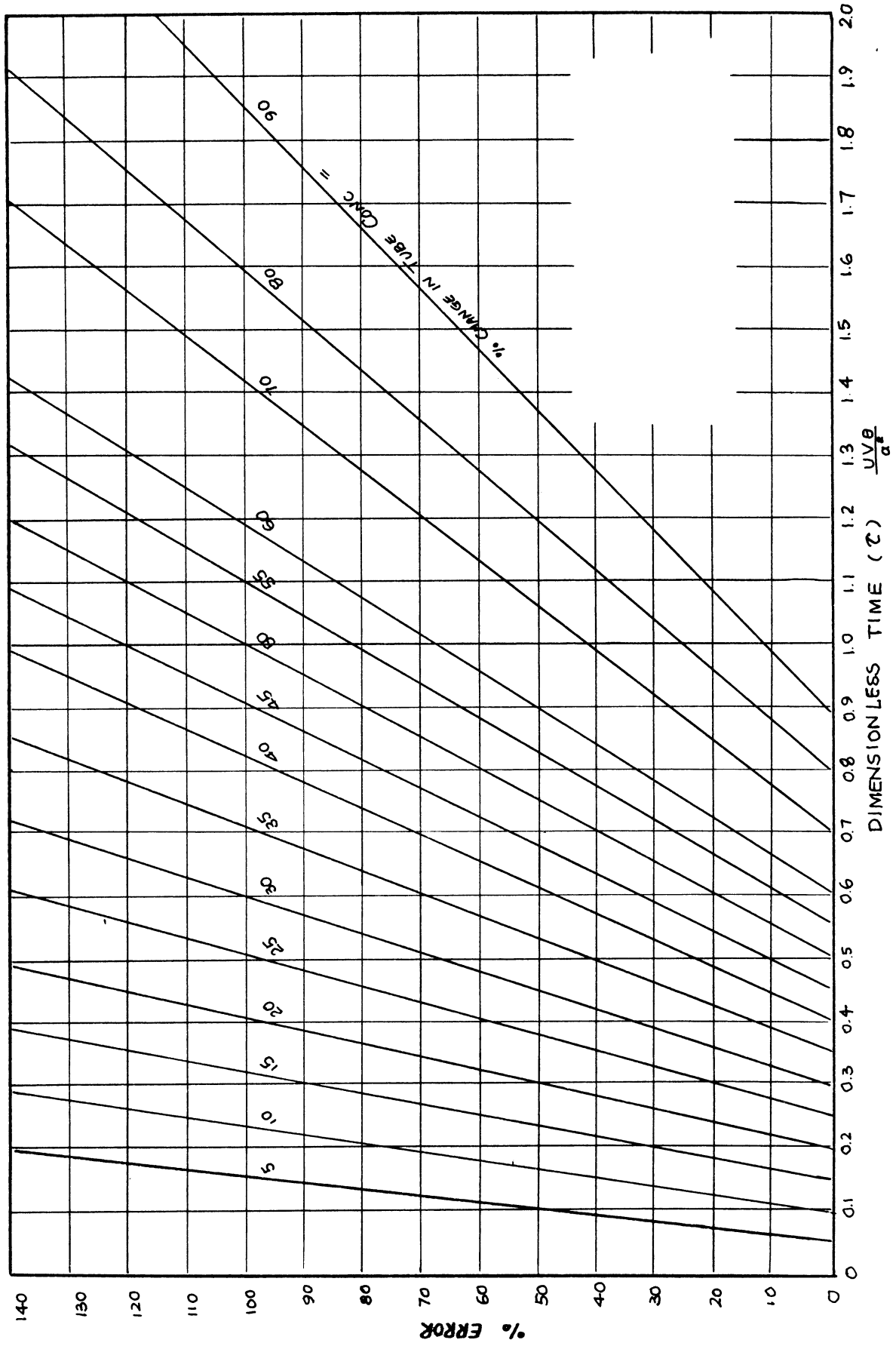

Figure 6. Per Cent Error in Mobility vs. Dimensionless Time (τ).

included in Tables XVI and XVII for each run. One might expect that since back diffusion errors cause low values of mobility, the highest experimental mobility is the best approximation of the true value. Such an assumption however, neglects errors from other sources. As can be seen from the data on nickel at 500°C, the back diffusion error, as calculated by the above procedure, is not the maximum with the lowest determined mobility.

Included in Tables XVI and XVII is an estimate of the error resulting from chemical analysis. As previously mentioned, a number of blank capillaries were analysed with each run to obtain the reservoir composition. From these data an estimate can be made of the standard deviation of an individual analysis for each run. By use of Figure 5 then, it is possible to estimate the deviation of the mobility as a result of errors in the chemical analysis. The average of this deviation divided by the square root of the number of measurements can then be compared to the statistical deviation of the average mobility. For the Ni binaries the estimated chemical analysis deviation is approximately 30% of the observed deviation of the mobility, whereas for Pd-Bi it is better than 100%. From Table XVI then, it appears that the chemical analysis error is limiting for Pd-Bi and the back-diffusion error is limiting for Ni-Bi.

Some of the raw data was not included in the average shown in Tables XVI and XVII. This data was rejected either because of high back diffusion errors or experimental irregularities. Some difficulty was encountered with Mg and U reacting with the pyrex capillaries. In attempting to eliminate the back diffusion errors, some of the capillaries were bent into a U shape. Theoretically, this would isolate the convective currents in each leg of the U. The results however, were inconclusive.

TABLE XVI

DATA ON Ni-Bi AND Pd-Bi

Capillary	Avg. Observed Composition, Wt. %	Temperature, °C	δ_1 (a)	% Error Due to Back Diffusion	Mobility, u x 10^4 $cm^2/V\text{-}sec$	Std. Dev. of Avg. Mobility x 10^4	Dev. of Avg. Mobility at 95% C.L. x 10^4 (St. t Dist.)
			Nickel in Bismuth				
40-1	.482 Ni	499	0.58	30	4.06		
40-2	.482	499	0.47	62	4.13		
43-1	.486	500	1.53	29	5.10		
43-2	.486	500	0.57	0	6.97		
47-1	.494	500	0.27	51	4.60		
Average	.486	500	$\frac{.68}{\sqrt{5}} = .30$	34	4.99	1.18	1.47
			Nickel in Bismuth				
50-2	.484 Ni	800	0.58	26	7.21		
52-1	.501	797	0.38	40	6.85		
52-2	.501	797	0.44	12	8.11		
Average	.495	798	$\frac{.46}{\sqrt{3}} = .27$	26	7.39	0.37	1.61
			Palladium in Bismuth				
1-A	.213 Pd	453	----	0	2.32		
1-C	.213	453	----	0	3.35		
2-A	.163	453	2.00	0	3.49		
2-B	.163	453	2.12	0	3.05		
Average	.188	453	$\frac{2.06}{\sqrt{2}} = 1.03$	0	3.05	0.26	0.82

(a) Deviation in u resulting from chemical analysis error (95% Conf. Level, Student t Dist.).

TABLE XVII

DATA ON TERNARIES

Capillary	Avg. Observed Composition, Wt. %	Temperature, °C	δ_1 (a)	% Error Due to Back Diffusion	Mobility, u x 10^4 $cm^2/V\text{-}sec$	Std. Dev. of Avg. Mobility x 10^4	Dev. of Avg. Mobility at 95% C.L. x 10^4 (St. t Dist.)
			Copper in Cu-Ni-Bi				
CT-2-2	.493 Cu	499	0.18	31	1.52		
CT-2-1	.493	499	0.24	29	1.54		
Average	.493	499	$\frac{.21}{\sqrt{2}} = .15$	30	1.53	--	--
			Copper in Cu-Mg-Bi				
CT-2-1	.372 Cu	344	2.20	40	1.43		
CT-3-1	.372	344	1.92	30	1.39		
CT-3-2	.372	344	0.58	0	3.74		
Average	.372	344	$\frac{1.57}{\sqrt{3}} = .91$	23	2.18	1.35	3.24
			Nickel in Ni-Mg-Bi				
CT-1-1	.299 Ni	350	1.37	113	2.55		
CT-1-2	.299	350	0.85	111	2.61		
Average	.299	350	$\frac{1.11}{\sqrt{2}} = .78$	112	2.58	--	--
			Nickel in Ni-Cu-Bi				
CT-2-1	.466 Ni	499	0.49	19	4.42		
CT-2-2	.466	499	0.39	42	4.15		
Average	.466	499	$\frac{.44}{\sqrt{2}} = .28$	31	4.28	--	--
			Magnesium in Mg-Ni-Bi				
CT-1-1	.269 Mg	350	1.28	80	6.03		
CT-1-2	.269	350	0.79	70	6.22		
Average	.269	350	$\frac{1.04}{\sqrt{2}} = .74$	75	6.10	--	--
			Magnesium in Mg Cu-Bi				
CT-3-1	.262 Mg	344	1.58	24	8.85		
CT-3-2	.262	344	1.38	32	8.26		
CT-3-3	.262	344	1.10	22	8.52		
Average	.262	344	$\frac{1.35}{\sqrt{3}} = .78$	26	8.54	.29	.71
			Uranium in U-Cu-Bi				
C-58	.142 U	475	0.63	0	3.69		
C-59-1	.154	475	1.26	60	1.98		
C-59-2	.154	475	0.41	11	2.79		
Average	.150	475	$\frac{.77}{\sqrt{3}} = .45$	24	2.82	.86	2.07

(a) Deviation in u resulting from chemical analysis error (95% Conf. Level, Student t Dist.).

Discussion of Results--The results of the experiments are summarized in Table XVIII and Figure 7. For the sake of comparison, the results of J. C. Angus on Cu-Bi, Zr-Bi, Mg-Bi, and U-Bi, taken with the same apparatus, are included. Whenever possible the solute was run into the capillaries, but in some of the ternaries the solutes migrated in opposite directions. The data for the ternary systems are based on only 2 to 4 experiments and hence are subject to large errors. They do, however, confirm that small additions of a second solute do not have a strong effect on the mobility of the first. As mentioned in the introduction, this work was originally initiated by the idea that electrotransport might afford a method of in-place separation of certain fission products from uranium in the fuel of a liquid-metal nuclear reactor. The results indicate that Cu and probably Mg could be separated from uranium in liquid Bi.

The Ni-Bi binary was run at two temperatures. These values are suspect because of the high back diffusion error and the relatively high scatter. However, they indicate a mild temperature dependence of the same magnitude found by Mangelsdorf for Hg-Cd[117] and by Schwarz for Ag-Zn.[149] The values found for the mobility in this study are of the same order of magnitude as those in liquid mercury at and around room temperature. This result might be expected, since the diffusion coefficient in various liquid metal systems is roughly the same.

In the experiments which gave large back diffusion errors it was possible to determine S from Figure 2, since the point would be off the linear portion of the curve. The diffusion coefficient could then be calculated from these values because u had been determined. The average

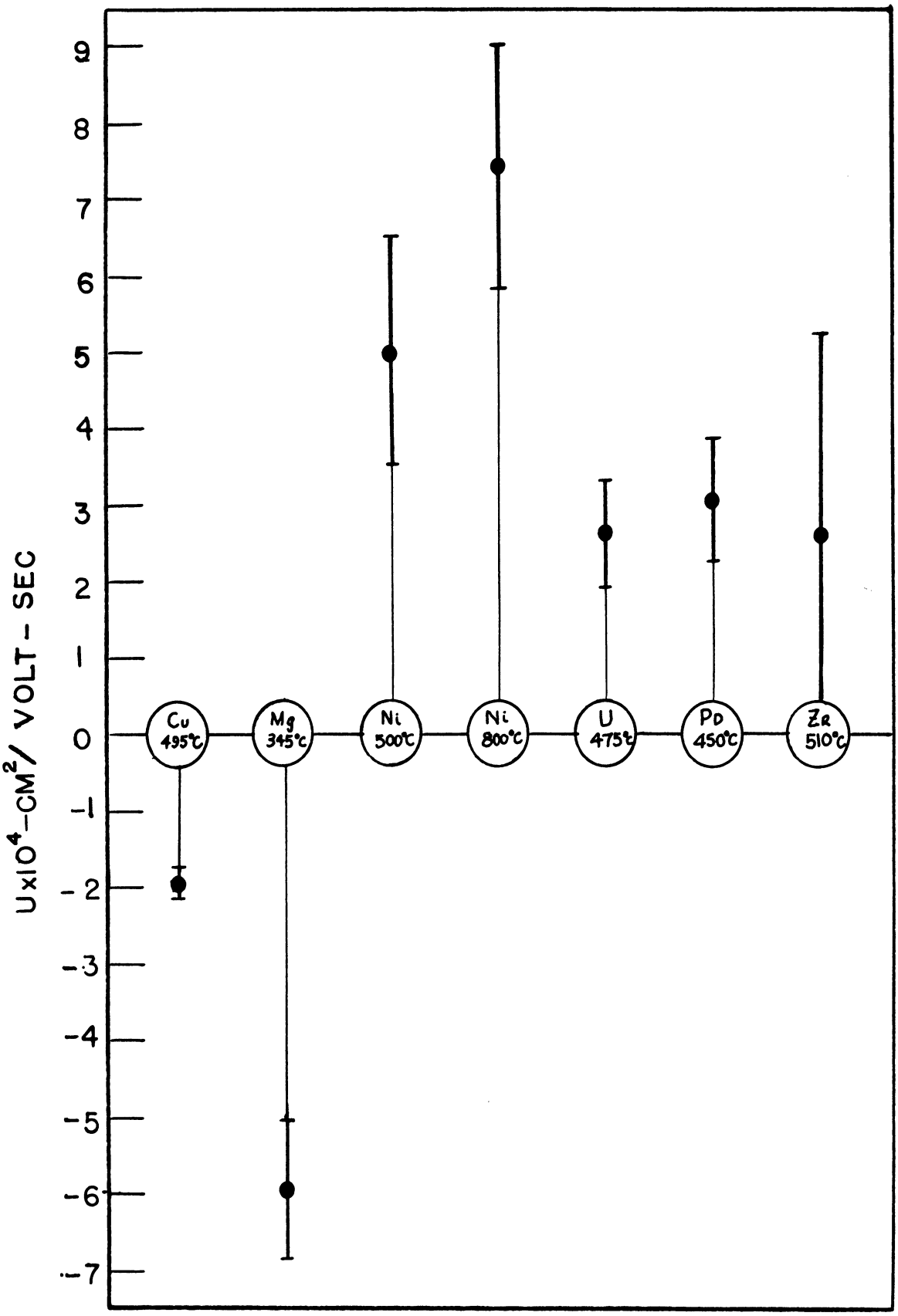

Figure 7. Mobilities in Bismuth.

TABLE XVIII

SUMMARY OF DATA BY CHEMICAL ANALYSIS TECHNIQUE

Migrating Element	Alloy	Temperature, °C	Avg. Composition of Migrating Element, Wt. %	(a) Average Mobility, u x 10^4 cm^2/V-sec	(b) Statistical Deviation in Average Mobility x 10^4
Palladium	Pd-Bi	453	.188	+3.05	0.82
Nickel	Ni-Bi	500	.486	+5.0	1.5
	Ni-Bi	798	.498	+7.4	1.6
	Ni-Cu-Bi	499	.497	+4.3	-(c)
	Ni-Mg-Bi	350	.286	+2.6	-
Uranium	U-Cu-Bi	475	.150	+2.8	2.1
	U-Bi(d)	478	.113	+2.57	0.67
Copper	Cu-Ni-Bi	499	.493	-1.5	-
	Cu-Mg-Bi	344	.372	-2.2	3.2
	Cu-U-Bi	475	.480	-2.1	0.6
	Cu-Bi(d)	495	.491	-1.95	0.28
Magnesium	Mg-Cu-Bi	344	.262	-8.5	0.7
	Mg-Ni-Bi	350	.269	-6.1	-
	Mg-Bi(d)	345	.508	-5.97	0.91

(a) Based on resistivity of pure bismuth.
(b) Deviation at 95% Conf. Level, Student t Dist.
(c) Only two measurements.
(d) Work of J. C. Angus.

value for D, determined in this manner, was around 25 x 10^{-5} cm^2/sec. This value is higher by a factor of about 5 than the usual values of D in liquid metals. This result might be taken as evidence of convective mixing within the tube. Hence, D must be interpreted as an effective diffusion coefficient.

It may be concluded that better experiments could be made by using longer capillaries with more than one bend, and by developing chemical analysis techniques which give high precision on small sample weights (0.1 gm). The method appears to be quite versatile because of its simplicity, so that extension to high melting metals such as iron seems quite feasible.

Electrical Resistivity Technique

In an effort to obtain more quantitative results, a new technique was developed which employed resistivity measurements as a tool for analysing the capillary composition. Such a technique has been employed in the past by Schwarz,[2] Mangelsdorf,[121] Drakin[113] and others. However, none of these authors have directly measured the electrical mobility at temperatures above 150°C. The development of this technique turned out to be quite difficult. The first major difficulty was encountered in the construction of a cell which would operate at high temperatures and be simple enough that it could be reused a number of times without breaking. This development took a little over a year; the details are described in Appendix F. The second difficulty resulted in a lack of reproducibility of the data, which was traced to a generation of a stray potential at the electrode contacts. Locating and eliminating this difficulty took about one year; the details are described in Appendix G. Only the final experimental design is discussed in this chapter.

Experimental Design and Calculation of Mobility--Electrotransfer experiments are easily carried out at constant current. Therefore, the resistivity of a segment of the capillary may be obtained by simply measuring the voltage drop across two probes along the length of the capillary. The concentration of the solute may then be determined from the concentration versus resistivity curve for the system being studied. If a number of probes are placed along the length of the capillary, it is possible to obtain an estimate of the concentration profile. Such an analytical technique has the advantage that it allows one to follow the concentration change during the actual experiment.

The capillary cells and the experimental apparatus used in this work are shown in Figure 8. After heating to temperature under vacuum, the capillaries are lowered beneath the surface of the molten alloy and then filled by introducing helium pressure. Current is passed down one tube and up the other and the voltage drop at the probes is measured as a function of time with a null detector. Analysis of the circuit diagram for Figure 8 will show that the measured voltage is the drop over the length of the capillary. The design of the cells at the upper electrode is fairly critical and is discussed in detail in Appendix G.

A mass balance across the capillary mouth gives the following expression for the total flux of component 1 across the mouth,

$$J_1 = \frac{1}{A_e} \frac{dN_1'}{d\theta} , \qquad (149)$$

where subscript e refers to conditions at the entrance of the capillary. The term $dN_1'/d\theta$ may be determined from the rate of change of the voltage drop if the relation between resistivity and concentration is known.

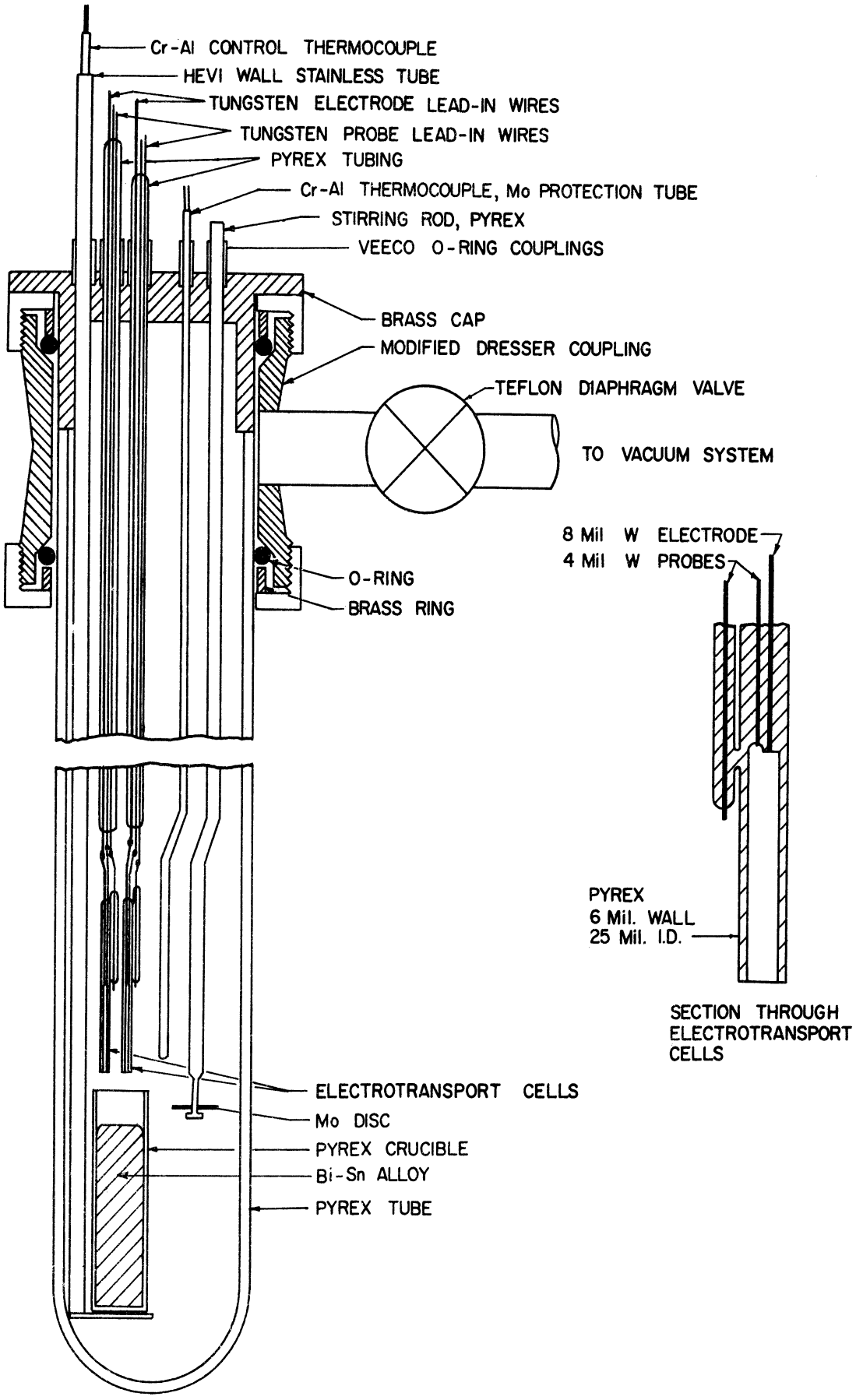

Figure 8. Electrotransport Cell -- Resistivity Type.

The voltage drop is related to the resistivity through Ohm's law,

$$V = \rho_m \frac{L}{A_m} I , \tag{150}$$

where the subscript m designates the mean value over the length of the cell. Since the current is held constant during an experiment the changing resistivity is related to the changing voltage as,

$$d\rho_m = \frac{A_m}{LI} dV . \tag{151}$$

Data on resistivity as a function of mole fraction is fairly easy to obtain experimentally. The relation may be expressed mathematically as follows,

$$X_1 = \phi(\rho) , \tag{152}$$

where ϕ represents a general function. The mole fraction is an unknown function of the position in the capillary so that the mean value of the mole fraction over the length of the capillary may be written as,

$$(X_1)_m = \frac{1}{L} \int_0^L X_1(Z)dZ , \tag{153}$$

where L is the length of the capillary. This may be written in terms of resistivity by substitution of Equation (152),

$$(X_1)_m = \frac{1}{L} \int_0^L \phi \left[\rho(Z)\right] dZ. \tag{154}$$

Since the resistivity is measured over the length of the capillary, only the mean value is known and consequently, $\rho(Z)$ is an unknown function. If one assumes however, that the function ϕ is linear, it may be brought outside of the integral to give,

$$(X_1)_m = \phi\left[\frac{1}{L}\int_0^L \rho(Z)\,dZ\right] = \phi\,(\rho_m)\,, \tag{155}$$

since the term in brackets is the definition of ρ_m. Hence, it has been shown that if the resistivity of a binary alloy is a linear function of mole fraction, the mean value of the resistivity over the tube length is the same linear function of the mean mole fraction over the tube length. If the linear function between mole fraction and resistivity is written as,

$$X_1 = f\cdot\rho + b, \quad \text{and } (X_1)_m = f\cdot\rho_m + b, \tag{156}$$

then Equation (151) may be written in terms of mole fraction as,

$$d\,(X_1)_m = \frac{f\cdot Am}{LI}\,dV\,. \tag{157}$$

Now, the mass transport across the capillary mouth may be written as a function of the mean mole fraction within the capillary as follows,

$$dN_1' = A_m L\,(\partial N_1/\partial X_1)_m\,d(X_1)_m\,. \tag{158}$$

Combining Equations (149), (157) and (158) the following expression is obtained,

$$J_1 = \frac{(dN_1/dX_1)_m f}{A_e}\cdot\frac{dV/d\theta}{I/A_m^2}\,. \tag{159}$$

This expression assumes that the resistivity is a linear function of mole fraction.

In this work the Bi-Sn system was chosen for analysis. It was necessary to determine the resistivity-mole fraction relationship at the temperatures of interest. The results of this work are given in detail in Appendix H. The resistivity versus mole fraction in this system was found to be linear between 0 and 95 atomic % bismuth.

Equation (159) is the expression for the total flux of component 1 with respect to the observer across the mouth of the capillary tube. There is a relationship between this flux and the corresponding flux of component 2 which may be derived as follows. Consider as a system under analysis the binary alloy contained within the fixed volume of the capillary cell. In the electrotransport experiments the composition is not uniform over the cell length. A mean composition may be defined as,

$$(N_1)_m = \frac{1}{L} \int_0^L N_1(Z)\, dZ \,. \tag{160}$$

From a differential balance the total volume may be expressed as,

$$V' = A \int_0^L \bar{V}_1(Z) N_1(Z)\, dZ + A \int_0^L \bar{V}_2(Z) N_2(Z)\, dZ \tag{161}$$

In an ideal solution the partial molar volumes are independent of composition and would therefore the independent of position, Z, in an electrotransport experiment. Consequently, Equation (161) reduces to the following form for an ideal system,

$$1 = \bar{V}_1(N_1)_m + \bar{V}_2(N_2)_m \,. \tag{162}$$

This means that for an ideal binary solution at constant temperature and pressure, the total volume is fixed once the mean composition is determined. The total volume is therefore independent of the solute distribution. Since the partial molar volumes are constant in an ideal solution, Equation (162) may be differentiated to give,

$$\bar{V}_1 d\,(N_1) + \bar{V}_2 d(N_2) = 0. \tag{163}$$

Multiplying by the overall volume which is constant Equation (163) becomes,

$$\bar{V}_1 d N_1' + \bar{V}_2 d N_2' = 0 \qquad (164)$$

If this expression is combined with Equation (149) written for component 2 as well as component 1, the following relation is obtained,

$$J_1\bar{V}_1 + J_2\bar{V}_2 = 0 . \qquad (165)$$

This result shows that for an ideal solution there is zero net volume transport across the capillary mouth.

Some data were found in the literature on the variation of specific volume with mass fraction for the Bi-Sn system. These data were converted to molar quantities and are shown graphically in Figure I-1. The graph indicates that the partial molar volumes are approximately constant in the Bi-Sn system. Hence, Equation (163) can be applied in this work. It was shown in Chapter IV that under the constant volume restriction of Equation (165) the flux equations for the mass transfer across the capillary mouth may be written as,

$$J_1 = (U_{12}N_1N_2\bar{V}_2E)_e , \qquad (166)$$

$$J_2 = (U_{21}N_1N_2\bar{V}_1E)_e , \qquad (167)$$

where the subscript e has been added to specify that the equations refer to the conditions at the capillary entrance. Combining Equation (159) with Equation (166) the following expression is obtained for U_{12},

$$U_{12} = \frac{f}{(X_1X_2\rho)_e} \frac{dV/d\theta}{(I/A_m)^2} \left[\frac{\bar{V}_e^2(dN_1/dX_1)_m}{(\bar{V}_2)_e}\right]. \qquad (168)$$

If Equation (159) is rewritten for component 2 and then combined with Equation (167) the analogous expression for U_{21} is obtained,

$$U_{21} = \frac{-f}{(X_1 X_2 \rho)_e} \frac{dV/d\theta}{(I/A_m)^2} \left[\frac{\bar{V}_e^2 (dN_2/dX_2)_m}{(\bar{V}_1)_e} \right]. \qquad (169)$$

It is necessary that U_{12} be equal to the negative of U_{21}. For the case of complete mixing it is shown in textbooks on thermodynamics that Equation (163) may be written without restriction to ideal solutions as,

$$\bar{V}_1 dN_1 + \bar{V}_2 dN_2 = 0. \qquad (170)$$

Dividing by the differential of the mole fraction and rearranging one has,

$$\frac{dN_1}{dX_1} = \frac{\bar{V}_2}{\bar{V}_1} \frac{dN_2}{dX_2} . \qquad (171)$$

Since the system under consideration is ideal, the partial specific volumes will be the same at the capillary entrance as at all other points in the capillary. Hence the mean value of the above function over the capillary length becomes,

$$\left(\frac{dN_1}{dX_1}\right)_m = \frac{(\bar{V}_2)_e}{(\bar{V}_1)_e} \left(\frac{dN_2}{dX_2}\right)_m . \qquad (172)$$

If this result is substituted into Equation (169), it can be seen that the expression for U_{21} reduces to the negative of U_{12}, as given in Equation (168).

It is possible to make a slightly further simplification in the expressions for the differential mobility. If one expresses the concentration of component 1 as

$$N_1 = X_1 / \bar{V} , \qquad (173)$$

the following expression can be obtained by differentiation,

$$\frac{dN_1}{dX_1} = \frac{1}{\bar{V}} \left(1 - \frac{X_1}{\bar{V}} \frac{d\bar{V}}{dX_1}\right) . \qquad (174)$$

The total molar specific volume may be expressed in general as follows,

$$\bar{V} = \bar{V}_2 + X_1 \quad (\bar{V}_1 - \bar{V}_2) . \qquad (175)$$

This expression may be rearranged to give,

$$\frac{\bar{V}_2}{\bar{V}} = 1 - \frac{X_1}{\bar{V}} (\bar{V}_1 - \bar{V}_2) = \left(1 - \frac{X_1}{\bar{V}} \frac{d\bar{V}}{dX_1}\right) . \qquad (176)$$

Combining Equations (174) and (176) one has,

$$\frac{dN_1}{dX_1} = \frac{\bar{V}_2}{\bar{V}^2} \quad . \qquad (177)$$

Since $\bar{V}_2$ is constant the mean value over the tube length may be written as,

$$\left(\frac{dN_1}{dX_1}\right)_m = (\bar{V}_2)_e \, (1/\bar{V}^2)_m . \qquad (178)$$

Consequently, the bracketed term of Equation (168) reduces to $\bar{V}_e^2 \cdot (1/\bar{V}^2)_m$. At zero time in an electrotransport experiment this term would be exactly 1. During an experiment its value would be a function of time, and should therefore produce a variation in $dV/d\theta$ since all of the other terms in Equation (168) are constant. The V vs θ curves were found to be quite linear over the initial portion of the experiments so that variations in the above term appeared to be negligible. The bracketed term of Equation (168) was therefore taken to be one. Hence both Equations (168) and (169) reduce to the following expression,

$$U_{12} = -U_{21} = \frac{f}{(X_1 X_2 \rho)_e} \cdot \left[\frac{\Delta V / \Delta \theta}{(I/A_m)^2} \right] . \qquad (179)$$

This is the final expression used to calculate the differential mobility.

In this technique, the design of the experiment is not nearly as critical as with the chemical analysis technique, since one is not faced with the problem of balancing two errors. The back diffusion error is simply eliminated by measuring $\Delta V / \Delta \theta$ only over the initial portion of the experiment where V varies linearly with θ. Figure 9 is presented to illustrate this point. It can also be seen from this figure that the non-linearity due to back diffusion occurs much later for the case where the solute is run into the tube, as was predicted by the solution to the differential equation. In order to minimize analytical errors it is desirable to have the linear portion of the voltage versus time curve as long as possible. The longer the linear portion the more accurately $\Delta V / \Delta \theta$ may be determined. The non-linearity is the result of back diffusion at the capillary mouth, and for a given set of experimental conditions will be delayed in proportion to the capillary length. The time to a given error due to non-linearity may be estimated from the solutions to the differential equations shown in Figures 2 and 4.

Experimental Procedure--The apparatus is shown in Figure 8. The pyrex capillaries were 3 cm long with an inside diameter of approximately 0.6 mm. The wall thickness was around 0.15 mm. The probes and electrode were soldered to the .012-in. tungsten lead-in wires with "Nioro" Au-Ni solder. The molybdenum sheet stirrer has been described in discussion of the previous technique. Molybdenum tubing was employed to shield the

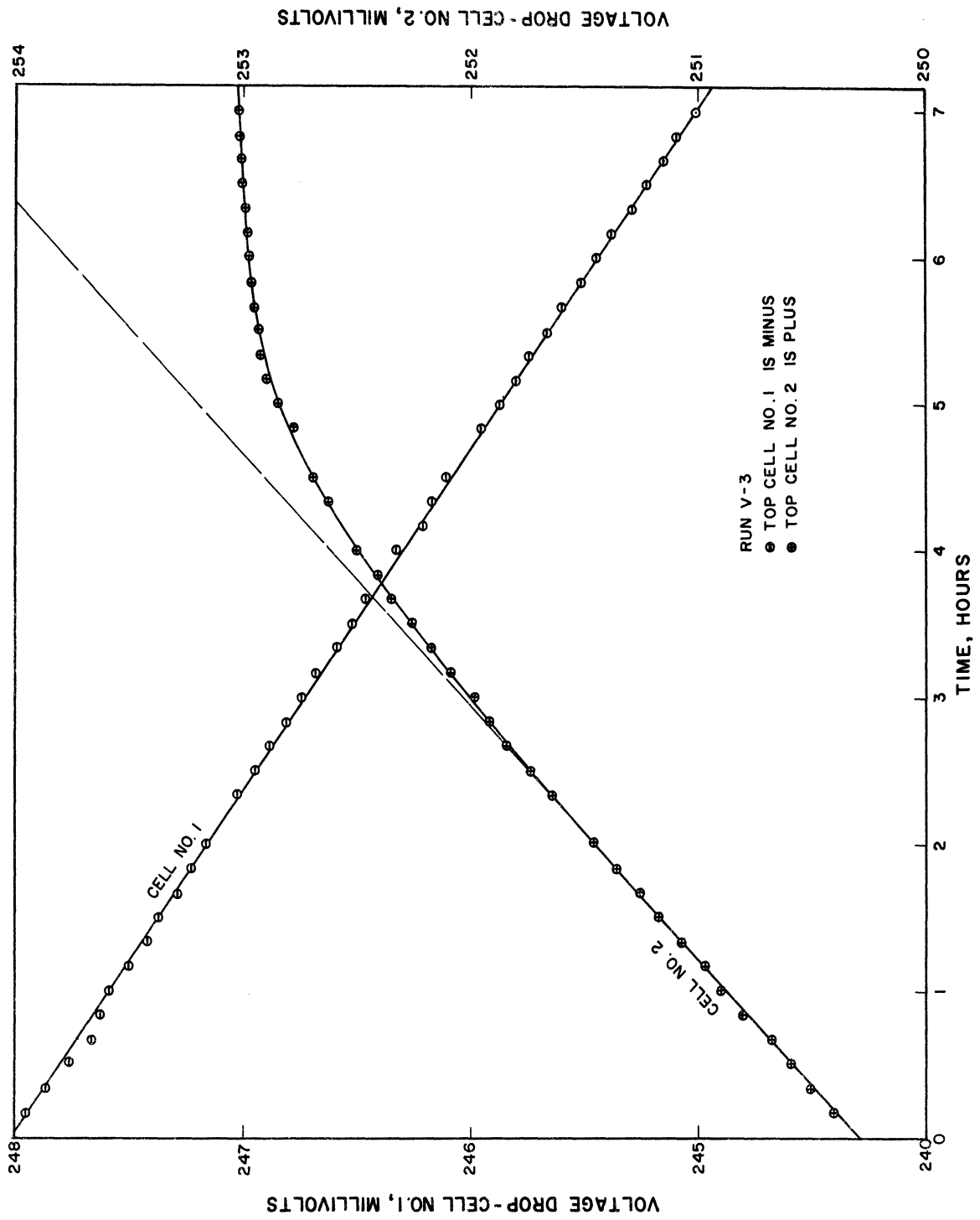

Figure 9. Voltage Drop Across Cell versus Time.

Chromel-Alumel thermocouple used to measure the bath temperature. The alloy was held in a pyrex crucible fastened to the end of a stainless steel rod which could be rotated and moved up and down. All of the rods or tubes coming through the brass cap could be rotated or translated through vacuum tight O-ring Veeco Couplings or CVC seals. The voltage measurements were taken with a Leeds and Northrup K-3 potentiometer and a null detector.(1) On the low range which extends from 0 to 160 mv, this instrument can measure to 0.1 micro-volts. The potentiometer was connected to each of the voltage probes with a Leeds and Northrup thermocouple switch. A Hevi Duty resistance wound hinged furnace was used to maintain temperature. The furnace had three zones which could be controlled independently. Consequently, it was possible to adjust the temperature gradient in the crucible to avoid bulk convection. The potentiometer was sensitive enough to pick up the bulk convection as a rapid fluxuation in the temperature measurement. A temperature gradient of 0.5 °C/cm was sufficient to eliminate this convection. The temperature was controlled with a Wheelco proportionating controller. The temperature would cycle slowly with a maximum variation of 2°C over a 3 hour run. The control thermocouple was placed inside of the stainless steel rod used to hold the crucible. The current was supplied by a Kepco rectifier modified to be current-controlling. The current was determined by measuring the voltage drop across a maganin shunt which was calibrated against Leeds and Northrup 0.1 ohm No. 301185 standard resistor. The current regulation varied from 1 part in 3000 in some 3 hour runs to 1 part in 500 in other 3 hour runs.

---

(1) The model numbers of the equipment are given in Appendix J.

In all runs the short time flucuation was very low, being on the order of 1 part in 100,000 over 2 minute intervals. The temperature was measured with matched 28 gauge Chromel-Alumel thermocouples calibrated as discussed previously. All temperature measurements were made using an ice-bath cold junction. The details of the vacuum system are shown in Figure 10. The system was capable of pulling a vacuum of 10^{-5} mm Hg at the gauge point as measured on a McLeod gauge. This was sufficient to maintain the surface of liquid bismuth metallic bright at temperatures between 271 and 600°C. The manufacturer and the quoted purity on the bismuth and tin metal used in these experiments are listed in Table XIX.

TABLE XIX

PURITY AND SOURCE OF ELEMENTS USED

Tin-City Chemical Co.	Bismuth-Belmont Smelting
Fe - 0.4 ppm	Fe - 5 ppm
Pb - 0.5 ppm	Pb - 1 ppm
Sb - Not detectable	Sb - 1 ppm
Cu - Not detectable	Cu - 1 ppm
Ni - Not detectable	Ag - 1 ppm
Sn - 99.99+%	Zn - 5 ppm
	Bi - 99.9986%

The following procedure was used to make a run. The alloy, previously vacuum cast to the diameter of the pyrex crucible, was placed in the crucible. The apparatus was then heated to around 530°C and held overnight. The alloy was stirred in the evening and again a few times in the morning before starting a run. After cooling to the operating temperature the melt was raised up around the capillaries, which were then filled by the introduction of one atmosphere of helium gas. The helium

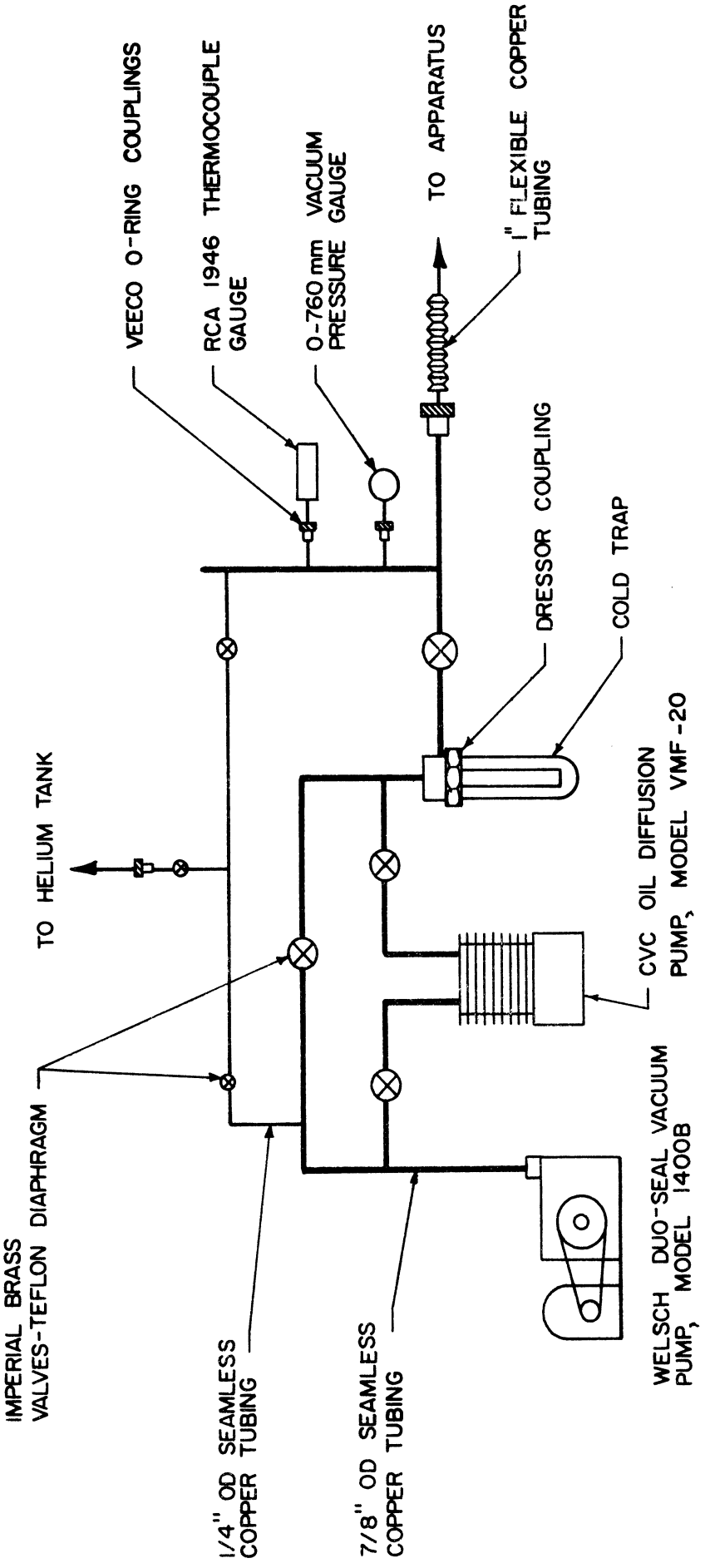

Figure 10. Vacuum System.

was admitted slowly through the liquid nitrogen cold trap to remove condensable impurities. The current was then switched by means of a relay from a dummy load to the capillaries. As in the previous technique, it was passed down one tube and up the other. The voltage readings were measured every 10 minutes in the initial experiments and every 5 minutes in the rest of the experiments. The run-time was generally 3 hours. The voltage reading sequence was as follows: Temperature - Cell - Shunt - Temperature. The two temperature readings were averaged in proportion to the sequence of the four readings. Only one shunt reading was required because, as noted above, the short time current variation was very low. After the run the current was switched back to the dummy load, and the zero current potential was measured for comparison to its value measured at the beginning of the experiment. The crucible was lowered and a vacuum was pulled on the apparatus. Fortunately, the alloys did not wet the pyrex capillaries, so that the surface tension force was directed downward once the upper surface formed inside the capillary. This force, plus the gravitational force, plus the differential pressure force due to the absence of the helium was sufficient to cause the tubes to empty very cleanly. Another run could then be started after sufficient outgassing. It was found that two hours of outgassing with occasional stirring was sufficient to produce successful runs.

The capillaries were prepared and calibrated in the following manner. Pyrex No. 7740 glass was used in all experiments. The critical geometry at the electrode was produced by trial and error using a miniature tip on a gas-osygen torch and a binocular microscope. As mentioned in Appendix G, it was necessary that the probe did not extend down beyond the tip of the shielding on the electrode. After attachement to the lead-in

wires the oxide surface was removed from the electrode and probes of the capillary cells by electroetching with 20% KOH solution and A.C. current. The capillaries were cleaned between runs of different composition using conc. HNO_3 and distilled water. After making new capillaries, it was generally necessary to also clean with a 5% solution of HF acid. To perform these operations a small rig was made with which a liquid could be squirted through a AISI 304 stainless steel tube having an outside diameter of 13 mils. This tube could be moved up and down inside of the capillary, thereby flushing it with liquid or emptying it with suction. The cleanliness of the tubes before a run proved to be quite important. A binocular microscope was very useful in guiding the cleaning process.

It was necessary to know the mean capillary cross-sectional area, Am, quite accurately, since it enters as the square in the calculation of U_{12}. The area was determined by first measuring L/Am from resistance measurements on mercury, and then determining the capillary length, L. The capillaries were cleaned as described above and then outgassed at 530°C for a few hours under vacuum. After cooling to room temperature they were filled with pure mercury, (see Appendix J for purity), as described above, and a current density of 0.3 amps/mm^2 was passed through them. A series of voltage measurements on the temperature, current shunt, and cell probes was then made in the sequence described above. Ten measurements were made, altering the polarity on each measurement to eliminate any non-linear effects. The ratio L/Am was then determined from the average value using Ohm's law and the averaged data in the International Critical Tables, (vol. 6, p. 136), on the resistivity of pure mercury. The length of the capillary was determined with the aid

of the binocular microscope. The capillary was positioned vertically and the hair line was aligned with the electrode. The scope was then lowered until the hair line was aligned with the mouth of the tube. The traverse of the scope was measured with Johansson blocks and a dial indicator which could be read to ±.0001 in.

Discussion of the Technique

As mentioned previously, the final mobility is determined by averaging experiments in which the solute was run out of the capillary with those having the solute moved into the capillary. This procedure has certain advantages. Due to the I^2R heating within the capillary metal there will be a small temperature gradient at the mouth which may give rise to a flux of solute due to thermal diffusion. Reversing the polarity does not change the direction of this flux, so that in one case it would add to the electrotransport flux and in the other it would subtract; it would thereby be eliminated from the average value. Any spurious addition to the electrotransport flux which did not reverse itself with polarity change would likewise be eliminated from the average value. A flux due to gravitational force would thus be eliminated.

The current density in this work ranged from 180 to 970 amps/cm^2. One would therefore, expect a considerable temperature rise within the capillary due to I^2R heat generation. As an approximation, it was assumed that all of the heat generated in a unit length of the metal column passes through a unit length of the capillary walls. A simple calculation was then made to determine the temperature rise as a function of current density, based on the thermal conductivity of the Pyrex glass and assuming perfect contact at the walls. If the latter assumption is correct, this calculation

should give an upper limit of expected temperature rise. This was found to be the case in experiments conducted on liquid mercury around room temperature, (see Appendix K). Figure 11 gives the maximum temperature rise expected in these experiments. Hence the maximum expected temperature rise was only 0.65°C in the worst case, (Run V-17). The results in Appendix K indicate that the true temperature rise was roughly 3/4 or less of this maximum value. However, the results of Run E-17 in Appendix G indicate the possibility that the temperature rise was as high as 2.4°C. The reliability of this result is uncertain. In any case, the inability to exactly determine the temperature of the capillary metal does not produce an appreiciable error in the result. To obtain accurate values of $\Delta V/\Delta\theta$, it is only necessary to determine variations in the capillary metal temperature, which may be determined from variations of the bath temperature at the outside wall of the capillary. The error in the reported temperature of the mobility due to temperature rise is probably ± 1°C, which is within the accuracy of the thermocouple calibration.

The mole fraction of the alloy was determined directly from the weighed-in values. Since very little oxide formed on the alloy during a run, one would expect this procedure to be quite good. However, the vapor pressure of bismuth was high enough that some vapor deposited bismuth was found on the cool section of the outer pyrex tube when outgassed under vacuum at 530°C. Depending on the size of the alloy charge, this prefernetial loss of bismuth metal could cause an appreciable error in the use of the weighed-in composition. The error would be a maximum in alloys containing small amounts of bismuth. In order to check this error an analytical scheme was worked up and is described in Appendix L. At the end of a

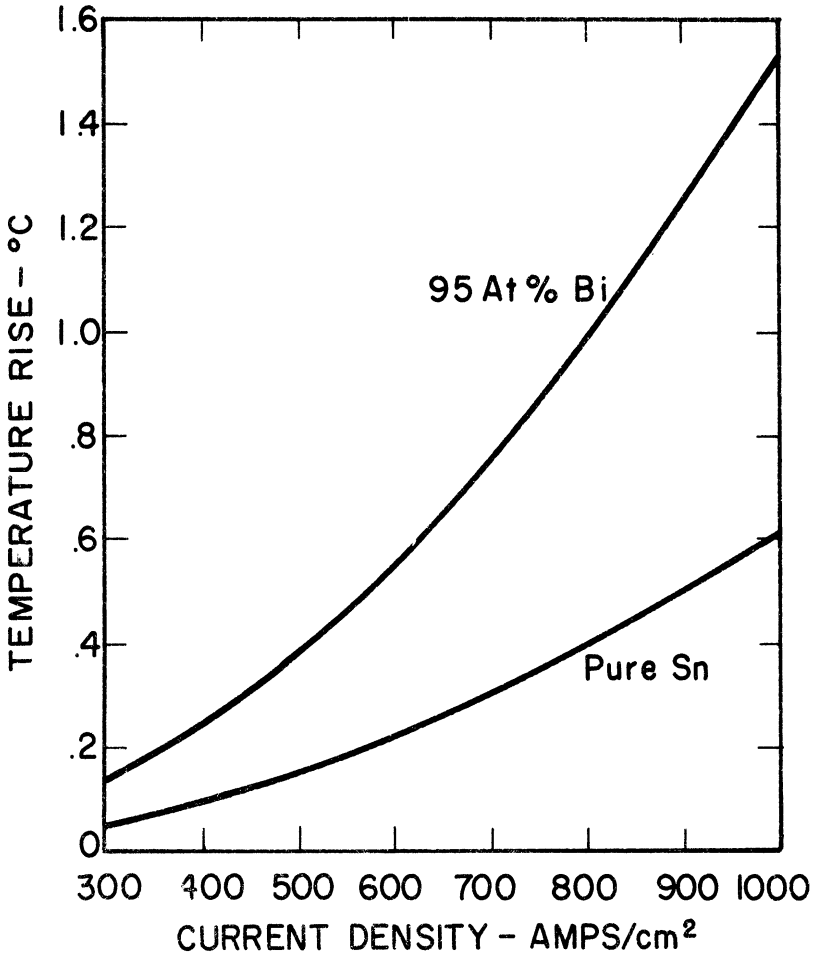

Figure 11. Temperature Rise Inside of Electrotransport Cells Due to I^2R Heating at 520°C.

number of experiments with a given alloy, a few one gram samples were taken from the liquid alloy by lowering a capillary into the melt, filling, and then raising before solidification. The results of the chemical analyses are shown in Table XX. The results agree with the weighed in values within experimental limits.

TABLE XX

CHEMICAL ANALYSIS OF Bi-Sn ALLOYS

Run	No. of Previous Fillings	Previous Outgassing Temp.	Weighed-in Composition	Measured Composition
V-22	6	530°C	1.72 Wt.%	1.70 Wt.%
V-8	3	625°C(1)	8.45	8.57
V-9	8	550°C	8.45	8.48
V-10	25	530°C	8.45	8.42
V-13	4	530°C	30.72	30.78

(1) Two previous outgassings at this temperature overnight.

It can be seen that even after 25 fillings and a number of outgassings at relatively high temperatures, the composition did not vary measurably in the alloy used in Runs V-8 to V-10. Consequently, the weighed-in analysis was used in all of the calculations.

In order to check the technique and make sure that there were no gross errors in the method of calculation, experiments were done on the Hg-Cd system around room temperature, and the results compared to those of Mangelsdorf[121] and Schwarz.[149] The experiments were made on an amalgam containing 1 At.% Cd. The data of Larsen[150] corrected to constant temperature was used to determine the slope of the resistivity vs. mole fraction curve. The data is very nearly linear between 0 and 1.5 At.% Cd The data of Bornemann[151] on a 1 At.% Cd amalgam was used to determine the slope of the resistivity temperature curve, which was needed to correct

the readings to constant temperature. The resistivity of the amalgam was determined by extrapolation of the voltage vs. time curve back to zero time. The results agreed with Bornemann to within 0.4%. The mobility was calculated with the assumption of dilute solutions, $\bar{V}_2 N_2 \cong 1$ and $X_2 \cong 1$, so that the results could be compared directly to the literature data. The results are shown in Table XXI; there appears to be good agreement. From an extrapolation of the data of Mangelsdorf on the temperature dependence, the data points at 25 and 27°C would be increased by only 0.1×10^{-4} $cm^2/V\text{-}s$ at 43°C. It is interesting to note that Mangelsdorf made his measurements by running the Cd out of a capillary, while Schwarz made his by running the Cd into a capillary. In this work running the Cd out of the capillary gave a higher value than running it into the capillary. The value in the table is the average of the two, which appears to agree quite well with the average of the literature data.

TABLE XXI

RESULTS ON THE Hg-Cd SYSTEM

Author	Conc. At%	Temp °C	Mobility - u_{Cd} $cm^2/V\text{-}sec \times 10^4$
Mangelsdorf[121]	1	27	10.3
Schwarz[149]	Dilute	25	9.7
Run V-23	1	43	10.0

Treatment of Data and Experimental Results--The determination of the change of voltage with time, $\Delta V/\Delta\theta$ requires that both the current and the temperature be held constant throughout the run. Even with the excellent controlling equipment used in this work, the control of current and temperature over a 3 hour run was not good enough to give precise results, since the effect being examined is quite small. As mentioned

earlier, the current and the temperature were recorded with each data point. In processing the data all of the points were corrected to a standard current and a standard temperature, arbitrarily chosen to correspond to the values of the $n/2$ data point where n is the total number of points used in determining $\Delta V/\Delta\theta$. The voltage increment required to correct the data to constant current may be calculated directly from Ohm's law as,

$$\Delta V \text{ (due to current variation)} = \frac{V_c}{V_s}\left[(V_s)_o - V_s\right], \qquad (180)$$

where $(V_s)_o$ is the voltage drop across the shunt at the standard current value, and V_c is the voltage drop across the capillary cell. The voltage increment required to correct the data to constant temperature may also be calculated from Ohm's law, but requires in addition, the slope of the resistivity vs. temperature curve, $\Delta\rho/\Delta T$.

$$\Delta V \text{ (due to temp. variation)} = \frac{\Delta\rho}{\Delta T}\frac{\Delta T}{\Delta V_{tc}}\left(\frac{1}{\rho}\right)\left[(V_{tc})_o - V_{tc}\right]. \qquad (181)$$

Here, $(V_{tc})_o$ is the voltage output of the thermocouple at the standard temperature, and $(\Delta T/\Delta V_{tc})$ is a characteristic of the thermocouple material used. The effectiveness of this correction may be seen by reference to Figure 12. In this run the maximum current variation was 1 part in 700, and the maximum temperature variation was 1.6°C.

The voltage readings were recorded directly onto IBM cards and processed in a digital computer. The temperature vs. EMF characteristic of the Chromel-Alumel thermocouples was fitted to a curve so that the temperature conversion was made in the program. Data was kindly supplied by Corning Glass Works on the thermal expansion of the Pyrex No. 7740

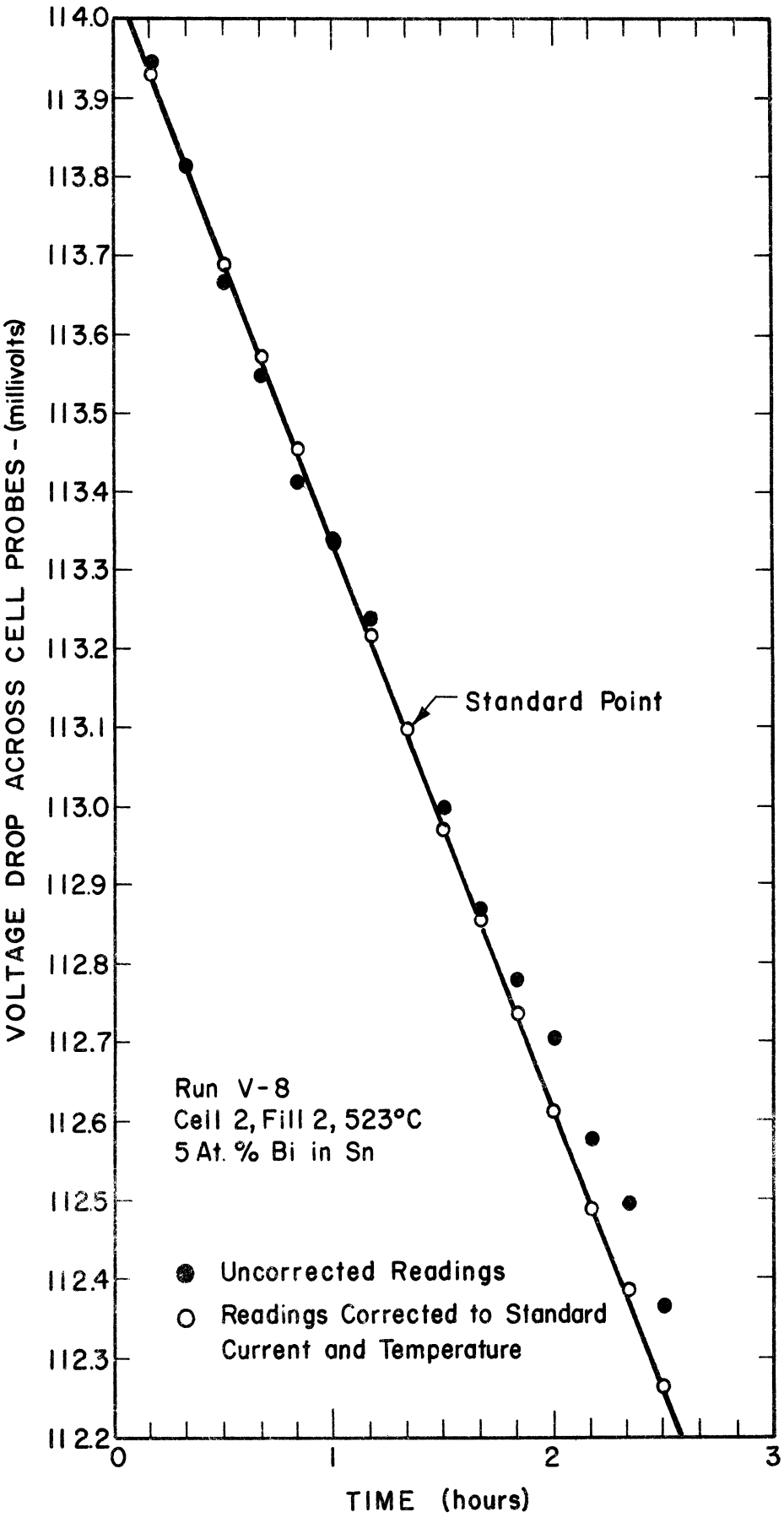

Figure 12. Typical Result of Voltage Drop Across Cell vs. Time.

used in the capillaries. The program included a correction for variation of A_m with temperature based on this data. The program corrected the data to the standard current and temperature according to the above relations and also typed out a plot of the corrected voltage readings versus time on the IBM printer. This plotting method is only an approximation, but it proved to be of sufficient accuracy to determine the number of data points lying on the linear portion of the V vs θ curve. These points from the linear portion were then fitted to a straight line by the method of least squares in a second program. The slope and a number of statistical parameters measuring the "degree of fit" were printed out, along with the average current, average temperature, and the term in brackets in Equation (179). By extrapolating the curve to zero time it was possible to obtain a measure of the initial resistivity of the alloy. The program also printed out this value. The computer output for all of the data is shown in Table M-1. Three statistical parameters are presented, the standard deviation of the slope, the percent standard deviation of the slope, and the maximum deviation from the final curve.

Six different cells were used throughout the course of this work. The average value for the mean area, A_m, of each cell, determined as described above, is shown in Table M-2. The percent standard deviation refers to the determination of A_m/L. It can be seen that the measurements are quite precise.

The weighed-in value of the weight and atom percent bismuth in the alloy of each run are given in Table M-3. The remaining parameters used in the calculation of the differential mobility are given in Table M-4. The slope of the resistivity versus mole fraction curve, 1/f, is taken

from the data of Appendix H. The final value of the differential mobility for each run, as calculated from Equation (179), is given in Table M-1.

A tabular summary of all of the processed data is shown in Table XXII. The weighed-in compositions are quoted for all values. The temperatures are those of the standardized couples. The resistivity has been corrected to the quoted temperature values from the standard temperature used in processing the data. The mobility was determined as follows. The values for all of the runs in which the solute was run out of the tube were averaged. Also, the values for the runs where the solute was run into the tubes were averaged. The quoted mobility is the average of these two average values. In all cases the value of the mobility was slightly smaller when the bismuth was run out of the tube. The mean value of the difference of the two averages for all quoted values is 0.035×10^{-3} $cm^2/V\text{-}sec$. Half of the measurements for each quoted value were taken with a different cell, so that each value is averaged over two cells. The standard deviation of the average mobility was determined as the average of the two standard deviations of the mobilities determined with opposite polarity. The following expression was used,

$$\sigma_{Ave} = \frac{1}{2}\left[\frac{(B \cdot \sigma_{out})^2}{N_{out}} + \frac{(B \cdot \sigma_{in})^2}{N_{in}}\right]^{\frac{1}{2}}, \qquad (182)$$

where subscript "in" refers to the solute being run into the tube, σ is the standard deviation of the mobility values, N is the number of measurements, and B was determined from the value of $(N-1)$ on a Student-t distribution at a confidence level of 95%.

The precision of the resistivity data turned out to be remarkably good. This was very encouraging because it meant that the cells must have

TABLE XXII

SUMMARY OF Bi-Sn RESULTS

Run No.	Composition At. % Bi	Temp., °C	Resistivity, μohm-cm	Dev.* of Avg. Res.	% Dev. of Avg. Res.	Mobility x 10^3 cm^2/V-sec	Dev. of Avg. Mobility x 10^3	% Dev. of Avg. Mobility	No. of Measurements
V-22	0.986	257	49.067	.110	.224	1.522	.565	37.1	4
V-22	0.986	378	52.324	.175	.335	1.741	.346	19.9	4
V-22	0.986	518	56.079	.117	.209	2.060	.738	35.8	4
V-10	4.98	250	51.896	.027	.052	1.488	.010	0.7	8
V-10	4.98	351	54.723	.037	.068	1.675	.012	0.7	8
V-10	4.98	450	57.410	.038	.066	1.790	.027	1.5	8
V-7,8,9	4.98	518	59.210	.022	.037	1.863	.007	0.4	18
V-10	4.98	599	61.398	.070	.114	1.923	.065	3.4	10
V-12	9.96	516	63.255	.017	.027	1.801	.018	1.0	8
V-21	20.12	220	62.869	.020	.032	1.283	.014	1.1	4
V-21	20.12	338	66.505	.019	.029	1.506	.021	1.4	4
V-13	20.12	518	71.941	.017	.024	1.687	.020	1.2	8
V-19	38.57	177	76.359	.055	.072	0.993	.102	10.3	4
V-19	38.57	297	80.650	.052	.037	1.223	.022	1.8	4
V-14	38.57	517	88.141	.016	.018	1.457	.012	0.8	8
V-20	57.59	197	92.564	.154	.166	0.858	.122	14.2	4
V-20	57.59	318	97.460	.070	.072	1.024	.057	5.6	4
V-16	57.59	520	105.389	.032	.030	1.204	.022	1.8	8
V-18	78.80	248	111.070	.032	.029	0.691	.048	7.0	4
V-18	78.80	368	116.419	.049	.042	0.823	.022	2.7	4
V-15	78.80	520	123.455	.014	.011	0.943	.012	1.3	8
V-17	94.84	518	136.408	.039	.029	0.780	.070	9.0	8

*Student t Dist., 95% Conf. Level.

filled almost perfectly in each run, i.e., there was negligible bubble formation. It also affords further evidence that there was negligible composition change from run to run. The resistivity data from all of the electrotransport runs have been corrected from the standard temperature used in computing the slope of the V vs θ curve to the average temperature of the individual runs. The corrected data have been averaged and are shown in Table M-5. The precision may be compared to that obtained in the direct resistivity measurements described in Appendix H. It appears to be approximately the same for both techniques. The values of the resistivity found from the extrapolated electrotransport data are plotted on those determined at much lower currents in Figures H-4 and H-5. The temperature dependence agrees very well, but in the three cases where the composition was the same, the absolute values appear to be off slightly. The source of this error is unknown. In any case, the disagreement is quite small, amounting to only 0.26% in the worst case. This is probably within the experimental accuracy with which the temperature is known, due to the I^2R heating within the tube in the electrotransport runs, and the inaccuracy of the temperature measurements.

Compared to the precision of transport properties such as the diffusion coefficient, the precision of the differential mobility appears quite good. The large scatter in the data for the 1 At% Bi alloy was due to the fact that $\Delta V/\Delta\theta$ is a function of mole fraction, so that low values of mole fraction give small changes in voltage with corresponding small precision.

The liquid properties of an alloy are frequently best characterized by the increment of temperature above the liquidus rather than by the

absolute temperature. Consequently, the low temperature data was taken at 30 and 150°C above the liquidus. In addition, an isotherm was measured at 518°C. The results are presented graphically in Figure 13. The precision of the values at 30°C above the liquidus for 38, 57, and 78 At% Bi is relatively low. This is probably due to the fact that these points lie within the "V-notch" of the liquidus line. Consequently, when the solute is run into the tubes the solid solution components would freeze out at the electrode. The temperature dependence of the data is presented in Figure 14. The liquidus temperature for each alloy is joined by a cross hatched line. The data at 4.98 At% Bi appears to justify drawing a smooth curve through the data at the other compositions where only three temperatures were investigated.

As mentioned earlier, all but some of the initial experiments were run for 3 hours. In runs V-7 and V-8, containing 5 At% Bi, the current was reversed after 2.83 and 2.67 hours respectively, and the run continued for an additional 5 hours. The data obtained after reversing the migration direction are quite interesting. In other runs made under similar operating conditions but with uniform concentration distribution at time zero, it was established that the V vs Θ curve was linear for approximately 2.67 hours when the bismuth was run into the tubes and for at least 3 hours when the bismuth was run out of the tubes. After reversing the polarity on those tubes in which the Bi was first run outward, the linear portion was lengthened from 2.67 hours to 4.83 hours. This result was interpreted as follows. The initial removal of Bi from the tube before reversing the direction of migration caused a depletion of the Bi concentration within the tube predominantly at the electrode end. Consequently, after

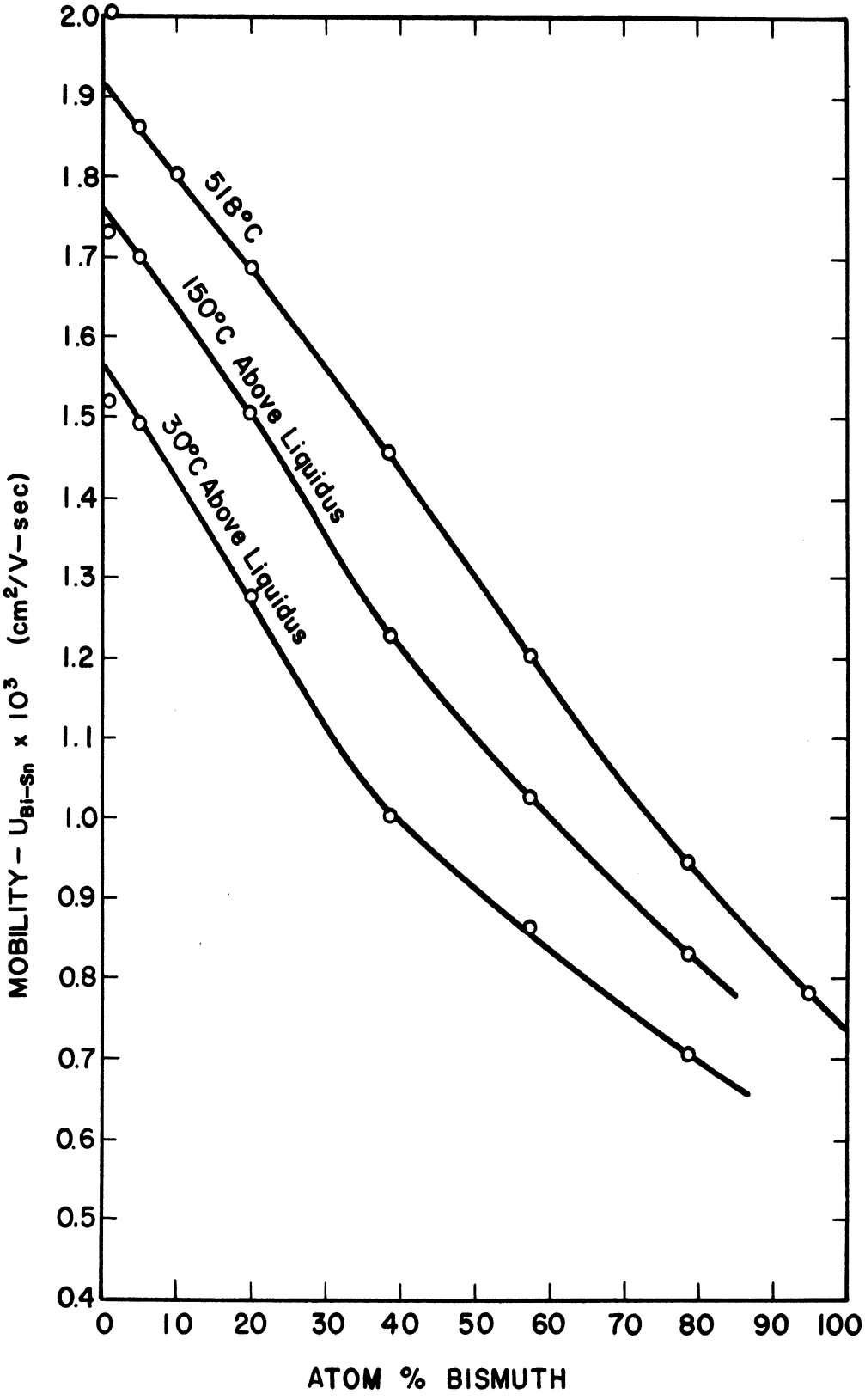

Figure 13. Experimental Results -- Differential Mobility vs. Composition.

NOTE: Not all of the data points were taken at exactly 30 and 150°C above the liquidus. Consequently, some of the points on the lower two curves were extrapolated from Figure 14.

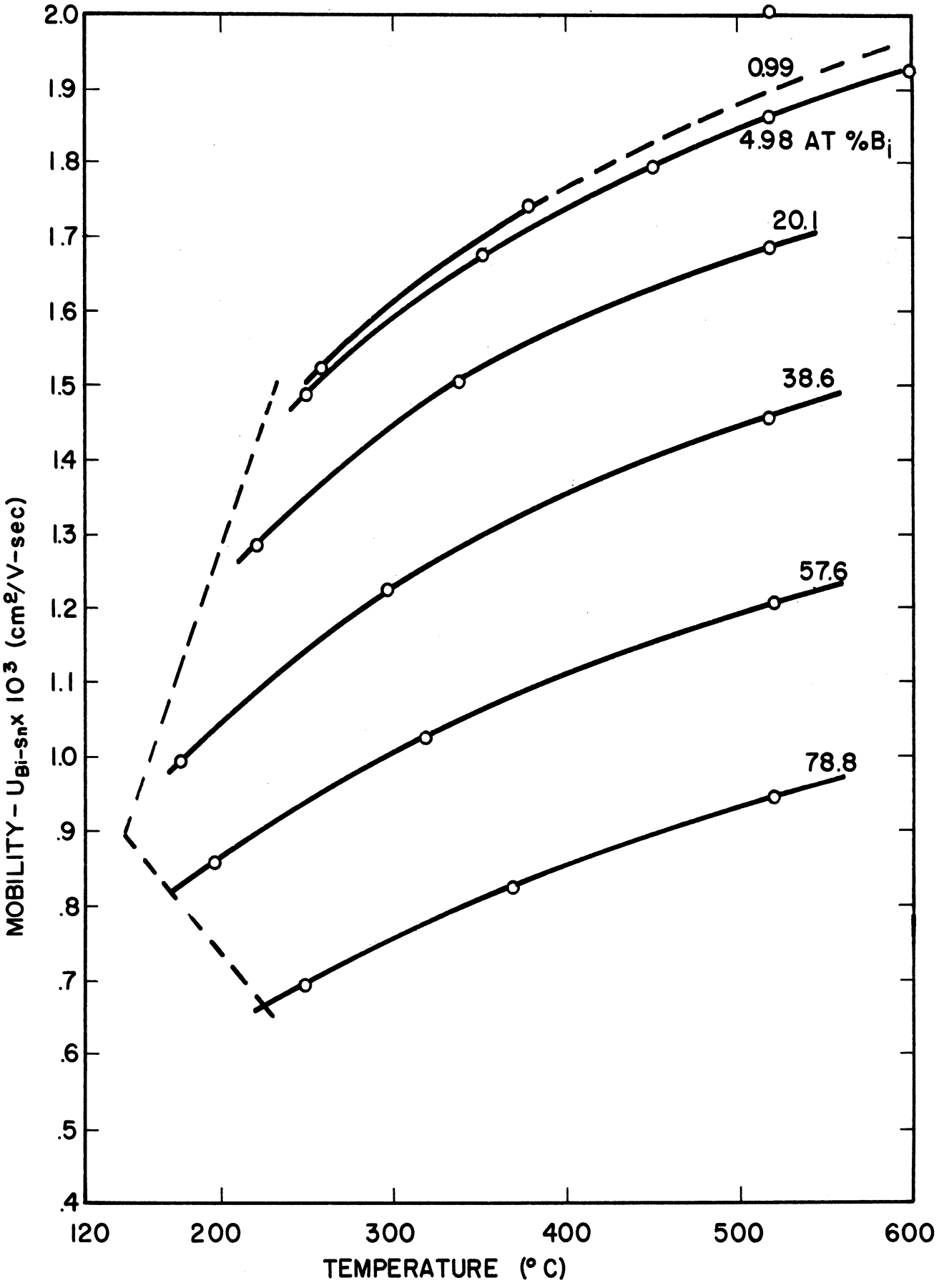

Figure 14. Experimental Results -- Differential Mobility vs. Temperature, Parameters of At.% Bismuth.

reversal it took longer for the concentration wave to build up and move down the tube than in the usual case where the concentration distribution was uniform at at time zero. The resulting data is marked with an asterisk in Table M-1. It might be noted that since this procedure gives a longer linear portion to the V vs θ curve, it affords a possible means of obtaining more precise data. In the case where the Bi was first run into the tubes, the data became non-linear after reversal in only 1.33 hours, whereas in the normal procedure it remained linear for at least 3 hours. The initial influx of Bi before reversal caused a concentration buildup within the capillary. One might expect this non-uniform concentration distribution to move outward upon polarity reversal thereby causing a concentration gradient to appear at the mouth sooner than in the case of uniform initial concentration. Such an explanation would also predict that the initial slope of the V vs θ curve should be greater than in the normal case of uniform initial composition. This was found to be the case experimentally. The data obtained in these tubes could not, therefore, be used to calculate mobilities.

Some additional interesting results were obtained concerning the determination of the effective diffusion coefficient from the non-linear portion of the data. Since the runs were only made for 3 hours, it was frequently impossible to determine when the V vs θ curve became non-linear. The following unexpected results were obtained, however; the V vs θ curve became non-linear in less than 3 hours when the Bi migrated into the tubes in all of the runs except those at 1 At% Bi. The V vs θ curve was still linear after 3 hours in all of the runs where the Bi migrated out of the tubes. As mentioned earlier, it is possible to calculate the

diffusion coefficient from the non-linear portion of the data by use of the solution of the partial differential equation shown in Figure 2. The runs made with 5 At% Bi at 520°C and 2 amperes all became non-linear at around 2.67 hours when the Bi migrated inward. The corresponding effective diffusion coefficient from the figure was found to be 25×10^{-5} cm^2/sec. The value found by Niwa[153] at 500°C was approximately 6×10^{-5} cm^2/sec. Hence, there appears to be considerable convection when Bi is run upward into the tubes.

Discussion of Errors--The accuracy of the data is probably most subject to error in the values used for the resistivity variation with composition. This value is inherently difficult to measure because it is the slope of the experimental data. The accuracy may be fairly good however, since the precision of this slope measurement was quite good. It can be seen from Table H-5 that the percent deviation of the least square fit is only about 0.7%.

The current density enters the mobility calculation as the square, (see Equation 179), and consequently errors in its determination would be doubled in the mobility. The main source of error in the current density is in the determination of the mean area of the capillary, since the current may be determined quite precisely. As can be seen from Table M-2 the value of A_m/L was determined quite precisely from the mercury calibration. The determination of L was also fairly precise, but was probably the limiting error because of the irregularities at the upper electrode in the cells. Since each mobility was determined from an average over two different cells, it is possible to give a qualitative check of cell calibrations. Table XXIII is a comparison of the average value of the

mobility using only cell 1 to the average value using only cell 2. It does appear that cell 1 gives slightly higher results than cell 2. In view of the inherent scatter in the data, however, the error appears to be tolerably small, being less than 1.5% in the worst case. It is possible to make a check on the A_m/L calibration of the cells from the resistivity data obtained from the electrotransport runs. It can be seen from Table M-5 that the average values of the resistivity obtained from the two cells were slightly different. The values obtained from cell 1 are, on the average, 0.019 μΩ-cm higher than those obtained from cell 2. This value is a deviation of only .034%. Hence, this result is experimental evidence that the determination of L was the limiting error in calibrating the cells.

TABLE XXIII

COMPARISON OF RESULTS FROM DIFFERENT CELLS

Temp °C	Ave U_{12} Cell 1 $cm^2/V\text{-}sec.$	Ave U_{12} Cell 2 $cm^2/V\text{-}sec.$	Difference $U_{cell\ 1} - U_{cell\ 2}$	Ave.Std. Dev.(1)
250	1.493×10^{-3}	1.482×10^{-3}	$-.011 \times 10^{-3}$	$.010 \times 10^{-3}$
351	1.678	1.673	-.005	.011
450	1.800	1.779	-.021	.026
518	1.869	1.858	-.011	.007

(1) Student t Distribution, 95% Confidence Level

The voltage change with time turned out to be quite linear. The standard deviation on the least square fit of the data was computed for each run and is shown in Table M-1. It can be seen that the data of Figure 12 are a typical result. The percent standard deviation of $\Delta V/\Delta\theta$ appears, on the average, to be around 1 to 2%. Consequently, the main scatter in the mobility may be attributed to the determination of $\Delta V/\Delta\theta$. Due to inherent inaccuracies almost invariably present in experiments

of this nature, it was felt that the precision of the $\Delta V/\Delta\theta$ measurement was suitably good.

Examination of Equation (125) reveals that U_{12} should be independent of current density if the effective valence does not vary with current density. Since the effective valence is a function of ion valence and ion-electron scattering cross section, it would seem that it would be independent of current density. It was pointed out in Chapter III that both Huntington and Kuz'menko have found the mobility to be independent of current density in self-electrotransport in solids. However, Wever has found a current density dependence in electrotransport in the Cu-Al system. It therefore seemed advisable to check the dependence of U_{12} on the current density. The results of this work are shown in Table XXIV. The results indicate no measurable effect within the limits of experimental error. The range of variation of current density was not very large, but it does cover, fairly adequately, the range of field intensities used in these experiments. It is therefore felt that the results are independent of the current densities used.

TABLE XXIV

VARIATION OF MOBILITY WITH CURRENT DENSITY

Run	Current Density amps/cm^2	$U_{Bi\text{-}Sn}$ cm^2/V-sec.	No. of Measurements
V-9	502	1.848×10^{-3}	2
V-9	663	1.858	6
V-9	820	1.849	2

Examination of the geometry of the cell at the electrode end, (see Figure 8), reveals that there is a small cavity which acts as a reservoir, since no current passes through it. When the solute is run out

of the tube, additional solute will enter the cell by diffusion out of the cavity and thus tend to make U_{12} lower than it should be. When the solute is run into the tube, some of it will be lost to the cavity by concentration gradient diffusion and again tend to make U_{12} lower than it should be. Consequently, the cavity presents a possible source of error. It was possible to estimate the size of the cavity with the binocular microscope. The cavity volume was approximately 0.3% of the total volume with an entrance area approximately 1/3 the cross sectional area of the capillary. If an instantaneous concentration change of 50% is assumed at the cavity entrance, the mass flow across the cavity mouth due to diffusion is still negligible compared to the electrotransport mass flux.

Discussion of Results--The properties of the Bi-Sn system have been fairly well investigated. The data gathered by Kubaschewski[152] indicate that the system approximates an ideal solution. Niwa[153] has shown that the mutual diffusion coefficient varies linearly with mole fraction at 500°C. The viscosity data of Golik[154] shows a linear variation with mole fraction down to 10°C above the liquidus. In addition, it has been found in this work that resistivity varies linearly with mole fraction down to at least 180°C. Electron diffraction[155,156] and x-ray[157] studies of the system indicate a tendency for microheterogeneity in the melt, decreasing as the temperature is increased above the liquidus. However, the degree of microheterogeneity is not as complete as that found in the Bi-Pb and Sn-Pb systems. Nevertheless, it is quite possible that at temperatures just above the liquidus, the liquid Bi-Sn alloys consist of two types of clusters; one composed predominantly of Sn and the other predominantly Bi. Apparently, such clustering has no anomalous effect

on the variation of the thermodynamic properties, diffusion coefficient, viscosity and resistivity with composition. Since the degree of clustering is a function of the temperature above the liquidus, anomalies in the liquid structure at various compositions would probably best show up on a plot of a physical parameter against composition at a constant temperature above the liquidus. In accord with this thinking the differential mobility was determined at 30 and 150°C above the liquidus as shown in Figure 13. The variation from linearity appears to be more a function of temperature than of the corresponding position on the phase diagram. To check this, mobilities were extrapolated from Figure 14 at 300 and 400°C and are shown in Figure 15 along with the data at 518°C. The variation with composition does appear to be practically linear at constant temperature.

The temperature dependence of U_{12} is not linear but appears to decrease with increasing temperature. It can also be seen from Figure 14 that the temperature dependence is stronger toward the high Sn side.

It is possible to analyse these variations in terms of phenomenological parameters by means of Equation (125). Since the system is ideal, the thermodynamic factor $d \ln a_1 / d \ln N_1$ is identically one, under the assumption that the fractional change in density is negligible. As mentioned above, Niwa[153] has found the mutual diffusion coefficient to be a linear function of mole fraction at 500°C. He has also measured this coefficient in both dilute solutions of this system from 400 to 600°C. Consequently, it is possible to make a fairly good estimate of the mutual diffusion coefficient as a function of composition and temperature. Using Equation (125) then, the effective valence was calculated as a function of temperature and composition. The temperature variation is similar at

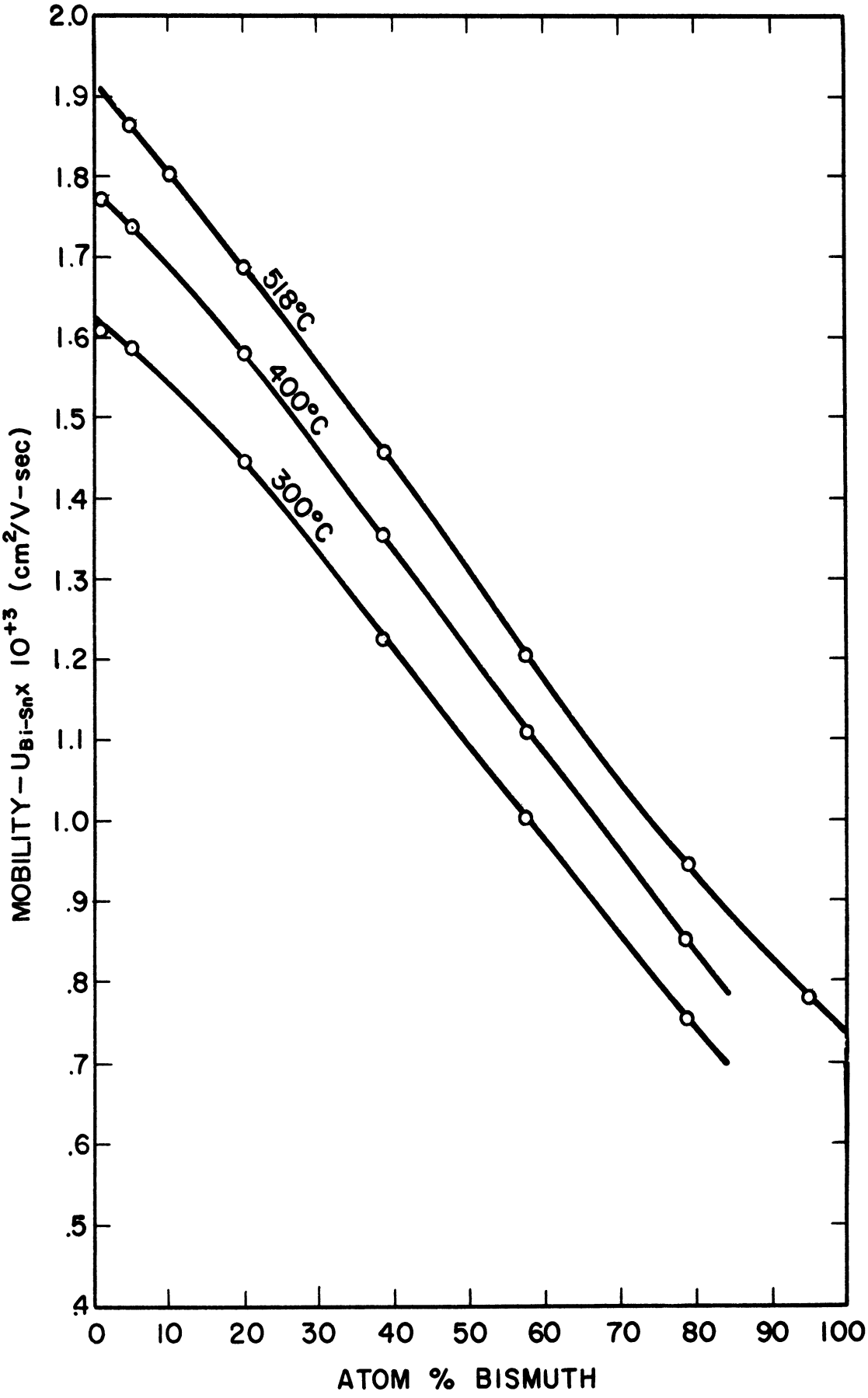

Figure 15. Isothermal Variation of Differential Mobility with Composition.

each composition; the results for two compositions are shown in Figure 16. The results agree qualitatively with those reported on the temperature dependence of the effective valence in solids as discussed in Chapter III.

It was shown in Chapter IV that the effective valence could be written as,

$$Z_i^o = \left[Z_i - \frac{\delta_i}{e^2 \rho} \right]. \qquad (127)$$

Further evidence was cited that would lead one to assume that the true valence, Z_i, and the friction coefficient should be independent of temperature. Consequently, a plot of Z_i^o (T) versus $1/\rho(T)$ would be a straight line from which one might determine the true valence and the friction coefficient. This plot has been constructed at each composition and in no case was it found to be linear; two examples are shown in Figure 17. These results indicate that either Z_i and/or δ_i vary with temperature, or that Equation (127) must be modified to include cathode-directed momentum transfer from defect electrons. As mentioned in Chapter III, Smolin has carried through an analysis including cathode-directed momentum transfer which predicts a hyperbolic relationship between $Z_i^o(T)$ and $1/\rho(T)$. Since other evidence indicates that Z_i and δ_i are temperature independent and that Smolin's analysis is questionable, (see Chapter IV), the above result might be interpreted as an indication that the migrating species is not the individual ions but rather clusters of ions whose size decreases as the temperature is increased.

The results of Figure 17 are, of course, subject to any errors inherent in Niwa's data on the diffusion coefficients. Because it is not

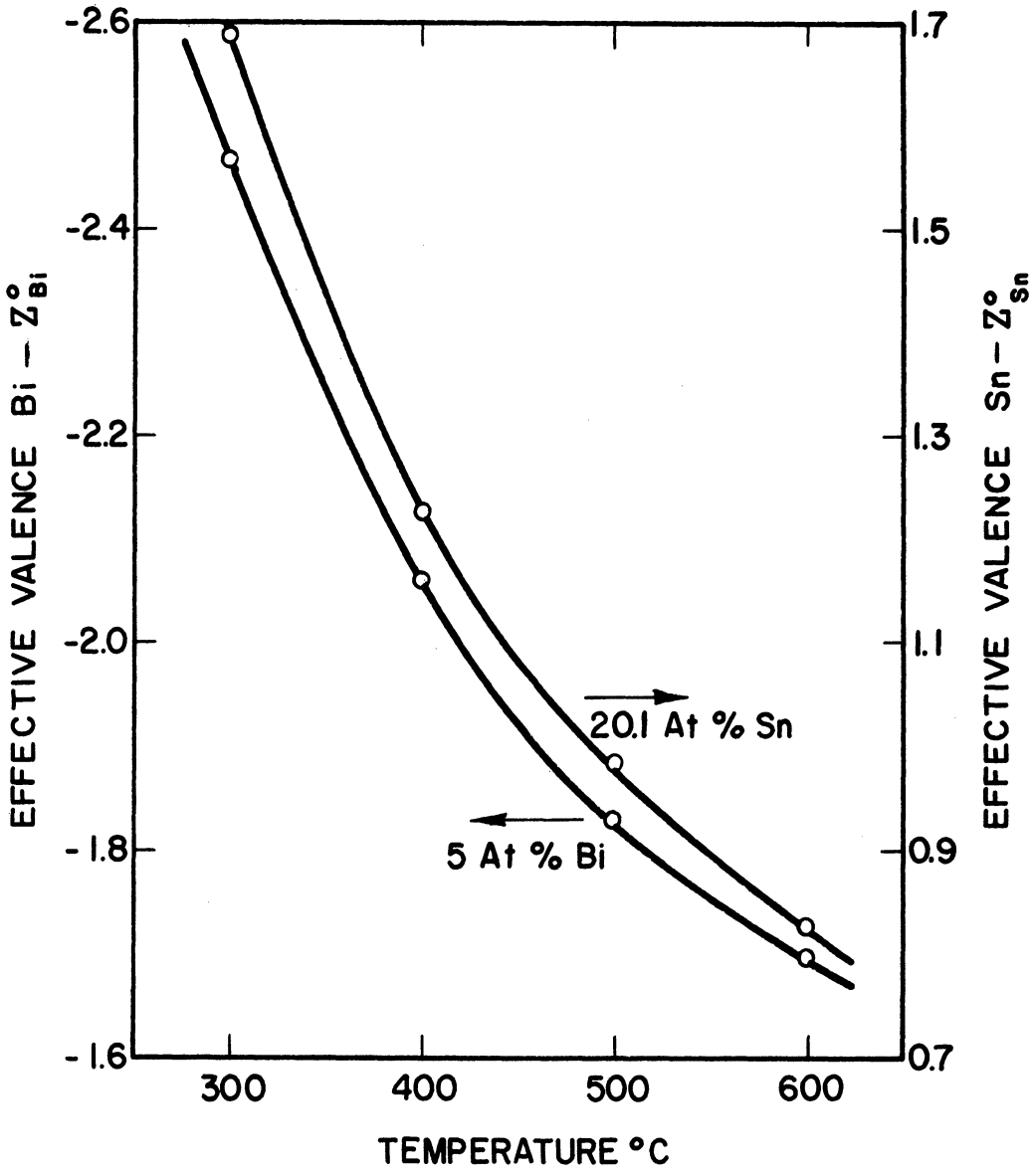

Figure 16. Variation of Effective Valence with Temperature.

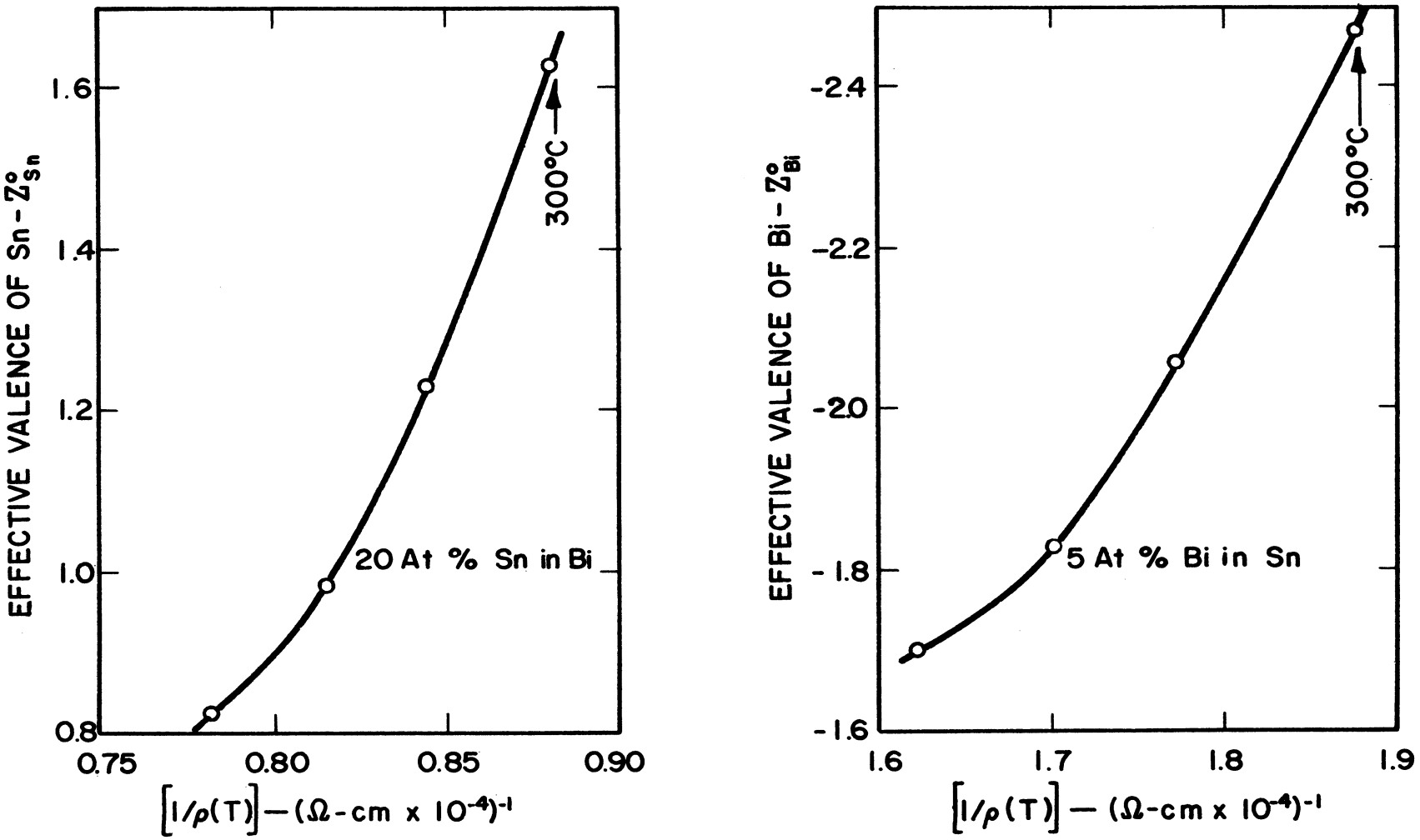

Figure 17. Effective Valence vs. Reciprocal Resistivity as a Function of Temperature.

possible to predict the temperature variation of Z_i^o, the temperature variation of the differential mobility cannot be used to estimate the activation energy for diffusion.

The variation of effective valence versus mole fraction has been calculated and is shown in Figure 18. Rather smooth curves are obtained which converge to zero for the pure metal. The convergence simply expresses the fact that in this gross phenomenological treatment no net motion is observed in pure metals. The negative values for Bi indicate that the electron friction force predominates while the positive values for Sn mean that the field force predominates.

Belashchenko[117] concluded that Z_1, Z_2 and δ_1/δ_2 are independent of composition. If Z_i and δ_i were independent of composition, a plot of $Z_i^o(X)$ vs. $1/\rho(X)$ should give a straight line. This plot of the data at 500°C is shown in Figure 19. At lower temperatures the curve in the bismuth data is more pronounced, and the tin data is curved concave upwards. In both cases it appears that as the temperature increases the plots of $Z_i^o(X)$ vs. $1/\rho(X)$ become more linear. On the basis of the above analyses this would indicate that Z_i and δ_i become independent of composition as the temperature is increased. Extrapolation of the tin data to the zero value of the abscissa at 500°C gives a true valence for Sn in Bi of $^+1.8$ on the basis of Equation (127). Similarly, an extrapolation of a forced straight line through the bismuth data gives a true valence of Bi in Sn of +1.4. The recent work of Cusack[31] and Tieche[139] on Hall coefficients in liquid metals indicate that molten metals may be described quite completely with the free electron gas model using the valence as the free electron to atom ratio. On this basis the above obtained values appear to be of the correct sign but slightly small.

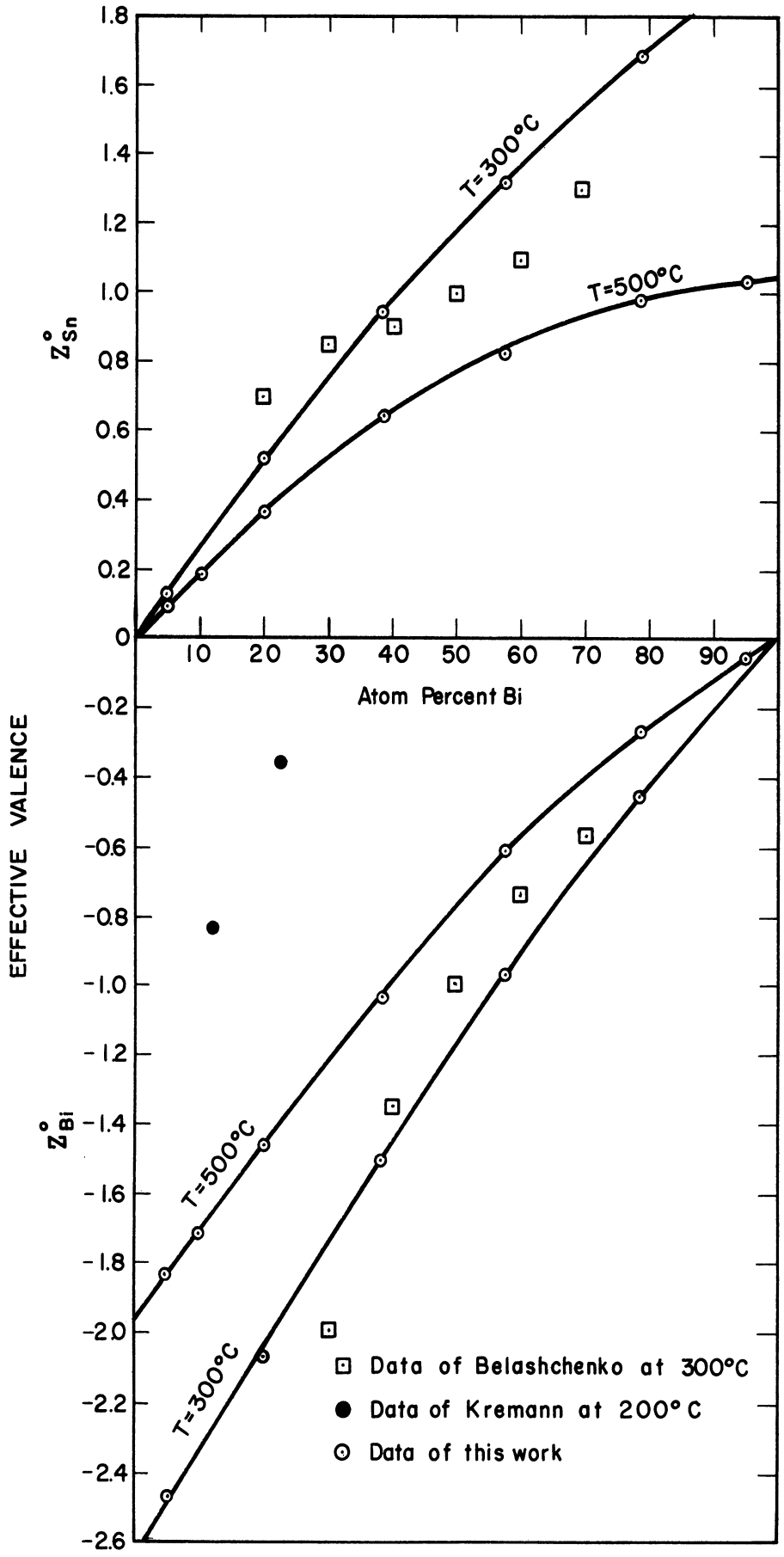

Figure 18. Variation of Effective Valence with Composition.

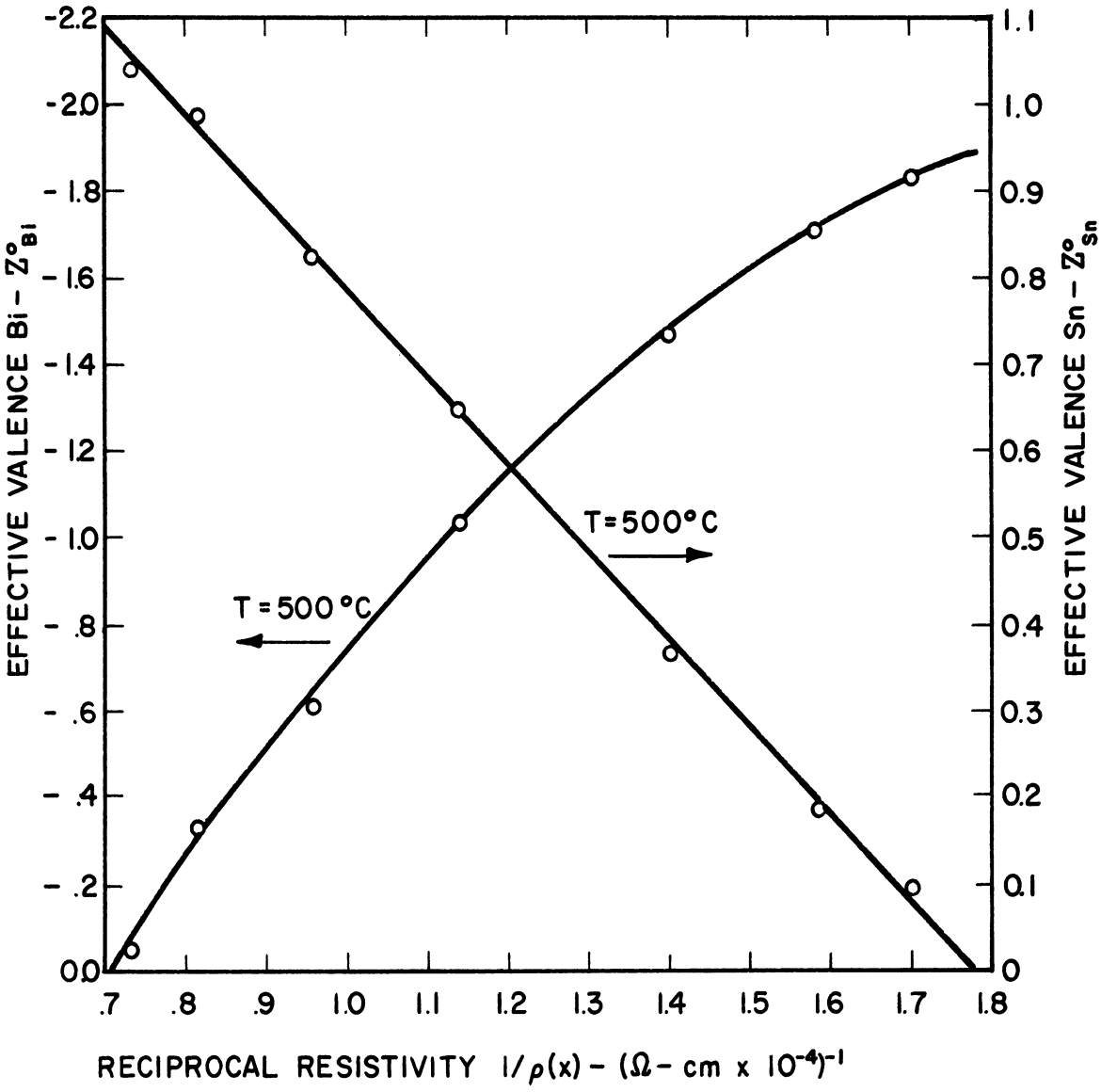

Figure 19. Effective Valence vs. Reciprocal Resistivity as a Function of Composition.

The gross picture of the above analysis lacks the detail to say anything about the actual mechanism of transport. It might be that migration occurs predominantly from activated ions or by the movement of clusters. As discussed in Chapter II such a detailed analysis quickly becomes very complex. If the moving species were predominantly clusters, one would expect them to break up at higher temperature. Since the friction coefficient and volume of such clusters would vary with temperature, this model would account for the non-linearity of the $Z_i^o(T)$ vs $1/\rho(T)$ found in this work. It might also account for the non-linearity of $Z_i^o(X)$ vs $1/\rho(X)$ at the lower temperature. Such conclusions, however, require the above analysis to be applied to clusters rather than the individual ion species. The true valence would then be the cluster valence.

Electrotransport in the Bi-Sn system has been studied by a number of previous investigators. The first investigation was reported by Kremann and Rehenburg.[158] These authors limited their experiments to four hours so that none of them reached steady-state conditions. Kremann, Kreighammer and Troster[159] reinvestigated the system using experimental times of 18 to 24 hours. With current densities above 800 amps/cm^2 the experiments appeared to have reached steady-state conditions for these experimental times in 15 cm capillaries. In both of these works the Bi migrated to the anode as in the present investigation. These investigators did not attempt to make any particular correlation of their data, which is reported as mole fraction Sn versus capillary position. Hence, the effective valence may be calculated from steady-state experiments by the following rearranged form of Equation (139),

$$Z_i^o = \frac{kT}{e\rho\,(I/A)} \frac{d \ln X_i}{dZ} \quad . \tag{183}$$

Some of Kremann's data which appeared to have reached the steady-state have been analysed and are shown in Figure 18. Previous authors[2] in discussing Kremann's data have concluded that convection currents where present, probably due to the use of large diameter horizontal capillaries. This would account for the low Z_i^o values of Kremann shown in Figure 18. In addition to convection errors this method of determining Z_i^o is subject to any errors introduced by segregation upon freezing. It is also necessary to assume a mean value for resistivity, although this difficulty can be overcome by proper analysis of the data.

Most of the Russian investigators reference a review article by Romadin[160] which is unavailable in the U. S. libraries. According to Esin,[161] Romadin has studied the Bi-Sn system and has also found that Bi migrates to the anode. However, he observed the effect to be only 14% as large as Kremann found; a result which seems erroneously low in view of the other work on this system.

As mentioned in Chapter III, Drakin has also studied the Bi-Sn system and found that Bi migrated to the anode. However, his work was done in the "V-notch" of the phase diagram and may not be analysed in terms of the effective valence.

The most recent investigation of the Bi-Sn system was done by Belashchenko[117] using the steady state method with chemical analysis. He has analysed his data in terms of the effective valence using Equation (139). The results are shown in Figure 18 and appear to agree fairly well with those of this investigation.

Reference to Figure 2 indicates that when the solute is run into the tube the linear portion of the V vs θ curve should be considerably longer than when the solute is run out of the tube. The solution shown in Figure 2 is limited by the assumption that the mole fraction of solute does not reach 1.0 when the solute is run inward. This limitation is most probably met in the experiments with only 5 At% solute which were run for 3 hours and produced a 20% change in the mean concentration in the case of highest mobility. In any case, it is intuitively apparent that the linear portion should be longer when the solute is run into the tubes, since in this case the mole percent solute at the electrode end can increase from 5 to 100% whereas when the migration direction is outward, the maximum mole percent solute change is only 5 to 0%. In the former case then, one would expect the concentration wave to move down the tube more slowly than in the latter for the same rate of transfer across the tube mouth. Some early results obtained in Run V-3 and shown in Figure 9, confirm this analysis. The alloy was 5 At% Sn, and when the Sn was run inward the linear portion was found to last for 30 hours. When the Sn was run outward the curve became non-linear after only 2.67 hours. Runs made at 5 At% Bi however, gave contrary results. When the solute was run inward the curve became non-linear after only 2.67 hours, but still remained linear after 3.33 hours when the solute was run outward. Longer time runs were not made. This result may be interpreted as evidence that when Bi migrates into the capillary the effective diffusion coefficient becomes very large due to some type of convection. The Bi atoms are heavier than Sn atoms and hence migration inward increases the density of the liquid at the top of the tube relative to that at the

bottom. Such a condition is unstable and would tend to produce convection. It would be interesting to conduct an experiment with the tubes inverted so that the mouth was facing upward with the electrode at the bottom.

CHAPTER VI

SUMMARY AND CONCLUSIONS

A brief discussion of the recent theories which have appeared in the literature is presented. A comparison of the different theories shows a strong similarity between some of them.

The recent experimental work is reviewed. The review covers electrotransport in solid metals, liquid metals and solid semiconductors. The work on electrotransport in solid metals is discussed under three categories depending on whether the migrating species is, (a) the pure metal, (b) an interstitial solute or (c) a solid solution solute. The liquid metals are discussed under two categories, (a) separation of alloy components and (b) separation of the isotopes of a pure metal. It is apparent that a large portion of the current work on electrotransport is being done in Russia.

A simple phenomenological discription of electrotransport in liquid metals is developed in which a differential mobility is defined. This differential mobility is equal to the difference of the individual mobilities. The differential mobility is related to the mutual diffusion coefficient through a parameter which is a measure of the effective valence of the migrating species. This effective valence is a function of the true valence and the electron-ion scattering cross section. An expression is presented for the effective valence which can be derived under certain limiting conditions from four of the theories discussed in Chapter 2.

Two different experimental methods have been developed for quantitatively determining the differential mobility at high temperatures.

Contrary to many of the older methods, both of these methods are free from errors due to convective mixing and segregation on freezing. The first method was developed in collaboration with fellow-graduate student John C Angus, and is distinguished from the second method in that the composition change is measured by chemical analysis rather than electrical resistivity. Solutes of Pd and Ni in molten bismuth were studied with this method. A number of ternaries consisting of two solutes dissolved in bismuth were also studied with this method. The precision of this technique was relatively low. The deviation of the average at the 95% confidence level on a Student-t distribution was around 15% for 7 "good" runs. In the second method the solute change was determined by measuring the corresponding resistivity change. The Bi-Sn system was chosen for analysis and the resistivity versus composition and temperature was determined. The differential mobility was determined as a function of composition and temperature. This technique was refined, after much experimental difficulty, to be quite precise. The deviation of the average at the 95% confidence level on a Student-t distribution was on the average, 1% for 8 runs.

The data collected with the first method verify that the mobility at higher temperatures is of the same order of magnitude as that found in mercury at room temperature. The temperature dependence of the mobility of Ni in Bi was also found to be roughly the same as that found for mercury systems around room temperature. The addition of a second solute did not appreciably affect the mobility of the first in the systems studied. Consequently, in answer to the orginal question which motivated this

work, it is possible to separate uranium solute from Cu and Mg dissolved in liquid bismuth.

The data collected with the second method are the first really quantitative results on the differential electric mobility at high temperatures as a function of temperature and composition. The high precision of the method is in sharp contrast with the precision generally achievable in liquid diffusion measurements. The mobility varies almost linearly with composition at constant temperature. The variation with composition at 30°C above the liquidus shows no anomalies above the eutectic. The mobility increases non-linearly with temperature. The increase becomes less at higher temperatures and is smaller on the high bismuth side of the system. The results were analysed on the basis of a simple phenomenological approach. Literature data was used for the mutual diffusion coefficient. The effective valence was found to decrease with temperature in accord with the results on solid metals. The expression derived for the effective valence indicates that either: (a) It is necessary to include the momentum transfer from defect electrons in deriving an expression for the effective valence, or (b) The charge of the migrating species or the electron-ion scattering cross sections are functions of temperature. They are also a function of composition but become less so as the temperature is increased and are independent of composition for the migrating tin species at 500°C. This allows the true valence of Sn to be estimated as + 1.8 in Bi at 500°C. It is possible to interpret these results as an indication that electrotransport occurs by the movement of clusters.

The present results were compared to literature data on electrotransport in the Bi-Sn system. It was necessary to use literature data on the mutual diffusion coefficient because of the different method of investigation. The work of Kremann [158, 159] and Romadin[160] appears to be low and that of Belashchenko [117] appears to be approximately the same as that found in this work.

The effective diffusion coefficient was found to be much larger when the Bi was migrated upward into the capillaries than vice versa. This was interpreted as a result of the unstable density gradient produced. Hence, it appears that it is very important in steady-state experiments, such as conducted by the above authors, to arrange the polarity so that the less dense metal migrates downward.

REFERENCES

1. M. Gerardin, "De l'action de la pile sur les sels de potasse et de soude et sur les alliages soumis a la fusion igne'e," Compt. Rend., 53, 727-730 (1861).

2. K. E. Schwarz, Electrolytic Migration in Liquid and Solid Metals, Johann Ambrosius Barth, Leipzig 1940; also, Edwards Brothers, Ann Arbor, Michigan, 1945.

3. W. Jost, Diffusion in Solids, Liquids, Gases, Academic Press, New York, 1952.

4. W. Seith, Diffusion in Metals, Sec. Ed., Springer, Berlin, 1955.

5. A. Einstein, "Motion of Suspended Particles on the Kinetic Theory," Ann. Physik, 17, 549-560 (1905).

6. J. Bardeen (see footnote 8, page 1404), "Diffusion in Binary Alloys," Phys. Rev., 76, No. 9, 1403-1405 (1949).

7. J. Bardeen and C. Herring, "Diffusion in Alloys and the Kirkendall Effect," Atom Movements, ASM, Cleveland, Ohio, 1951.

8. A. D. LeClaire and A. B. Lidiard, "Correlation Effects in Diffusion in Crystals," Phil. Mag., 1, No. 6, 518-527 (1955).

9. K. Compaan and Y Haven, "Correlation Factors for Diffusion in Solids," Trans. Far. Soc., 52. 786-801 (1956).

10. J. Frenkel, Kinetic Theory of Liquids, Dover, 1955.

11. C. H. Ma and R. A. Swalin, "Self Diffusion in Liquid Tin," J. of Chem. Phys., 36, No. 11, 3014-3018 (1962).

12. F. Skaupy, "The Electrical Conduction in Metals," Verhandl. deut. Physik Ges., 16, 156-167 (1914).

13. G. N. Lewis, E. Q. Adams, E. H. Lanman, "Electrical Transference in Amalgams," J. Am. Chem. Soc., 37, 2656-2663 (1915).

14. C. Wagner, "Interpretation of the Electrolytic Current Conducting Constituent in Amalgams and Other Alloys," Z. physik. Chem., B15, 347-352 (1932).

15. P. C. Mangelsdorf, Jr., "Transport Processes in Liquid Alloys. II The Electrical Force on An Ion," J. Chem. Physics, 33, No. 4, 1151-1161 (1960).

16. H. B. Huntington and A. R. Grone, "Current Marker Motion in Gold Wires," J. Phys. Chem. Solids, 20, Nos. 1/2, 76-87 (1961).

17. K. Schwarz, "On the Theory of the Electrolytic Phenomenon in Metallic Solutions," Z. physik. Chem., A164, 223 (1933).

18. J. C. Angus, The Electrolysis of Some Liquid Metal Alloys, Thesis Dissertation, University of Michigan, January, 1961.

19. V. B. Fiks, "On the Mechanism of the Mobility of Ions in Metals," Fiz. Tver. Tela, 1, No. 1, 1959, [Sov. Phys.--Sol. State, 1, No. 1, 14-28 (1959)].

20. N. F. Mott and H. Jones, The Theory of the Properties of Metals and Alloys, Dover Pub. Inc., New York, 1958; also, Clarendon Press, Oxford, England, 1936.

21. M. D. Glinchuk, "The Theory of Electrotransport in Solid Metal Crystals," Ukr. Fiz. Zhurn., 4, No. 5, 684-685 (1959).

22. S. Brown and S. J. Barnett, "Carriers of Electricity in Metals Exhibiting Positive Hall Effects," Phys. Rev., 87, 601-607 (1952).

23. A. Klemm, "Isotope Transference and Self Transference in Metals," Z. Naturforschung, 9a, 1031-1035 (1954).

24. S. E. Bresler and G. E. Pikus, "On the Theory of the Separation of Isotopes and of Components of Alloys by the Passage of Current Through Liquid Metal," J. Tech. Phys. (USSR), 28, 2282-2288 (1958), [Sov. Phys.--Tech. Phys., 3, 2094-2100 (1958)].

25. V. L. Ginzburg, "Electron-Inertia Experiments with Metals and the Hall Effect," Chem. Abstracts, 53, 16707e.

26. A. R. Grone, "Current-Induced Marker Motion in Copper," J. Phys. Chem. Solids, 20, Nos. 1/2, 88-93 (1961).

27. H. B. Huntington and Siu-Chung Ho, "Electromigration in Metals," Japanese Conference on Crystal Lattice Defects, Kyoto, Japan, Sept. 7-12 (1962). To be published in J. Phys. Soc., Japan.

28. C. Bosvieux and J. Friedel, "On the Electrolysis of Metallic Alloys," J. Phys. Chem. Solids, 23, 123-136 (1962).

29. P. C. Mangesldorf, Jr., "Electrolysis and Diffusion Liquid Alloys," Metallurgy Society Conference (AIME), Vol. 7, 428-445, Interscience Pub. (1961).

30. L. G. Schulz, "The Experimental Study of the Optical Properties of Metals and the Relation of the Results to the Drude Free Electron Theory," Advanc. Phys., 6, 102-144 (1957).

31. N. Cusack and P. Kendall, "The Hall Coefficient of Liquid Mercury," Phil. Mag., 6, 419-427 (1961).

32. Y. Tieche, "Hall Effect of Liquid Mercury," Helv. phys. Acta, 33, 963-966 (1960).

33. P. C. Mangelsdorf, Jr., "The Role of Thermal Diffusion in the Electrolytic Separation of Isotopes in Liquid Metals," J. Chem. Phys., 32, 293-295 (1960).

34. P. G. deGennes, "Isotopic Separation by Passage of Current in a Metal," J. Phys. Rad., 17, 343-346 (1956).

35. A. Klemm, "Thermodynamics of the Transport Processes in Ion Mixtures and Its Application to Salts and Metals Containing Isotopes," Z. Naturforschung, 8a, 397-400 (1953).

36. R. W. Laity, "An Application of Irreversible Thermodynamics to the Study of Diffusion," J. Phys. Chem., 63, 80-83 (1959).

37. L. Onsager, "Theories and Problems of Liquid Diffusion," Ann. N.Y. Acad. Sci., 46, 241-265 (1945).

38. A. Klemm, "Isotopic Transference and Self Transference in Metals," Z. Naturforschung, 9a, 1031-1035 (1954).

39. E. Haeffner, "A New Method of Changing the Isotope Abundance of Mercury," Nature, 172, 775-776 (1953).

40. B. Baranowski, "Thermodynamical Theory of Separation of Components in Binary Liquid Alloys in an Electric Field," Roczniki Chem., 29, 129-131 (1955).

41. B. Baranowski, "A Certain System of Thermodynamic Forces and Flows in a Binary Electrolytic Solution," Roczniki Chem., 29, 586-593 (1955).

42. B. Baranowski, "Migration of Components of Binary Liquid Metallic Alloys in the Electric Field from the Point of View of Thermodynamics of Irreversible Processes," Pol. Akad. Nauk, Bull. Ser. Sci., Math. Astron., 3, No. 2, 117-120 (1955).

43. B. Baranowski, "The Seith-Wever Effect Interpreted from the Point of View of Thermodynamics of Irreversible Processes," Pol. Akad. Nauk, Bull. Ser. Sci., Math. Astron., 4, No. 7, 465-468 (1956).

44. B. Baranowski and A. S. Cukrowski, "Transport Processes in Iso- and Polythermal Binary Solid Metal Alloys," Pol. Akad. Nauk, Bull. Ser. Sci. Chimiques, 10, No. 3, 135-141 (1962).

45. D. K. Belashchenko and A. A. Zhukhovitskii, "Theory of Electrical Transport," Zhur. Fiz. Khim., 35, 1921-1926 (1961), [Rus. J. Phys. Chem., 35, No. 9, 944-947, (1961)].

46. D. K. Belashchenko and B. S. Bokshtein, "Theory of Electrical Transport II. Multicomponent Metallic Systems," Zhur. Fiz. Khim., 35, 2228-2233 (1961), [Rus. J. Phys. Chem., 35, No. 10, 1099-1101 (1961)].

47. K. G. Denbigh, The Thermodynamics of the Steady State, Wiley, New York, 1951.

48. B. Baranowski and A. S. Tsukrovskii, "Comments on the Paper by Belashchenko and Zhukhovitskii, Theory of Electrical Transport," Zh. Fiz. Khim., 36, No. 9, 2096-2097 (1962).

49. D. K. Belashchenko and A. A. Zhukhovitskii, "Reply to ... Comments on ...," Zh. Fiz. Khim., 36, No. 9, 2098 (1962).

50. S. I. Drakin, "Transfer and Distribution of the Components of Metal Alloys in an Electric Field," Zhur. Fiz. Khim., 27, 1586-1591 (1953).

51. B. Baronowski, "Some Remarks on the Work of S. I. Drakin," Zhur. Fiz. Khim., 28, 1676-1677 (1954).

52. K. P. Gurov, "The Theory of Diffusion Movement and Electron Transfer in Metals and Metallic Solid Solutions," Fiz. Metal. Metalloved., 11, No. 4, 496-506 (1961), [Phys. Metals and Metallog., 11, No. 4, 18-29 (1961)].

53. Th. Heumann, "Electrolytic Transport in Metallic Solutions," The Physical Chemistry of Metallic Solutions and Intermetallic Compounds, Vol. 1, Paper 2C, Her Majesty's Stationary Office, London, 1959.

54. H. Wever, "Transport Experiments on Solid Copper," Z. Elektrochem., 60, 1170-1175 (1956).

55. H. Wever, "Electrolytic Transport and Conduction Mechanism in Iron and Nickel," The Physical Chemistry of Metallic Solutions and Intermetallic Compounds, Vol. 1, Paper 2L, Her Majesty's Stationary Office, London, 1959.

56. H. Wever and W. Seith, "New Results on the Electrolysis of Solid Metal Phases," Z. Elektrochem., 59, 942-946 (1955).

57. A. R. Grone, "Current-Induced Marker Motion in Copper," J. Phys. Chem. Solids, 20, No. 1/2, 88-93 (1961).

58. P. P. Kuz'menko and E. I. Khar'kov, "Migration of Silver on Passing Direct Current Through It," Ukr. Fiz. Zhur., 3, 528-536 (1958).

59. P. P. Kuz'menko and E. I. Khar'kov, "Electric Transfer in Cd and Zn," Ukr. Fiz. Zhur., 4, 537-539 (1959).

60. E. I. Khar'kov and P.P. Kuz'menko, "Electric Transfer in Sn, Pb, Ag, and Cu," Ukr. Fiz. Zhur., 5 428-429 (1960).

61. P. P. Kuz'menko and E. I. Khar'kov, "Electric Transport in Solid Aluminum," Ukr. Fiz. Zhur., 4, 401-402 (1959).

62. P. P. Kuz'menko and V. S. Grom, "Electrical Transfer of Gold in Solid Gold," Ukr. Fiz. Zhur., 6, 140-142 (1961).

63. P. P. Kuz'menko, "Mechanism of Mobility and Effective Charges of Ions in Metals," Ukr. Fiz. Zhur., 7, Nos.2/3, 117-131 (1962).

64. P. P. Kuz'menko and E. I. Khar'kov, "Determination of the Degree of Ionization of Atoms in the Crystal Lattice by the Electric Transfer Method," Ukr. Fiz. Zhur., 5, 430-431 (1960).

65. I. N. Frantsevich, "An Investigation of Electric Transport in Solid Solutions of Metals Using Radiactive Isotopes," UNESCO/NS/RIC/29, Pergamon Press, London, 1957.

66. I. N. Frantsevich, D. F. Kalinovich, I. I. Kovens'kii and V. V. Pen'kovs'kii, "The Acceptor Role of Iron in an Iron-Carbon Alloy," Doklody Acad. Nauk SSSR, 121, 277 (1958), [Sov. Phys.--Doklady, 3, 842-844 (1958)].

67. I. N. Frantsevich, D. F. Kalinovich, I. I. Kovens'kii and V. V. Pen'kovs'kii, "On the Migration of Solid Metal Solution Components in a Direct Current Field III," Ukr. Fiz. Zhur., 3, No. 4, 552-559 (1958).

68. I. N. Frantsevich, D. F. Kalinovich, I. I. Kovens'kii and M. D. Smolin, "Some Quantitative Relationships of the Process of the Donor-Acceptor Reaction in Metal Alloys," Fiz. Tver. Tela, 1, No. 1, 62-66 (1959), [Sov. Phys.--Sol. State, 1, No. 1, 58-61 (1959)].

69. S. D. Gertsriken, I. Ya. Dekhtyar, V. S. Mikhalenkov, and V. M. Fal'chenko, "Study of Electrical Transfer in Steels by the Method of Inert Tags," Ukr. Fiz. Zhur., 6, No. 1, 129-135 (1961).

70. S. D. Gertsriken, I. Ya. Dekhtyar, V. S. Mikhalenkov, and E. G. Madatova, "Study of the State of Atoms in Solid Iron-Aluminum Solutions by the Electrical Transfer Method," Ukr. Fiz. Zhur., 5, No. 1, 79-87 (1960).

71. S. D. Gertsriken, I. Ya. Dekhtyar, V. S. Mikhalenkov, and E. G. Madatova, "The Electrolytic Conductivity of the Iron-Aluminum Alloys in the Solid State," Issled. po Zhar. Splavam, Akad. Nauk SSSR, Inst. Met. im A.A. Babikova, 6, 99-104 (1960).

72. F. Claisse and H. P. Koenig, "Thermal and Forced Diffusion of Oxygen in β-Titanium," Acta Met., 4, 650-654 (1956).

73. I. H. de Boer and J. D. Fast, "Electrolysis of Solid Solutions of Oxygen in Metallic Zirconium," Rec. Trav. Chim., 59, 161-167 (1940).

74. W. Seith and Th. Daur, "Electrical Transport in Solid Alloys," Z. Elektrochem., 44, 256-260 (1938).

75. A. Coehn and W. Specht, "The Contribution of Protons to the Electric Conductivity in Metals," Z. Phys., 62, 1-31 (1930).

76. C. Wagner and G. Heller, "The Rate of Migration of Protons in an Electric Field in the α Phase of the System Palladium-Hydrogen," Z. Phys. Chem. Abt. B, 46 242-249 (1940).

77. J. M. Williams and C. L. Huffine, "Solid State Electrolysis in Yttrium Metal," Nuclear Sci. and Eng., 9, 500-506 (1961).

78. V. I. Yavoiskii and D. F. Chernega, "Motion of Hydrogen in Solid Steel Under the Effect of an Electric Field," Stal, 16, 790-793 (1956).

79. I. N. Frantsevich, D. F. Kalinovich, I. I. Kovens'kii, "The Problem of the State of Carbon in Iron and Steel," Fiz. Metal. Metalloved., 8, No. 4, 574-578 (1959), [Phys. Metals Metallog., 8, 93-97 (1959)].

80. D. F. Kalinovich, "Electrical Transport in Interstitial Solid Solutions," Fiz. Tverd. Tela, 3, 1117-1121 (1961), [Sov. Phys.-- Sol. State, 3, No. 4, 812-815 (1961)].

81. Yu. F. Babikova and P. L. Gruzin, "Study of the Electrolytic Transport of Carbon in Steel by Means of Radioactive Tracers," Fiz. Metal. Metalloved., 5, No. 2, 225-260 (1957), [Phys. Metals Metallog., 5, 57-61 (1957)].

82. P. L. Gruzin, Yu. F. Babikova, Yu. A. Polikarpov, and G. B. Fedorov, "Investigation into Carbon Atom Mobility and Atomic Interaction in Alloys by the Use of Tracer Techniques," UNESCO/NS/RIC/28, Pergamon Press, London, 1957.

83. I. N. Frantsevich, D. F. Kalinovich, I. I. Kovens'kii, V. V. Pen'kovs'kii, "On The Migration of Solid Metal Solution Components in a Direct Current Field I", Ukr. Fiz. Zhur., 3, No. 1, 124-134 (1958).

84. P. L. Gruzin, Yu. F. Babikova, Yu. A. Polikarpov, A. N. Tirkina, G. B. Fedorov, E. V. Borisov, S. V. Zemskii, N. P. Peregudov, and M. A. Shumilov, "Investigation of the Mobility of Carbon Atoms in Steel and Alloys with Carbon 14," Problemy Metalloved. Fiz. Metal., No. 5, 327-365 (1958).

85. I. N. Frantsevich and I. I. Kovens'kii, "Ion Migration of Carbon in Metals of the Iron Group," Dopovidi Akad. Nauk, Ukr. R.S.R., No. 9, 1169-1171 (1961).

86. I. N. Frantsevich and I. I. Kovens'kii, "On the State of Carbon in Titanium, Tantalum and Tungsten," Dopovidi Akad. Nauk, Ukr. R.S.R., No. 11, 1471-1474 (1961).

87. M. D. Smolin and I. N. Frantsevich, "Application of the Method of Electric Transport to the Study of Metals and Alloys," Fiz. Tver. Tela, 3, 2115 (1961), [Sov. Phys.--Sol. State, 3, No. 7, 1536-1541 (1962)].

88. D. F. Kalinovich, I. I. Kovens'kii, and M. D. Smolin, "Diffusion and Electrolytic Transport of Chromium in Molybdenum," Fiz. Metal. Metalloved., 11, No. 2, 307-308 (1961), [Phys. Metals Metallog., 11, 148-150 (1961)].

89. I. N. Frantsevich, D. F. Kalinovich, I. I. Kovens'kii, and M. D. Smolin, "The Electrical Transfer of Tungsten in Nickel-Tungsten Alloys," Inzhener. Fiz. Zhur., Akad. Nauk Belorus. S.S.R., 2, No. 4, 47-51 (1959).

90. I. N. Frantsevich, D. F. Kalinovich, I. I. Kovens'kii, V. V. Pen'kovs'kii and M. D. Smolin, "Electrodiffusion of Tungsten in an Iron-Tungsten Alloy," Dopovidi Akad. Nauk, Ukr., R.S.R., No. 7, 736-739 (1958).

91. I. N. Frantsevich, D. F. Kalinovich, I. I. Kovens'kii and M. D. Smolin, "Migration of the Components of Iron-Tungsten Alloys in a Constant Electric Field," Izvest. Akad. Nauk SSSR., Otdel. Tekh. Nauk Met i Toplivo, No. 1, 71-74 (1959).

92. I. N. Frantsevich, D. F. Kalinovich, I. I. Kovens'kii and M. D. Smolin, "Donor-Acceptor Interactions of Components in a Binary Fe-Cr Alloy," Inzhener. Fiz. Zhur., Akad. Nauk. Belorus. S.S.R., 2, No. 9, 62-68 (1959).

93. I. N. Frantsevich, D. F. Kalinovich, I. I. Kovens'kii and V. V. Pen'kovs'kii, "On the Migration of Solid Metal Solution Components in a Direct Current Field II," Ukr. Fiz. Zhur., 3, Supplement to No. 1, 64-68 (1958).

94. D. F. Kalinovich, I. I. Kovens'kii, M. D. Smolin, and I. N. Frantsevich, "The Mobility of Chromium Atoms in a Nickel-Chromium Alloy Under the Influence of a Constant Electric Field," Fiz. Metal. Metalloved., 10, No. 1, 42-46 (1960), [Phys.Metals Metallog., 10, No. 1, 41-44 (1960)].

95. D. F. Kalinovich, I. I. Kovens'kii, M. D. Smolin, and I. N. Frantsevich, "Diffusion of Nickel in a Ni-Mo Alloy in an Electric Field," Inzhener. Fiz. Zhur., Akad. Nauk. Belorus. S.S.R., 4, No. 5, 108-110 (1961).

96. M. D. Smolin and I. N. Frantsevich, "Investigation of the Effect of Temperature on the Migration of Elements in Alloys of High Melting Point Metals," Dokl. Akad. Nauk SSSR., 136, 81-83 (1961), [Sov. Phys.--Doklady, 6, No. 1, 66-67 (1961)].

97. I. N. Frantsevich and M. D. Smolin, "Concentration Dependence of the Electrotransport of Ni-Cr Alloy Components," Dopovidi Akad. Nauk Ukr. R.S.R., No. 7, 908-910 (1961).

98. D. F. Kalinovich, I. I. Kovens'kii, M. D. Smolin, "Electrical Transfer of Tungsten in Cobalt," Fiz. Metal. Metalloved., 13, No. 6, 930-931 (1962).

99. E. I. Khar'kov and P. P. Kuz'menko, "Electrical Transfer of Iron and Aluminum in Fe-Al Alloys," Ukr. Fiz. Zhur., 4, No. 3, 389-398 (1959).

100. P. P. Kuz'menko, E. I. Khar'kov, and G. P. Grinevich, "Diffusion and Electric Transfer in Ag-Zn Alloys, Ukr. Fiz. Zhur., 5, No. 5, 683-688 (1960).

101. P. P. Kuz'menko and L. F. Ostrovs'kii, "Electrotransfer of Small Amounts of Zinc and Silver in Solid Aluminum," Ukr. Fiz. Zhur., 6, No. 3, 525-530 (1961).

102. P. P. Kuz'menko, L. F. Ostrovs'kii, and V. S. Koval'chuk, "Mobility of Antimony, Iron, Cobalt in Copper," Fiz. Tver. Tela, 4, No. 2, 490-493 (1962), [Sov Phys.--Sol. State, 4, No. 2, 356-358 (1962)].

103. P. P. Kuz'menko, L. F. Ostrovs'kii, and V. S. Koval'chuk, "Mobility of Small Amounts of Tin in Copper and Silver," Fiz. Metal. Metalloved., 13, 406-410 (1962).

104. P. P. Kuz'menko, "Determination of the Effective Charge of Impurities in a Metal from Residual Electric Resistance," Ukr. Fiz. Zhur., 6, No. 1, 116-120 (1961).

105. O. Kubaschewski and K. Reinartz, "Electrical Transport Measurements for the Investigation of the Heteropolarity of Solid Intermetallic Phases," Z. Elektrochem., 52, 75-86 (1948).

106. C. S. Fuller and J. C. Severiens, "Mobility of Impurity Ions in Germanium and Silicon," Phys. Rev., 96, No. 1, 21-24 (1954).

107. C. J. Gallagher, "Electrolysis of Copper in Solid Silicon," J. Phys. Chem. Sol., 3, 82-86 (1957).

108. I. I. Ibragimov and A. A. Kuliev, "Electrical Transport of Thallium in Polycrystalline Selenium," Fiz. Tver. Tela, 3, No. 11, 3330-3335 (1961), [Sov. Phys.--Sol. State, 3, No. 11, 2418-2421 (1962)].

109. B. I. Boltaks, G. S. Kulikov, and R. Sh. Malkovich, "Electrical Transport of Gold in Silicon," Fiz. Tver. Tela, 2, No. 10, 2395-2399 (1960), [Sov. Phys.--Sol. State, 2, No. 10, 2134-2137 (1960)].

110. V. B. Fiks, "Entrainment of Ions by Electrons in Semiconductors," Fiz. Tver. Tela, 1, 1321 (1959), [Sov. Phys.--Sol. State, 1, 1211-1214 (1959)].

111. B. P. Konstantinov and L. A. Badenko, "An Electrical-Diffusion Study of the Behavior of Indium and Antimony Impurities in Germanium," Fiz. Tver. Tela, 2, No. 11, 2696-2702 (1960), [Sov. Phys.--Sol. State, 2, No. 11, 2400-2405 (1961)].

112. S. I. Drakin, "A New Method of Separation of Eutetic Alloys," Izvest. Sektora. Fiz. Khim. Anal. Akad. Nauk. SSSR., 20, 341-344 (1950).

113. S. I. Drakin and A. K. Maltsev, "Electrodiffusion in Alloys of Potassium and Sodium," Zhur. Fiz. Khim., 31, 2036-2041 (1957).

114. S. I. Drakin, Yu. K. Golubkova, and E. P. Ushakova, "Electrodiffusion in Dilute Solutions of Lead and Mercury in Metallic Potassium," Zhur. Fiz. Khim., 34, 866-871 (1960), [Rus. J. Phys. Chem., 34, No.4, 411-414 (1960)].

115. S. I. Drakin, T. N. Sergeeva, and U. N. Rusakova, "Electrodiffusion in K-Tl, Na-Hg, Na-Pb, and Na-Cd Alloys," Zhur. Fiz. Khim., 35, 1125-1132 (1961), [Russ. J. Phys. Chem., 35, No. 5, 551-555 (1961)].

116. D. K. Belashchenko, "Electron Transport in Liquid Alloys of the Bismuth-Tin System," Izvest. Vysskikh Ucheb. Zavedenii SSSR, Khim. i Khim. Tekh., No. 2, 285-287 (1960).

117. D. K. Belashchenko, "Mechanism of Electrotransfer in Liquid Binary Metallic Alloys," Izvest. Vysshik Ucheb. Zavedenii SSSR, Chernaya Met., No. 9, 5-12 (1961).

118. D. K. Belashchenko, "Kinetic Properties of Liquid Metallic Alloys," Izvest. Akad. Nauk. SSSR, Otdel. Tekh. Nauk, Met. i Toplivo, No. 6, 89-93 (1960).

119. D. K. Belashchenko, "Electrical Transport in Dilute Metallic Solutions," Zhur. Fiz. Khim., 35, No. 8, 1875-1876 (1961), [Rus. J. Phys. Chem., 35, No. 8, 923-924 (1961)].

120. D. K. Belashchenko, and G. A. Grigor'ev, "An Investigation of Electro-transport of Impurities in Molten Metals," Izvest. Vysshikh Ucheb. Zavedenii SSSR, Chernaya Met., No. 11, 116-121 (1961).

121. P. C. Mangesldorf, Jr., "Transport Processes in Liquid Alloys, I: A Transport Cell for Liquid Alloys," J. Chem. Phys., 30 1170-1179 (1959).

122. M. A. Rabkin, "Electrolytic Transfer of Carbon in Liquid Iron-Carbon Alloys," J. Applied Chem. USSR, 30, 832-835 (1957).

123. V. I. Yavoiskii and G. I. Batalin, "Removal of Hydrogen from Metals by Employment of an Electric Field," Trudy Nauch.--Tekh. Obshchestva Chernoi Met., 4, 74-88 (1955).

124. J. C. Angus and E. E. Hucke, "The Electrolysis of Sodium Amalgams," J. Phys. Chem., 65, 1549-1551 (1961).

125. A. Lunden, C. Reutersward, and A. Lodding, "Isotopic Effect Produced by Current Passage in Molten Potassium Metal," Z. Naturforsch., 10a, 924-926 (1955).

126. A. Lodding, A. Lunden and H. von Ubisch, "The Temperature Dependence of the Isotope Effect due to Current Flow in Molten Indium Metal," Z. Naturforsch., 11a, 139-142 (1956).

127. A. Lunden, A. Lodding and W. Fischer, "Isotope Effect Induced by Current in Molten Lithium Metal," Z. Naturforsch., 12a, 268-269 (1957).

128. A. Lodding, "Isotope Transport in Molten Rubidium Metal at Different Temperatures," Z. Naturforsch., 14a, 7-9 (1959).

129. A. Lodding, "Temperature Dependence of the Isotope Effect in Current Carrying Liquid Alkali Metals," Z. Naturforsch., 14a, 934-937 (1959).

130. A. Lodding, "New Measurements of the Haeffner Effect in Rb, K and In," Z. Naturforsch., 16a, 1252-1253 (1961).

131. E. Haeffner, "A method of Changing the Isotope Abundance in Mercury," Nature, 172, 775-776 (1953).

132. E. Haeffner, Th. Sjoborg, S. Lindhe, "The Isotope Effect of a Direct Electric Current Through Liquid and Solid Metal," Z. Naturforsch., 11a, 71-75 (1956).

133. I. V. Bogoyavlenskii, V. N. Grigor'ev, N. S. Rudenko, and D.G. Dolgopolov, "Change in the Isotopic Composition of Mercury in a D.C. Field," Zhr. Ehsptl i Teoret. Fiz., 33, 581-587 (1957), [Sov. Phys.--JETP, 6, No. 3, 450-454 (1958)].

134. I. V. Bagoyavlenskii, V. N. Grigor'ev, and N. S. Rudenko, "Effect of Temperature on the Change in Isotopic Composition of Liquid Mecury in a D.C. Field," Zhur. Ehsptl. Teoret. Fiz., 37, 1241-1246 (1959), [Sov. Phys. -- JETP, 10, 884-887 (1960)].

135. G. Neif and Etienne Roth, "On the Phenomena of the Separation of Isotopes Produced by Passage of an Electric Current in a Liquid Metal," Compt. Rend., 239, 162-164 (1954).

136. M. M. Goldman, G. Nief, and E. Roth, Influence of Temperature Upon the Isotopic Separation Under the Effect of Direct Current in Gallium," Compt. Rend., 243, 1414-1416 (1956).

137. A. Lodding, Isotope Transport Phenomena in Liquid Metals, Gothenburg Studies Phys., 1, 71 pp., Almquist and Wiksell, Stockholm, Sweden, 1961.

138. L. S. Darken, "Diffusion, Mobility, and Their Interrelation Through Free Energy in Binary Metallic Systems," Trans. AIME, 175, 185-194 (1948).

139. G. Busch and Y. Tieche, "Hall Effect of Liquid Metals," Helv. Phys. Acta, 35, No. 4 and 5 (1962).

140. G. E. Pikus and V. B. Fiks, "Electrokinetic Effects in Liquid Metals," Fiz. Tver. Tela, 1, 1062-1071 (1959), [Sov. Phys.--Sol. State 1, 972-980 (1959)].

141. V. B. Fiks and G. E. Pikus, "Electrokinetic Effects and the Viscosity of Electrons in Liquid Metals. II," Fiz. Tver. Tela, 1, 1147-1158 (1959), [Sov. Phys.--Sol. State, 1, 1049-1059 (1959)].

142. A. Klemm, "Electrokinetics of Liquid Metals," Z. Naturforsch., 13a, No. 12, 1039-1043 (1958).

143. H. Knof and A. Klemm, "The Temperature Dependence of Electroendosmosis of Mercury," Z. Naturforsch., 14a, 1020-1023 (1959).

144. M. Mason and W. Wever, "The Settling of Small Particles in a Fluid," Phys. Rev., 23, 412-426 (1924).

145. R. Furth, "Over the Problem of Diffusion in a Gravitational Field," Z. Physik, 40, 351-363 (1926).

146. S. R. DeGroot, "Theory and Phenomenology of the Soret Effect," Physica, 9, 699-708 (1942).

147. L. Kholkanov and S. I. Drakin, "Derivation and Solution of the Differential Equation Describing the Transport of Material by Electrodiffusion in Metallic Alloys," Khim. i Khim. Tekhnol., 3, 14-19 (1960).

148. J. D. Verhoeven, J. C. Angus, W. C. Bouwsma, and E. E. Hucke, "The Determination of Electrical Mobilities in Molten Alloys," University of Michigan Research Report No. 2917-1-T, (1960).

149. K. Schwarz, "A New Method for Direct Measurement of Electrolytic Migration Velocity in Metallic Solutions," Z. Electrochem., 44, No. 9, 648-651 (1938).

150. A. Larsen, "Conductivity of Dilute Amalgams," Annal. Physik, 1, 123-131 (1900).

151. K. Bornemann and G. von Rauschenplat, "The Electrical Conductivity of Metal Alloys in the Liquid State," Metallurgie, 9, 473-486, 505-515 (1912).

152. O. Kubaschewski and E. L. Evans, Metallurgical Thermochemistry, Pergamon Press, New York, 1958.

153. K. Niwa, M. Shimoji, S. Kado, Y. Watanabe, and T. Yokokawa, "Studies on Diffusion in Molten Metals," Trans. AIME, 209, 96-101 (1957).

154. A. Z. Golik, N. A. Ryndich and S. A. Babenko, "Viscosity of the Sn-Bi System," Ukr. Fiz. Zhur., 3, No. 3, 365-369 (1958).

155. A. I. Bublik and A. G. Buntar, "Electron Diffraction Study of the Structure of Liquid Metals and Alloys," Kristallog., 3, 32-42 (1958), [Sov. Phys.--Crystallog., 3, 31-40 (1958)].

156. N. V. Alexeyev and Ya. I. Gerasimov, "On the Structure of Molten Bismuth-Tin Alloys," Dokl. Akad. Nauk SSSR., 121, 488 (1958) AEC-tr-3516.

157. A. S. Lashko, "X-Ray Investigation of the Structure of Some Liquid Metallic Systems," Zhur. Fiz. Khim., 33, 1730-1738 (1959), [Rus. J. Phys. Chem., 33, No. 8, 133-137 (1959)].

158. R. Kremann and P. Gruber v. Rehenburg, "Over the Electrolysis of a Few Tin Alloys," Z. Anorg. Allg. Chem., 140, 1-21 (1924).

159. R. Kremann, H. Krieghammer and A. Troster, "The Electrolytic Conduction in Molten Metal Alloys, XII. The Electrolysis of Bismuth-Tin Alloys," Monat. Chem., 46, 531-539 (1925).

160. K. P. Romadin, "Electrolytic Transfer in Liquid and Solid Metallic Solutions," Trans. of the N.E. Zhukovsky Air Force Adad., Ed. 167, 1947.

161. O. A. Esin and P. U. Gel'd, Physical Chemistry of Pyrometallurgical Processes. Part II. The Interaction of Liquids with Gases and Solid Phases, 1954, AEC-tr-3439, Book 2.

162. S. Epstein and J. R. Weeks, Private Communication, Brookhaven, National Labs., New York.

163. W. Seith and H. Wever, "A New Effect in the Electrolytic Transfer in Solid Alloys," Z. Elektrochem., 57, 891-900, (1953).

164. D. K. Belashchenko and G. A. Grigor'ev, "Electrical Transport of Thallium and Cobalt in Liquid Metallic Solutions,"Izv. Vysshikh Ucheb. Zavedenii, Chernaya Met., 5, No. 1, 124-130 (1962).

165. S. E. Bresler and G. E. Pikus, "Separation of Ions According to Their Mobility," J. Tech. Phys. (USSR), 26, 109-125, (1956), [Sov. Phys.--Tech. Phy., 1, 102-118 (1956)].

APPENDICES

APPENDIX A

SIMILARITIES BETWEEN DIFFERENT THEORIES

I. RELATION BETWEEN THE THEORIES OF FIKS AND HUNTINGTON

The collision rate, A_i, is defined as follows,

$$\frac{\text{electron coll. on atom i}}{\text{sec}} = n_e \bar{v}_e A_i \ . \tag{A-1}$$

The mean free time for electron collisions with atoms i is defined as τ_i. Hence the collision rate for an individual electron is $1/\tau_i$. Making a collision balance on a unit volume gives the relation between τ_i and A_i.

$$\frac{1}{\tau_i} = n_i \bar{v}_e A_i \ . \tag{A-2}$$

The resistivity attributable to atoms i can then be written as,

$$\Delta\rho_i = \frac{m_e^*}{n_e e^2 \tau_i} = \frac{m_e^* \bar{v}_e n_i A_i}{n_e e^2} \ . \tag{A-3}$$

The total resistivity is written as,

$$\rho_o = \frac{m_e^*}{n_e e^2 \tau} = \frac{m_e^* \bar{v}_e}{n_e e^2 \ell} \ . \tag{A-4}$$

The quotient becomes,

$$\frac{\Delta\rho_i}{\rho_o} = n_i A_i \ell \ . \tag{A-5}$$

If the electron concentration is taken to be exactly $\bar{Z}$ times the total atom concentration, the expression can be written as,

$$\bar{Z} \frac{n_o}{\rho_o} \frac{\Delta\rho_i}{n_i} = n_e A_i \ell. \tag{A-6}$$

Substituting into Fiks' Equation (15) we have,

$$F_{ei} = -eE\bar{Z}\frac{\Delta\rho_i}{\rho_o} \cdot \frac{n_o}{n_i} \quad . \tag{A-7}$$

The net force on an ion can then be expressed as,

$$F_i = eE\left[Z_i - \bar{Z}\frac{\Delta\rho_i}{\rho_o}\frac{n_o}{n_i}\right] . \tag{A-8}$$

II. RELATION BETWEEN THE THEORIES OF MANGELSDORF AND HUNTINGTON

If the electron friction force from Mangelsdorf's treatment, Equation (33), is equated to that of Fiks' analysis, Equation (15), the following relation is obtained,

$$\delta_i n_e \bar{v}_{ei} = eEn_e \ell A_i \quad . \tag{A-9}$$

The average electron velocity $\bar{v}_e$ can be expressed from Ohm's law as

$$\bar{v}_e = \frac{\sigma \cdot E}{n_e e} \quad . \tag{A-10}$$

The conductivity can be expressed as,

$$\sigma = \frac{n_e e^2 \tau}{m_e^*} = \frac{n_e e^2 \ell}{m_e^* \bar{v}_e} \quad . \tag{A-11}$$

Combining these three equations, the following expression is obtained for the friction coefficients defined by Mangelsdorf,

$$\delta_i = m_e^* \bar{v}_e A_i \quad . \tag{A-12}$$

Substituting into Equation (A-2) a relation between the friction coefficient and the electron collision time is obtained,

$$\frac{1}{\tau_i} = \frac{n_i \delta_i}{m_e^*} \quad . \tag{A-13}$$

The resistivity decrement due to component i can now be written as,

$$\Delta\rho_i = \frac{m_e^*}{n_e e^2 \tau_i} = \frac{n_i \delta_i}{n_e e^2} \cdot \tag{A-14}$$

Combining this equation with Equation (35) gives,

$$\frac{\overline{Z}}{\delta}\ \delta_i = \overline{Z}\,\frac{\Delta\rho_i}{\rho_o} \cdot \frac{n_o}{n_i}\ , \tag{A-15}$$

where the free electron to atom ratio has been taken as the average valence, $\overline{Z} = n_e/n_o$. Combining with Equation (37) the net force per ion can be written as,

$$F_i = eE\,[Z_i - \overline{Z}\,\frac{\Delta\rho_i}{\rho_o}\,\frac{n_o}{n_i}] \cdot \tag{A-16}$$

III. RELATION BETWEEN FRICTION COEFFICIENTS AND SCATTERING CROSS SECTIONS

The expansion of Equation (53) in Klemm's treatment for the case of self transport gives the following expression for the thermodynamic force on the activated ions,

$$F_A = r_{Au} X_u v_{Au} + r_{Ae} X_e v_{Ae} \cdot \tag{A-17}$$

The second term is taken to be the contribution of the electron friction to the force on the activated ions. Hence, this term may be related to the expression given by Mangelsdorf in Equation (33) to obtain the following relationship between the electron-ion friction coefficients of the two authors,

$$\delta_i = \frac{r_{ie} X_e}{n_e} = \frac{r_i}{n_o} \cdot \tag{A-18}$$

From Equation (A-11) Klemm's friction coefficients are related to Fiks' scattering cross section as follows,

$$r_i = m_e^* \bar{v}_e n_o A_i \ . \qquad \text{(A-19)}$$

APPENDIX B

SOLUTION OF THE PARTIAL DIFFERENTIAL EQUATION

Equation (144) $$\frac{\partial C}{\partial t} = \frac{\partial^2 C}{\partial X^2} - S\frac{\partial C}{\partial X}$$

Conditions of experiment:

$$C = 1 \qquad \text{for} \qquad X = 0, \quad t > 0$$

$$\frac{\partial C}{\partial X} - SC = 0 \qquad \text{for} \qquad X = 1, \quad t > 0$$

$$C = 1 \qquad \text{for} \quad 0 \leq X \leq 1, \quad t = 0$$

$$C = \exp SX \qquad \text{for} \quad 0 \leq X \leq 1, \quad t = \infty$$

Solutions:

$S = 2$

$$C(X,t) = \exp SX + A_o X \exp(X-t) + \sum_{n=1}^{\infty} C_n \sin\beta_n X \exp\left[\frac{SX}{2} - (\beta_n^2 + \frac{S^2}{4})t\right]$$

$S > 2$

$$C(X,t) = \exp SX + B_o \sinh \alpha X \exp\left[\frac{SX}{2} + (\alpha^2 - \frac{S^2}{4})t\right] + \sum_{n=1}^{\infty} C_n \sin\beta_n X \exp\left[\frac{SX}{2} - (\beta_n^2 + \frac{S^2}{4})t\right]$$

$S < 2$

$$C(X,t) = \exp SX + \sum_{n=1}^{\infty} C_n \sin\beta_n X \exp\left[\frac{SX}{2} - (\beta_n^2 + \frac{S^2}{4})t\right]$$

$$A_o = -\frac{6}{e}$$

$$B_o = \frac{16\,\alpha S \cosh\alpha \exp(-S/2)}{(S^2-4\alpha^2)(S-2\cosh\alpha^2)} \qquad C_n = \frac{-16\,\beta_n S \cos\beta_n \exp(-S/2)}{(S^2+4\beta_n^2)(S-2\cos^2\beta_n)}$$

The eigen values α and β_n are the roots of the following eigen functions:

$$\alpha(\coth\alpha) = S/2$$

$$\beta_n(\cot\beta_n) = S/2$$

TABLE B-1

ROOTS OF THE EQUATION TAN[X] - [2/S]X = 0

S	1	2	3	4	5
+ 100.00	3.2056172	6.4107036	9.6147541	12.8173131	16.0179926
+ 50.00	3.2717219	6.5390146	9.6211306	13.0473806	16.2853314
+ 20.00	3.4761403	6.8862352	10.2211104	13.4996040	16.7402823
+ 15.00	3.5877884	7.0367250	10.3693928	13.6342584	16.8602097
+ 10.00	3.7902224	7.2502483	10.5531104	13.7893118	16.9925900
+ 9.00	3.8492006	7.3016646	10.5938960	13.8224306	17.0202835
+ 8.00	3.9164354	7.3559270	10.6358514	13.8561267	17.0483005
+ 7.00	3.9926471	7.4128592	10.6788567	13.8903313	17.0766005
+ 6.00	4.0781497	7.4721926	10.7227710	13.9249699	17.1051395
+ 5.00	4.1725967	7.5335684	10.7674349	13.9599617	17.1338722
+ 4.00	4.2747822	7.5965460	10.8126733	13.9952220	17.1627513
+ 3.00	4.3826255	7.6606214	10.8582999	14.0306627	17.1917287
+ 2.00	4.4934094	7.7252518	10.9041216	14.0661939	17.2207552
+ 1.00	1.1655611	4.6042167	7.7898837	10.9499436	14.1017251
+ 0.50	1.3932490	4.6587782	7.8220315	10.9727946	14.1194627
+ 0.10	1.5383044	4.7017550	7.8476103	10.9910251	14.1336292
+ 0.05	1.5547176	4.7070778	7.8507972	10.9933001	14.1353983
+ 0.01	1.5676067	4.7113277	7.8533449	10.9951195	14.1368132
- 0.01	1.5739729	4.7134497	7.8546182	10.9960289	14.1375206
- 0.05	1.5865524	4.7176881	7.8571634	10.9978474	14.1389351
- 0.10	1.6019972	4.7229751	7.8603425	11.0001196	14.1407028
- 0.50	1.7155071	4.7648089	7.8856740	11.0182600	14.1548269
- 1.00	1.8365972	4.8158423	7.9170526	11.0408298	14.1724320
- 2.00	2.0287578	4.9131804	7.9786657	11.0855384	14.2074367
- 3.00	2.1746260	5.0036452	8.0384627	11.1295434	14.2421016
- 4.00	2.2889297	5.0869850	8.0961635	11.1727058	14.2763529
- 5.00	2.3806444	5.1633054	8.1515643	11.2149058	14.3101229
- 6.00	2.4556438	5.2329384	8.2045313	11.2560430	14.3433507
- 7.00	2.5179545	5.2963423	8.2549929	11.2960368	14.3759824
- 8.00	2.5704315	5.3540318	8.3029291	11.3348255	14.4079711
- 9.00	2.6151525	5.4065327	8.3483619	11.3723648	14.4392772
- 10.00	2.6536624	5.4543537	8.3913455	11.4086265	14.4698680
- 15.00	2.7859313	5.6385305	8.5727360	11.5706762	14.6113962
- 20.00	2.8627725	5.7605579	8.7083138	11.7026780	14.7334723
- 50.00	3.0213230	6.0459048	9.0765155	12.1151150	15.1627701
- 100.00	3.0800690	6.1605913	9.2420008	12.3246945	15.4090185

TABLE B-1 (Concluded)

ROOTS OF THE EQUATION $\tan[X] - [2/S]X = 0$

	S	6	7	8	9	10
+	100.00	19.2164807	22.4125469	25.6060382	28.7968724	31.9850272
+	50.00	19.5122876	22.7290015	25.9365234	29.1359838	32.3284680
+	20.00	19.9558194	23.1542562	26.3407046	29.5184941	32.6898572
±	15.00	20.0626079	23.2499016	26.4270081	29.5969499	32.7616747
+	10.00	20.1774438	23.3510065	26.5171686	29.6782238	32.8356100
+	9.00	20.2011714	23.3717323	26.5355518	29.6947324	32.8505862
+	8.00	20.2250979	23.3925884	26.5540253	29.7113060	32.8656107
+	7.00	20.2491969	23.4135576	26.5725767	29.7279352	32.8806767
+	6.00	20.2734415	23.4346216	26.5911932	29.7446115	32.8957773
±	5.00	20.2978034	23.4557621	26.6098623	29.7613253	32.9109058
+	4.00	20.3222538	23.4769601	26.6285710	29.7780673	32.9260552
±	3.00	20.3467635	23.4981967	26.6473060	29.7948283	32.9412186
+	2.00	20.3713029	23.5194525	26.6660542	29.8115987	32.9563890
±	1.00	17.2497818	20.3958423	23.5407082	26.6848024	29.8283692
+	0.50	17.2642798	20.4081028	23.5513301	26.6941724	29.8367514
±	0.10	17.2758653	20.4179034	23.5598226	26.7016650	29.8434548
+	0.05	17.2773126	20.4191279	23.5608838	26.7026013	29.8442925
+	0.01	17.2784702	20.4201073	23.5617326	26.7033503	29.8449626
-	0.01	17.2790489	20.4205970	23.5621571	26.7037248	29.8452977
-	0.05	17.2802063	20.4215764	23.5630058	26.7044737	29.8459678
-	0.10	17.2816528	20.4228004	23.5640667	26.7054098	29.8468054
∓	0.50	17.2932151	20.4325870	23.5725500	26.7128960	29.8535042
-	1.00	17.3076405	20.4448034	23.5831433	26.7222463	29.8618724
-	2.00	17.3363779	20.4691674	23.6042847	26.7409160	29.8785865
-	3.00	17.3649267	20.4934161	23.6253509	26.7595337	29.8952633
-	4.00	17.3932439	20.5175229	23.6463238	26.7780870	29.9118938
-	5.00	17.4212891	20.5414616	23.6671861	26.7965638	29.9284692
-	6.00	17.4490243	20.5652079	23.6879210	26.8149521	29.9449807
-	7.00	17.4764146	20.5887383	23.7085125	26.8332405	29.9614200
-	8.00	17.5034282	20.6120311	23.7289453	26.8514179	29.9777788
-	9.00	17.5300362	20.6350660	23.7492049	26.8694738	29.9940492
-	10.00	17.5562132	20.6578243	23.7692776	26.8873980	30.0102236
-	15.00	17.6799601	20.7669265	23.8664224	26.9747260	30.0894095
-	20.00	17.7908353	20.8672381	23.9573676	27.0575502	30.1652365
-	50.00	18.2197675	21.2858232	24.3603021	27.4423964	30.5312497
-	100.00	18.4952593	21.5836396	24.6743180	27.7673940	30.8629136

TABLE B-2

ROOTS OF THE EQUATION $\tanh[X] - [2/S]X = 0$

S	ROOT
+ 3.0	1.2878394
+ 4.0	1.9150080
+ 5.0	2.4640596
+ 6.0	2.9847045
+ 7.0	3.4935397
+ 8.0	3.9568430
+ 9.0	4.4988869
+ 10.0	4.9995456
+ 15.0	7.4999954
+ 20.0	9.9999999

APPENDIX C

CALIBRATION OF THERMOCOUPLES

In all of this work the temperature was measured with matched 28 ga. Chromel-Alumel thermocouple wire taken from the same spool. The couples were beaded with a torch and insulated from the metal protection tube with two-hole ceramic insulators. The metal protection tubes were welded shut on the bottom and the thermocouple bead was percussion welded to the closed end.

A number of thermocouples were calibrated against a Pt-10 Rd thermocouple which had been calibrated by the National Bureau of Standards. The procedure was as follows. The stirrer was removed from the apparatus shown in Figure 8 and replaced with the standard thermocouple enclosed within a molybdenum protection tube. The tips of the standard couple and the couple to be calibrated were held in contact with each other by means of wires. The apparatus was then heated to temperature with the same furnace and temperature controller used in the resistivity technique, and described in Chapter V. The two couples were immersed in a bath of liquid bismuth which was contained in the crucible shown in Figure 8. The temperature was determined by alternately measuring the standard couple and the Cr-Al couple and averaging the results. In addition to standardization against the Pt-10 Rd couple, the melting point of bismuth was also checked. The results for three couples are shown in Table C-1.

Thermocouples No. 1 and No. 2 were used in the chemical analysis technique and thermocouple No. 3 was used in the resistivity technique.

TABLE C-1

CALIBRATION OF THERMOCOUPLES[a]

Measured EMF Pt-Rd[b]	Temp. from Standard Calibration[c]	Cor. from Nat. Bur. Std. Calibration	Corrected Temp. °C	Measured EMF Cr-Al	Temp. from Standard Calibration[c]	Temp. Correction Required
			Thermocouple No. 1			
5.270	604.5	-0.7	603.8	25.152	605.4	-1.6
4.367	514.8	-0.6	514.2	21.276	515.0	-0.8
1.543	212.7	-0.2	212.5	8.657	213.0	-0.5
1.008	147.9	-0.1	147.8	6.058	148.2	-0.4
0.309	51.6	0.0	51.6	2.151	53.2	-1.6
			Thermocouple No. 2			
4.295	507.5	-0.6	506.9	21.009	508.8	-2.1
3.772	454.1	-0.5	453.6	18.606	452.4	+1.2
3.059	379.8	-0.3	379.5	15.467	378.0	+1.5
2.543	324.7	-0.3	324.4	13.160	322.8	+1.6
1.660	226.1	-0.2	225.9	9.101	224.2	+1.7
			Thermocouple No. 3			
4.4324	520.3	-0.6	519.7	21.623	522.9	-3.2
3.7486	451.9	-0.5	451.4	18.683	454.0	-2.6
3.2366	398.5	-0.4	398.1	16.419	400.5	-2.0
2.7669	348.8	-0.3	348.5	14.314	350.5	-2.0
2.3126	299.6	-0.2	299.4	12.232	300.6	-1.2
2.0596	271.6	-0.2	271.3[d]	11.107	273.2	-2.1

(a) All temperatures are degrees centigrade based on the International Temperature Scale 1948.
(b) Thermocouple No. 1035408 calibrated by National Bureau of Standards.
(c) National Bureau of Standards Circular 561.
(d) Known temperature of bismuth melting point.

Unfortunately, the thermocouple used in Runs V-7 to V-15 was ruined by a leak in the Mo protection tube before it was calibrated. However, since that couple was made from wire off the same spool as the above three, a correction of -2°C was applied to all of the data in Runs V-7 to V-15. The same correction was applied to the data in Runs V-15 and V-23, in which thermocouple No. 3 was used. It seems fairly certain that the temperature is probably correct to $\pm$1°C. In view of the large scatter in the chemical analysis data, the temperature corrections were not applied to that data.

A number of attempts were made to calibrate a Ta-W thermocouple. These couples were not beaded; they were joined by immersing the exposed tips, separated by about 2 mm, into a liquid metal bath. The EMF-Temp. characteristics of these couples were not very reproducible. However, the slope of the curve was approximated over a number of calibrations for use in some of the work described in Appendices G and K. At room temperature the slope was .004 mv/°C, and at 440°C it was .016 mv/°C.

APPENDIX D

ANALYTICAL PROCEDURES USED WITH THE CHEMICAL ANALYSIS TECHNIQUE

D-1. SPECTROPHOTOMETRIC DETERMINATION OF URANIUM IN BISMUTH

I. INTRODUCTION

Uranium is determined spectrophotometrically at 412 mμ and 390 mμ as the dibenzoylmethane-uranium complex. The applicable range is 50 to 120 μg of uranium; up to 300 mg of bismuth can be tolerated. This method has been used for samples containing 99 per cent bismuth and 1000 ppm uranium with respect to bismuth.

The bismuth is complexed with diaminocyclohexane tetraacetic acid (DCTA), and the uranium is complexed with dibenzoylmethane. The dibenzoylmethane-uranium complex is extracted into amyl acetate, and the absorbance of the resulting organic layer is measured at two wavelengths.

II. APPARATUS

Spectrophotometer, Beckman Model DU with tengsten lamp and blue-sensitive cell. Absorption cells, 1 cm. path length, corex or quartz (pyrex cells also seem to be satisfactory).

III. REAGENTS

1. Nitric acid, concentrated, reagent grade
2. Ammonium hydroxide, 5 M
3. Hydrochloric acid, 3 M
4. Saturated ammonium chloride solution

5. Bromcresol green indicator solution, 0.04 per cent

6. Dibenzoylmethane solution, one per cent in ethanol (absolute or 95 per cent)

7. Amyl acetate, reagent grade. The isoamyl acetate was the only amyl acetate available in a reagent grade; consequently, it was used since the original reference did not specify which ester was used.

8. Diaminocyclohexane tetraacetic acid (DCTA) solution: 100 g. is dissolved in 300 ml of 5 M NaOH; after dissolution the pH is adjusted to 5.2 with HCl and NaOH; finally the solution is diluted to 500 ml.

IV. PREPARATION OF SAMPLES

1. Weigh the bismuth sample and dissolve in concentrated nitric acid.
2. Transfer to a volumetric flask and dilute to the mark with water. This dilution should be such that an aliquot no larger than 10 ml will be required for an analysis.

V. PROCEDURE

1. Withdraw an aliquot (no more than 10 ml) containing 50 to 100 μgms. of uranium and no more than 300 mg of bismuth. Transfer to a 60-ml separatory funnel. (See Note 1).

2. Add water to bring volume up to 10 ml.

3. Add 5 ml of the DCTA solution (see Note 2).

4. Add three drops of the bromcresol green indicator solution.

5. Add dropwise ammonium hydroxide, 5 M, and/or hydrochloric acid, 3 M, until the solution just turns from blue to yellow.

6. Add 5 ml of saturated ammonium chloride solution.

7. Add water to make the volume about 20 ml (see Note 3).

8. Add 1.00 ml (pipet) of dibenzoylmethane solution while rotating the funnel (see Note 4).

9. Immediately add from an eye dropper 12 drops of 5 M ammonium hydroxide.

10. Add 10.00 ml (pipet) of amyl acetate.

11. Shake the contents of the funnel thoroughly and allow the two layers to separate (see Note 5). Centrifuge for one minute.

12. Pipet enough of the organic layer (top layer) into the absorption cell to fill it.

13. Measure the absorbance at 412 mμ and at 390 mμ against a blank which has been prepared in the same manner as the sample using water instead of a uranium containing sample (see Notes 6 and 7).

VI. NOTES AND PRECAUTIONS

1. A 10-ml aliquot is maximum because the final volume of the aqueous layer is 20 ml, and 10 ml of reagents must be added.

2. Five ml of DCTA will keep in solution about 300 mg of bismuth. If a precipitate does occur, add more DCTA.

3. The diluted solution should be clear at this point; if not, probably insufficient DCTA was added.

4. After the addition of dibenzoylmethane, the solution will be turbid and a small amount of precipitate will be present. Keep the dibenzoylmethane in ethanol solution tightly stoppered to prevent volatilization.

5. The two layers should be clear now with the aqueous layer colored blue and organic layer yellow. The intensity of the yellow color will be determined by the amount of uranium present.

6. Unless one has tightly stoppered absorption cells, it will be necessary to work rapidly during the photometry because of the volatility of amyl acetate.

7. It has been found that soapy water followed by thorough rinsing with water and a final rinse with acetone will clean the absorption cells very nicely.

VII. CALCULATIONS

The concentration of uranium is read from a calibration curve of absorbance versus uranium concentration which is best prepared from a series of standard uranium solutions. These solutions should be treated in the same manner as the sample and their absorbances read at the two wavelengths.

$$\% \text{ U} = \frac{\mu\text{g of U read from calibration curve}}{1000 \times \text{sample wt. in mg}} \times \frac{\text{dilution volume}}{\text{aliquot volume}} \times 100$$

$$\text{ppm U} = \frac{\mu\text{g of U} \times 10^6}{1000 \times \text{sample wt. in mg}} \times \frac{\text{dilution volume}}{\text{aliquot volume}}$$

The concentration of the uranium as read from the 412 mμ curve should agree with that read from the 390 mμ curve. The two readings taken together should show if any interference is present. The ratio of absorbances A(412 mμ): A(390 mμ), is constant at 1.9 to 2.0 over the range studied (50 to 120 μg U).

VIII. REFERENCES

(1) H. L. Finston, Brookhaven National Laboratory, private communication.

(2) J. H. Yoe, F. Will III, and R. A. Black, Anal. Chem., 25, 1200 (1953).

D-2. DETERMINATION OF MAGNESIUM IN BISMUTH ALLOYS

I. INTRODUCTION

Magnesium is determined titrimetrically employing versene (ethylenedinitrilo) tetraacetic acid disodium salt as the titrant and Eriochrome-black-T as the indicator.[1] Magnesium forms a wine-red complex with the indicator that changes to a deep blue color at the end-point upon titration with versene.

II. INTERFERENCES

1. Uranium interference is removed by complexation of the uranyl ion with carbonate. $(UO_2(CO_3)_3^{-4})^2$.

2. Zirconium interference is removed by precipitation as a hydroxide.

3. Bismuth interference is removed by precipitation as a mixture of BiOCl and $Bi(OH)_3$. The presence of BiOCl promotes the formation of a granular precipitate, thereby minimizing absorption and occlusion.

III. APPARATUS

Beckman pH meter, Buchner type funnels with fritted disc (medium porosity).

IV. REAGENTS

1. Hydrochloric acid - 2N

2. Eriochrome-black-T indicator. Dissolve 0.2 grams of the indicator in 50 ml of methanol, reagent grade, containing two grams of hydroxylamine hydrochloride.

3. Standard magnesium solution. Dissolve six grams of magnesium, reagent grade, in dilute hydrochloric acid and dilute to one liter. Dilute a portion of stock solution 1:100 to obtain a final solution containing 0.06 mg Mg/ml.

4. Versene (ethylenodinitrito) tetraacetric acid disodium salt standard solution. Dissolve four grams of the component in one liter of water. A portion diluted 1:10 will yield a titer of approximately 0.027 mg Mg/ml. Solution is standardized accurately against standard Mg solution, containing approximately 600 mg Bi/ml.

5. Bismuth stock solution was prepared by dissolving high purity bismuth (15.2471 grams) in nitric acid, (concentrated) and diluting with water, yielding 30.49 mg Bi/ml.

6. Buffer. Dissolve 67.5 grams of ammonium chloride in 200 ml of distilled water, add 570 ml of concentrated ammonium hydroxide, dilute to one liter. Final pH is 10.

7. Sodium hydroxide - 0.5N.

8. Sodium Carbonate solution. Dissolve ten grams of sodium carbonate in water and dilute to 100 ml.

V. PREPARATION OF SAMPLES

1. Weigh the sample, transfer the weighed sample to a beaker, add sufficient water to cover the sample and add concentrated nitric acid.

2. Following dissolution, heat samples to near boiling in order to expel dissolved nitrogen oxides. Cool, transfer to a suitable size volumetric flask and dilute to mark with water. Dilution should be such that a five to ten ml aliquot will be required for analysis.

VI. PROCEDURE

1. Remove an aliquot portion of sample 5-10 ml containing approximately 0.5-1 mg Mg and transfer to a beaker.

2. Add 5 ml of 2N hydrochloric acid.

3. Add sodium hydroxide 0.5N slowly, with stirring, until the mixture attains a pH of 2, as measured by a pH meter, then add 2 ml of sodium carbonate solution (0.1 gm/ml) and resume addition of sodium hydroxide until the mixture attains a pH of 9.

4. Allow the precipitate formed to stand five to ten minutes.

5. Filter thru a fritted disc funnel (medium porosity).

6. Transfer filtrate to a 500 ml erlenmeyer flask.

7. Add 2.5 ml of buffer solution (pH 10).

8. Add 20 drops of Eriochrome-black-T indicator solution.

9. Titrate with standard versene solution until solution changes from wine-red color to a deep blue (see Note 2).

VII. CALCULATIONS

$$\% \text{ Mg} = \frac{(\text{ml versene})(\text{titer})(\text{dilution ml})(100)}{(\text{wt. gms. sample})(\text{aliquot})(10^3)}$$

VIII. NOTES

(1) Standardization of the versene solution against a magnesium solution containing a large excess of bismuth compensates for these quantities of bismuth which may not be completely removed through precipitation.

(2) Near the end-point the solution will appear blue with a red tinge, care must be taken to assure the complete absence of red at the end-point.

IX. REFERENCES

(1) Charlot and Bezier, Quantitative Inorganic Analysis, (John Wiley and Sons, Inc., N.Y., 1957) p. 471.

(2) H. Willard and H. Diehl, Advanced Quantitative Analysis, (d. van Nostrand Company, Inc., N.Y., 1943) p. 364.

D-3. SPECTROSCOPIC DETERMINATION OF COPPER IN BISMUTH

I. INTRODUCTION

The spectrophotometric method for the determination of copper reported by G. Frederick Smith and W. H. McCurdy, Jr.[1] and Y. Yshihara and Y. Taguchi[2] was successfully applied to the determination of copper in the presence of uranium and large quantities of bismuth.

Copper is extracted from an aqueous solution of pH 5-6 as a neocuproine complex with isoamyl alcohol and measured at 454 mμ. Beer's law is obeyed over the range of 0.15 to 10.6 ppm copper in isoamyl alcohol. The method is quite selective for copper and may be used in the presence of many cations and anions. A minor modification of the original procedure was made in order to more rapidly determine the pH of the aqueous phase prior to extraction.

II. INTERFERENCES

Smith reported that no cation other than the cuprous ion formed a colored complex that was extractable under the conditions employed. The chloride, sulfate, nitrate, perchlorate, tartrate, citrate and acetate anions do not interfere. Many other anions that either react with hydroxylamine or give a yellow colored solution may be eliminated by employing suitable conditions. The following cations were found to produce no detectable interference:

Cation	Weight Ratio Cation: Cu^{+1}
Bi^{+3}	28,000: 1
UO_2^{+2}	234: 1

III. APPARATUS

Beckman DU Quartz Spectrophotometer with tungsten lamp.

IV. REAGENTS

1. Concentrated nitric acid.
2. p-Bromocresol green, 0.04 per cent aqueous solution.
3. Ammonium hydroxide - 5 M.
4. Hydrochloric acid - 1 M.
5. Hydroxylamine hydrochloride, 30 per cent, aqueous solution.
6. Sodium citrate, 30 per cent, aqueous solution.
7. Neo-cuproine, 0.1 per cent ethanol - water solution (1.9 by volume).
8. Isoamyl alcohol (Reagent Grade). (See Note 3).

V. PROCEDURE

1. Dissolve the bismuth alloy in concentrated nitric acid. Heat to expel nitrogen oxides, cool and dilute to volume.
2. Transfer an aliquot of sample containing 5 to 75 μg copper to a 60 ml separatory funnel.
3. Add 10 ml hydroxylamine hydrochloride (30 per cent).
4. Add 2 ml of sodium citrate (30 per cent).
5. Add 2 drops of p-Bromocresol green.
6. Add ammonium hydroxide (5M) and/or hydrochloric acid (1M) till the solution changes from a blue to a green-yellow color.
7. Add 8 ml of sodium citrate.
8. Add 2 ml of neo-cuproine solution (0.1 per cent) with mixing.
9. Make up to a volume of 30 ml with distilled water.

10. Add 10 ml of sioamyl alcohol and shake for 20 seconds. Allow the phases to separate.

11. Remove a portion of the organic phase and measure the absorbancy at 454 mμ against a reagent blank.

VI. CALIBRATION CURVE

A calibration curve was prepared from a stock solution of copper (99.9 per cent) in 1N nitric acid. Amounts of bismuth up to 47,860 μg and uranium up to 400 μg were added to 1.71 μg copper without any noticeable interference.

VII. NOTES

1. The complex contains a molar ratio of copper to neocuproine of 1:2 with copper present as the cuprous (Cu^{+1}) ion.

2. p-Bromocresol green indicator (pH 3-5) was introduced for determining the pH of the aqueous phase prior to extraction. The indicator exhibited an absorbancy of 0.010/1 drop at 454 mμ, a sufficiently low value to permit its use in the determination.

3. This solvent exhibits a nauseating odor and should be used in a hood.

4. Addition of sodium citrate prevents hydrolysis and precipitation of heavy metals during the subsequent neutralization operation.

5. Exactly 2 drops of indicator are used in both blank and sample (see Note 1).

6. Complex formation, for all practical purposes, occurs instantaneously.

7. Smith[1] performed two extractions. However, it was found in this laboratory that one 10 ml extraction was sufficient to remove the copper complex. The use of a single extraction significantly decreased the time required to perform the analysis.

REFERENCES

(1) G. F. Smith and W. H. McCurdy, Jr., Anal. Chem., 24, 371 (1952).

(2) Y. Yshira and Y. Taguchi, Japan Analyst, 6, 588 (1957).

D-4. SPECTROPHOTOMETRIC DETERMINATION OF PALLADIUM IN BISMUTH ALLOYS

I. INTRODUCTION

The spectrophotometric method for the determination of Palladium reported by Oscar Menis and T. C. Rains, Anal. Chem., 27, (12), 1932 (1955) has been applied to the analysis of bismuth alloys containing Palladium concentrations as low as 20 ppm. The presence of Uranium and high concentrations of bismuth in the alloys necessitated a more rigid control of the acidity and time for color formation than is implied in the original reference.

The absorbancy of the palladium-alpha-furildioxime complex is measured at 380 mμ in chloroform, following extraction from a 1.3 N acid aqueous mixture. Time for color formation is exactly 5 minutes, if the time exceeds 30 minutes, bismuth causes interference. An acidity of 1.3 N in the aqueous phase prevents the precipitation of bismuth in any of the alloys analyzed, including alloys containing the minimum amount of palladium (20 ppm) and allows complete color development to occur in 5 minutes.

II. APPARATUS

Beckman DU Quartz Spectrophotometer with tungsten lamp; absorption cells 1 cm; 50 ml burette.

III. REAGENTS

1. Alpha-Furildioxime 1% solution. Prepare by dissolving 1 gm. of the reagent in 30 ml of ethanol and diluting to 100 ml with water (see Note 1).

2. 0.500 N Sodium hydroxide.

3. Concentrated nitric acid.

4. Phenolphthalein indicator.

5. Chloroform. Reagent grade.

IV. PROCEDURE

1. Dissolve the sample in concentrated nitric acid and dilute to volume. Final normality of the sample solution should not exceed 3 N.

2. Remove an aliquot of sample solution and determine the free acid content using standard base and phenolphthalein indicator, e.g., total equivalents of base required minus the number of equivalents of base required minus the number of equivalents of bismuth present (see Note 2).

3. Transfer an aliquot of sample solution containing 5.75 µg to 57.5 µg Pd to a 60 ml separatory funnel.

4. Add 2 N hydrochloric acid and water, sufficient to yield 35 ml total volume of a 1.3 N solution. The reagent blank should be the same acidity as the sample solution and should contain 321 mg bismuth (see Note 2).

5. Add 1 ml of α-furildioxime (1% alcohol-water solution) while rotating the funnel. Allow the mixture to stand exactly 5 minutes.

6. Add 10 ml of chloroform, shake for 20 sec., allow the phases to separate and transfer the lower organic layer to a 25 ml volumetric flask. Time elapsed between the addition of alpha-furildioxime and the final extraction should not exceed 10 minutes.

7. Dilute the organic extracts to 25 ml with chloroform and mix thoroughly.

8. Add 0.3 gms. sodium sulfate, anhydrous, to chloroform extracts to remove traces of water.

9. Measure the absorbancy of the sample at 380 mµ against the reagent blank containing bismuth.

V. CALIBRATION CURVE

A stock solution of palladium was prepared by dissolving the pure metal (99.9%) in concentrated nitric acid containing a small amount of hydrochloric acid, heating the mixture till the evolution of Cl_2 ceased and diluting to volume. Aliquot portions of the palladium stock solution were then treated according to the above procedure. Bismuth and uranium were added to the palladium aliquots and produced no effect upon the observed absorbancy of the palladium-alpha-furildioxime complex under the conditions of acidity and time for color development cited in the procedure.

VI. CALCULATIONS

1. Normality of sample solution:

$$N(\text{as free acid}) = \frac{(\text{Volume base ml})(\text{N base})\ \frac{\text{wt. sample gms.}}{69.6}\ \frac{\text{aliquot sample ml}}{\text{Dilution ml}}}{(\text{aliquot sample ml})}$$

2. Volume of 2.00 N hydrochloric acid required to prepare 1.3 N sample solution for extraction:

$$\text{ml of 2.00 N HCl required} = \frac{(35\text{ ml})(1.3\text{ N}) - (\text{aliquot sample ml})(N_S)}{(2.00\text{ N})}$$

N_S = Normality of sample as determined from (1).

3. Per cent composition:

$$\%\ \text{Pd} = \frac{(\mu\text{g Pd})(\text{Dilution ml})(100)}{(\text{ml aliquot})(\text{gms. sample})(10^6)}$$

VII. NOTES

1. The reagent must be purified before use through recrystallization from water. If further purification is desired see, Reed, S. A. and Bank, C. U., Proc. Acad. Sci., 55, 267 (1948).

2. 321 mg bismuth represent the largest amount of bismuth encountered with the alloys studied in the aliquot used for the analysis.

D-5. SPECTROPHOTOMETRIC DETERMINATION OF NICKEL

I. INTRODUCTION

Nickel (II) dimethylglyoximate is slightly soluble in chloroform and other organic solvents yet it is immiscible with water. Since the solubility of nickel dimethylglyoximate in water is much less than in chloroform, small amounts of nickel can be effectively extracted in this way. The uniqueness of this procedure is that few other metals form chloroform soluble dimethylglyoxime complexes and thus a selective separation of nickel can be obtained in this way.

The absorbance of the nickel dimethylglyoxime complex is measured at 460 millimicrons. The range for this method is between 5 to 90 micrograms of nickel per 25 mls.

II. APPARATUS

The Beckman Model DU Spectrophotometer with tungsten lamp; fused silica cells having a path length of 10 mm.

III. REAGENTS

Ammonium hydroxide, 1:50 solution

Ammonium hydroxide, concentrated

Amonium persulfate, 10% solution

Chloroform, reagent grade

Dimethylglyoxime
- 1% alcoholic solution
- 2.5% solution in 1 M sodium hydroxide

Hydroxylamine hydrochloride, 10% solution

Phenolphthalein indicator

Sodium citrate, 20% solution

Sodium hydroxide, 10M

Hydrochloric acid, 0.5 M

IV. PROCEDURE

1. Pipet an aliquot of solution containing between 5 to 90 micrograms of nickel into a 125 ml separatory funnel.
2. Add 10 ml of 20% sodium citrate.
3. Add 2 ml of 10 per cent hydroxylamine hydrochloride solution.
4. Add 2 ml of 1 per cent alcoholic dimethylglyoxime solution.
5. Add 2 drops of phenolphthalein indicator.
6. Neutralize with concentrated ammonia, and then add three drops in excess. (Neutralize to pink)
7. Dilute to 60 ml and shake for 2 minutes with 20 ml of chloroform.
8. Separate the phases, and shake the chloroform with 10 ml of 1:50 ammonia for one minute; repeat the washing with another portion of ammonia and then separate the phases.
9. Shake the chloroform for one minute with 15 ml of 0.5 M hydrochloric acid to transfer the nickel to the aqueous phase.
10. To the acid solution add 2 ml of 2.5% dimethylglyoxime in 1 M sodium hydroxide.
11. Add 1 ml of 10 M sodium hydroxide.
12. Add 0.3 ml of 10 per cent ammonium persulfate solution.
13. Transfer to a 25 ml volumetric flask, dilute to volume after 10 minutes, and measure the absorbance at 460 millimicrons.

V. CALCULATIONS

The concentration of nickel is read from a calibration curve of absorbance versus the concentration of nickel, which is best prepared from a series of standard nickel solutions. These solutions should be treated in the same manner as the sample and their absorbance read at 460 millimicrons.

VI. REFERENCE

Sandell, E. B. Colorimetric Determination of Traces of Metals, Interscience Publications Inc., New York, 1959, p. 672 slt. procedure.

APPENDIX E

ORIGINAL DATA FROM CHEMICAL ANALYSES RUNS

TABLE E-1

RAW DATA FOR Bi-Ni AND Pd-Bi

Capillary	Migrating Element, Wt. %	Temp., °C	D.C. Amps*	Capillary I.D., cm	Capillary Length, cm	Time, hr	Final Wt., Migrating Element	Wt. Capillary Metal, gm	u x 10^4 cm^2/V-sec	Comments
						Nickel in Ni-Bi				
24-1	.462 Ni	500±2.5	+ .503	.05	2.3	21.5	.613	.0431	2.65	No stirring
24-2	.462	500±3.5	+ .503	.05	2.7	46.0	.704	.0551	2.52	
34-1	.466	496±3	+2.075	.104	4.39	24.0	.512	.3097	1.23	
34-2	.466	496±3	+2.055	.103	4.02	48.15	.503	.3199	0.53	
40-1	.482	499±5	+2.08	.0533	4.95	13.0	.711	.1090	4.06	
40-2	.482	499±5	+2.01	.0508	4.87	19.5	.780	.1288	4.13	
43-1	.486	500±3	+2.05	.05	5.21	8.17	.642	.1304	5.10	Hairpin cap
43-2	.486	500±3	+2.06	.05	5.34	12.92	.876	.1142	6.97	Hairpin cap
47-1	.494	500±5	+2.10	.05	5.12	12.23	.701	.1386	4.60	
50-2	.484	800±10	+1.97	.05	5.11	11.45	.855	.1130	7.21	100°C temp. cycle for 1 hr
52-1	.501	797±3	+2.05	.05	5.4	12.42	.909	.1133	6.85	
52-2	.501	797±3	+2.11	.05	4.9	9.08	.872	.1115	8.11	
55-1	.496	797±10	+4.17	.1	5.0	16.37	.619	.4304	2.96	
57-2	.447	790±10	+4.00	.1	5.0	20.43	.618	.3732	3.30	
						Palladium in Pd-Bi				
1-A	.213 Pd	453	+1	.076	6.10	10.0	.222	.2711	2.32	
1-C	.213	453	+1	.084	5.07	24.0	.243	.2759	3.35	
2-A	.166	453	+1	.059	7.20	14.0	.186	.1927	3.49	
2-B	.166	453	+1	.067	5.39	14.0	.186	.1863	3.05	

*Sign of current indicates capillary polarity.

TABLE E-2

RAW DATA FOR TERNARY SYSTEMS

Ternary	Capillary	Migrating Element, Wt. %	Temp., °C	D.C. Amps*	Capillary I.D., cm	Capillary Length, cm	Time, hr	Final Wt., Migrating Element	Wt. Capillary Metal, gm	u x 10^4 cm^2/V-sec	Comments
					Copper Ternaries						
Ni-Cu-Bi	CT-2-2	.493 Cu	499±5	+2.05	.075	4.85	24.0	.422	.2533	1.52	
Ni-Cu-Bi	CT-2-1	.493	499±5	+2.11	.075	5.23	18.0	.437	.2517	1.54	
Mg-Cu-Bi	CT-3-1	.372	344±3	-1.96	.10	5.08	14.5	.388	.4428	1.43	
Mg-Cu-Bi	CT-3-2	.372	344±3	-2.01	.10	5.29	17.5	.391	.4501	1.39	
Mg-Cu-Bi	CT-3-3	.372	344±3	-1.95	.10	5.25	21.0	.434	.4310	3.74	
U-Cu-Bi	C-58	.470	475±5	+3.17	.070	10	37.42	.316	.3797	2.14	Hairpin tubes
U-Cu-Bi	C-59-1	.486	475±5	+3.48	.075	10	24.17	.399	.5039	2.26	Hairpin tubes
U-Cu-Bi	C-59-2	.486	475±5	+4.15	.075	10	39.73	.333	.4565	1.78	Hairpin tubes
					Nickel Ternaries						
Mg-Ni-Bi	CT-1-1	.299 Ni	350±5	-2.02	.10	5.1	27.0	.244	.4395	2.55	Wall reaction
Mg-Ni-Bi	CT-1-2	.299	350±5	-2.06	.10	5.1	40.0	.219	.4348	2.61	Wall reaction
Cu-Ni-Bi	CT-2-1	.466	499±5	+2.11	.075	5.23	18.0	.619	.2517	4.42	
Cu-Ni-Bi	CT-2-2	.466	499±5	+2.05	.075	4.85	24.0	.646	.2533	4.15	
					Magnesium Ternaries						
Ni-Mg-Bi	CT-1-1	.269 Mg	350±5	-2.02	.10	5.1	27.0	.364	.4395	6.03	Wall reaction
Ni-Mg-Bi	CT-1-2	.269	350±5	-2.06	.10	5.1	40.0	.418	.4348	6.22	
Cu-Mg-Bi	CT-3-1	.262	344±3	-1.96	.10	5.08	14.5	.332	.4428	8.85	
Cu-Mg-Bi	CT-3-2	.262	344±3	-2.01	.10	5.29	17.5	.342	.4501	8.26	
Cu-Mg-Bi	CT-3-3	.262	344±3	-1.95	.10	5.25	21.0	.362	.4310	8.52	
					Uranium Ternaries						
Cu-U-Bi	C-58	.142 U	415±5	+3.17	.070	10	37.42	.222	.3797	3.69	
Cu-U-Bi	C-59-1	.154	475±5	+3.48	.075	10	24.17	.179	.5039	1.98	
Cu-U-Bi	C-59-2	.154	475±5	+4.15	.075	10	39.73	.230	.4565	2.79	

*Sign of current indicates capillary polarity.

APPENDIX F

DEVELOPMENT OF A RESISTIVITY TYPE CELL

I. INTRODUCTION

Both Schwarz[2] and Mangelsdorf[121] have performed electrotransport experiments in capillary cells in which they followed the composition profile by continuously monitoring the resistivity. Because of material problems these cells could not be used at higher temperatures. The initial experimental work in this area was devoted to the development of resistivity type cells which could be used up to temperatures around 600°C.

II. FIRST CELL DESIGN

There are certain basic requirements which must be met in the cell design. First, it is necessary that the dimensions of the transport channel be of capillary size in order to avoid convection currents. The probes must be introduced into the channel without distorting the channel. Distortion of the channel does not affect the electrotransport since the divergence of the mass flow is independent of area. Frequently, however, it makes it difficult to accurately determine the dimension of the segments between probes along the capillary. Contrary to resistivity work, the area and not the area to length ratio is needed in this work. It is also necessary to use materials for the channel and the probes which are not corroded by the liquid metals at the temperature of operation. And lastly, it is very desirable to have a method of emptying the channel before the alloy solidifies in order that the cell may be reused.

It was not possible to use a noble metal such as platinum for an electrode material in this work, since they have a slight solubility

in the Bi-Sn alloys at 500°C. This proved to be a major disadvantage. The choice of electrode material was fairly well limited to the refractory metals, W, Ta, and Mo. Of these, tungsten is the most conveniently used. A number of materials were considered for the transport channel. An interesting design was considered, using Ta or Al which have stable oxides. A capillary channel would be cut into the metal and then oxidized slightly for the electrical insulation required if resistivity probes are to be used. Such a cell has the advantage that it would be a good sink for the I^2R heat generated. It proved to be too difficult because of troubles arising in introducing the resistivity probes. It was finally decided to use pyrex capillary tubing and tungsten wires for probes. Tungsten has the advantage that diameters less than .040-in. readily form a glass to metal seal with Pyrex No. 7740 glass. The tungsten oxides formed on the free surfaces when sealing to the Pyrex are readily removed by etching. Pyrex is inert to most of the low melting alloys up to 600°C.

The Pyrex capillary tubing commercially available has a relatively thick wall of around 2.5 mm. In order to insert a probe through this thick wall without distorting the capillary channel it is necessary to first drill a hole through the wall. The capillary diameter was only .020-in. (0.5 mm) so that it was necessary to use very small wires for probes. This produced the problem of drilling holes 6 mils or less through 2.5 mm of Pyrex. Two methods were attempted, one using a high velocity stream of abrative particles and the other an ultrasonic drill. The latter method proved successful. The technique was refined by trial and error to the point where 3 mil holes could be made consistantly.

The first cell design is shown in Figure F-1. In addition to the tungsten probes, Ta probes were also sealed into the capillary. The Ta and W probes formed a thermocouple with the molten alloy acting as the connecting medium. The glass-work entailed shielding the probes and sealing them into the small holes so that just the tip protruded into the channel. This work was very delicate and required a high degree of glass-working ability. An excellent job was done by Mr. George Killich. All of the materials coming through the brass cap were sealed vacuum tight. The upper electrode came just to the edge of the capillary channel. The lower electrode protruded across the channel, thereby blocking the channel to the passage of molten metal. A small pin-hole remained, however, so that gas pressure could be transmitted through the capillary channel.

To fill the channel a small pressure of helium was first introduced into the chamber. Both valves were then closed, the vacuum system turned on, and the molten alloy raised over the down-spout. The small valve was then opened until a length of metal exactly equal to the length of the transport channel was drawn into the capillary. The alloy was then lowered, the valve closed and the apparatus tapped gently. The tapping caused the lower surface to form inside the capillary giving an additional upward force due to the convex surface and thereby pushing the metal around into the channel. The metal was stopped and held by the lower electrode. After a run the metal could be simply blown out of the capillary with helium.

A 12 point recorder was used to measure the voltage drop across each of the segments as a function of time. A schematic diagram is shown in Figure F-2. The constant current D.C. power supply is described in

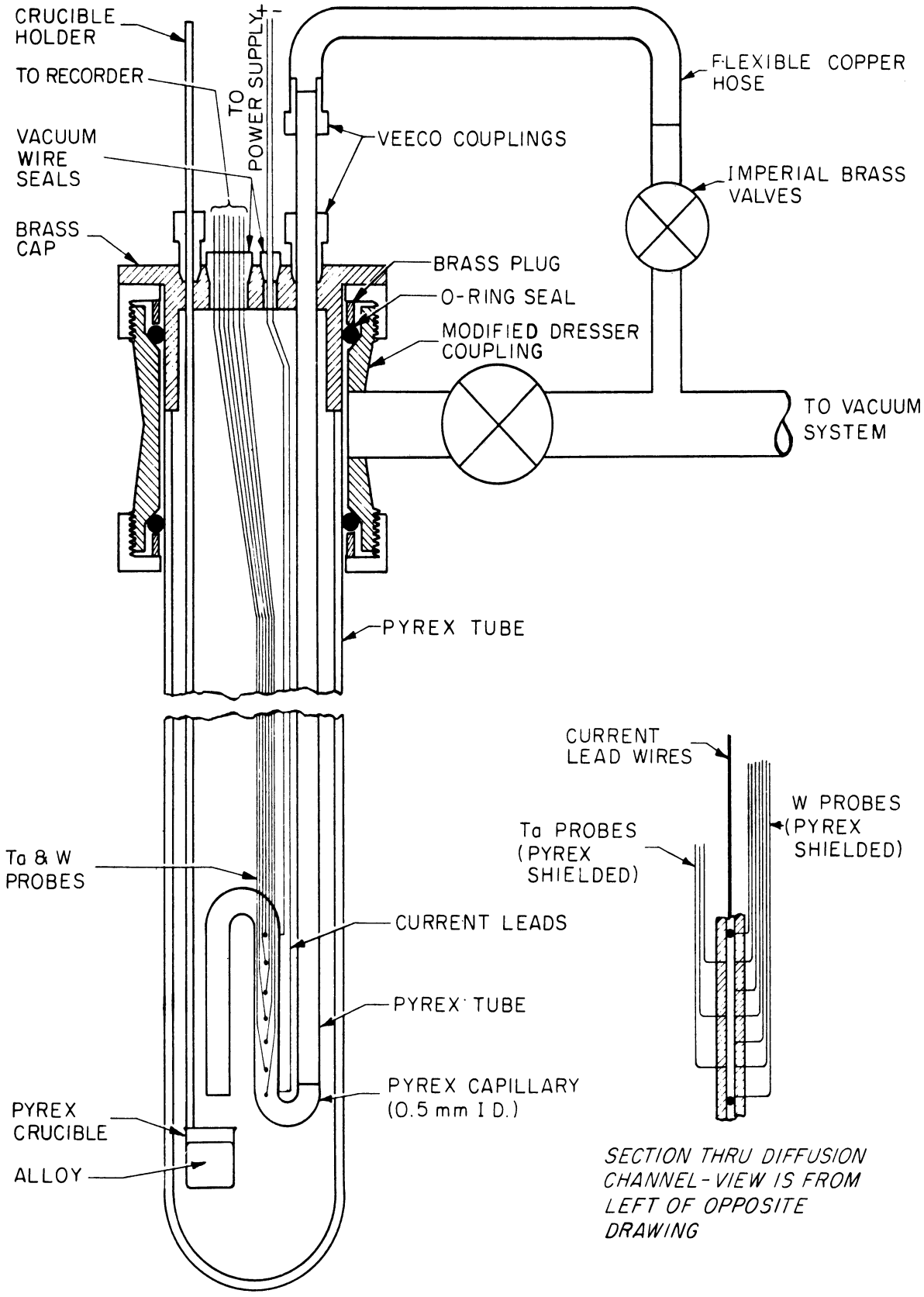

Figure F-1 Electrodiffusion Cell -- Resistivity Type.

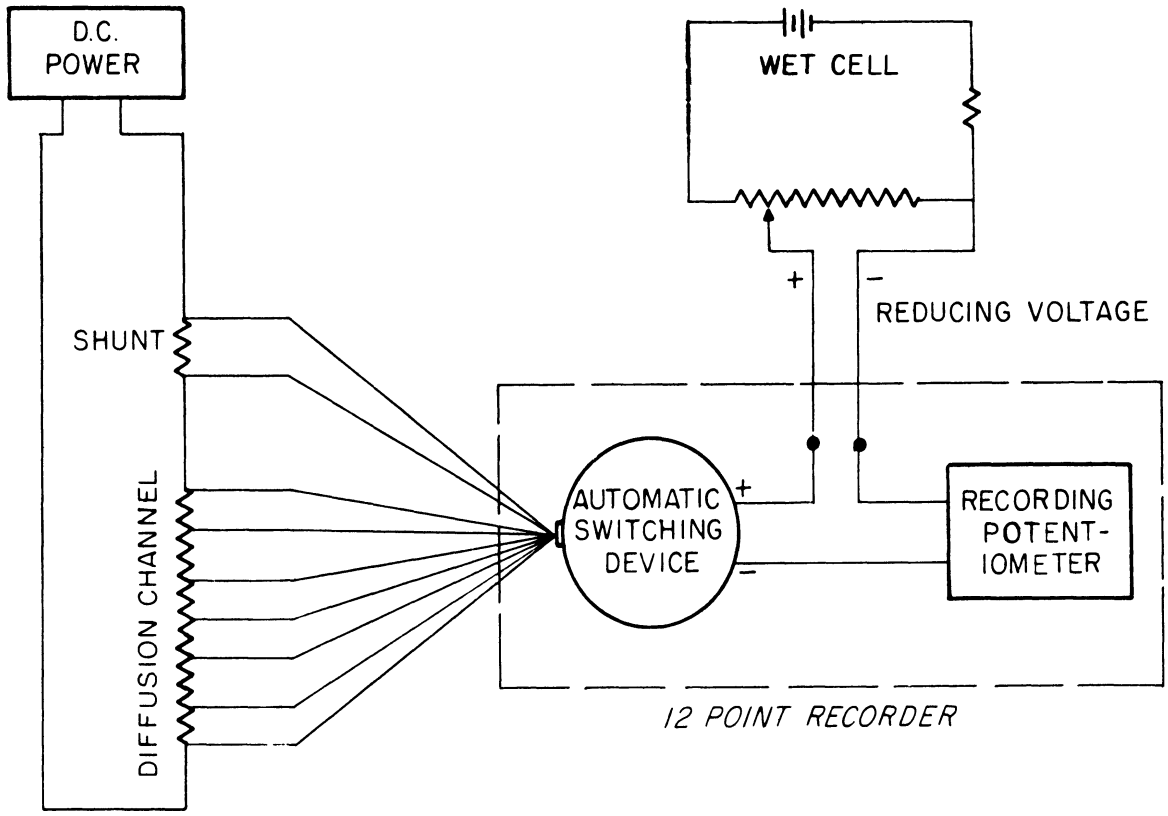

Figure F-2 Electrical Circuitry.

Chapter V. The long time current variation was not negligibly small so that it was necessary to monitor the current and correct the data for current variation. The percent change of the voltage across each probe was quite small. To measure this change accurately with the recording device it was necessary to use a low scale (0 - 2.5 mv) on the recording potentiometer. The segment voltages were reduced to this scale by a constant reducing voltage of opposite polarity in a series circuit. Since data was recorded over a number of hours it was not necessary to run the recorder continuously. A circuit was designed which automatically turned the switching and recording portion of the controller on for one cycle over the 12 points at intervals of n minutes, where n could be varied from 5 minutes upwards.

The cell was first calibrated using pure mercury. The calibration was carried out in a manner similar to that described in Chapter V. The ratio of $(A_m/L)_i$ for each segment, i, was determined with Hg and the segment length, L_i, was determined with a binocular microscope.

The first cell design was constructed and operated successfully on a Bi-Sn alloy. It proved to be rather tedious to fill the cell with exactly the right length of alloy. The temperature measuring scheme did not work out successfully because the Temp-EMF relation for Ta-W, joined by liquid alloy, was not reproducible. This difficulty is discussed in Appendix K. The temperature was then measured by a thermocouple placed at the outside wall of the capillary Because of these two difficulties this design was dropped in favor of a second design.

III. SECOND CELL DESIGN

The details of this design are shown in Figure F-3. The materials

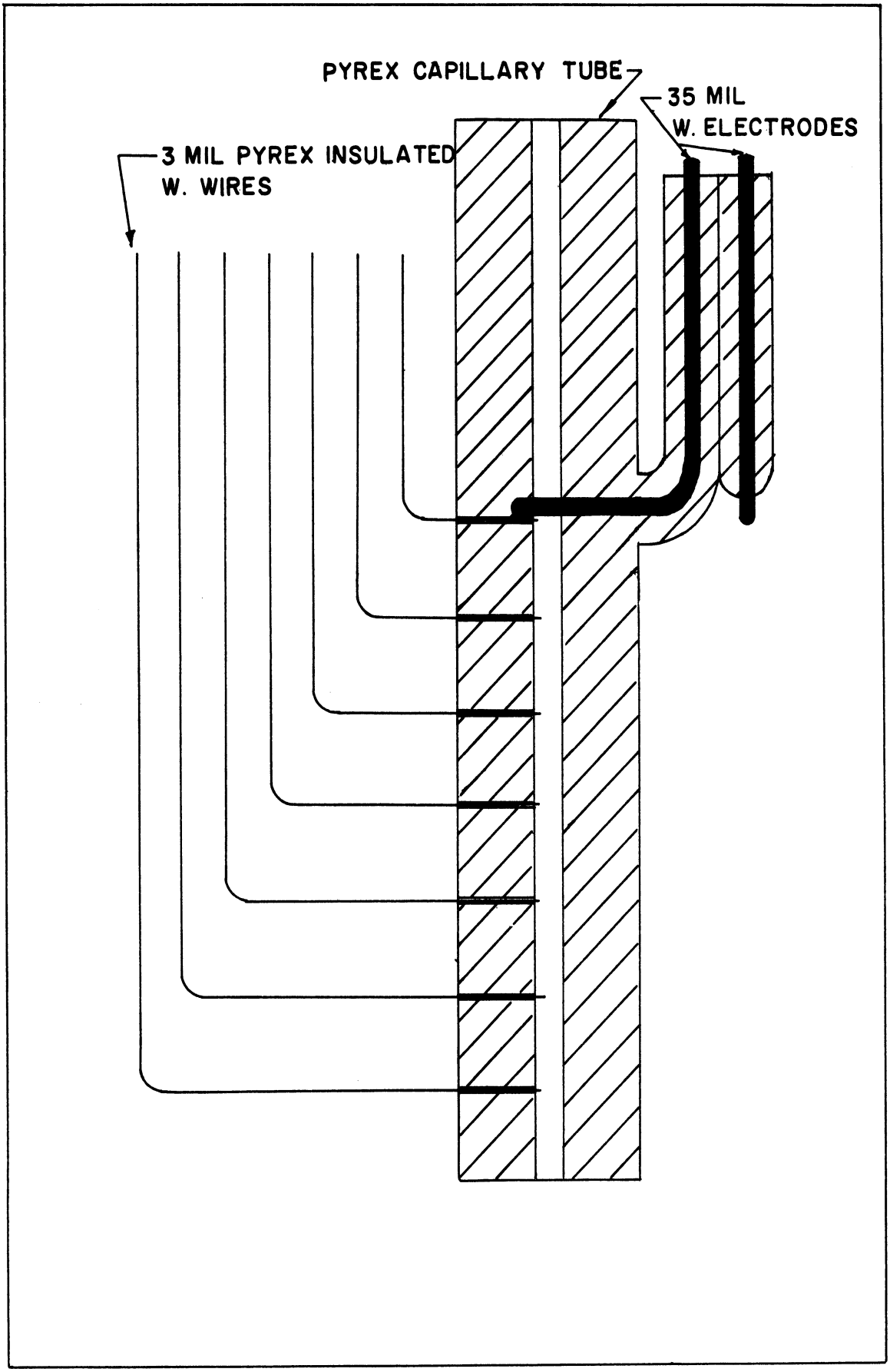

Figure F-3 Modification of Resistivity Cell to a One-Ended Reservoir Geometry.

are the same as in the first design. The cell was positioned at the end of the vertical tube in Figure F-1, with the open end down. The alloy was contained in a long crucible which could be raised up around the cell so that the entire capillary channel was surrounded by a liquid metal bath. The temperature was measured by a thermocouple placed next to the capillary within the metal bath. The capillary channel was filled by either introducing pressure through the large valve or drawing a slight vacuum through the small valve. In either case the metal was forced to stop at the inside electrode, since the opening there was large enough to pass helium gas but not liquid metal. The cells were emptied by simply blowing the metal out of the capillary. Cells of this design proved to be much easier to fill than cells of the previous design.

Measurements were successfully made on the Hg-Sn system around room temperature with cells of this design. A mobility value of 5.1×10^{-4} $cm^2/V\text{-}sec$ was obtained compared to 5.3×10^{-4} by Schwarz and 6.4×10^{-4} by Mangelsdorf. The reproducibility, however, was not very good.

Three different cells of this design were constructed. To clean the cells after a run, it proved necessary to insert a small tube up the capillary channel, so that an acid solution might be squirted against the upper electrode and past each of the probes. In the course of this process it was very difficult to avoid contact with the probes. All three cells were ruined after only a few runs were made; the tips of some of the probes were broken off in the cleaning process. This was extremely discouraging since a large amount of effort was required to construct, connect, and calibrate each of these cells.

IV. THIRD CELL DESIGN

The third type of cell was designed with an emphasis on simplicity. The design is shown on the left of Figure G-1. The dimensions of the cell and the details of the experimental operation are essentially the same as those discussed in Chapter V. A critical point which made this type at all feasible was the fact that it could be emptied by simply drawing a vacuum upon it. This resulted because the Bi-Sn alloys did not wet the Pyrex. One of the major advantages of these cells in addition to their simplicity and ease of construction was the thin wall thickness (.006-in.). The temperature rise due to I^2R heating was considerably less than in the previous design where the wall thickness was greater by a factor of 16. Some of the first data taken with cells of this design are shown in Figure 9.

APPENDIX G

ELIMINATION OF SPURIOUS INTERFACE POTENTIALS

I. INTRODUCTION

After development of the Type 1 cell shown on the left of Figure G-1 it became quite easy to check the reproducibility of the results. Some of the first results with Type 1 cells are shown in Figure 9. These results are typical of the very good linearity of the data obtained in all of the initial work. Unfortunately, however, the precision of the slope of these V vs θ curves was very poor; the slopes varied by as much as 20% on runs made with the same cell under identical conditions. Considerable experimental effort was required to locate the source of this error.

II. EXPERIMENTAL WORK

The first two runs, Runs V-1 and V-2, were made on an alloy containing 0.5 At% Sn. The values of $\Delta V/\Delta\theta$ obtained at this low concentration were so small that the precision was very poor. Runs V-3 to V-6 were then made at 5 At% Sn in Bi, and the results are shown in Table G-1. For the eight experiments the deviation of the average amounted to 15%. This seemed extremely inconsistant with the high linearity of each run.

In addition to the lack of reproducibility of the data, another anomaly was encountered in the calibration of the cells with pure mercury. This calibration yields the mean value of the length to area ratio, L/A_m, for the cells; the experimental procedure is described in Chapter V. The results of the calibrations are shown in Table G-2. The precision of the data was low relative to the precision generally attainable in electrical

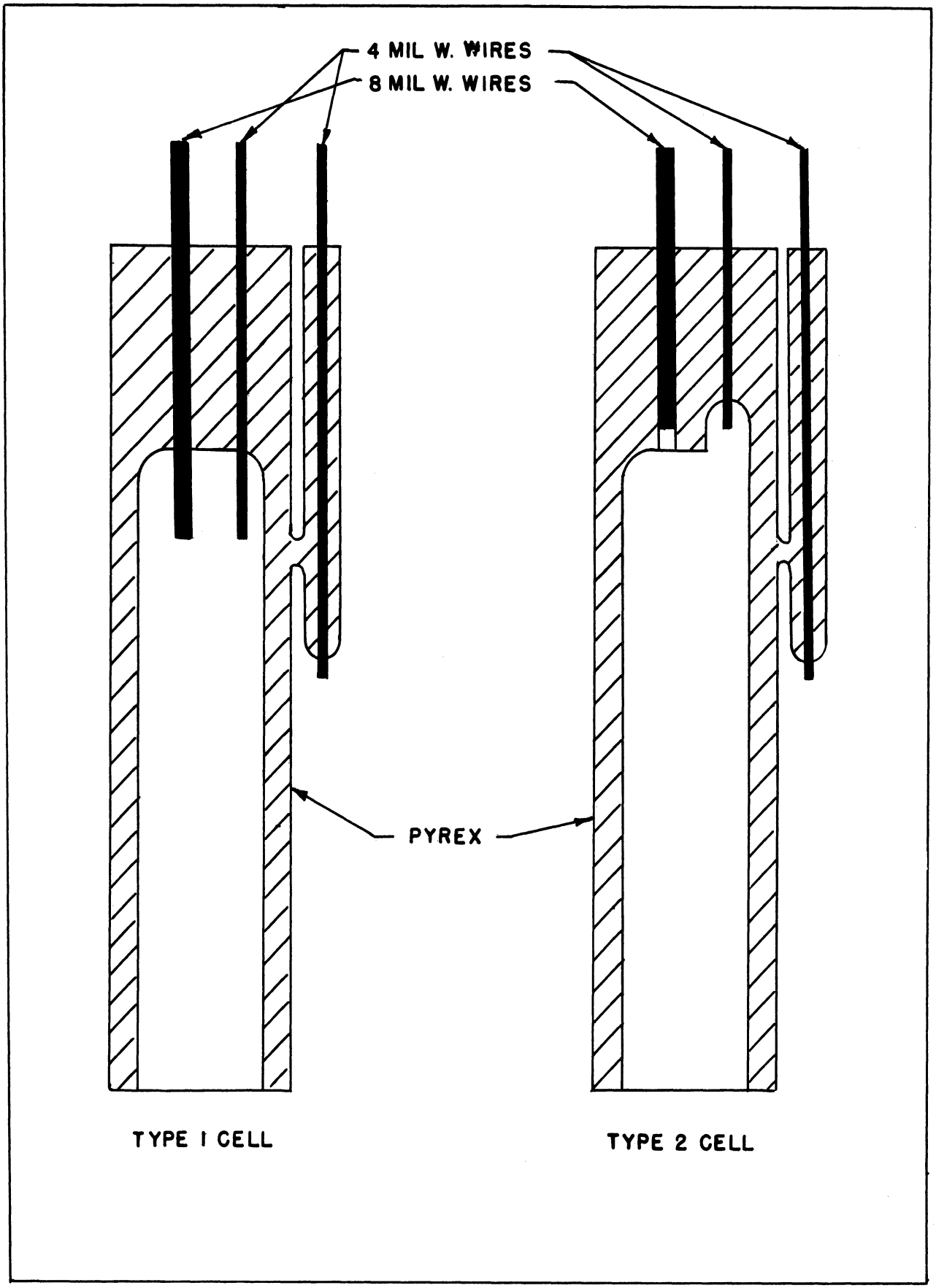

Figure G-1. Details of Electrotransport Cells.

measurements of this type, and the drift between calibrations was unexplainable.

TABLE G-1

DIFFERENTIAL MOBILITY USING TYPE 1 CELLS

Run	Cell	U_{Bi-Sn} $cm^2/V\text{-}sec \times 10^3$	I/A $amps/cm^2$	Temp. °C
V-3	1	.571(1)	622	374
V-3	2	.765*	640	374
V-4	1	.644*	619	375
V-4	2	.551	638	375
V-5	1	.758	619	383
V-5	2	.776*	638	383
V-6	1	.755	617	385
V-6	2	.694*	636	385
Ave Mobility:		.690; Dev. of Ave.(2):		.103

(1) Asterisk indicates solute migrated inward rather than outward.
(2) Deviation of Average Mobility, determined as described in Chapter V, Equation (180).

TABLE G-2

CALIBRATION OF CELLS USED IN RUN V-3

Calibration	Cell	$\frac{L}{A_m} \times 10^3$, cm^{-1}	% Standard Deviation	No. of Points
1	1	892.71	1.2	6(1)
2	1	906.70	0.98	17
3	1	918.01	1.9	10
1	2	892.27	0.065	6
2	2	905.85	0.50	17
3	2	928.46	0.38	10

(1) Each point is the average of two measurements of opposite polarity.

Following these results, experiments were conducted to locate the source of error causing the lack of precision. The experimental program turned out to be quite extensive and is reviewed here by reference to each experiment. Unless otherwise stated, pure Bi was used as the molten metal, the tube length was 2.5 cm, and the current density was approximately 650 amps/cm^2.

Run E-1: Cells: Type 1 from V-1 to 6; Temp: 376, 379, 416°C.

Purpose: To check the voltage variation using pure Bi. One would expect the voltage drop across the cell to approximate a horizontal straight line as a function of time.

Results: The voltage drop across the cells was found to vary considerably with time. In six different experiments the voltage increased 4 times and decreased twice in a non-linear fashion, random with respect to polarity. The rate of voltage change decreased with time, but was still changing, even after 45 hours.

Run E-1A: Cells: Type 1 from E-1; Temp: 365°C.

Purpose: It was felt that the variation might be due to absorbtion of helium on the cell walls or to slight pressure changes, since the runs were made at an absolute pressure of 660 mm Hg.

Results: The voltage across the cells containing pure Bi was measured as the pressure was varied from .005 mm to 660 mm Hg. A small effect was found, but it was negligible compared to variations encountered in Run E-1.

Run E-2: Cells: Type 1, made up new (not KOH etched); Temp: 379°C.

Purpose: To check voltage variation in pure Bi using oxidized probes.

Results: The results of 4 experiments gave the same random results as Run E-1 with one exception; the voltage variations appeared to be much larger.

Run E-2A: Cells: Same as E-2; Temp: 379°C.

Purpose: The variation might have been caused by a varying thermoelectric output between the probes inside and outside of the cell. If the temperature inside the cell were changing with time due to varying contact resistance at the electrode, this would cause a varying thermoelectric output since the outside probe was held at the bath temperature.

Results: The voltage decay across the cell was measured after shutting off the current. If it did not drop immediately to a steady value this would be an indication of, at least, the presence of a thermoelectric effect. The decay rate was relatively slow, indicating the possibility of a thermoelectric effect.

Run E-3: Type 1 with withdrawn probe; Temp: 383°C.

Purpose: The maximum internal heat generation was most probably produced at the electrode-metal contact. If the voltage variation was due to a thermoelectric effect, it could be reduced by withdrawing the inside probe from the vicinity of the electrode-metal contact.

Results: Two cells were made up with the inside probes withdrawn 2.2 cm above the electrode. The alloy travelled up a small cavity to contact the probes. The results were again a random change of about the magnitude found in Run E-1.

Run E-4: Cells: Type 1 with large electrode; Temp: 373°C.

Purpose: To check the effect of using a larger electrode.

Results: Cells were made up using 12 mil W for electrodes. Results were again a random voltage change.

Run E-5: Cells: Type 1 with additional inside Ta probe; Temp: 375°C.

Purpose: (a) To check the relative W-Bi vs. Ta-Bi thermoelectric voltage. If the Ta-Bi thermoelectric voltage were much smaller, Ta might be a better probe material. (b) To check the internal heating on start-up. (c) To check the temperature lag. If the inside temperature were continually changing due to I^2R heat, and if there was an appreciable temperature lag to the measuring thermocouple in the bath, then an apparent voltage would result. (d) To check the absolute voltage variation when the polarity was reversed.

Results: Two cells were made up with an additional 6 mil Ta probe adjacent to the inside 4 mil W probe. Previous data had been measured on the thermoelectric output of Ta-W thermocouples connected through molten Bi-Sn (see Appendix K). (a) The thermoelectric output of Ta-Bi was greater than that of W-Bi. (b) The temperature rise inside of the tube relative to the bath appeared to be on the order of 2°C. (c) Voltage variation using the inside Ta-W thermocouple was the same as using the bath thermocouple. (d) A relatively large absolute voltage difference was found when the polarity was reversed. The variation was practically instantaneous. It was as large as 8 mv out of 250 mv in some cases, and somewhat spurious with time.

Run E-6: Cells: From Run E-5; Temp: 380°C.

Purpose: To check the effect of pressure upon the change in voltage when the polarity was reversed.

Results: Experiments were run at an absolute pressure of 160 mm Hg and then at 710 mm Hg. The absolute value of the voltage difference on polarity reversal was independent of this pressure change.

Runs E-7, 8: Cells: Shunt-type using W (see Figure G-2); Temp: 380°C.

Purpose: Somewhere in the electrical circuit there was a non-linearity giving rise to the absolute value of the voltage difference upon polarity reversal. The purpose here was to pinpoint the non-linearity.

Results: Two shunt-type cells as shown at the top of Figure G-2 were made up. Reversing the polarity produced a 0.15 mv change out of 260 mv across the probes. A change of 3 to 12 mv out of 350 mv was produced across the upper probe and a probe attached to the outside of the cell in contact with the bath. This circuit contained a W-Bi interface. The result was fairly conclusive evidence that the non-linearity was being produced at the W-Bi interface rather than at some other point in the circuit.

Run E-9: Cells: Shunt-type using Ta and Mo; Temp: 302, 380°C.

Purpose: To check the non-linear voltage change across the Mo-Bi and Ta-Bi interfaces.

Results: The absolute value of the voltage change on polarity reversal was about the same for Mo-Bi as for W-Bi, but was smaller by a factor of 2 for Ta-Bi.

Run E-10: Cells: Type 2--KOH etched; Temp: 473°C.

Purpose: It was fairly certain that the non-linear potential was generated at the W-Bi interface. In all probability the tungsten surface was coated with a thin layer of WO_3 even though it had been etched. WO_3, as well as the oxides of Ta and Mo, are semiconducting materials, and metal-semiconductor interfaces are frequently rectifying; copper oxide rectifiers are a typical example. Consequently, the varying voltage could be accounted for if the semiconducting properties of the oxide varied as a run progressed.

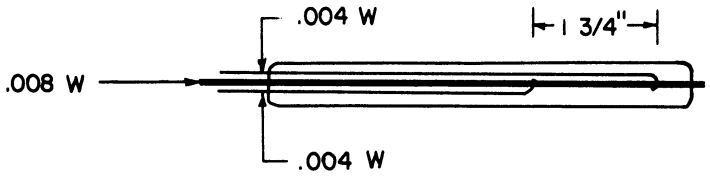

TUNGSTEN SHUNT

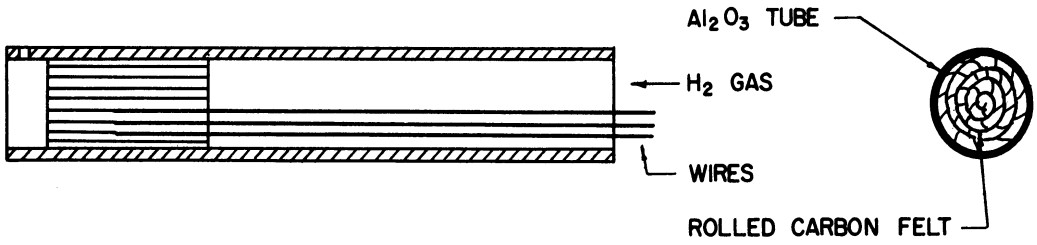

FINAL SETUP FOR CARBURIZING TUNGSTEN WIRES

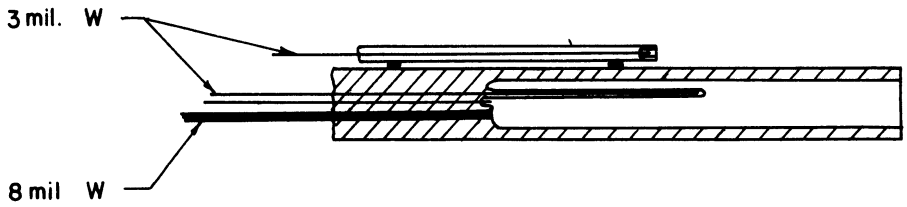

EXPERIMENTAL ELECTROTRANSPORT CELL

Figure G-2. Miscellaneous Experimental Apparatus.

In fact, any variation in the rectifying characteristics of the interface due to a physical or chemical change would account for the random results. The results of Run E-2 supported this theory. This interface difficulty could have easily been overcome by using a noble metal for the electrodes and probes. This was not possible since the noble metals are soluble in Bi-Sn alloys at 500°C. To eliminate the difficulty arising from a rectifying interface potential the Type 2 cell shown in Figure G-1 was developed. Analysis of this cell will reveal that the voltage drop across the W-Bi interface is not measured by the probes. In addition, there is no point in the probe circuit where the electrotransport current passes through a W-Bi interface.

Results: The absolute value of the voltage change on current reversal ranged from only 0.2 to 0.6 mv. This was only slightly larger than the value found for the shunt cell of Runs 7, 8 and was probably due to non-linearities in the external circuit. It compared to values of around 5 mv on similar runs with Type-1 cells. In addition, the V vs θ curve was horizontal over a 7 hour run for the first time.

Run E-11: Cells: Two new Type 2 cells--KOH etched; Temp: 430°C.

Purpose: To recheck Run E-10 with new cells.

Results: The ΔV on polarity reversal ranged from 0.15 to 0.46 mv. The V vs θ curves were horizontal over 8 hours.

Run E-12: Cells: Two new Type 2 cells with bigger openings at the electrode--KOH etched with AC current; Temp: 375, 500°C.

Purpose: To determine the limits of precision.

Results: The ΔV on polarity reversal ranged from .35 to .65 mv. However, a large voltage variation was found with time; it was always positive,

whereas in runs on cells of Type 1 it had also been negative. It ranged from +90 to +370 μV/hr at $I/A = 650$ amps/cm^2 and was fairly linear.

Run E-13: Cells: From E-12; Temp: 485°C.

Purpose: The cells in Run E-12 had accidentally been vapor coated with Bi before the run was made. This run was made to see if the deposit had caused the bad results.

Results: Same as E-12, with $\Delta V/\Delta\theta$ ranging from +110 to +113 μV/hr.

Run E-14: Cells: From E-13--cleaned and etched; Temp: 445°C.

Purpose: To check the possibility of a short across the Pyrex glass, and also to rerun cells.

Results: The resistance at temperature across the probes before filling but after immersion in the molten bath was 50,000 ohms. Placing 50 D.C. volts across the empty immersed cells gave a probe reading of only 3 μV. Hence, leakage across the glass was assumed negligible. The ΔV on current reversal was +.18 and +.26 mv. The voltage variation, $\Delta V/\Delta\theta$, was +90 and +50 μV/hr.

Run E-15: Cells: From E-14--cleaned and oxidized; Temp: 495°C.

Purpose: To check the effect of oxidizing the electrode and probes.

Results: The following treatment was given to the cells to form an oxide layer of 6000 Å thickness. After cleaning with HNO_3 and HF and etching with KOH until shiny, the cells were vacuum annealed at 480°C for 12 hours. They were then held under an absolute pressure of 76 mm of pure oxygen for 2 hours at 504°C. This treatment should produce a 6000 Å layer of WO_3 on the tungsten surface.(G-1) The oxide layer apparently accentuated the voltage change. The voltage variation $\Delta V/\Delta\theta$, was +830 and +1140 μV/hr.

Run E-16: Cells: One cell from Run E-11 and one shunt-type cell; Temp: 500°C; I/A: 650 and 325 A/cm^2.

Purpose: (a) To recheck the cell used in Run E-11 after etching with AC current. (b) To check the effect of current on $\Delta V/\Delta\theta$. (c) To check the value of $\Delta V/\Delta\theta$ obtained on the type of shunt shown in Figure G-2.

Results: (a) The cell from Run E-11 no longer produced a flat $\Delta V/\Delta\theta$ curve. (b) At a current density of 650 A/cm^2 the value of $\Delta V/\Delta\theta$ was +450 μV/hr; at 325 A/cm^2 the V vs θ slope was +220 μV/hr. Hence the variation appeared to be linear with current density. (c) The value of $\Delta V/\Delta\theta$ for the shunt was approximately zero. The ΔV on reversing the current polarity was 0.12 mv for both the cell and the shunt at 650 A/cm^2.

Run E-17: Cells: Type 2 with a second W probe inside one of them and a second Ta probe inside the other; Temp: 499°C.

Purpose: (a) To check the potential between two W probes in the cavity next to the electrode. (b) To check the result using Ta-Ta as probes. (c) To check the temperature change inside and out on starting. (d) To check the voltage variation, $\Delta V/\Delta\theta$, using an inside thermocouple for temperature corrections.

Results: Two cells were made up with two probes in the cavity next to the electrode. In one cell both inner probes were W and the other contained one Ta and one W probe. (a) Even though the inner probes were in the cavity where none of the electrotransport current passed through them, the current caused a potential of +40 μV to be induced across the W-W probes under one polarity, and -60 μV under the opposite polarity. The thermoelectric output of the Ta-W probes in the other

cell was also affected by the current, making a 70 μV jump when the polarity was reversed. In both cases however, this potential was relatively time independent, having a $\Delta V/\Delta\theta$ of 1 μV/hr. (b) The value of $\Delta V/\Delta\theta$ obtained with Ta probes was approximately the same as with W probes. (c) Taking into account the effect of current on the Ta-W output, the inside capillary temperature appeared to be either 0.2 or 2.4°C higher than the bath temperature. (d) The value of $\Delta V/\Delta\theta$ using the Ta-W couple for temperature corrections was roughly the same as with the bath thermocouple. The values of $\Delta V/\Delta\theta$ were +80 μV/hr and +180 μV/hr.

Run E-18, 19: Cells: Type 2 with WC probes; Temp: 449°C.

Purpose: From previous work it had been concluded that the non-linearity, and possibly the variation with time of the cell voltage resulted from the rectifying properties of the tungsten oxide-bismuth interface. Since tungsten monocarbide is an electronic conductor(G-2) the WC-Bi interface should not be rectifying. It was therefore decided to construct cells using WC probes.

Development of WC Probes: A rather thorough literature survey was conducted on the formation and properties of tungsten carbides. Two carbides are formed, WC and W_2C, both of which are electronic conductors. The monocarbide is more stable chemically and has a higher conductivity, being 40% that of the pure metal. Following references such as Newkirk,(G-3) the first wires were carburized by passing a mixture of H_2 and CH_4 over them at high temperatures. This method was not very successful and a better method was finally developed. Graphite felt was plugged into the end of an Al_2O_3 tube and the ends of the wires to be carburized were pushed into the felt as shown in Figure G-2. The W wires had previously

been etched in a solution of 4 parts conc. HF to 1 part conc. HNO_3 for 30 seconds to a minute. The tube was placed in the cool end of a Leco tube furnace and flushed with He gas for a half hour or so before they were pushed into the hot zone at 2500°C. They were then flushed with hydrogen which was first purified by passage through a liquid nitrogen cold trap. After 6 to 10 hours the hydrogen was replaced by helium and the tube was slowly withdrawn from the furnace. This method proved successful in preferentially carburizing just one end of the wires. Considerable effort was made to insure that WC had formed on the wires. The monocarbide is a steel gray color and it is insoluble in the above acid solution, while both W and W_2C are soluble. The carburized wires which had a steel gray appearance were insoluble in the acid solution. An x-ray picture was then taken on one of these wires by rotating it in a Debye camera. The picture was taken for 3 1/2 hours using cobalt radiation with a power setting of 10 ma at 40 KW. The strong lines corresponded nicely to WC with a few W_2C lines showing up. None of the oxide lines appeared. The x-ray specimen was then mounted along with other carburized wires for metallographic examination. The wires were first electrolytically coated with iron out of a solution containing 288 gms of $FeCl_2$ and 57 gms of NaCl dissolved in 1000 mil H_2O and heated to 185°F. After polishing they were mounted and examined metallographically. Both the W_2C and the WC layer could be seen. The W_2C layer was columnar as described in the literature. By etching with the $HF\text{-}HNO_3$ solution the Fe and W_2C were dissolved leaving only a skeleton of WC along the outside edge. This was a beautifully graphic proof of the WC layer. On an 8 mil sample from one run the WC layer

was 2 microns thick and the W_2C was roughly 5 microns thick. The cells were made up using probes of 4 mil WC coated wire. Unfortunately the Pyrex did not seal well to the WC coat because of bubble formation. It sealed well enough however, to make up the cells. It was necessary to be sure that the WC was not oxidized in the sealing process. Fortunately, WC does not air oxidize until 500-520°C.[G-4] The seals were made inside the outer pyrex tube while flushing with a stream of helium gas.

Results: A fairly linear variation of V with θ over 9 hours was found, with $\Delta V/\Delta\theta$ being +230 μV/hr.

Run E-20: Cells: Type 2 with WC probes; Temp: 446°C.

Purpose: To recheck the results of Run E-18, 19.

Results: This run was made with the polarity reversed on a new WC probe cell. The initial voltage variation was quite rapid but fell off to a linear value of +150 μV/hr. Hence, it appeared quite conclusively, that the voltage change was not overcome with the use of an electronic conducting probe.

Run E-21: Cells: Type 2--newly made; Temp: 460°C.

Purpose: To check the outgassing procedure.

Results: It had been noticed that sometimes when the cells were lowered into the melt, small bubbles were evolved even after vacuum outgassing. After outgassing at 500°C the cells were lowered into the melt a few times before final filling. The results were negative. The values of $\Delta V/\Delta\theta$ were +510 and +420 μV/hr.

Run E-22: Cells: Type 2 from Run E-21; Temp: 500°C.

Purpose: The cells used in the successful runs of E-10 and E-11 were etched with DC current while the cells used in later runs were etched with AC current. In this run one cell was DC etched and the other AC etched. In addition the cells were cleaned with a $Na_2Cr_2O_7 + H_2SO_4$ cleaning solution to insure clean tube walls.

Results: Contact was lost on the DC etched cell in the first fill. The $\Delta V/\Delta\theta$ of the AC etched cell was +1720 μV/hr. In the second fill the DC etched cell gave a $\Delta V/\Delta\theta$ of +140 μV/hr and the AC etched cell gave +160 μV/hr.

Run E-23: Cells: Modified Type 2; Temp: 505°C.

Purpose: A method was found for coating the W probes with a thickness of pyrex 1 mil or less. A cell was then made up as shown in the bottom of Figure G-2. Note that the tip of the lower inside probe is shielded from the electrotransport current by the Pyrex coating. By measuring the voltage drop across the inner probes, the voltage variation across the electrode segment could be determined. The voltage drop across the lower segment could also be measured between the lower inner probe and a probe in the bath. If the voltage variation were produced by an effect at either the electrode or the tube mouth it would show up as a zero $\Delta V/\Delta\theta$ for one segment and not the other.

Results: The voltage variation across the electrode section was +40 μV/hr. The voltage variation across the whole cell was +50 μV/hr.

Run E-24: Modified Type 2; Temp: 500°C.

Purpose: Two new cells were made up to check the purpose stated for Run E-25 more thoroughly.

Results: The electrode segment of cell 1 gave a $\Delta V/\Delta\theta$ of +40 μV/hr, the lower segment gave +330 μV/hr and the overall value was +310 μV/hr. Hence for this cell the change was produced in the lower segment. For cell 2 the $\Delta V/\Delta\theta$ of the electrode segment was +120 μV/hr, the lower segment was +70 μV/hr and the overall value was measured as +190 μV/hr. Hence in this cell the change seemed to be fairly uniformly spread over the cell, with a slightly greater contribution from the electrode end. This was interpreted as evidence that the change probably resulted from a changing column diameter due to gas formation on the capillary walls.

Run E-25: Cells: From E-24; Temp: 292°C.

Purpose: If the interpretation of Run E-24 were correct, the difficulty might be alleviated by better outgassing. A quartz outer tube was obtained and the cells and melt were outgassed at 630°C with considerable stirring of the melt by the Mo stirrer arrangement shown in Figure 8. The run was made about 200°C lower than the usual experimental temperature.

Results: The $\Delta V/\Delta\theta$ for the electrode segment of Cell 1 was +64 μV/hr, the lower segment gave -28 μV/hr and the overall value was +40 μV/hr. This was the first negative value encountered on a Type 2 cell. The $\Delta V/\Delta\theta$ for the electrode segment of Cell 2 was +80 μV/hr, the lower segment was approximately zero and the overall value was +93 μV/hr. These values are only approximations, since the data is scattered. They indicate, however, that in both of these experiments the predominate change occurred at the electrode segment.

Run E-26: Cells: From Run E-25; Temp: 338°C.

Purpose: According to qualitative information in the literature, the solubility of helium in molten metals is negligibly small. The previous

runs were made under 600 to 700 mm of He pressure. Before introducing the helium the metal had been thoroughly outgassed to the point where no gas bubbles were visible upon stirring. After a 3 hour run under helium a vacuum was again pulled and the metal was stirred. This process evolved about 5 to 10 cm^3 of gas at the vacuum pressure. The gas formed evenly throughout the crucible right down to the bottom of a column of metal about 4 inches high. Consequently, the helium must have penetrated into the melt by some process. It was felt that since the argon atom is much larger it would probably not be entrained in the melt as much as the helium atom. And consequently by using an argon atmosphere, the $\Delta V/\Delta\theta$ variation might be overcome if it were due to a helium film at the capillary wall.

Results: The run was made after a number of outgassings followed by argon flushing. The value of $\Delta V/\Delta\theta$ in the electrode segment of cell 1 was +80 μV/hr. For cell 2 all 3 values were zero. These results were encouraging, but a strange difficulty arose. For some reason when argon was used the potentiometer reading on the cells became very unstable. A satisfactory explanation of this phenomena was never obtained. The instability was large enough to prohibit the use of argon in the actual runs.

Run E-27: Cells: From Run E-26; Temp: 308°C.

Purpose: (a) To see if keeping the charge under argon for a more extended period helped. (b) To check the ΔV on reversing the current polarity.

Results: (a) The $\Delta V/\Delta\theta$ value for the upper electrode segment of cell 1 was +27 μV/hr, the lower segment gave -17μV/hr and the overallvalue was +9 μV/hr. The variation in cell 2 was again approximately zero. (b) The ΔV on current reversal was zero for all three values in cell 1. In cell 2

however, the reversal gave a ΔV of 0.4 mv for the electrode segment, zero for the lower segment and 0.4 mv overall. This would appear to indicate that the non-linearity resulted in the neighborhood of the electrode. The results also indicate that the $\Delta V/\Delta\theta$ was very small if not zero when argon was used for pressure.

Run E-28: Cells: From Run E-27; Temp: 500°C.

Purpose: Calculations had been made which showed that the voltage readings were extremely sensitive to the diameter of the capillary column. For the condition of these experiments, a deposit of 1 micron of gas on the capillary wall would produce a voltage change of 1690 μV. In addition, such a deposit would always cause a positive value of $\Delta V/\Delta\theta$, independent of polarity; which was in agreement with previous experimental results. Consequently, the apparatus shown in Figure G-3 was designed so that the Bi could be distilled under a high vacuum, directly within the electrotransport equipment. This distillation column was placed within the electrotransport apparatus, shown in Figure 8, through the coupling which introduced the stirring rod. The cells were withdrawn to the cooler end of the furnace and a temperature of 975°C was held for around 21 hours. This was sufficient time to distill 370 gms of Bi and also provide considerable refluxing. The vacuum within the chamber was transmitted into the column through a 1 inch hole in the top wall of the distillation column. After distilling, the empty quartz crucible, fitted with a strip of Mo as shown in Figure G-3, was rotated under the column into a position such that the Mo strip contacted the knock-out plug. The crucible was raised, lifting the knock-out plug, and the metal flowed slowly into the crucible. Meanwhile, the cells had been positioned in a cooler

section of the furance where they had simultaneously been outgassed. Consequently, after cooling to the desired temperature, a run could be made in the usual manner. Helium gas was again used for filling the tubes.

Results: The results were negative, with $\Delta V/\Delta\theta$ being +115 μV/hr.

Run E-29b: Cells: Type 2 from Run E-21; Temp: 500°C.

Purpose: To recheck the results of Run E-28.

Results: The $\Delta V/\Delta\theta$ for cell 1 was +102 μV/hr and for cell 2 it was +70 μV/hr. The ΔV on polarity reversal was 0.2 mv for cell 1 and .06 mv for cell 2. Helium gas was again used. The distillation had no effect. If the trouble were produced by a gas deposit on the capillary walls it seems unlikely that the gas had originated within the bismuth.

Run E-30: Cells: Type 2 from Run E-29b; Temp: 518°C.

Purpose: To check the voltage variation with time using pure Sn rather that pure Bi.

Results: The value of $\Delta V/\Delta\theta$ was zero within the limits of measurements over an experiment time of 11 hours. The value of ΔV on polarity reversal was .02 mv. The results were astonishingly constant in view of the extreme difficulty previously encountered with pure Bi.

Run E-31: Cells: Type 2--one from Run E-30 and one new cell made up 3 cm long; Temp: 527°C.

Purpose: To repeat a run with pure Sn.

Results: Again the results were very encouraging. $\Delta V/\Delta\theta$ was zero within the limits of measurements. The value of ΔV on reversing polarity was .02 mv for cell 1 and .05 mv for cell 2. The results are shown in Figure G-4.

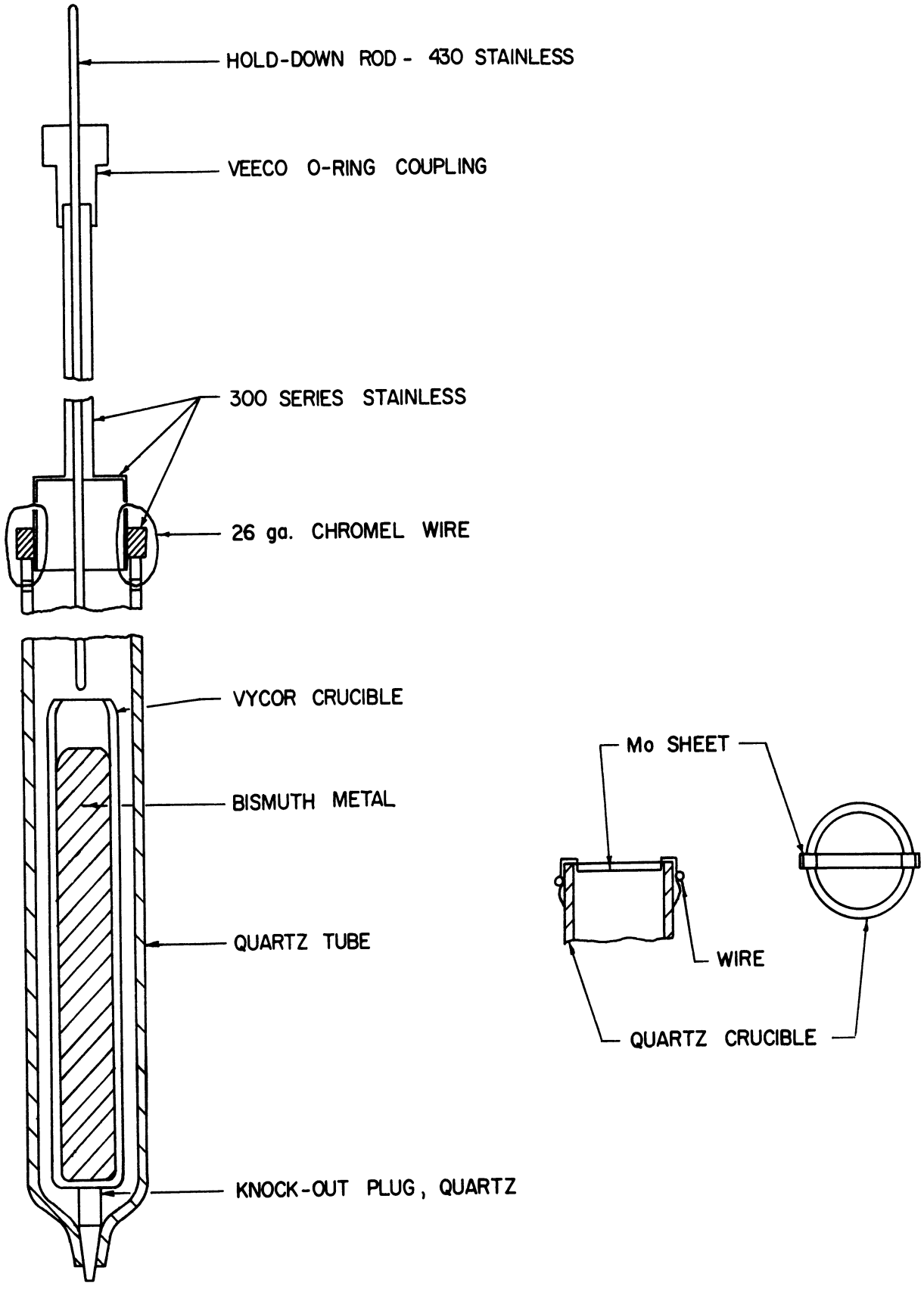

Figure G-3 Apparatus for Distilling Bi Inside of Electrotransport Equipment.

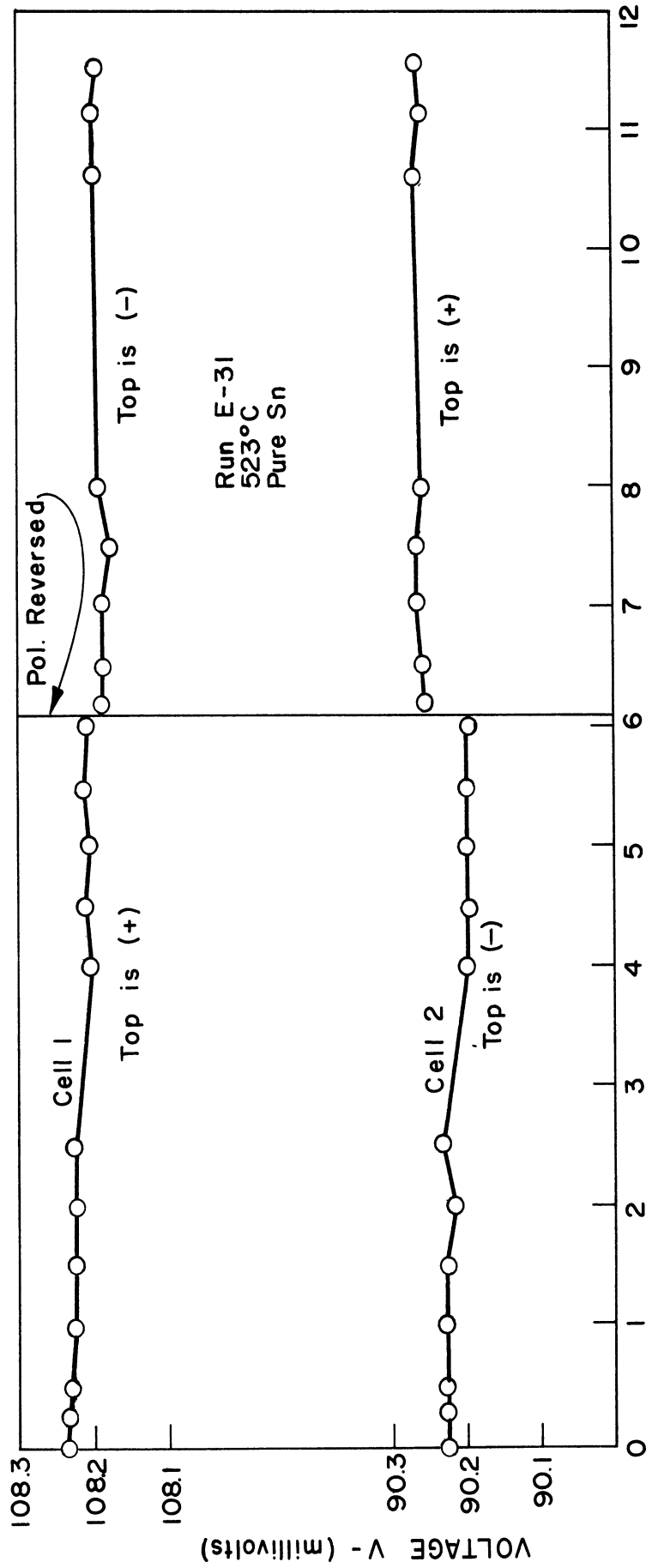

Figure G-4 Voltage Drop Across Cell Probes vs. Time.

III. CONCLUSIONS

After Run E-31 it was decided to measure the reproducibility of the mobility on the high Sn side of the system using Type 2 cells. Runs were made with 5 At% Bi at 520°C. The initial experiments were Runs V-7, 8, 9 shown in Table M-1. The reproducibility was extremely good, being much better than the previous results on a 5 At% Sn alloy using Type 1 cells, as shown in Table G-1. The rest of the phase diagram was then covered by increasing the Bi content and carefully checking the reproducibility. It was thought that the reproducibility would probably fall off as pure bismuth was approached. This did not happen however, even up to 95% Bi. The scatter in this 95% value is higher than the other values as can be seen in Table XXII. It is quite certain, however, that this is a result of using a lower sensitivity on the potentiometer due to the high resistance of this alloy. This difficulty was overcome in Runs V-1 to V-6, where the same composition was studied, by placing a reducing potential of opposite polarity in series with the cell potential.

During the course of the experiments, six different Type 2 electrotransport cells were used. The calibration of these cells is shown in Table M-2. The precision of the calibration may be compared with that for the Type 1 cells shown in Table G-2. The better precision of the Type 2 cells is additional proof that the electrode arrangement used in the Type 2 cells was the necessary modification required to overcome the lack of precision encountered in Runs V-1 to V-6.

The inability to eliminate $\Delta V/\Delta\theta$ for pure Bi using Type 2 cells is still a mystery. In view of the extensive experimental work done

in Runs V-10 to V-29b, the following conclusions are made. The source of the positive $\Delta V/\Delta\theta$ value is not due to (a) a changing temperature lag, (b) a changing thermoelectric potential, (c) a changing non-linear potential characteristic at the probe-metal interface, (d) a depositing of gas, initially contained within the bismuth, upon the tube walls, and (e) current leakage through the Pyrex at the elevated operating temperatures. In view of the experimental work, the best hypothesis is that somehow the He gas is slowly deposited on the capillary walls, thereby causing a minute change in the capillary diameter. This is supported by the fact that, (a) the overall $\Delta V/\Delta\theta$ is always positive, (b) the calculated value of $\Delta V/\Delta r$ is 1690 μV/micron of deposited gas, (c) a large amount of He is evolved from the melt after a run, and (d) the $\Delta V/\Delta\theta$ effect is very nearly zero using argon. It is required, however, that the helium deposit be roughly constant over the whole length of the capillary, since $\Delta V/\Delta\theta$ is not produced exclusively at either the electrode segment or lower segment of the capillary.

IV. REFERENCES

(G-1) E. A. Gulbransen and W. S. Wysong, Trans. AIME 175, 611-27 (1948).

(G-2) K. Becker, Phys. Zeit. 34, 185-196 (1933).

(G-3) A. E. Newkirk and I. Aliferis, J. Am. Ch. Soc. 79, 4629-31 (1957).

(G-4) A. E. Newkirk, J. Am. Ch. Soc. 77, 4521-22 (1955).

APPENDIX H

RESISTIVITY OF THE Bi-Sn SYSTEM

I. INTRODUCTION

In order to determine the electrical mobility with the resistivity technique it is necessary to know the variation of resistivity with composition. A fairly extensive literature search indicated that Northrup[H-1] was the only investigator who has reported on the resistivity as a function of composition in the Bi-Sn system. He presents graphical data at 300°C which shows the resistivity to be a linear function of mole fraction. A private communication to the laboratory where this work was done, revealed that a tabulation of the data was no longer available. In discussion of the Bi-Sn system, Golik[H-2] refers to a study of the conductivity of the system by Gaibullaev and Regel.[H-3] This reference could not be found in the United States library system. Consequently, it was necessary to experimentally determine the resistivity-composition-temperature relationship for the Bi-Sn system.

II. EXPERIMENTAL PROCEDURE

Cell Design -- A rather sophisticated electrodless method has recently become quite popular for the measurement of the resistivity in liquid metals.[H-4] Since the Bi-Sn system has rather mild corrosive effects, the more conventional technique was used for these measurements. The cell design is shown in Figure H-1 . The resistivity is determined by simply measuring the voltage drop across the

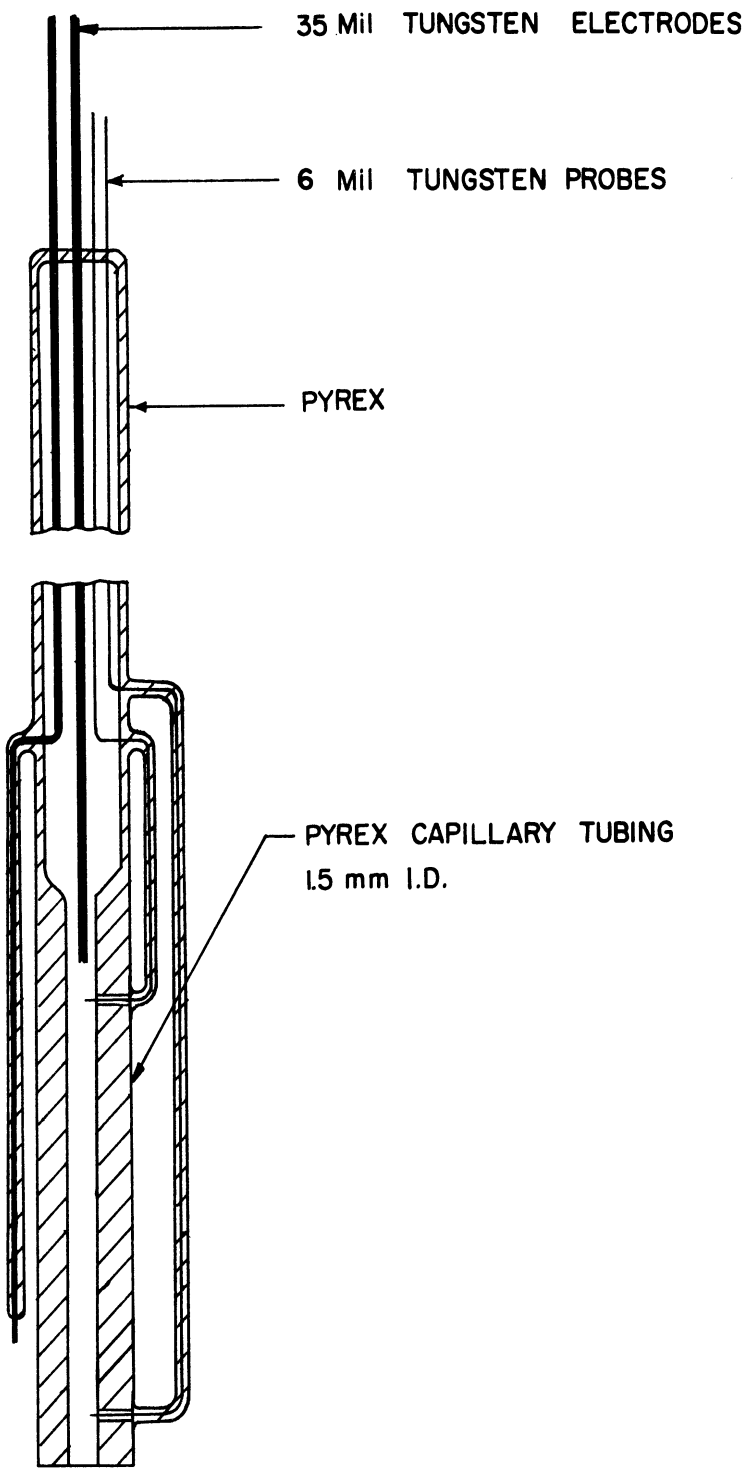

Figure H-1 Pyrex Resistivity Cell.

two probes with a known current passing through the metal within the capillary channel. The mean value of the length to area ratio of the capillary channel is first determined by a calibration with pure mercury.

The construction of these cells was facilitated by the development of an ultrasonic drilling technique. This technique was used to drill a 6 mil hole through the wall of the Pyrex capillary tube. It was thereby possible to seal in the tungsten probes with a minimum distortion of the inside capillary wall. In this type of experiments it is not necessary that the area of the capillary be constant. However, irregularities at the probes introduced by normal glass blowing techniques increase the possibility of bubble formation and consequent error.

Two cells of the type shown in Figure H-1 were constructed. Cell No. 1 had an I.D. of 2 mm and Cell No. 2 an I.D. of 1.5 mm. The distance between probes was 2 inches.

Measurement Procedure -- The two cells were positioned next to each other in a vacuum chamber through a modified Dresser coupling, in a manner analogous to the electrotransport cells shown in Figure 8. The cells were separated by a stainless steel rod which held two Pyrex crucibles containing the alloy under study. The rod could be rotated so that one crucible would be positioned under each cell. The cells could be quickly filled and emptied by raising and lowering the stainless rod. A separate 28 ga. Chromel-Alumel thermocouple was used to measure the temperature of each cell. The thermocouples were shielded

in AISI No. 430 ferritic stainless tubing having an O.D. of 3/32". Since tin dissolves iron, the stainless was shielded with a thin-walled Pyrex tubing (wall thickness--approximately 0.1 mm) in all of the runs except pure bismuth. The stainless fit snugly into the Pyrex shielding which was held tightly against the outside wall of the resistivity cell. The Pyrex crucibles had an I.D. of 17 mm and were filled with a 3 inch height of alloy. With this arrangement it was possible to measure the resistivity of two alloys during the same run.

The furnace, temperature controlling equipment, power supply, and potentiometer used in this work have been described in Chapter V and Appendix J. The vacuum equipment is shown in Figure 10.

The pure Bi and Sn metal was first vacuum cast into cylinders having a diameter slightly smaller than the I.D. of the Pyrex crucibles. The cylinders were then cut into sections and the desired alloy ratio was determined by weighing. The bismuth used in this work was 99.998% pure and the tin 99.999%. A detailed analysis of the purity is given in Table XIX. To make a run the alloy was heated slightly above the operating temperature and outgassed under vacuum. It was stirred by raising and lowering a number of times around the cells. The temperature was then lowered to the desired value and the crucibles were raised up around the cells. All of the resistivity runs were made under vacuum. A current of 1/4 ampere was then passed through the electrodes of each cell in a series circuit. The current was determined from the measurement of the voltage drop across a maganin shunt,

which had previously been calibrated against a standard 0.1 Ω Leeds and Northrup shunt (No. 301185). The temperature measurements were made using an ice bath cold junction. To overcome any possible non-linearities in the circuit, each point was the average of two measurements having opposite polarities. The polarity was reversed instantaneously by means of a relay circuit. The sequence of measurements after filling the cells was as follows: Temperature, Shunt, Cell 1, Shunt, Cell 2, Temperature, Reverse the Polarity, repeat the sequence. The temperature was taken as the average and the current was determined from the shunt reading preceding the respective cell reading. To reduce errors due to improper filling of the capillaries a number of measurements were taken at each temperature, after emptying and filling again.

Processing Data -- The raw data was processed directly in a digital computer. The program computed the resistivity from the average of the values of opposite polarity. The value of L/A_m was corrected for cell expansion from data on the thermal expansion of No. 7740 Pyrex glass, supplied by Corning Glass Works. The thermocouple readings were converted to the corresponding temperature value by the program. The EMF-Temperature characteristic of the Chromel-Alumel couples had been fitted to two straight lines. The program typed out the raw input data and the calculated resistivities along with the standard deviation of the average resistivity at each temperature. The tabulated results are shown in Table H-1 .

TABLE H-1

SUMMARY OF DATA FROM RESISTIVITY MEASUREMENTS

Run No.	Cell	Composition At. % Bi	Temperature, °C	Resistivity, μohm-cm	Standard Deviation, σ	Std. Dev. Avg. Res.*	No. of Measurements**
R-2	1	100	499.6	139.237	.219	.230	6
R-2	2	100	504.3	139.796	.109	.114	6
R-3	1	100	496.3	139.261	.058	.054	7
R-3	2	100	500.6	139.751	.101	.094	7
R-3	1	100	449.7	136.720	.074	.118	4
R-3	2	100	453.2	137.127	.116	.185	4
R-3	1	100	398.4	134.003	.071	.113	4
R-3	2	100	402.8	134.162	.029	.046	4
R-3	1	100	347.7	131.218	.103	.164	4
R-3	2	100	353.1	131.556	.091	.145	4
R-3	1	100	295.7	128.444	.056	.089	4
R-3	2	100	300.9	128.710	.149	.237	4
R-4	2	78.80	446.9	120.330	.036	.057	4
R-4	2	78.80	402.7	118.281	.019	.030	4
R-4	2	78.80	354.6	116.087	.015	.024	4
R-4	2	78.80	299.7	113.578	.024	.038	4
R-4	2	78.80	251.9	111.318	.037	.059	4
R-4	1	57.59	444.2	102.664	.248	.395	4
R-4	1	57.59	400.4	100.443	.034	.054	4
R-4	1	57.59	352.9	98.564	.044	.070	4
R-4	1	57.59	297.8	96.430	.051	.081	4
R-4	1	57.59	250.5	94.557	.085	.136	4
R-6	1	38.57	491.2	87.338	.021	.032	4
R-6	1	38.57	444.3	85.762	.011	.018	4
R-6	1	38.57	396.0	84.126	.044	.070	4
R-6	1	38.57	347.3	82.409	.041	.065	4
R-6	1	38.57	294.6	80.624	.024	.038	4
R-6	1	38.57	250.5	79.080	.007	.011	4
R-6	2	18.84	492.9	69.926	.015	.024	4
R-6	2	18.84	447.2	68.599	.033	.053	4
R-6	2	18.84	398.6	67.146	.047	.075	4
R-6	2	18.84	349.8	65.659	.039	.062	4
R-6	2	18.84	296.9	64.070	.021	.033	4
R-6	2	18.84	252.8	62.712	.005	.008	4
R-5	1	0.0	499.3	54.801	.024	.038	4
R-5	2	0.0	498.9	54.674	.029	.046	4
R-5	1	0.0	448.6	53.441	.033	.053	4
R-5	2	0.0	448.4	53.371	.012	.019	4
R-5	1	0.0	398.5	52.065	.016	.025	4
R-5	2	0.0	398.4	52.056	.014	.022	4
R-5	1	0.0	351.6	50.836	.004	.006	4
R-5	2	0.0	351.7	50.796	.020	.032	4
R-5	1	0.0	298.8	49.438	.010	.016	4
R-5	2	0.0	298.9	49.399	.013	.021	4
R-5	1	0.0	243.7	47.907	.006	.010	4
R-5	2	0.0	243.7	47.877	.004	.006	4

*Deviation at 95% Conf. level, Student t Dist.

**Each measurement is the average of two values of opposite polarity.

Possible Errors -- Since the capillary channels were 2 inches long between probes, it was necessary to minimize the temperature gradient within the cells so that the temperature could be accurately known. This was done by adjustment of the three independently controlled zones of the furnace. It was not possible to hold the temperature gradient to zero over the two inch length; a 1 to 2°C gradient was found to be stable. Consequently the temperature profile was first determined for each run by moving the thermocouple vertically. The thermocouple was then placed at the position corresponding to the mean value of the temperature over the distance between the probes.

The current of 1/4 amp corresponded to a density of 1.41 A/cm^2 in the 1.5 mm I.D. cell and 0.80 A/cm^2 in the 2 mm cell. It was felt that the I^2R heat produced at these densities was negligible. No temperature rise was detected. In addition, the results on the resistivity of the pure metals measured with both cells agreed quite well (see Table H-1).

The weighed-in composition was used in presenting the data. There is the possibility that these values might differ from the true values due to preferential vaporization or some other cause. This possibility was checked experimentally and the results are discussed in Chapter V. The alloys containing 38.57, 57.59, and 79.80 atom percent Bi were used in both the resistivity determinations and the electrotransport runs.

The Chromel-Alumel thermocouples used in this work were calibrated against the melting point of pure bismuth. The results are presented in Table H-2 .

TABLE H-2

CALIBRATION OF THERMOCOUPLES

Melting Point Pure Bismuth	Value Measured by t.c. No. 1	Value Measured by t.c. No. 2
271.3°C(1)	271.5°C	271.5°C

(1) International Temperature Scale 1948.

Because of the excellent agreement the temperature values were used directly, without correction.

The cells were calibrated at room temperature using the mercury listed in Appendix J. The calibration was made in the same manner in which the resistivity was determined. A recheck of the calibration revealed a slight variation. For the remaining runs then, the cells were calibrated after every run. The results are shown in Table H-3 .

TABLE H-3

CALIBRATION OF RESISTIVITY CELLS

Calibration	Cell	L/A cm^{-1}	Per Cent Standard Deviation	No. of Points(1)
1	1	199.18	0.30	8
2	1	199.10	0.21	12
3	1	198.76	0.45	12
4	1	198.03	0.10	8
1	2	296.71	0.47	8
2	2	296.46	0.14	12
3	2	296.32	0.17	12
4	2	296.48	0.07	8

(1) Each point is the average of two measurements of opposite polarity.

It is interesting to compare these results to the calibrations of the Type 2 electrotransport cells shown in Table M-2 . The electrotransport calibrations are considerably more precise. The source of the relative lack of precision of the above calibration is probably a result of the current passing through the portion of the probe which protrudes into the capillary.

III. DISCUSSION OF RESULTS

As a check on the experimental technique, the resistivity-temperature relation for the pure metals was compared to data that could be found in the literature. The results are presented graphically in Figure H-2 for Sn and Figure H-3 for Bi. The agreement appears to be quite satisfactory. A few points seem worth noting here. Roll's[H-4] electrodeless method appears to give results slightly higher than the average literature data. There appears to be an error somewhere in the liquid metal wire technique used by Pietenpol.[H-9] Scala[H-7] has interpreted his results on pure tin to indicate that all of the old data were slightly high due to trace impurities. In view of the high purity of the tin used in this work it would appear that Scala's conclusion may be erroneous. Either Scala's high purity results are wrong, or the purity quoted by the City Chemical Company, on their pure tin in Table XIX, is wrong. An independent check of the tin purity was not made.

The temperature variation of the Bi-Sn alloys is shown in Figure H-4 . The linearity of the data with temperature appears to be quite good. The circled data on this plot are from the electrotransport runs and are discussed in Chapter V. The data was fitted to a straight line by the

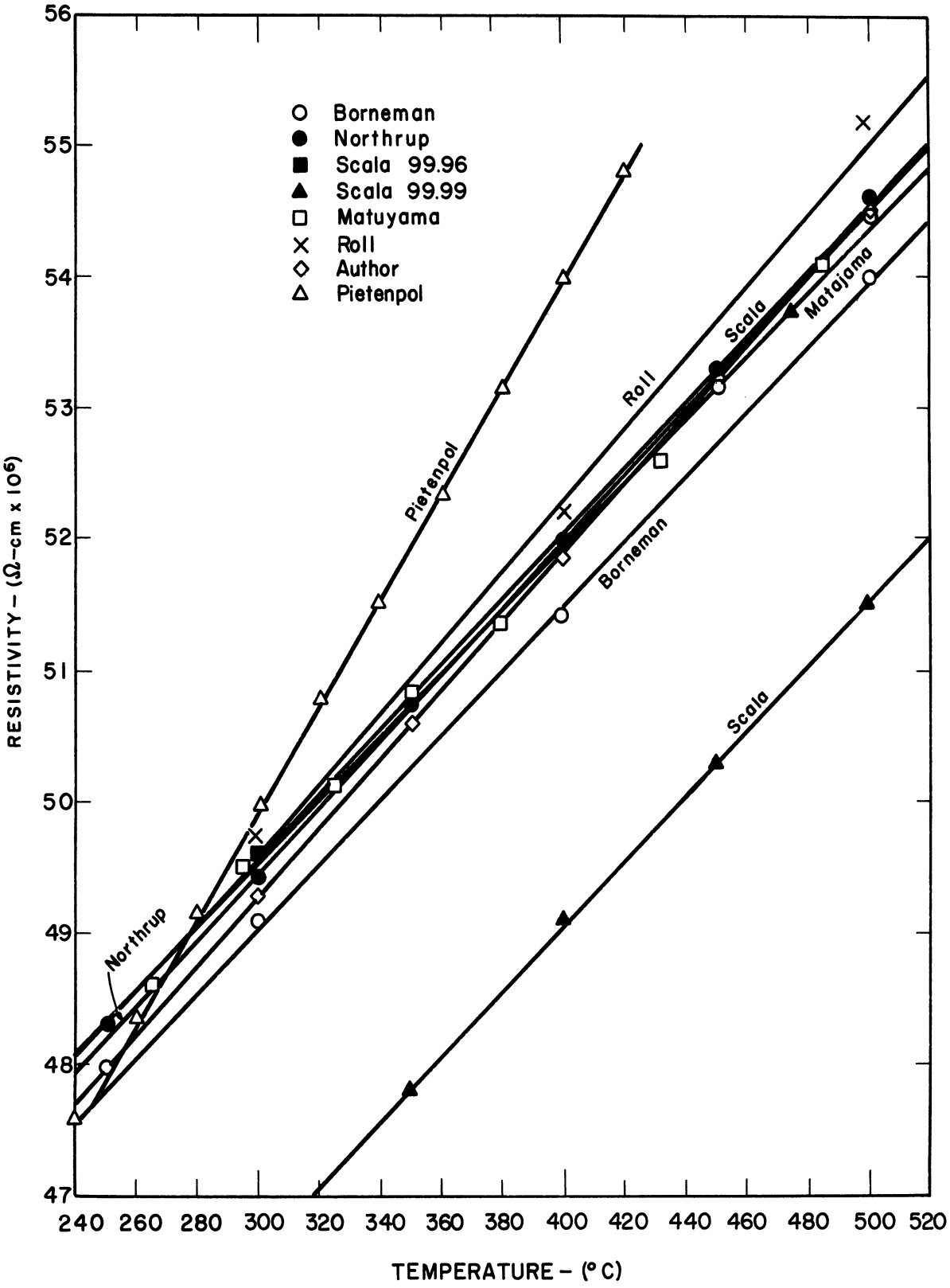

Figure H-2 Resistivity vs. Temperature for Pure Tin (99.999%).

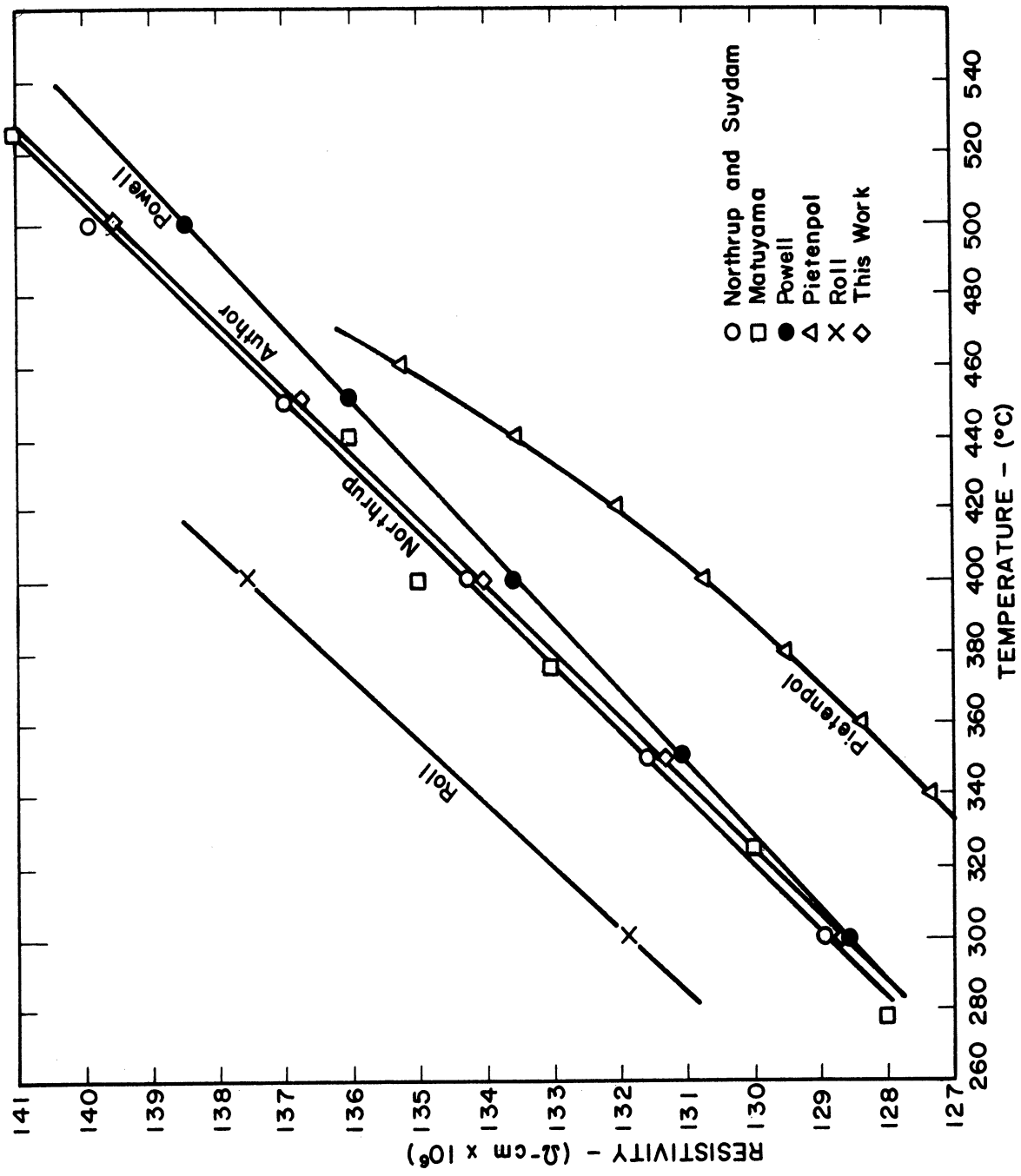

Figure H-3 Resistivity vs. Temperature for Pure Bismuth (99.998%).

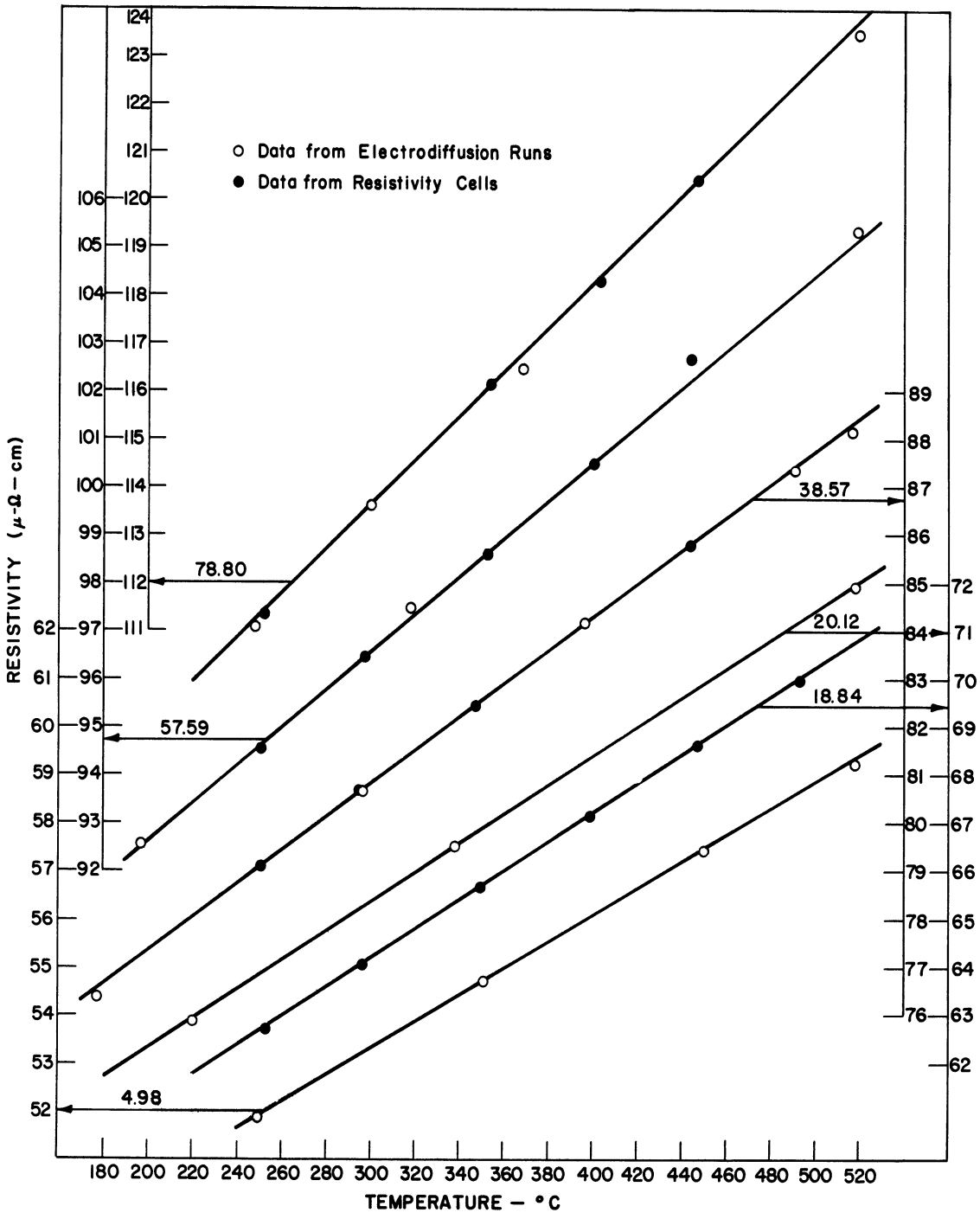

Figure H-4. Resistivity vs. Temperature -- Bismuth Tin Alloys, Parameters of At.% Bismuth.

method of least squares on a digital computer. The equation may be written as:

$$\rho = mT + b. \qquad \text{(H-1)}$$

The results are summarized in Table H-4 .

TABLE H-4

RESISTIVITY VS. TEMPERATURE

Composition At % Bi	Slope - m $\mu\Omega$ - cm/^{o}C	Intercept - b $\mu\Omega$ - cm
100.00	.054253	112.382
78.80	.046109	99.727
57.59	.039196	84.744
38.57	.034335	70.496
18.84	.030080	55.131
0.00	.026761	41.397

A plot of the resistivity at a constant temperature as a function of composition was determined for various temperatures from the above equations. The data from 0 to 78.80 At % Bi appeared to be very close to linear at the temperatures examined (250^{o}C to 601^{o}C), and the data over the entire composition range was not far from linear. The resistivity, as calculated from the above equations, was then fitted to the following straight line function of mole fraction, at all of the temperatures at which electrotransport experiments were made,

$$\rho = \frac{1}{f} X_{Bi} + b'. \qquad \text{(H-2)}$$

Only the data from 0 to 78.8 At % Bi were used. The results are presented in Table H-5 . Five points were used in these calculations. The maximum deviation of a point and the standard deviation of the slope are also presented. It can be seen that the data appears to approximate a straight

line quite well. The maximum deviation appears to be less than 1% in the worst case.

TABLE H-5

RESISTIVITY VS. COMPOSITION

Temperature °C	Slope $(\frac{1}{r})$ μΩ-cm x 10^{-2}	Intercept b' μΩ - cm	Maximum Dev. μΩ-cm	Percent Std. Dev. of Slope
181	.7887	46.126	-.36	.64
199	.7934	46.572	-.40	.67
223	.7992	47.192	-.41	.65
252	.8063	47.941	-.42	.64
260	.8082	49.148	-.42	.64
300	.8180	49.181	-.44	.63
320	.8229	49.698	-.44	.63
340	.8278	50.215	-.45	.63
353	.8309	50.552	-.46	.64
371	.8353	51.016	-.46	.65
380	.8375	51.248	-.47	.65
452	.8551	53.109	-.49	.70
520	.8717	54.867	-.52	.76
601	.8915	56.958	-.55	.85

The slope of Equation (H-1) appears to vary quite smoothly with composition as shown in Figure H-5. The slope of Equation (H-2) is an extremely linear function of temperature as shown in Figure H-6.

IV. CONCLUSIONS

The resistivity of the Bi-Sn system has been determined as a function of composition and temperature by a conventional technique. The variation of resistivity with temperature was found to be linear as in similar liquid metal systems. The variation of resistivity with mole fraction was found to be nearly linear over the whole system, and linear to within a 1% maximum deviation from 0 to 78.80 At% Bi. This supports the results published by Northrup.(H-1)

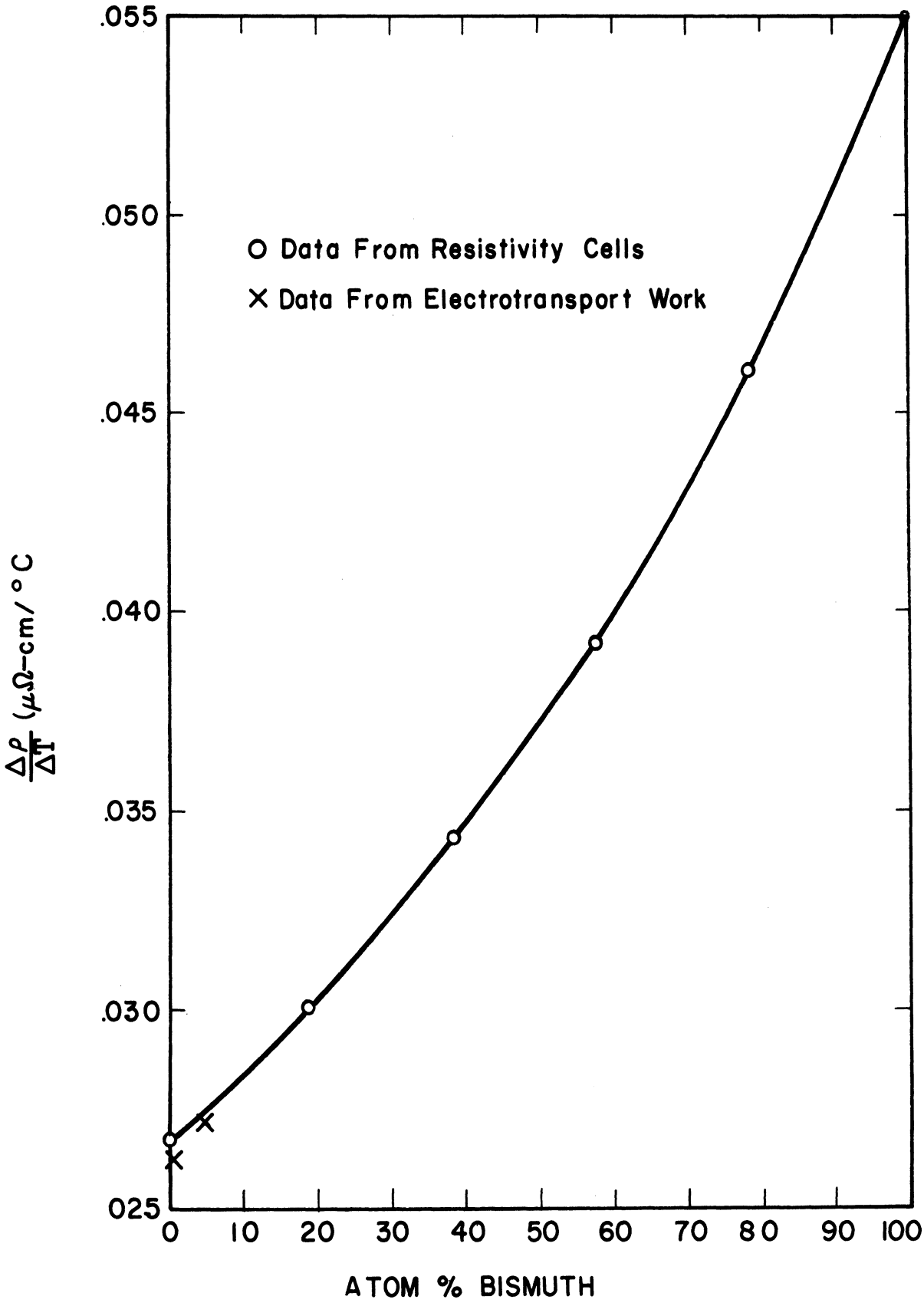

Figure H-5 Slope of Resistivity vs. Temperature as a Function of Mole Fraction.

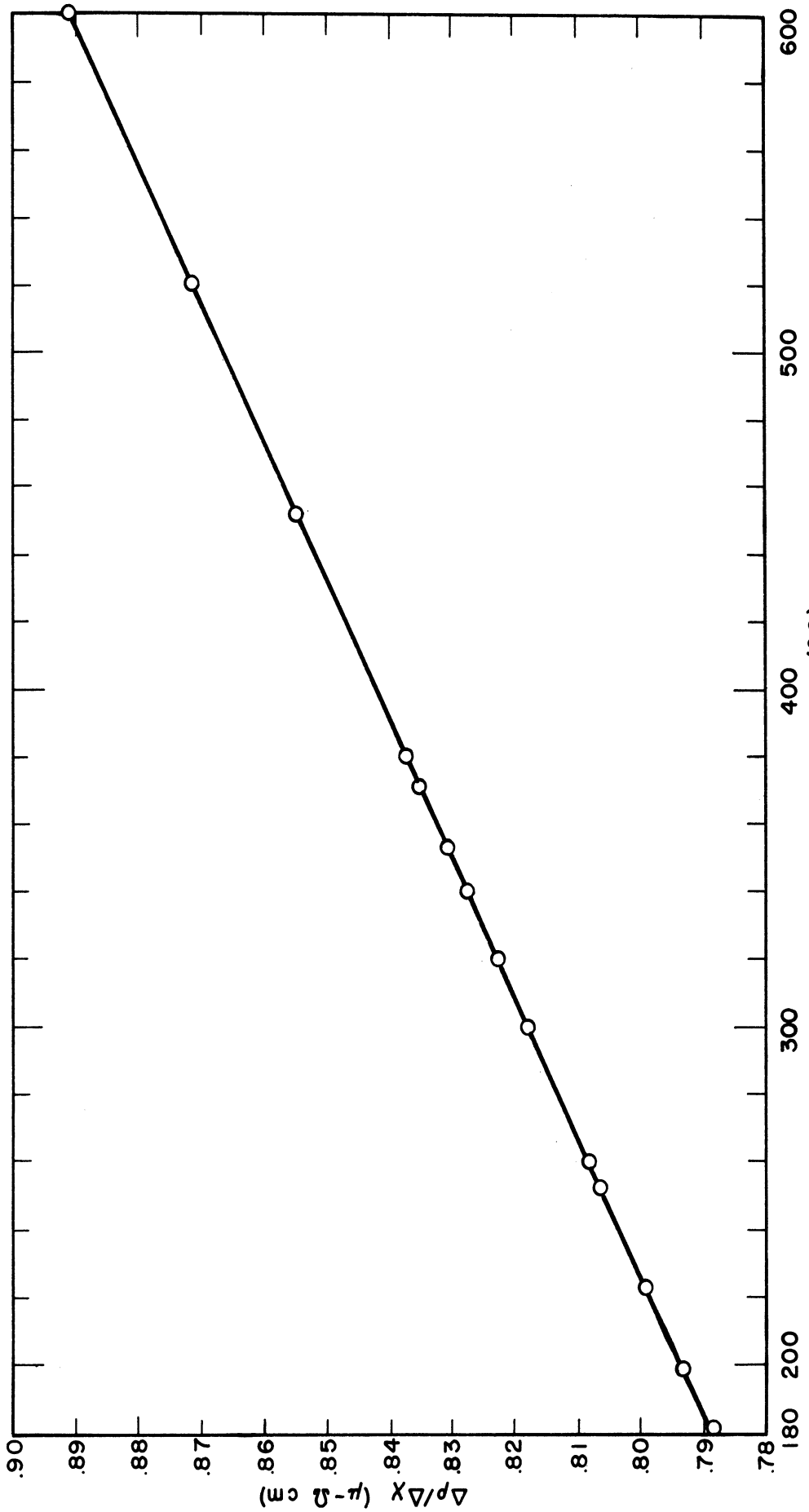

Figure H-6 Slope of Resistivity vs. Mole Fraction as a Function of Temperature.

The conclusion of Scala,[H-7] that the old data on the resistivity of pure tin was high due to trace impurities, appears erroneous.

More precise resistivity data could probably have been measured using the Type 2 electrotransport cells shown in Figure G-1.

V. REFERENCES

(H-1) E. F. Northrup and R. G. Sherwood, J. Frank. Inst. 182, 477-509 (1916).

(H-2) A. Z. Golik, N. A. Ryndich and S. A. Babenko, Ukr. Fiz. Zhur. 3, No. 3, 365-9 (1958).

(H-3) F. Gailbullaev and A. R. Regel, Doklady na Soveshchanii po Zhidkomu Sostoianiiu, K. G. U., (1957).

(H-4) A. Roll and H. Motz, A. Metallk. 48, 272-80 (1957).

(H-5) K. Bornemann and P. Muller, Metallurgie, 7, 396-402 (1910).

(H-6) E. F. Northrup and V. A. Suydam, J. Frank. Inst. 175, 153-61 (1913).

(H-7) E. Scala and W. D. Robertson, Trans. AIME, 197, 1141-44 (1953).

(H-8) Y. Matuyama, Sci. Reports Tohoko Imp. Univ. 16, 447-74 (1927).

(H-9) W. B. Pietenpol and H. A. Miley, Phys. Rev. 34, 1588-1600 (1927).

(H-10) R. W. Powell and R. P. Tye, Proc. Conf. Thermo. and Transport Properties Fluids, 182-7 (London, 1957).

APPENDIX I

DATA ON THE SPECIFIC VOLUME OF THE Bi-Sn SYSTEM

A literature survey was undertaken to obtain all available data on the specific volume of the molten Bi-Sn system. Chemical Abstracts was used as the main reference; it was searched from the present back to 1910. This system has been studied by the first three investigators listed below. Of these studies, the work by Matuyama[I-2] is the most precise and appears to be the most accurate.

The data of the three investigators is shown graphically in Figure I-1 after conversion to molar specific volume. With the best fit of this data it appears that the molar specific volume is linear with mole fraction. It might be noted here that Kirshenbaum[I-4] has recently published some new data and a thorough literature survey on the specific volume of liquid tin.

REFERENCES

(I-1) K. Bornemann and P. Siebe, Z. Metallk., 14, 329-34 (1922).

(I-2) Y. Matuyama, Tohoku, Imp. Univ. Sci. Repts., 18, 19-41 (1929).

(I-3) M. Plusse, Z. Anorg. Chemie, 93, 1-45 (1915).

(I-4) A. Kirshenbaum and J. Cahill, Trans. ASM, 55, 844-48 (1962).

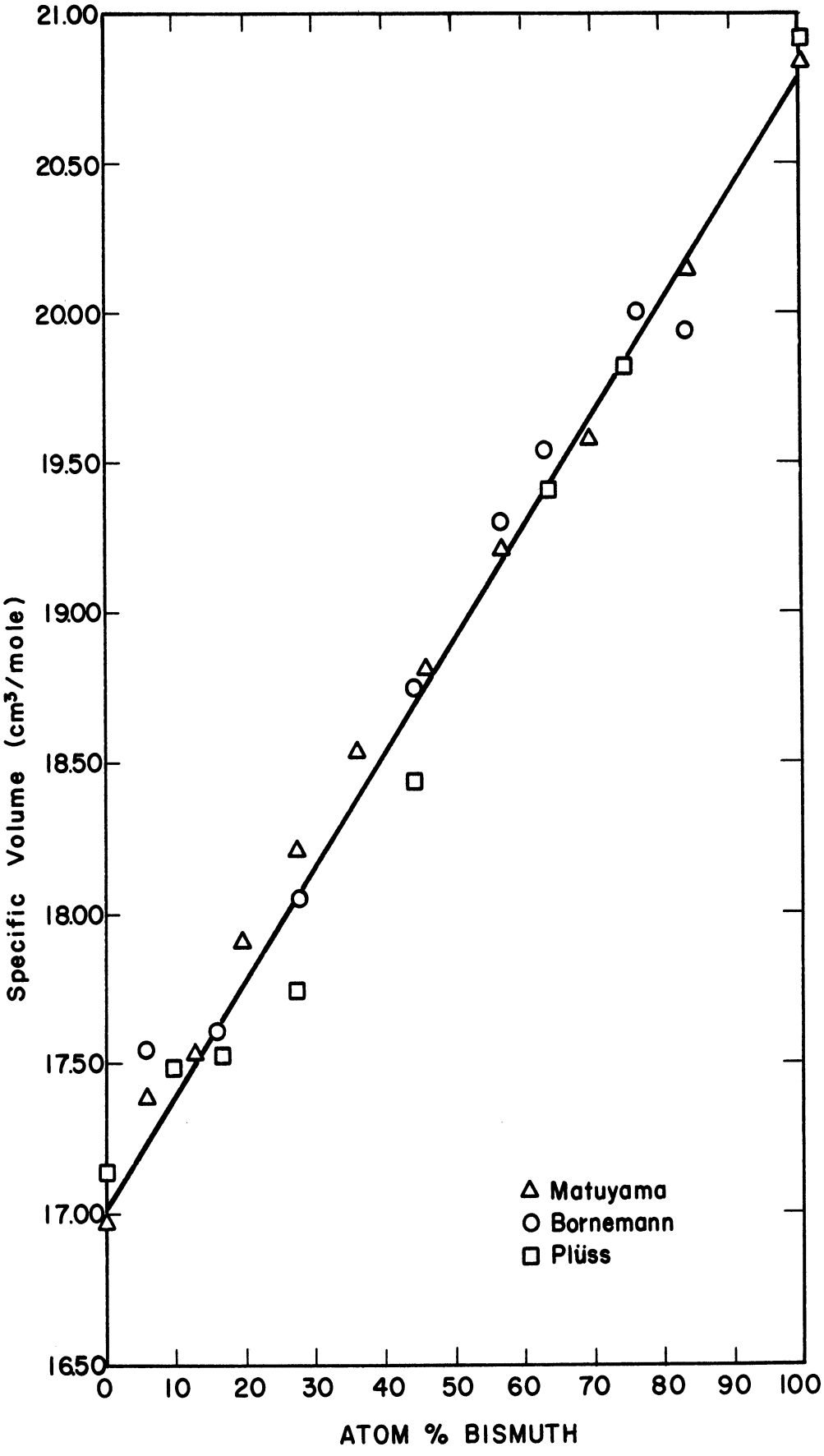

Figure I-1 Literature Data on Molar Specific Volume vs. Mole Fraction for the Bi-Sn System.

APPENDIX J

DATA ON EXPERIMENTAL EQUIPMENT

1. D. C. Power Supply

   Kepco Instruments
   Flushing New York
   Model SC-32-5

2. Temperature Controlling Equipment

   Wheelco Instrument Division
   Barber-Coleman Company, Rockford, Illinois
   Model 407 Capacitrol
   Model 350 Reference Voltage Source
   Lindburg Engineering Company
   Chicago, Illinois
   5KVA Tapped Reactrol Transformer

3. Voltage Measuring Equipment

   Leeds and Northrup
   Philadelphia, Pennsylvania
   K-3 Potentiometer
   Model 9834 Null Detector
   Standard Cell No. 708730
   Eppley Laboratory, Inc.
   Newport, Rhode Island

4. Resistance Wound Furnace

   Hevi Duty Electric Company
   Milwaukee, Wisconsin
   Type M-3018-S

5. Mercury Used in Calibrations

   Mallinkrodt AR
   Base Metal 1 ppm
   Foreign Metals 5 ppm

6. Vacuum Equipment

   Consolidated Vacuum Corporation
   Rochester, New York
   Model 1400B Duo Seal Vacuum Pump
   Model VMF 20 Air Cooled Oil Diffusion Pump

APPENDIX K

TEMPERATURE RISE WITHIN THE CAPILLARIES

I. APPROXIMATE CALCULATION

An estimate of the temperature rise was made in the following manner. All of the I^2R heat generated per unit length was assumed to pass through a unit length of the tube wall. The heat balance is,

$$0.239 \frac{I^2R}{\ell} = \frac{q}{\ell} , \qquad \text{(K-1)}$$

where q is the heat transfer rate in cal/sec and the conversion factor 0.239 is the number of cal/joule. Substituting for q and the resistance, R, one obtains,

$$0.239 \frac{I^2\rho}{A} = \frac{2\pi k \Delta T}{\ell n(r_o/r_i)} , \qquad \text{(K-2)}$$

where k is the thermal conductivity of the Pyrex cells, r_o is the outside capillary radius and r_i the inside radius. The thermal conductivity of bismuth is about a factor of 10 higher than that of Pyrex so that the temperature variation inside the capillary is neglected. Also, the temperature measured by the thermocouple in the molten alloy reservoir next to the tube wall is assumed to be approximately the same as the temperature of the wall. In the Bi-Sn experiments the average capillary dimensions were as follows: O.D. = 37 mils, ID = 24 mils. Data was supplied by the Corning Glass Works on the thermal conductivity of No. 7740 Pyrex glass from -95°C to 200°C. Extrapolation of this data to 500°C gives a value of .004 cal/cm-sec-°C. The expression for the temperature rise can be written as

$$\Delta T = \frac{(0.239) \cdot \rho \cdot r_i^2 \cdot \ell n(\frac{r_o}{r_i})}{2k} \left(\frac{I}{A}\right)^2 , \qquad (K\text{-}3)$$

and substitution of the above values gives,

$$\Delta T = .01127\ \rho\left(\frac{I}{A}\right)^2 . \qquad (K\text{-}4)$$

This is the expression used to derive the curve in Figure 11.

II. EXPERIMENTAL DETERMINATION

With the cell shown in Figure F-1 it was possible to check the accuracy of Equation (K-3). The cell was filled with liquid mercury and heat was supplied from an external furnace. The temperature was measured at the outside wall of the capillary channel after immersion in a bath of liquid mercury. The temperature was measured with the Ta-W couple inside the cell and a Chromel-Alumel couple in the mercury bath. The Ta-W couple was thereby calibrated against the Chromel-Alumel couple. Alternating current was then passed through the cell electrodes at room temperature and the apparatus was allowed to come to thermal equilibrium. The temperature inside the cell was recorded with the Ta-W couple and the outside wall temperature was measured by the Chromel-Alumel couple, thereby giving a direct measure of the temperature rise inside the cell due to I^2R heating. Alternating current was used to eliminate any electrode effects on the Ta or W probes. The results for the upper and the middle Ta-W couple are shown in Figure K-1; the lower couple did not make contact. The theoretical curve was calculated from Equation (K-3). It appears that the equation does represent an upper limit for the expected temperature rise.

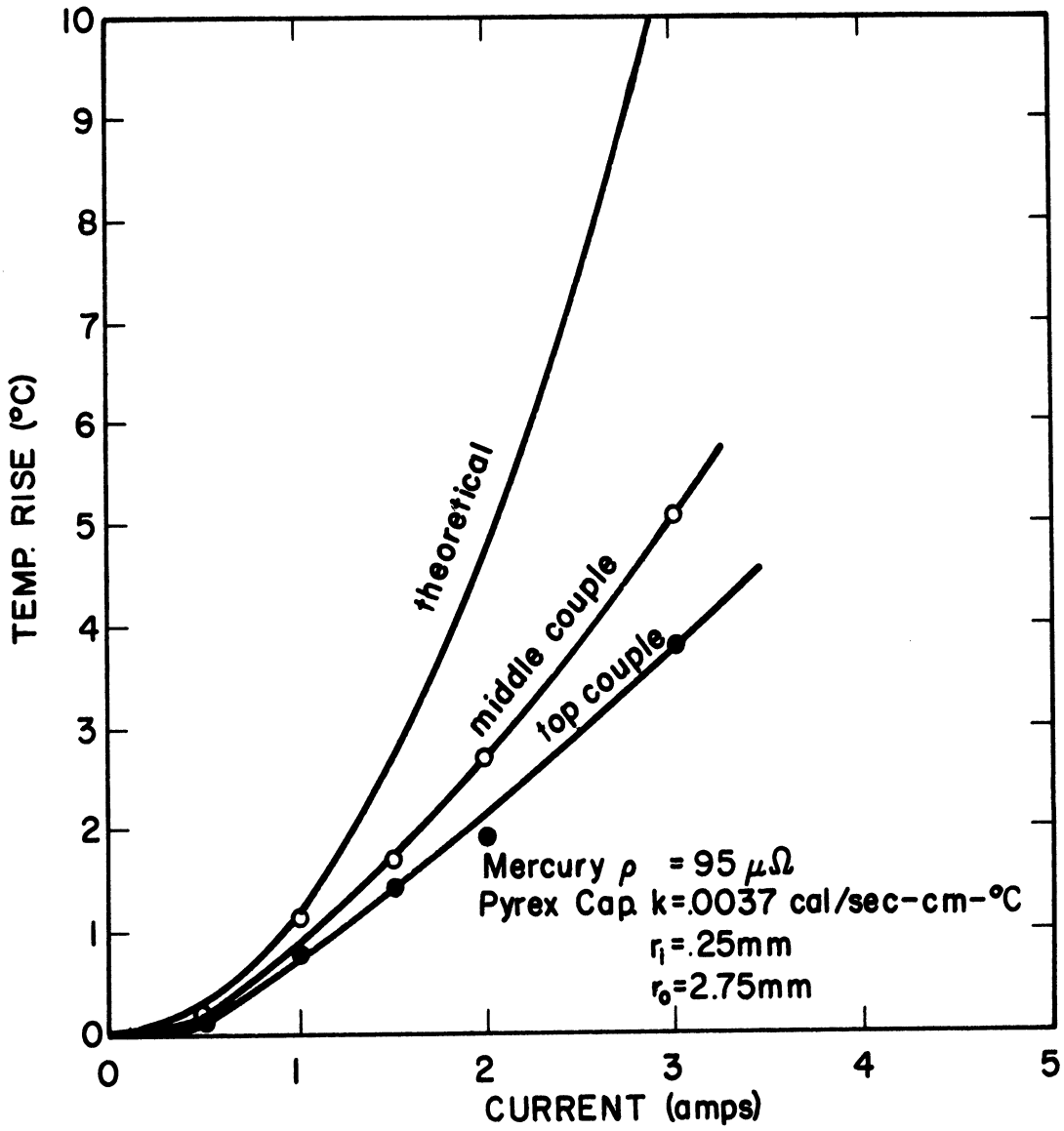

Figure K-1 Experimental Determination of Temperature Rise Inside of Capillary Due to I^2R Heating.

APPENDIX L

ELECTROLYTIC DETERMINATION OF BISMUTH IN BISMUTH-TIN ALLOYS

I. INTRODUCTION

Bismuth is determined electrolytically by weighing the amount of bismuth metal deposited on a copper gauze electrode. This method is most accurate for amounts of bismuth in the range 100 to 200 mg in concentration of approximately 1 mg bismuth per ml solution. This procedure is used for samples containing 1 to 100% bismuth in tin.

The bismuth is dissolved in hot nitric acid while the tin is complexed with hydrofluoric acid. Bismuth is plated quantitatively on copper gauze from this solution, washed with water and alcohol, and dried at 110°C.

II. APPARATUS

The basic apparatus is a DC power supply with a rheostat used to vary current. The electrodes are a platinum anode and a copper gauze (100 mesh) cathode. A source of heat for constant temperature electroplating and a mechanical stirrer are also necessary.

III. REAGENTS

Hydrofluoric acid, 50%, reagent grade

Nitric acid, 1:1 concentrated nitric acid

Tartaric acid, 50%

Absolute ethanol

IV. PREPARATION OF SAMPLES

1. Weigh the bismuth sample and dissolve in 1:1 nitric acid plus 50% hydrofluoric acid. Use no more than 5 ml of the 50% hydrofluoric acid per liter of solution to avoid serious etching.

2. Cool and then transfer bismuth solution to a 500 ml volumetric flask partially filled with water and dilute to mark. The solution is transferred to a tincture bottle and the volumetric glassware is rinsed out.

V. PROCEDURE

1. Place an aliquot containing approximately 100 to 200 mg bismuth in a 250 ml beaker.

2. Add 5 ml of 50% hydrofluoric acid and enough 1:1 nitric acid to make 150 ml of solution 0.5 N in nitric acid. (8 ml 1:1 nitric acid per 150 ml of solution.)

3. Add 25 ml 50% tartaric acid and dilute to 150 ml with hot distilled water. Final desired temperature is 90°C.

4. Adjust the rheostat on the DC power supply so that the current is 3.0 amps when the cathode and anode are shorted. (See Note 1)

5. Insert electrodes into the hot bismuth solution and begin stirring. (See Note 2)

6. Adjust the current in the solution to 3.0 amps, and the temperature should be 90-93°C. The stirring is continued with constant current and temperature for 20 minutes.

7. After 20 minutes of plating, leave the current on and rinse the copper gauze electrode according to the following procedure: All rinse solutions must be in the temperature range of 3° to 10°C.

   A. Dip gauze once in 600 ml beaker of distilled water.
   B. Dip gauze once in second 600 ml of distilled water.
   C. Dip gauze once in 1000 ml beaker of distilled water.
   D. Dip gauze once in 250 ml beaker of absolute alcohol. (See Note 3)

8. Carefully disconnect gauze from cathode and dry in oven at 100°C.

9. Cool, weigh, and clean gauze.

IV. NOTES AND PRECAUTIONS

1. Cathode should be previously weighed. Cleaning procedure: Dissolve bismuth off copper gauze with 1:1 nitric acid, then wash gauze well with 3 N hydrochloric acid. Rinse with distilled water and dry in oven at less than 150°C.

2. The stirring is especially important in the first ten minutes because this gives an even, cohesive plating of bismuth. Arsenic, Antimony, and Copper were found to interfere by plating out with the bismuth.

3. Extreme caution must be employed in these rinses to avoid losing the bismuth plating of the gauze. The rinses also must have a pH of 7.

VII. CALCULATIONS

Per cent Bismuth = (weight of cathode + bismuth) - (weight of cathode)/weight of sample.

VIII. REFERENCES

Goldberg, C, Metallurgia, 42, 108 (1950), "Rapid Determination of Bismuth in Bismuth-Tin and Bismuth-Tin Cadmium Alloys."

APPENDIX M

SUMMARY OF DATA FROM RUNS USING RESISTIVITY ANALYSES

TABLE M-1

PROCESSED DATA FROM COMPUTER

Cell	Fill	Initial Resistivity, μohm-cm	Std. Temp., mv	Avg. Temp., °C	Current Density, amps/cm^2	% Std. Dev. of $\Delta V/\Delta\theta$	Std. Dev. of $\Delta V/\Delta\theta$	Max. Dev. in $\Delta V/\Delta\theta$	$\frac{\Delta V/\Delta\theta}{(I/A)^2}$ $\frac{V/sec}{(amps/cm^2)^2}$	$U_{Bi-Sn} \times 10^3$ cm^2/V-sec
					Run No. V-7					
1	1	59.226	21.444	519.6	663.8	1.70	.012	.036	.464205	1.90217
2	1	59.278	21.450	519.9	662.3	.36	.003	.012	- .452520	1.85429
2*	1	58.249	21.464	519.2	661.5	.82	.006	.014	.463826	1.90062
					Run No. V-8					
1	1	59.313	21.665	524.2	662.3	1.29	.009	.010	- .453679	1.85351
1*	1	58.341	21.605	522.8	661.4	1.10	.008	.007	.463101	1.89200
2	1	59.310	21.651	524.2	660.9	.65	.005	.010	.459356	1.87670
1	2	59.397	21.683	524.8	663.7	.36	.003	.024	.457081	1.86740
2	2	59.265	21.686	524.7	662.4	1.44	.010	.012	- .452386	1.84822
					Run No. V-9					
1	1	59.209	21.496	520.0	663.9	1.16	.008	.048	.457719	1.87560
2	1	59.176	21.498	520.0	662.6	1.08	.008	.008	- .450407	1.84563
1	2	59.188	21.508	520.4	662.9	.65	.005	.007	- .450740	1.84700
2	2	59.214	21.504	520.4	661.5	1.70	.012	.027	.455648	1.86711
1	3	59.169	21.478	519.7	664.9	1.01	.007	.013	- .451832	1.85147
2	3	59.212	21.482	519.7	663.5	1.33	.010	.018	.453926	1.86005
1	4	59.276	21.543	520.9	821.1	1.05	.012	.025	.452789	1.85539
2	4	59.214	21.549	520.8	819.4	1.09	.010	.016	- .449887	1.84350
1	5	59.252	21.487	519.8	502.2	1.57	.006	.008	.457311	1.87392
2	5	59.174	21.485	519.8	501.1	1.38	.006	.010	- .444885	1.82301

*Unusual initial conditions, see Chapter 5.

TABLE M-1 (Continued)

Cell	Fill	Initial Resistivity, μohm-cm	Std. Temp., mv	Avg. Temp., °C	Current Density, amps/cm^2	% Std. Dev. of $\Delta V/\Delta\theta$	Std. Dev. of $\Delta V/\Delta\theta$	Max. Dev. in $\Delta V/\Delta\theta$	$\frac{\Delta V/\Delta\theta}{(I/A)^2}$ $\frac{V/sec}{(amps/cm^2)^2}$	$U_{Bi-Sn} \times 10^3$ cm^2/V-sec
					Run No. V-10					
1	1	57.342	18.589	452.0	665.4	1.40	.009	.011	.422726	1.82106
2	1	57.366	18.587	452.0	664.1	1.24	.008	.010	- .412272	1.77603
1	2	57.427	18.649	452.9	666.4	1.46	.010	.025	.421386	1.81529
2	2	57.462	18.646	452.8	665.1	.82	.005	.010	- .408175	1.75838
1	3	57.388	18.574	451.5	667.4	.92	.006	.012	- .409880	1.76572
2	3	57.421	18.575	451.5	666.1	1.05	.007	.007	.422544	1.82028
1	4	57.454	18.583	451.6	667.3	1.18	.008	.030	- .417135	1.79698
2	4	57.402	18.585	451.6	665.9	1.95	.013	.024	.409209	1.76283
1	5	54.717	14.406	352.7	667.2	1.40	.008	.003	- .357174	1.66164
2	5	54.743	14.405	352.7	665.8	1.57	.009	.007	.362780	1.68773
1	6	54.689	14.416	353.3	666.5	.61	.003	.005	- .359723	1.67350
2	6	54.721	14.418	353.3	665.1	1.53	.009	.011	.365649	1.70107
1	7	54.754	14.414	353.7	665.3	.82	.005	.005	.361911	1.68368
2	7	54.721	14.416	353.7	663.8	.96	.005	.005	- .356816	1.65998
1	8	54.720	14.371	352.5	665.9	1.81	.010	.010	.363540	1.69126
2	8	54.626	14.374	352.5	664.7	.98	.006	.004	- .353215	1.64323
1	9	51.868	10.192	251.4	666.5	1.73	.008	.011	.297012	1.50134
2	9	51.844	10.199	251.5	664.9	1.41	.007	.006	- .289520	1.46347
1	10	51.908	10.253	252.2	667.6	3.06	.014	.005	.299739	1.51512
2	10	51.881	10.249	252.4	666.2	1.47	.007	.009	- .290406	1.46794
1	11	51.915	10.227	251.3	661.9	1.38	.006	.004	- .293494	1.48355
2	11	51.933	10.229	251.2	660.8	1.17	.005	.005	.297518	1.50389
1	12	51.889	10.210	251.4	664.7	1.55	.007	.004	- .291340	1.47267
2	12	51.903	10.209	251.4	663.3	2.02	.009	.008	.295352	1.49295

TABLE M-1 (Continued)

Cell	Fill	Initial Resistivity, μohm-cm	Std. Temp., mv	Avg. Temp., °C	Current Density, amps/cm^2	%Std. Dev. of $\Delta V/\Delta\theta$	Std. Dev. of $\Delta V/\Delta\theta$	Max. Dev. in $\Delta V/\Delta\theta$	$\frac{\Delta V/\Delta\theta}{(I/A)^2}$ $\frac{V/sec}{(amps/cm^2)^2}$	$U_{Bi-Sn} \times 10^3$ cm^2/V-sec
					Run No. V-10 (Concluded)					
1	13	61.480	24.988	602.3	661.2	.98	.008	.015	- .489188	1.89096
2	13	61.459	24.987	602.2	659.9	1.05	.009	.029	.518428	2.00398
1	14	61.328	24.935	601.2	662.7	1.29	.009	.031	- .444960	1.71999
2	14	61.317	24.932	601.2	661.3	1.03	.009	.046	.537411	2.07736
1	15	61.460	24.937	601.0	663.3	2.32	.018	.010	.497013	1.92120
2	15	61.327	24.941	601.0	661.9	2.58	.019	.025	- .476283	1.84107
1	16	61.406	24.950	601.0	663.2	1.90	.016	.050	.529894	2.04831
2	16	60.194	24.948	601.0	663.2	.82	.006	.016	- .483135	1.86756
1	17	61.444	24.900	600.4	662.1	1.76	.014	.007	.499556	1.93103
2	17	60.172	24.897	600.3	662.1	1.35	.011	.013	- .498073	1.92530
					Run No. V-12					
3	1	63.339	21.523	520.8	647.4	1.36	.018	.009	.912992	1.84890
4	1	63.355	21.524	520.8	646.1	.67	.009	.012	- .868433	1.75866
3	2	63.277	21.441	519.0	490.3	1.15	.009	.005	.910125	1.84309
4	2	63.292	21.441	518.7	489.6	.58	.004	.005	- .871674	1.76523
3	3	63.226	21.395	517.5	491.1	.68	.005	.010	- .878062	1.77816
4	3	63.236	21.394	517.6	490.4	.83	.006	.008	.893915	1.81027
3	4	63.199	21.345	516.5	491.2	.72	.006	.011	- .882220	1.78658
4	4	63.201	21.345	516.7	491.1	1.12	.009	.008	.896312	1.81512

TABLE M-1 (Continued)

Cell	Fill	Initial Resistivity, μohm-cm	Std. Temp., mv	Avg. Temp., °C	Current Density, amps/cm^2	% Std. Dev. of $\Delta V/\Delta\theta$	Std. Dev. of $\Delta V/\Delta\theta$	Max. Dev. in $\Delta V/\Delta\theta$	$\frac{\Delta V/\Delta\theta}{(I/A)^2}$ V/sec / (amps/cm^2)^2	$U_{Bi-Sn} \times 10^3$ cm^2/V-sec
					Run No. V-13					
3	1	72.000	21.570	521.9	492.5	.47	.007	.011	- 1.67830	1.66650
4	1	72.012	21.568	521.9	491.6	1.03	.015	.023	1.71575	1.70365
3	2	71.888	21.399	517.9	329.0	.28	.002	.005	- 1.68213	1.67027
4	2	71.860	21.399	518.0	328.9	.94	.006	.012	1.71150	1.69943
3	3	71.956	21.547	520.8	328.7	1.06	.007	.009	1.75486	1.74249
4	3	71.973	21.545	520.9	328.1	.78	.005	.009	- 1.65662	1.64494
3	4	71.899	21.464	519.5	328.3	1.24	.008	.008	1.73745	1.72520
4	4	71.913	21.473	519.4	327.8	.65	.004	.005	- 1.65668	1.64500
					Run No. V-14					
3	1	88.125	21.440	518.8	296.0	1.28	.011	.006	2.71230	1.49141
4	1	88.131	21.437	518.8	295.5	.68	.006	.015	- 2.57192	1.41422
3	2	88.120	21.425	518.6	280.4	1.34	.010	.005	2.71056	1.49046
4	2	88.116	21.428	518.5	279.9	.80	.006	.004	- 2.57127	1.41386
3	3	88.110	21.416	518.3	274.3	.70	.005	.004	- 2.61429	1.43752
4	3	88.109	21.425	518.2	273.9	.99	.007	.006	2.69711	1.48306
3	4	88.131	21.446	519.0	278.5	.58	.004	.006	- 2.61773	1.43941
4	4	88.173	21.448	519.0	278.1	1.07	.008	.012	2.70463*	1.48719

TABLE M-1 (Continued)

Cell	Fill	Initial Resistivity, μohm-cm	Std. Temp., mv	Avg. Temp., °C	Current Density, amps/cm^2	% Std. Dev. of $\Delta V/\Delta\theta$	Std. Dev. of $\Delta V/\Delta\theta$	Max. Dev. in $\Delta V/\Delta\theta$	$\frac{\Delta V/\Delta\theta}{(I/A)^2}$ $\frac{V/sec}{(amps/cm^2)^2}$	$U_{Bi-Sn} \times 10^3$ cm^2/V-sec
					Run No. V-15					
3	1	123.520	21.630	523.3	330.0	-1.26	.008	.007	-1.70063	.945839
4	1	123.604	21.635	523.3	329.5	1.32	.009	.014	1.69000	.939927
3	2	123.461	21.579	522.0	330.3	-1.37	.009	-.016	-1.68899	.939366
4	2	123.463	21.582	522.1	329.7	1.34	.009	.008	1.71324	.952853
3	3	123.456	21.578	522.1	330.8	1.54	.011	-.007	1.72696	.960485
4	3	123.449	21.579	522.1	330.2	-1.21	.008	-.009	-1.66823	.927819
3	4	123.402	21.539	520.8	332.3	.96	.007	.008	1.72124	.957302
4	4	123.375	21.534	520.8	331.8	-1.18	.008	.008	-1.65259	.919121
					Run No. V-16					
3	1	105.642	21.812	527.2	324.5	1.16	.012	.006	2.78725	1.24258
4	1	105.649	21.814	527.7	323.9	- .58	.006	-.018	-2.62894	1.17201
3	2	105.353	21.550	521.7	264.5	1.06	.007	.011	2.72721	1.21582
4	1	105.355	21.551	521.6	264.1	- .74	.005	-.005	-2.63092	1.17289
3	3	105.323	21.510	519.6	265.6	- .76	.005	.009	-2.68825	1.19845
4	3	105.331	21.511	519.3	265.2	1.27	.009	.007	2.69348	1.20078
3	4	105.281	21.495	520.6	264.8	- .78	.005	.027	-2.63438	1.17443
4	4	105.246	21.470	521.8	264.4	1.37	.009	-.024	2.8195	1.25696

TABLE M-1 (Continued)

Cell	Fill	Initial Resistivity, μohm-cm	Std. Temp., mv	Avg. Temp., °C	Current Density, amps/cm^2	% Std. Dev. of $\Delta V/\Delta\theta$	Std. Dev. of $\Delta V/\Delta\theta$	Max. Dev. in $\Delta V/\Delta\theta$	$\frac{\Delta V/\Delta\theta}{(I/A)^2}$ $\frac{V/sec}{(amps/cm^2)^2}$	$U_{Bi-Sn} \times 10^3$ cm^2/V-sec
					Run No. V-17					
3	1	136.372	21.498	520.3	362.7	-4.49	.009	.012	- .44998	.773921
4	1	136.382	21.498	520.2	362.1	4.60	.010	.009	.45881	.789107
3	2	136.367	21.494	520.5	650.4	-2.11	.014	.028	- .45326	.779562
4	2	136.436	21.491	520.5	649.4	2.33	.016	-.073	.45838	.788368
3	3	136.398	21.502	520.3	648.6	1.95	.013	.119	.45897	.789383
4	3	136.425	21.500	520.3	647.5	-2.88	.019	-.036	- .44327	.762380
3	4	136.400	21.509	520.2	650.1	2.17	.015	.035	.45932	.789984
4	4	136.484	21.510	520.2	649.1	-2.67	.018	-.045	- .44797	.770464
					Run No. V-18					
3	1	116.387	15.123	371.3	332.0	1.25	.007	.013	1.3533	.833470
4	1	116.425	15.134	371.1	331.4	-1.37	.007	.042	-1.3145	.809574
3	2	116.412	15.139	370.4	332.9	-1.16	.006	.015	-1.3253	.816226
4	2	116.446	15.122	370.3	332.2	1.18	.006	-.009	1.3498	.831315
3	3	111.040	10.141	249.2	332.1	-1.70	.007	.010	-1.0299	.689127
4	3	111.062	10.150	249.1	331.6	2.01	.008	.013	1.0372	.694011
3	4	111.068	10.180	251.0	445.0	2.11	.016	-.011	1.0560	.706591
4	4	111.116	10.177	250.7	444.1	-1.05	.007	.020	-1.0050	.672466
3	5	111.043	10.154	250.2	443.3	-1.18	.009	-.011	-1.0268	.687052
4	5	111.084	10.154	250.1	442.7	1.92	.014	-.017	1.0442	.698695

TABLE M-1 (Continued)

Cell	Fill	Initial Resistivity, μohm-cm	Std. Temp., mv	Avg. Temp., °C	Current Density, amps/cm^2	% Std. Dev. of $\Delta V/\Delta\theta$	Std. Dev. of $\Delta V/\Delta\theta$	Max. Dev. in $\Delta V/\Delta\theta$	$\frac{\Delta V/\Delta\theta}{(I/A)^2}$ $\frac{V/sec}{(amps/cm^2)^2}$	$U_{Bi-Sn} \times 10^3$ cm^2/V-sec
					Run No. V-19					
5	1	80.673	12.205	300.0	364.4	- .69	.006	-.048	-1.8785	1.20286
6	1	80.716	12.201	300.1	352.9	1.59	.014	-.007	1.9330	1.23776
5	2	80.620	12.154	298.8	298.7	1.18	.007	.006	1.9416	1.24326
6	2	80.621	12.157	298.9	289.6	-1.31	.007	-.008	-1.8846	1.20677
5	3	76.332	7.276	179.6	331.5	1.09	.006	.005	1.4270	1.00007
6	3	76.356	7.279	180.0	321.3	- .78	.004	-.007	-1.4013	.98206
5	4	76.432	7.329	182.3	331.3	- .90	.005	-.006	-1.3760	.96433
6	4	76.361	7.327	182.2	321.2	1.58	.009	.007	1.4657	1.02719
					Run No. V-20					
5	1	97.467	13.051	319.8	331.5	- .75	.006	-.016	-1.9663	1.00568
6	1	97.519	13.052	319.8	321.5	.11	.001	.007	2.0496	1.04829
5	2	97.453	13.034	320.3	332.9	1.64	.013	.008	2.0162	1.03121
6	2	97.408	13.034	320.1	322.7	- .92	.007	.045	-1.9772	1.01126
5	3	92.683	8.070	199.5	333.8	.85	.005	-.016	1.5857	.927714
6	3	92.475	8.058	199.6	323.6	- .74	.004	.016	-1.3024	.761969
5	4	92.510	8.034	199.1	330.2	-1.05	.006	-.019	-1.4381	.841360
6	4	92.576	8.027	198.5	320.1	1.48	.008	-.008	1.5407	.901387

TABLE M-1 (Continued)

Cell	Fill	Initial Resistivity, μohm-cm	Std. Temp., mv	Avg. Temp., °C	Current Density, amps/cm^2	% Std. Dev. of $\Delta V/\Delta\theta$	Std. Dev. of $\Delta V/\Delta\theta$	Max. Dev. in $\Delta V/\Delta\theta$	$\frac{\Delta V/\Delta\theta}{(I/A)^2}$ $\frac{V/sec}{(amps/cm^2)^2}$	$U_{Bi-Sn} \times 10^3$ cm^2/V-sec
					Run No. V-21					
5	1	66.482	13.862	339.8	365.4	- .67	.004	.006	-1.3022	1.47305
6	1	66.493	13.861	339.8	354.3	1.47	.009	.005	1.3585	1.53674
5	2	66.515	13.877	339.8	364.7	.65	.005	.006	1.3556	1.53345
6	2	66.494	13.876	339.9	353.6	- .79	.004	.009	-1.3091	1.48085
5	3	62.895	9.042	223.4	365.8	1.64	.008	-.010	1.0498	1.30060
6	3	62.875	9.048	223.3	354.7	-1.07	.005	.030	-1.0239	1.26851
5	4	62.860	9.006	221.8	364.9	- .89	.004	.006	-1.0205	1.26430
6	4	62.861	9.005	222.6	353.8	1.34	.006	-.005	1.0488	1.29936
					Run No. V-22					
5	1	52.424	15.599	381.2	811.6	4.47	.008	-.008	.075541	1.76970
6	1	52.261	15.605	381.3	786.9	-4.67	.008	-.020	-.074112	1.73622
5	2	52.386	15.500	379.8	972.0	4.07	.011	-.025	.077690	1.82004
6	2	52.232	15.507	379.7	942.4	-4.57	.010	-.018	-.069924	1.63811
5	3	49.150	10.576	260.1	962.4	3.94	.007	-.013	.056836	1.46876
6	3	49.035	10.564	260.0	932.7	-4.92	.009	.016	-.060490	1.56318
5	4	49.029	10.507	258.9	967.5	-4.03	.008	.020	-.056264	1.45397
6	4	49.115	10.513	258.9	938.0	4.92	.010	-.012	.061976	1.60158
5	5	56.039	21.501	520.1	934.2	-3.87	.011	.032	-.093539	1.96198
6	5	56.141	21.475	518.1	906.1	13.83	.045	-.017	.109941	2.30601
5	6	56.067	21.466	517.0	933.4	5.86	.018	-.006	.098906	2.07455
6	6	56.010	21.467	518.7	904.1	-3.34	.009	.011	-.090456	1.89731

TABLE M-1 (Concluded)

Cell	Fill	Initial Resistivity, μohm-cm	Std. Temp., mv	Avg. Temp., °C	Current Density, amps/cm^2	% Std. Dev. of $\Delta V/\Delta\theta$	Std. Dev. of $\Delta V/\Delta\theta$	Max. Dev. in $\Delta V/\Delta\theta$	$\frac{\Delta V/\Delta\theta}{(I/A)^2}$ $\frac{V/sec}{(amps/cm^2)^2}$	$U_{Bi-Sn} \times 10^3$ $cm^2/V\text{-}sec$
					Run No. V-23					
6	1	93.425	1.528	41.488	538.2	-2.69	.010	-.008	- .34868	.90308
6	2	93.856	1.702	45.372	541.3	2.58	.011	-.019	+ .42242	1.08902

TABLE M-2

CALIBRATION OF ELECTROTRANSPORT CELLS
USED IN RUNS V-7 TO V-22

Cell	$\left(\frac{Am}{L}\right) \times 10^3$, cm	L, cm	Am x 10^3, cm^2	% Std. Dev.	No. of Points
1	1.025	2.949	3.023	.032	6
2	1.044	2.901	3.030	.006	6
3	1.040	2.976	3.119	.005	6
4	1.025	3.025	3.074	.008	6
5	1.046	2.948	3.084	.003	5
6	1.026	3.099	3.181	.008	5

TABLE M-3

ORIGINAL WEIGHTS OF Bi-Sn ALLOY COMPONENTS

Runs	Wt. Bi, gm	Wt. Sn, gm	Wt. % Bi	At. % Bi
V-22	2.4369	138.930	1.72	.986
V-7,8,9,10	12.118	131.334	8.45	4.98
V-12	24.625	126.36	16.31	9.96
R-6-1	50.88	124.48	29.0	18.84
V-13,21	50.6345	114.20	30.72	20.12
R-6-2; V-14,19	92.32	83.52	52.50	38.57
R-4-1; V-16,20	135.06	56.501	70.6	57.59
R-4-2; V-15,18	176.05	26.903	86.8	78.80
V-17	191.920	5.934	97.2	94.84

TABLE M-4

DATA USED IN CALCULATING THE DIFFERENTIAL ELECTRIC MOBILITY

Run No.	Temp.,(a) °C	Sn(b) At. %	Bi(b) At. %	Initial(c) Resistivity, μohm-cm	1/f,(d) μohm-cm x 10^{-2}
V-7	518	95.02	4.98	59.210	.8710
V-8	522	95.02	4.98	59.319	.8720
V-9	518	95.02	4.98	59.210	.8710
V-10	450	95.02	4.98	57.416	.8544
V-10	351	95.02	4.98	54.723	.8301
V-10	249	95.02	4.98	51.896	.8056
V-10	599	95.02	4.98	61.365	.8909
V-12	516	90.04	9.96	63.255	.8705
V-13	518	79.88	20.12	71.941	.8710
V-14	517	61.43	38.57	88.141	.8708
V-15	520	21.20	78.80	123.455	.8716
V-16	520	42.41	57.59	105.389	.8716
V-17	518	5.16	94.84	136.408	.8710
V-18	369	21.20	78.80	116.419	.8347
V-18	248	21.20	78.80	111.070	.8052
V-19	298	61.43	38.57	80.650	.8174
V-19	180	61.43	38.57	76.359	.7888
V-20	318	42.41	57.59	97.460	.8222
V-20	197	42.41	57.59	92.564	.7930
V-21	338	79.88	20.12	66.505	.8270
V-21	221	79.88	20.12	62.869	.7989
V-22	378	99.014	.986	52.243	.8369
V-22	258	99.014	.986	49.067	.8078
V-22	517	99.014	.986	56.079	.8708
		At. % Hg	At. % Cd		
V-23	43	98.992	1.008	93.425	4.10
V-23	43	98.992	1.008	93.856	4.10

(a) Corrected with thermocouple calibration.
(b) Weighed-in values.
(c) Taken from electrotransport runs after correction to average temperature.
(d) From data in Appendix.

TABLE M-5

AVERAGE VALUES OF RESISTIVITY FROM ELECTROTRANSPORT RUNS

Run No.	Composition, At. % Bi	Temp., °C	Resistivity,(a) μohm-cm	Resistivity,(a) μohm-cm	Resistivity, μohm-cm	Std.(b) Dev.	Std. Dev.(c) Avg. Res.	No. of Measurements
			Cell 1	Cell 2	Average			
V-10	4.98	252	51.898	51.893	51.896	.026	.027	4
V-10	4.98	353	54.732	54.714	54.723	.035	.037	4
V-10	4.98	452	57.404	57.416	57.410	.036	.038	4
V-7,8,9	4.98	520	59.215	59.206	59.210	.041	.022	9
V-10	4.98	601	61.430	61.365	61.398	.065	.070	5(d)
			Cell 3	Cell 4	Average			
V-12	9.96	518	63.249	63.260	63.255	.015	.017	4
V-13	20.12	520	71.939	71.942	71.941	.016	.017	4
V-14	38.57	519	88.136	88.145	88.141	.015	.016	4
V-16	57.59	522	105.389	105.389	105.389	.030	.032	4
V-15	78.80	522	123.458	123.449	123.455	.013	.014	4
V-17	94.84	520	136.383	136.432	136.408	.036	.039	4
V-18	78.80	250	111.052	111.087	111.070	.027	.032	3
V-18	78.80	370	116.399	116.438	116.419	.027	.049	2
			Cell 5	Cell 6	Average			
V-21	20.12	222	62.875	62.863	62.869	.011	.020	2
V-21	20.12	340	66.506	66.502	66.505	.010	.019	2
V 19	38.57	179	76.372	76.345	76.359	.030	.055	2
V-19	38.57	299	80.638	80.661	80.650	.028	.052	2
V-20	57.59	198	92.595	92.532	92.564	.084	.154	2
V-20	57.59	320	97.458	97.461	97.460	.038	.070	2
V-22	0.986	259	49.076	49.058	49.067	.060	.110	2
V-22	0.986	380	52.404	52.243	52.324	.095	.175	2
V-22	0.986	520	56.063	56.094	56.079	.064	.117	2
V-23	1% Cd in Hg		--	93.630	--	.049	.44	2

(a) Values have been corrected from standard temperature to average temperature.
(b) As computed using the data from both cells, hence averaged over both polarities.
(c) At the 95% Conf. Level on a Student t Dist.
(d) The values from Cell 2, Fill 16 and 17 were rejected.